



UNIVERSITY OF
BIRMINGHAM

EXAMINING THE ROLES OF ENDOTHELIAL DERIVED GALECTINS IN VASCULAR INFLAMMATION

Abbey Lightfoot

A thesis submitted to the University of Birmingham
for the degree of DOCTOR OF PHILOSOPHY

Institute of Cardiovascular Science
College of Medical and Dental Sciences
University of Birmingham

February 2023

UNIVERSITY OF
BIRMINGHAM

University of Birmingham Research Archive

e-theses repository

This unpublished thesis/dissertation is copyright of the author and/or third parties. The intellectual property rights of the author or third parties in respect of this work are as defined by The Copyright Designs and Patents Act 1988 or as modified by any successor legislation.

Any use made of information contained in this thesis/dissertation must be in accordance with that legislation and must be properly acknowledged. Further distribution or reproduction in any format is prohibited without the permission of the copyright holder.

ABSTRACT

This thesis explores how galectins, sugar-binding proteins, influence leukocyte trafficking during inflammation. Galectins (Gal) are known to be involved in inflammation, but specific endothelial-galectin interactions remain unclear.

We investigated how inflammatory mediators and shear stress affect the production of endothelial galectins and found that Gal-9 was highly produced in response to virus-associated inflammatory mediators. In contrast, Gal-3 (Gal-3) was downregulated under the same conditions. Interestingly, blood flow patterns also influenced galectin production.

We studied the function of galectins using Gal-knockout mice for intravital microscopy to study leukocyte trafficking events in the absence of galectins, which we then mimicked using *in vitro* flow assays using siRNA-to knockdown galectin expression in human umbilical vein endothelial cells (HUVEC). Our results suggest that Gal-3 and Gal-9 have distinct roles in leukocyte trafficking. Finally, we used a galectin-peroxidase fusion protein to proximity label Gal-3 interactors on HUVEC in response to cytokine treatment, for downstream identification of novel interactors through mass spectrometry and validation experiments.

Overall, we show that galectins are emerging as complex glycan-binding proteins with context-dependent functions, presenting a rich area for further exploration into their contributions to immune homeostasis and potential therapeutic opportunities, particularly targeted to leukocyte-endothelial interactions.

“Joy for humans lies in human actions.

Human actions: kindness to others, contempt for the senses, the interrogation of appearances, observation of nature and of events in nature.”

Marcus Aurelius, *Meditations*

VIII, 26

“You are the universe experiencing itself...

...The hallucination of separateness prevents one from seeing that, to cherish the ego is to cherish misery.”

Alan Watts

"Craft your intention with purpose, summon courage as your companion, embrace the boundless possibilities of the world. Trust that destiny unfolds, effortlessly, when aligned with the rhythm of the universe.

Then, you'll see what a wonder it is to be alive.”

Abbey Lightfoot, using ChatGPT

ACKNOWLEDGEMENTS

Firstly, I'd like to thank the Wellcome Trust for providing the funds to support my research. A huge thank you to Steve, Graham, and Robin, for taking a chance on me. An extension of my thanks to Gerard Nash, for your comments and encouragement in my review meetings. Thank you to Asif and Helen, for your endless support and guidance, encouragement, and motivation to get sh*t done. My gratitude to UCB, for countless opportunities to learn, grow and surrender to the challenges associated with science. Thank you to ALL my collaborators, Dan, Jack, Dylan, other Dan, Shish, Peter, Deanoooo – absolute power in numbers, ey! The biggest thank you to the Huang research Group, Geno, Meg, Abdullah, Tim, Rick, Mia, Zak, Abbey, and Lu. What a trip of a lifetime that was.

A special thanks to the Research Nurses at Birmingham City Hospital and all the incredible women who donated their umbilical cords in the name of science. The LTG crew, especially Franzi, Sam, Sophie, Julia, Jeneffa, Areeba, Harry, Adel, Poppy, Kathryn, Ladi, Danielle, Ed and Ingrid. Plus, a shout out to the newbies – you guys are crushing it and I'm excited to keep an eye open for all your future endeavours!

MIDAS, Crème de la crème. Gosh, we really lucked out, didn't we? I couldn't have asked for a better bunch to guide me on this journey. Thank you, Lisa, Poppy, David, Rach and Sofia.

My thanks to all those I met along the journey, my reasons, my seasons, and my lifetimes. Jodie, Laurence, Dan, Ollie, but to name a few beyond those already mentioned.

Finally, my deepest thanks go to the beautiful souls in my life, who have supported me through all the peaks and the troughs.

To my love, William. Thank you for expanding my mind, my soul and my love for the world. I'm eternally grateful for everything you have to offer me. Cameron, my soul buddy - thank you for growing with me, for showing me the depths and the beauty of our minds.

I would like to express my deepest appreciation to Mum, for the invaluable lessons you imparted not through words, but through your actions. I am profoundly grateful for the impact of your teachings, which extend far beyond the pages of this thesis.

And to my oldest and most cherished friend, Faye. Even infinite words could not express the depth of love I have for you.

One final thanks to Me, for weaving my unique thread into the intricate tapestry of this wonderful game of the Universe. I see a bright and beautiful future.

Oh, what could be. Infinity has never looked so beautiful.

PUBLICATIONS TO DATE

1. Lightfoot A., Joeh E., Krautter F., Huang M. L., McGettrick H. M., Iqbal A. J., Elucidating the role of endothelial galectins in leukocyte trafficking. World Congress of Inflammation, Rome, Italy. June 2022. Pharmadvances doi: 10.36118/pharmadvances.2022.38
2. Lightfoot A, McGettrick H.M. (2021). Vascular Endothelial Galectins in Leukocyte Trafficking. Front. Immunol., Sec. Molecular Innate Immunity. doi.org/10.3389/fimmu.2021.687711

CONTENTS

CHAPTER 1: INTRODUCTION	1
1.1 OVERVIEW	2
1.2 <i>Endothelial Heterogeneity</i>	4
1.3 <i>Immune Response and Inflammation</i>	6
1.3.1 Capture and rolling	6
1.3.2 Activation and firm adhesion	7
1.3.3 Crawling and transendothelial migration	8
1.3.4 Role of haemodynamic forces in recruitment	10
1.4 <i>Galectins</i>	13
1.4.1 Regulation of galectin expression in inflammation	15
1.4.2 Leukocyte trafficking regulation by endothelial galectins	18
1.5 <i>Hypothesis and Aims</i>	23
CHAPTER 2: MATERIALS AND METHODS	24
2.1 <i>Ethics</i>	25
2.1.1 Human ethics	25
2.1.2 Mouse ethics	25
2.2 <i>Human endothelial cell isolation and culture</i>	27
2.2.1 Isolation of human umbilical vein endothelial cell (HUVEC) for cell culture	27
2.2.2 Expansion of cryopreserved endothelial cells	29
2.2.3 Washing and detachment of primary endothelial cells	29
2.2.4 Passaging of primary endothelial cells	29
2.2.5 Freezing of primary endothelial cells	30
2.2.6 Seeding of endothelial cells for experimental assays	30
2.2.7 SiRNA knockdown of HUVEC	31

2.2.8	Cytokine stimulation of HUVEC	32
2.2.9	Orbital shaking culture of HUVEC	32
2.2.10	Endothelial cell culture under flow using Ibidi Pump System	33
2.3	<i>Extraction of RNA and analysis of gene expression</i>	34
2.3.1	mRNA extraction	34
2.3.2	RNA Quality control	35
2.3.3	cDNA synthesis	35
2.3.4	Quantitative PCR (qPCR)	36
2.4	<i>RNA Sequencing</i>	38
2.4.1	Library Preparation	38
2.4.2	RNA sequencing analysis	38
2.5	<i>Analysis of Protein Expression and Binding</i>	40
2.5.1	Total protein isolation and quantification from adhered cells	40
2.5.2	Quantification of protein from lysates	40
2.5.3	Sodium dodecyl sulphate-polyacrylamide gel electrophoresis (SDS-PAGE)	42
2.5.4	Western Blot	42
2.5.5	Enzyme-linked immunosorbent assay (ELISA)	44
2.5.6	Immunofluorescence staining of HUVEC	44
2.5.7	Immunohistochemistry on frozen human tissue sections	46
2.6	<i>Human Blood Leukocyte Isolation</i>	48
2.7	<i>Flow Adhesion Assay</i>	49
2.8	<i>Proximity Labelling of Galectin Interactors On Endothelial Cells</i>	52
2.8.1	Validation and optimisation	52
2.8.2	Proximity labelling HUVEC in-situ for enriched proteomics analysis	55
2.8.3	Glycomics	60
2.8.4	In silico modelling of PXGal-3 interactions	62

2.8.5	Utilising ColabFold to model PXGal3-protein interactions	63
2.8.6	Direct ELISA for Gal-3 binding to recombinant CD38 and MMRN2	63
2.8.7	Co-Immunoprecipitation of PX-Gal3 interactors	64
2.9	<i>Mice used for experimental studies</i>	66
2.9.1	Complete blood count analysis	66
2.10	<i>Intravital Microscopy (IVM) Based Studies</i>	67
2.10.1	Cytokine-induced Inflammation	67
2.10.2	Pre-surgical Preparation	68
2.10.3	Exteriorisation of Cremaster Muscle	69
2.10.4	Analysis of IVM Images and Recordings	70
2.11	<i>Statistical analysis</i>	71
CHAPTER 3: CHARACTERISING THE REGULATORS OF ENDOGENOUS ENDOTHELIAL GALECTIN EXPRESSION		72
3.1	<i>Introduction</i>	73
3.2	<i>Shear regulation of endothelial galectins</i>	75
3.2.1	Orbital shaking culture of endothelial cells upregulates galectin transcription in vitro.	75
3.2.2	Investigating defined and complex shear stress patterns on galectin transcription in HUVEC using the ibidi culture system.	83
3.3	<i>Endogenous galectin expression is modulated in response to inflammatory mediators.</i>	90
3.4	<i>Characterisation of Galectin expression in human liver</i>	96
3.5	<i>Summary and Discussion</i>	102
3.5.1	Shear stress and pro-inflammatory mediators as regulators of galectin expression	102

3.5.2	Galectin expression in liver disease	104
CHAPTER 4: EXAMINING THE FUNCTION OF ENDOGENOUS ENDOTHELIAL		
GALECTINS IN LEUKOCYTE TRAFFICKING		107
4.1	<i>Introduction</i>	108
4.2	<i>Characterisation of global galectin knockout mice under resting conditions</i>	109
4.2.1	Endogenous Gal-3 and -9 are both required for controlled leukocyte rolling in the IL-1 β inflamed post-capillary venules of the cremaster	111
4.2.2	Endogenous Gal-3 and -9 are both required for controlled leukocyte rolling in the TNF- α inflamed post-capillary venules of the cremaster	118
4.3	<i>In vitro analysis of endothelial galectins under physiological shear stress</i>	124
4.3.1	Optimisation and validation of siRNA knockdown in HUVEC	124
4.3.2	Leukocyte trafficking is modulated in the absence of endothelial LGALS3 and LGALS9 function.	132
4.4	<i>Discussion</i>	135
4.4.1	Characterisation of galectin knockout mice	135
4.4.2	Flow adhesion assay	140
4.4.3	Limitations	141
CHAPTER 5: INVESTIGATING INTERACTIONS BETWEEN EXOGENOUS GALECTINS		
AND ENDOTHELIAL CELLS		144
5.1	<i>Introduction</i>	145
5.2	<i>Optimisation of proximity labelling galectin interactors on live cells</i>	146
5.3	<i>Identification of PX-Gal3 interactors by mass spectrometry</i>	158
5.4	<i>HUVEC N-Glycome profile changes in response to TNFα + IFNγ treatment</i>	165
5.5	<i>Validation of Galectin-3 interactors by in silico techniques</i>	167

5.6	<i>In vitro validation of Gal3 binding to CD38</i>	174
5.7	<i>Validation of MMRN2 binding</i>	177
5.8	<i>Discussion</i>	184
5.8.1	Optimisation of proximity labelling of HUVEC	184
5.8.2	Gal-3 interactions with CD38	188
5.8.3	MMRN2 interaction with Galectin-3.	189
5.8.4	Therapeutic potential	191
5.8.5	Limitations	192
	CHAPTER 6: CONCLUDING REMARKS AND FUTURE DIRECTIONS	194
6.1	<i>Concluding Remarks</i>	195
6.1.1	Concluding Remarks	195
6.1.2	Key Findings	195
6.1.3	Context-Dependent Functions	196
6.1.4	Implications for Atherosclerosis	197
6.1.5	Liver Pathogenesis and Beyond	198
6.1.6	Future Directions	199
6.1.7	Conclusion	200

LIST OF FIGURES

Figure 1: Glycan-binding proteins regulate endothelial-leukocyte interactions in inflammation.....	12
Figure 2: Structure and specificity of human endothelial-expressed β -galactoside binding galectins.	14
Figure 3: Schematic showing method for isolation of neutrophils from whole blood	48
Figure 4: Flow adhesion assay set up.....	49
Figure 5: In vitro analysis of the role of endothelial galectins in leukocyte trafficking under flow.....	51
Figure 6 (A-B): Intravital microscopy was used to investigate leukocyte trafficking events in vivo.	67
Figure 7: Endogenous endothelial galectin-3 and -9 expression is shear regulated.....	76
Figure 8: Concentration of soluble galectin decreases following culture with orbital shaking.....	79
Figure 9: Immunofluorescence staining of HUVEC grown in culture with orbital shaking show greater levels of galectin-3 and -9 positive staining.....	80
Figure 10: Immunofluorescence staining of HUVEC cultured under static conditions and 125 rpm orbital shaking show differential galectin-3 and -9 expression depending on shear stress.....	82

Figure 11: Galectin transcription in HUVEC following culture with low and high laminar shear stress over time relative to static control.	85
Figure 12: Endothelial cell morphology appeared directional with high laminar shear stress and less so with oscillating culture.	86
Figure 13: qPCR analysis of transcription of galectin genes in HUVEC following culture with low, medium, and high laminar or oscillatory shear stress over time relative to static control.	88
Figure 14 (A-D): Transcription of endogenous galectins is modulated in endothelial cells following stimulation with pro-inflammatory mediators.	92
Figure 15 (A-B): Expression of endogenous galectin-3 is modulated in endothelial cells following stimulation with inflammatory mediators.	93
Figure 16: Galectin-9 gene transcription is modulated by IFNα2 and IFNβ treatment.	94
Figure 17: Galectin genes are differentially transcribed in liver sinusoidal endothelial cells in response to pro-inflammatory stimuli.	97
Figure 18: Galectin-9 (Gal-9) was expressed highly in liver tissue sections from primary biliary cholangitis (PBC) patients.	99
Figure 19: Galectin-9 (Gal-9) was expressed highly in liver tissue sections from Hepatitis C (HepC) patients.	101
Figure 20 (A-B): Characterisation of galectin-knockout mice.	110

Figure 21 (A-I): Gr1+ leukocyte rolling flux and overall leukocyte numbers in post-capillary venules of IL-1β stimulated cremaster were significantly different across galectin-knockout and wildtype mice.	113
Figure 22 (A-B): Correlation matrix of IL-1β intravital microscopy data shows strong positive relationship between the leukocyte trafficking events of Gr+ cells and total leukocytes observed by brightfield.	115
Figure 23: Complete blood counts from mice following treatment with IL-1β and surgery for intravital microscopy.	117
Figure 24 (A-I): Mice deficient in both the Gal-3 and -9 genes show reduced transmigrated Gr1+ cells in post-capillary venules of TNFα stimulated cremaster.	119
Figure 25 (A-B): Correlation matrix of TNFα intravital microscopy data shows strong positive relationship between the leukocyte trafficking events of Gr+ cells and total leukocytes observed by brightfield.	121
Figure 26 (A-B): Complete blood counts from mice following treatment with TNFα and surgery for intravital microscopy.	123
Figure 27: Optimisation of siRNA knockdown of galectin-genes in HUVEC. .	125
Figure 28 (A-C): Optimisation of probe concentration for LGALS knockdown.	127
Figure 29: Optimised knockdown of galectin gene transcription in HUVEC by siRNA.	129

Figure 30: Protein expression analysis following galectin gene knockdown by siRNA.	131
Figure 31: Neutrophils show decreased ‘touch and go’, or non-stable interactions with inflamed HUVEC deficient in both the Gal-3 and -9 genes..	133
Figure 32: Proximity labelling of PFA-fixed PBMCs and HUVEC with PX-Gal3 in solution leads to a shift in side scatter, associated with aggregates.....	147
Figure 33: PX-Gal3 binding to live PBMCs causes a shift in the side scatter plot with increasing concentrations.....	148
Figure 34: rGal3 binding to live PBMCs does not cause a shift in side scatter plot with increasing concentrations.	149
Figure 35: rGal3 binding to live HUVEC does not cause a shift in side scatter plot with increasing concentrations.	150
Figure 36: PX-Gal3 binding to live PBMCs causes a shift in side scatter plot with increasing concentrations.....	151
Figure 37: No shift was observed in HUVEC scatter plot following incubation with increasing concentrations of PX-Gal3.	152
Figure 38: Proximity labelling technique damaged HUVEC monolayer.	154
Figure 39: Improved biotin labelling was observed in HUVEC with reduced incubation times with PX-Gal3.....	155
Figure 40: Sufficient biotin labelling was observed in HUVEC with reduced incubation times with biotin phenol.	156

Figure 41: Immunofluorescence validation of optimised proximity labelling conditions on HUVEC.	157
Figure 42: Mass spectrometry results from proximity labelling unstimulated HUVEC with PX-Gal3.	160
Figure 43: Mass spectrometry results from proximity labelling TNFα and IFNγ stimulated HUVEC with PX-Gal3.	161
Figure 44: Comparison of proteomics and transcriptomics dataset identifies differences between TNFα and IFNγ stimulated and untreated HUVEC that may be due to changes in glycosylation patterns.	163
Figure 45: N-glycomics profile differs between untreated and TNFα and IFNγ stimulated HUVEC.	166
Figure 46: Protein-protein interactions were determined by STRING analysis.	168
Figure 47: In silico modelling of PX-Gal3 using ColabFold.	169
Figure 48: In silico modelling was used to predict interactions with PXGal3.	171
Figure 49: In silico model of PX-Gal3 interaction with CD38.	172
Figure 50: Predicted residues facilitating interactions between PX-Gal3 and CD38 were determined by in silico modelling.	173
Figure 51: Confirmation of galectin-3 binding to CD38 by ELISA.	175
Figure 52: Galectin-3 binding to CD38 was outcompeted in the presence of lactose.	176

Figure 53: In silico model of PX-Gal3 interaction with Multimerin-2.....	178
Figure 54: Predicted residues facilitating interactions between PX-Gal3 and MMRN2 were determined in silico.	179
Figure 55: Galectin-3 binding to MMRN2 was not entirely glycan-dependent since binding was not fully inhibited in the presence of lactose.....	180
Figure 56: Western blot showing presence of Multimerin-2 bands following co-immunoprecipitation of PX-Gal3 in cell lysates.	182
Figure 57: Western blot showing Galectin-3 bands following co-immunoprecipitation of MMRN2 using rGal3.....	183

LIST OF TABLES

Table 1: Media and constituents used for human tissue cell culture.....	28
Table 2: List of FAM-labelled Taqman probes used for qPCR.	37
Table 3: Antibodies used for protein expression and binding assays.....	45
Table 4: Co-immunoprecipitation conditions for analysis of Gal-3-MMRN2 interactions.....	65
Table 5: Table of PX-Gal3 interactors with significant fold change difference in enrichment between treated and untreated HUVEC.....	164

LIST OF ABBREVIATIONS

Abbreviation	Definition
APC	Allophycocyanin
A260	Absorbance 260 nm
ACD	acid citrate dextrose anticoagulant
AcN	acetonitrile
AcOH	Acetic acid
AF647	AlexaFluor 647
ALD	Alcoholic Liver Disease
ANCOVA	Analysis of covariance
ANOVA	Analysis of Variance
APEX2	Ascorbate Peroxidase
AWERB	Animal Welfare and Ethics Review Body
B2ME	B-mercaptoethanol
BCA	Bicinchoninic acid
BSA	Bovine serum albumin
CaCl ₂	Calcium Chloride
CADM3	Cell Adhesion Molecule 3
CBC	Complete Blood Counts
CD38	Cluster of differentiation 38
CD77	Cluster of differentiation 77
cDNA	complimentary DNA
CLEC14A	C-type lectin CLEC14A
CO ₂	Carbon Dioxide
COVID-19	Coronavirus disease 2019
DAB	3,3'-diaminobenzidine
DAPI	4',6-diamidino-2-phenylindole
DEGs	Differentially Expressed Genes
dH ₂ O	deionised hydrogen dioxide (water)
DMEM	Dulbecco's modified Eagle's medium
DMSO	Dimethylsulfoxide
DNA	Deoxynucleic acid
DPBS	Dulbecco's phosphate buffered saline
DPX mount	Distyrene plasticiser xylene
DTT	Dithiothreitol
EC	Endothelial cells
EC ₅₀	Median effective concentration
ECL	Enhanced chemiluminescence
ECM	Extracellular Matrix
EDTA	Ethylene-(2,2)-diamine-tetracetic acid
ELISA	Enzyme Linked Immunosorbant Assay
eNOS	Endothelial nitric oxide synthase
EtOH	Ethanol
FBS	Fetal bovine serum
FCS	Fetal calf serum

FITC	Fluorescein isothiocyanate
FOV	Field of View
FSC	Forward scatter
GAGs	Glycosaminoglycans
Gal-1	Galectin-1
Gal-3	Galectin-3
Gal-3-/-	Galectin-3 knockout
Gal-3-/- Gal-9-/-	Galectin-3/Galectin-9 double knockout
Gal-8	Galectin-8
Gal-9	Galectin-9
Gal-9-/-	Galectin-9 knockout
GTF	Gene transfer format
H ₂ O ₂	Hydrogen Peroxide
HAEC	Human Aortic Endothelial Cell
HEPC	Hepatitis C
HEVs	High endothelial venules
His	Histamine
HRP	Horseradish peroxidase
HSS	High Shear Stress
HUVEC	Human umbilical vein endothelial cells
Hz	Hertz
IP	Intraperitoneal
I.S	Intrascrotal
I.V	Intravenous
ICAM1	Intercellular cell adhesion molecule 1
IFGR	Interferon gamma receptor
IFNs	Interferons
IFN γ	Interferon gamma
IFN α 2	Interferon alpha 2
IFN β	Interferon beta
IgG	Immunoglobulin
IHC	Immunohistochemistry
IL	Interleukin
IL-1 β	Interleukin-1 beta
iNOS	Inducible nitric oxide synthase
IQR	Interquartile range
IVC	Inferior Vena Cava
IVM	Intravital Microscopy
JAM	Junctional adhesion molecule
K ₂ CO ₃	Potassium Carbonate
KD	Knockdown
kDa	Kilodalton
KLF2	Krüppel-like factor 2
KO	Knockout
Lac	Lactose
LacNac	N-acetyllactosamine

LC	Liquid chromatography
LPS	Lipopolysaccharide
LSEC	Liver sinusoidal endothelial cell
LSS	Low shear stress
mAb	Monoclonal antibody
MFI	Median fluorescence intensity
MMRN2	Multimerin2
mRNA	Messenger RNA
MS	Mass Spectrometry
NaCl	Sodium Chloride
NaOH	Sodium Hydroxide
NF- κ B	Nuclear factor kappaB
NO	Nitric Oxide
NP40	Octylphenoxypolyethoxyethanol
Pa	Pascals
PAGE	Polyacrylamide Gel Electrophoresis
PAMPS	Pathogen Associate Molecular Patterns
PBC	Primary biliary cholangitis
PBMC	Peripheral blood mononuclear cells
PBS -/-	Phosphate buffered saline, without calcium and magnesium
PBS +/-	Phosphate buffered saline, with calcium and magnesium
PBSA	0.15% BSA
PBST	Phosphate buffered saline, with tween
PCA	Principal component analysis
PCR	Polymerase chain reaction
PE	Phycoerythrin
PECAM-1	Platelet/endothelial cell adhesion molecule 1
PEI	Polyethylenimine
PFA	Paraformaldehyde
Poly I:C	Polyinosinic:polycytidylic acid
PSC	Primary sclerosing cholangitis
PSGL-1	P-selectin glycoprotein ligand-1
PVDF	Polyvinylidene difluoride
PX-Gal3	Galectin-3 fusion protein with ascorbate peroxidase
RBC	Red Blood Cell
REC	Recording
rGal3	Recombinant Galectin-3 (CRD only)
rhBFGF	Recombinant Human Basic Fibroblast Growth Factor
rhEGF	Recombinant Human Epidermal Growth Factor
RIN	RNA integrity number
RIPA	Radioimmunoprecipitation assay buffer
RNA	Ribonucleic acid
RPM	Revolutions per minute
RT	Room Temperature
rTEM	Reverse Transendothelial Migration
SDS	Sodium dodecyl sulphate

SDS-PAGE	Sodium dodecyl sulphate polyacrylamide gel electrophoresis
SELE	E-selectin
SEM	Standard error of the mean
siRNA	Silencing RNA
SSC	Side Scatter
STAT	Signal Transducer and Activator of Transcription
T25	25 cm ² Tissue culture flask
TCEP	Tris(2-carboxyethyl)phosphine
TEAB	Triethylammonium bicarbonate
TFA	Trifluoroacetic acid solution
TLR2	Toll-like receptor 2
TMT	Tandem-Mass Tag
TNF α	Tumour Necrosis Factor alpha
VCAM1	Vascular cell adhesion molecule 1
VCR	Video cassette recorder
VE-Cadherin	Vascular endothelial cadherin
VEGF	Vascular Endothelial Growth Factor
VEGFR2	Vascular Endothelial Growth Factor Receptor 2
VLA	Very late antigen
VST	Variance Stabilising Transformation
WT	Wildtype

CHAPTER 1: INTRODUCTION

1.1 OVERVIEW

Inflammation is a protective and necessary response aimed at resolving perturbations in homeostasis within the body. This localised response is triggered by tissue injury, infection and/or other trauma resulting in a cascade of immunological responses that continue until damage is resolved. Inflammation can be classified as either acute or chronic; the five signs of acute inflammation are redness, swelling, heat, pain, and loss of function at the site of injury. These symptoms are brought about by an increase in white blood cells, cytokines and blood flow to the local area initiated by the innate immune response. This prompt response takes just a matter of seconds to commence, resulting in inflammation that may last between a few hours, a couple of days, or until the components of damaged tissue and infection are removed. In the case of chronic disease, inflammation can last a lifetime.

During onset of this inflammatory response, first-responders and tissue-resident leukocytes residing in the damaged area release soluble mediators that result in endothelial cell activation, whereby the expression of several adhesion molecules is upregulated to aid in subsequent leukocyte recruitment. Blood volume within the affected tissue becomes increased to facilitate this process, as well as increased vascular permeability in the surrounding blood vessels to allow the leakage of plasma fluid, resulting in oedema. This process generally takes place in the post-capillary venules of the skin and muscles, meanwhile, specialised endothelium which lines capillaries in the lung, liver and kidney are the facilitators of leukocyte trafficking in these tissues (Aird 2007).

Extravasation of leukocytes, namely neutrophils and macrophages, from nearby vessels towards the site of injury or infection is necessary for a specialised response

which is largely dependent on the initial insulting stimuli. For example, pathogen-associated molecular patterns on the surface of bacteria and viruses are recognised by pattern recognition receptors (PRRs), such as toll-like receptors (TLRs) which leads to activation of signalling pathways and subsequent NF- κ B, IRF and ERK-dependent gene transcription of pro-inflammatory soluble mediators, including IFNs, TNF α and IL-1 β (Parmar et al. 2006). The immune response raised in sterile inflammation is similar to that of infection, except damage-associated molecular patterns (DAMPs) of endogenous proteins are recognised by PRRs instead (Roh and Sohn 2018). Additional soluble mediators such as IL-33 and S100 proteins released from necrotic cells, are recognised by non-PRRs, or DAMP-specific receptors that include the class of Receptor for Advanced Glycation end-products (RAGEs). The expression of soluble mediators from innate immune cells following injury and infection act as chemical messengers to initiate responses from cells belonging to the adaptive immune system as well as triggering immunological memory. Initiation of the adaptive immune response is necessary for the body to recognise and resolve future incidents of previously encountered injury quickly and more efficiently, through the development of immunological memory within lymphocytes and natural killer cell population.

Inflammation is a critical response in the body's immune defence against injury and infection and is necessary for restoring homeostasis. If this response becomes dysregulated or remains unresolved, acute inflammation can soon turn chronic, resulting in disease. It is necessary to interrogate the mechanisms of the immune response and the specific interactions occurring at all stages of the process of inflammation, initiation and resolution, to understand which pathways or interactions might be becoming dysregulated in disease and could be druggable for treatment and even prevention of chronic disease.

1.2 Endothelial Heterogeneity

Endothelial cells (ECs) exhibit heterogeneity in structure, function, and gene expression across different vascular beds and organs. This heterogeneity is a fundamental property of the endothelium, allowing it to adapt to the diverse needs of underlying tissues and microenvironments. There are two substantial mediators of endothelial heterogeneity. Firstly, differences in the extracellular milieu; such as shear stress levels, blood components such as nutrients, toxins, and pH which EC's can sense and respond to these environmental cues, generating phenotypic differences across the vascular tree (Aird 2007). Secondly, epigenetic mechanisms that are site-specific properties "fixed" and retained even when ECs are cultured *in vitro*, providing genome-wide evidence for the importance of epigenetics in mediating differential gene expression (Chi et al. 2003).

Human umbilical vein EC (HUVEC) have been extensively used as a model for studying endothelial cell function and leukocyte recruitment in both static and flow systems due to their ability to become activated following treatment with inflammatory mediators and effectively support neutrophil adhesion and migration. ECs show intra-tissue heterogeneity within the vascular tree (arteries, veins, capillaries) and inter-tissue heterogeneity across different organs (Aird 2007). Macro-vessels, including veins and arteries, are critical for circulating blood throughout the body, delivering oxygen to vital organs and tissue and to the liver and kidneys for removal of waste products. The characteristics and functions of microvessels, such as arterioles and venules, is highly dependent on the environmental context in which they are found. Inter-tissue heterogeneity allows ECs to perform specialised functions, such as liver sinusoidal ECs (LSEC) which participate in metabolism and detoxification.

LSEC are the site at which leukocyte trafficking takes place within this tissue microenvironment (Shetty, Lalor, and Adams 2018). Large portal veins transport blood from the gastrointestinal tract to the liver, where blood travels through specialised sinusoidal capillaries to join the central vein. The hepatic arteries provide the necessary oxygen to the surrounding cells and tissue, flowing into the sinusoids where blood from the portal vein is cleansed before returning to the central vein and towards the heart. It is probable that the reason for differences in the blood vessels and ultimately the endothelial cells at each site is due to the spatial and temporal differences in the extracellular environment. Three subsets have been detailed: continuous, fenestrated, and discontinuous endothelium; defined as either tightly connected ECs surrounded by continuous basement membrane (continuous), a subset of which may contain holes or fenestra (fenestrated) to facilitate the selective exchange of nutrients, hormones, and waste products between the blood and surrounding tissues (Miyata 2015); and finally, endothelium containing fenestrae and a poorly formed basement membrane (discontinuous) (Favero et al. 2014). Tight cell-cell junctions of continuous endothelium are necessary and abundant in blood vessels forming the blood-brain barrier, preventing leakage and diffusion of substances by using only highly specific and regulated transportation mechanisms.

1.3 Immune Response and Inflammation

Leukocyte recruitment to the site of injury is a crucial event in the regulation of an inflammatory response. Tight regulation of interactions between the endothelium and circulating leukocytes is necessary to ensure a protective response to injury does not result in uncontrolled inflammatory disease. The leukocyte trafficking cascade is a crucial element to the inflammatory response and can be broken down into five major steps; Capture, rolling, firm adhesion, crawling and transmigration.

1.3.1 Capture and rolling

Glycans are one of the four major components that constitute cells, accompanied by nucleic acids, proteins, and lipids. Recognition of specific glycan motifs by glycan-binding proteins (lectins) is crucial for facilitating highly sophisticated cross-communication between leukocytes in the bloodstream and endothelial cells (ECs) lining the blood vessels (Krautter and Iqbal 2021). Several key lectins (E-, L- and P-selectins and Cluster of differentiation [CD] 44) have already been identified as important mediators of leukocyte recruitment and trafficking at the site of injury in the initial stages of the immune response (Krautter and Iqbal 2021).

Upon injury or infection, tissue-resident immune cells release pro-inflammatory factors such as reactive oxygen species (ROS) and proteases that partially degrade glycoprotein components of the glycocalyx; an EC-expressed matrix that serves to shield the vessel walls from direct exposure to blood components and flow (Sieve, Münster-Kühnel, and Hilfiker-Kleiner 2018; Reitsma et al. 2007). Glycosaminoglycans (GAGs) in the reduced layer of the glycocalyx bind and immobilise chemokines, accompanied by the activation of ECs leading to the upregulation of surface expressed

adhesion molecules (Marki et al. 2015). Hemodynamic forces facilitate the outward movement of leukocytes towards the endothelial wall, in a process known as margination, enabling interactions between leukocytes and the newly exposed adhesion molecules displayed on the endothelium (Marki et al. 2015).

The molecules facilitating the initial capture of leukocytes to the endothelium are formed from weak and low affinity interactions. Carbohydrate-binding proteins (lectins) displayed on the surface of activated ECs, namely selectins (E- and P-selectins), reduce the velocity of leukocytes rolling along the endothelium through binding to heavily glycosylated counter-receptors (PSGL-1, P-selectin glycoprotein ligand-1 [CD162]). This slow rolling facilitates leukocyte activation, whereby expression of ligands and receptors required for stable interactions and firm adhesion between leukocytes and endothelium are upregulated (**Figure 1A**) (Nourshargh and Alon 2014).

1.3.2 Activation and firm adhesion

Upon leukocyte activation, conformational changes in integrins (MAC-1, Macrophage antigen-1 [CD11b/CD18]; VLA-4, very late antigen-4 [CD49d/CD29]; and LFA-1, lymphocyte function-associated antigen-1 [CD11a/CD18]) are induced to facilitate firm adhesion of leukocytes to the endothelium. EC-expressed immunoglobulin superfamily adhesion molecules (ICAM-1, Intercellular Adhesion Molecule 1 [CD54] and VCAM-1, Vascular cell adhesion protein 1 [CD106]) serve as binding partners to leukocyte integrins (Herter and Zarbock 2013). These proteins are overexpressed in endothelial cells following stimulation with pro-inflammatory mediators and prime the ECs for leukocyte trafficking. This process of firm adhesion triggers the release of calcium ions (Ca^{2+}), following the engagement of integrin receptor-ligand complexes

that activate Phospholipase C (PLC) to mobilise inositol phosphate signalling molecule – IP₃, and diacylglycerol (DAG), and intracellular release of calcium ions from endoplasmic reticulum stores (Hellberg et al. 1996).

This interaction between integrins and adhesion molecules also initiates the reorganisation of the actin-cytoskeleton to facilitate spreading of leukocytes across the endothelium and for intraluminal crawling and transmigration into the tissue (Ley et al. 2007; Kinashi 2005).

1.3.3 Crawling and transendothelial migration

Leukocyte intraluminal crawling along the endothelium is driven by phosphatidylinositol-3 kinase (PI3K) phosphorylation of phosphatidylinositol (3,4,5)-biphosphate (PIP₂) to PIP₃ (triphosphate), and subsequent Rac1/2-mediated F-actin polymerisation to form cellular protrusions at the front of the neutrophil, taking the lead (Filippi 2019). Meanwhile, phosphatase and tensin homolog (PTEN)–mediated dephosphorylation of PIP₃ to PIP₂, and RhoA-driven actomyosin contraction at the rear of the cell allows the rest of the leukocyte to follow (Filippi 2019). Traversing of the leukocyte along the endothelium is required for initiation of transendothelial migration (TEM) to the tissues. Migration of leukocytes through the endothelium occurs either at endothelial junctions between ECs (paracellular) or through the body of the EC itself (transcellular), facilitated by leukocyte-integrin binding to junctional adhesion molecules (JAMs) and PECAM-1 [CD31] expressed on the EC surface (**Figure 1A**) (Ley et al. 2007). LFA-1, expressed on the neutrophil surface, provides the ligand for JAMs to initiate transmigration (Ostermann et al. 2002).

Moreover, it has also been discovered and described that neutrophils can engage in reverse transendothelial migration (rTEM) in which neutrophils migrate from the abluminal space into the luminal space in a process discovered to be dependent on JAM-C (Buckley et al. 2006; Woodfin et al. 2011). Whilst this process is necessary in preventing the accumulation of neutrophils at the site of inflammation and the subsequent resolution of inflammation, it is speculated that rTEM might also be responsible for initiating systemic inflammation (Xu et al. 2022).

Expression of selectins is low within the liver sinusoids since the low shear environment omits the requirement for tethering and rolling of leukocytes to the endothelium prior to trafficking (Shetty, Lalor, and Adams 2018). ICAM-1 and VCAM-1 are similarly upregulated in LSEC following their activation, with ICAM-1 mediating leukocyte binding through $\alpha\text{L}\beta 2$ receptors, and VCAM-1 mediating lymphocyte capture via $\alpha 4\beta 1$ integrin binding (Wilkinson, Qurashi, and Shetty 2020). Tissue-resident macrophages - Kupffer cells are the primary respondents to infection and inflammation in this microenvironment.

Whilst many aspects of the leukocyte trafficking cascade have been studied in detail, there remains more to uncover and understand. Specifically, the galectin family of glycan-binding proteins have recently come to light as functionally important immunoregulatory proteins with involvement in leukocyte activation, apoptosis and in mediating leukocyte adhesion and migration (**Figure 1B**) (Rabinovich et al. 2007) (Cooper et al. 2012). Enhancing our understanding of the regulators of galectin expression and their roles in mediating leukocyte trafficking, could uncover novel mechanisms of inflammation and highlight distinctive opportunities for the treatment of IMIDs.

1.3.4 *Role of haemodynamic forces in recruitment*

Tight regulatory mechanisms are required to ensure leukocyte recruitment occurs only when appropriate, as such ECs can detect and respond to environmental changes such as the haemodynamic forces of blood flow (Matharu et al. 2006; Nash, Buckley, and Ed Rainger 2004). Mechanosensitive proteins on the ECs recognise homeostatic continuous pulsatile and laminar blood flow which suppresses nuclear-factor kappa-B (NF- κ B) transcription factor via the MEK5/ERK5 (mitogen-activated protein kinase 5-extracellular signal-regulated kinase 5) pathway. Consequently, this prevents initiation of an inflammatory response through downregulating expression of adhesion molecules to ensure leukocytes are not unnecessarily or inappropriately recruited to the endothelium (Parmar et al. 2006).

The effects of haemodynamic forces also influence the various stages of the leukocyte trafficking cascade. Pre-exposure of neutrophils to 0.1-2.75 dyn/cm² shear stress has been reported to positively assist the neutrophil responses to chemoattractants, namely platelet-activating factor (Mitchell, Lin, and King 2014). One study reports that transitions between 'catch' and 'slip' neutrophil behaviours observed in the adhesion and rolling stages becomes stronger with increasing shear stress, as P-selectin complexes with P-selectin glycoprotein are first prolonged and then shortened to facilitate the movement of neutrophils along the endothelium (Marshall et al. 2003; Finger et al. 1996). Around 10-fold lower shear stress conditions (0.2 dyn/cm²) are favoured for the transition from selectin-mediated adhesion and rolling into firm adhesion, facilitated by integrin-interactions preceding transmigration (Lawrence et al. 1997). Finally, one study has reported that transmigration of leukocytes through inflamed endothelium is reliant on the presence of shear stress, not necessarily on the

magnitude of shear stress (Cinamon, Shinder, and Alon 2001). Contrary to this, another study reports that shear stress is not required for transmigration, though does accelerate the process (Kitayama et al. 2000). In summary, it is advantageous to study leukocyte-endothelial interactions as closely to physiological conditions as possible to mimic the events occurring *in situ*.

Another consideration is the interconnectedness of haemodynamics and the glycocalyx in blood vessels. The glycocalyx, a dense and uneven layer of glycoproteins and glycolipids covering the inner surface of blood vessels, serves several functions including acting as a mechanical sensor of blood shear force, a selective permeable barrier for the blood vessel wall, and a bridge for interactions between blood circulating cells and endothelial cells (Cosgun, Fels, and Kusche-Vihrog 2020). Research has identified the glycocalyx as a key mechano-sensor of the shear forces exerted by streaming blood onto the vascular endothelium that when damaged, can lead to endothelial dysfunction, inflammation, and coagulation cascades (Lupu, Kinasewitz, and Dormer 2020). Therefore, the integrity of the glycocalyx is vital for maintaining vascular homeostasis, and its disruption can play a role in various vascular diseases. In summary, the glycocalyx plays a crucial role in responding to haemodynamic forces, and its impairment can have significant implications for vascular function and health.

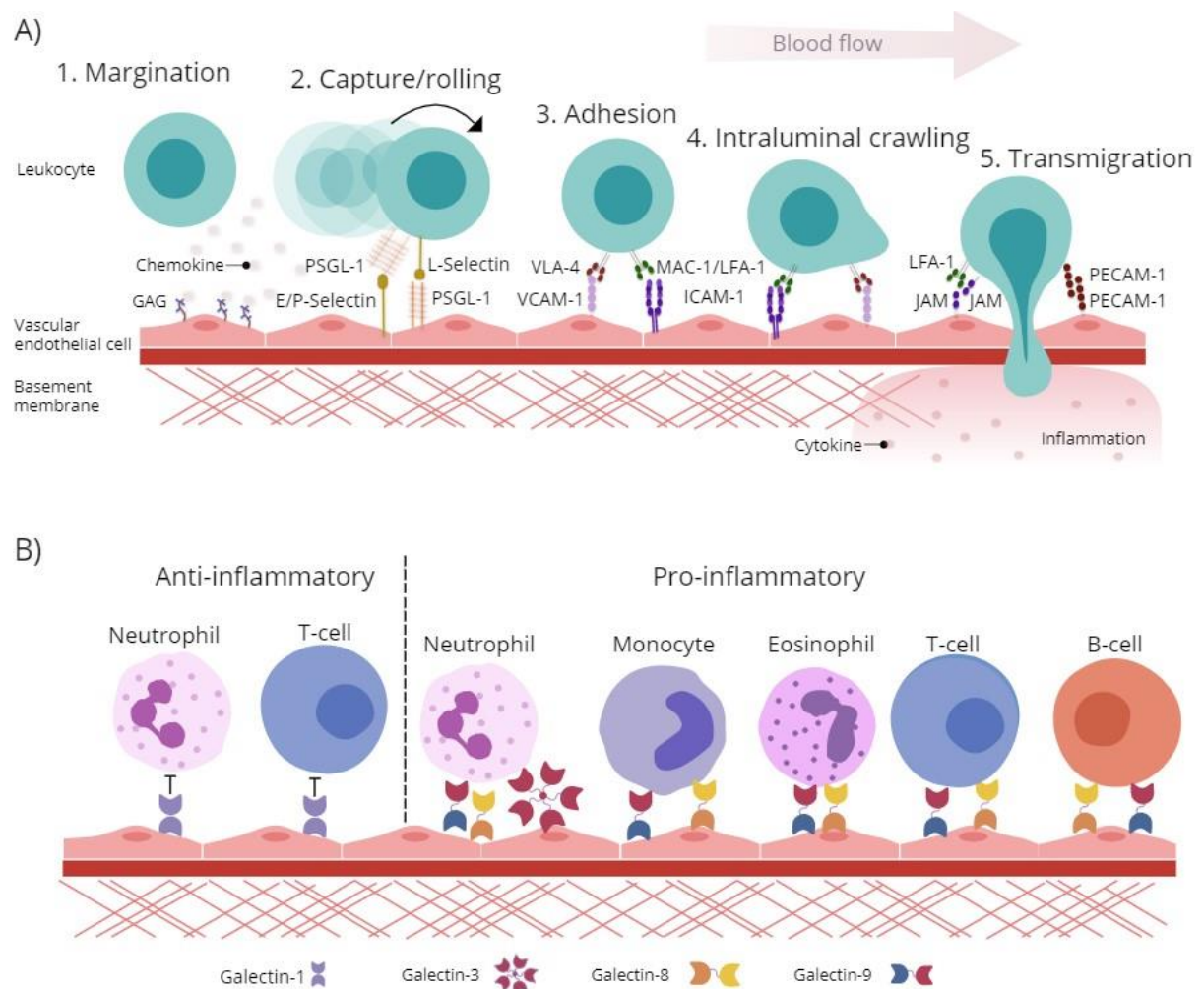


Figure 1: Glycan-binding proteins regulate endothelial-leukocyte interactions in inflammation.


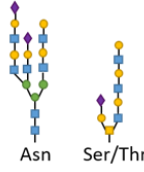
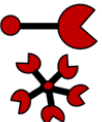
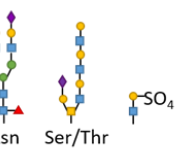
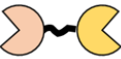
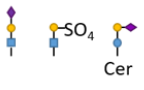
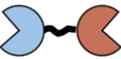
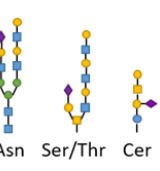
(A) Protein-protein and protein-glycan interactions are crucial regulators of leukocyte-endothelial interactions involved in the leukocyte adhesion cascade. Firstly, glycosaminoglycan (GAG)-presented chemokines promote leukocyte margination to the vessel wall. Capture and rolling of leukocytes along the endothelium is facilitated by interactions between selectins and their ligands such as P-selectin glycoprotein ligand (PSGL)-1. This interaction leads to cell activation and conformational changes in leukocyte integrins including Very Late Antigen (VLA)-4, Macrophage (Mac)-1 antigen and lymphocyte function-associated antigen (LFA)-1 that then interact with adhesion molecules such as Vascular Cell Adhesion Molecule (VCAM)-1 and Intracellular Cell Adhesion Molecule (ICAM)-1 to facilitate adhesion and intraluminal crawling. Finally, transmigration through the endothelial cell (EC) layer is mediated by homophilic interactions between platelet EC adhesion molecule (PECAM)-1 and junctional adhesion molecule (JAM). **(B)** β -galactoside binding galectins facilitate and inhibit leukocyte trafficking to the endothelium to promote pro- and anti-inflammatory responses. Galectin-1 inhibits leukocyte-endothelial interactions to promote an anti-inflammatory phenotype, whilst galectin-3, -8 and -9 facilitate pro-inflammatory leukocyte trafficking. Figure adapted from (Lightfoot, McGettrick, and Iqbal 2021).

1.4 Galectins

Galectins are a class of carbohydrate-binding proteins, specifically recognising β -galactoside-containing glycan side chains on proteins and lipids via their unique carbohydrate recognition domains (CRD) (Nabi, Shankar, and Dennis 2015). At present, 15 members of galectins have been identified in mammals, of which 12 are associated with genes found in humans (<https://www.ncbi.nlm.nih.gov/genbank/>) Galectins-1, -3, -8 and -9 are amongst the most studied members since many of their functions have been closely linked to inflammation and disease (Liu and Rabinovich 2010). Importantly, murine and human galectins share approximately ~79% protein sequence homology (Consortium 2020), allowing their function to be studied in pre-clinical murine models. Galectins can be classified into three distinct groups; prototype, tandem repeat, and chimeric as determined by their structural properties (**Figure 2**). Oligomerization of galectin monomers is typically required for the formation of functional galectin-glycan lattices on the surface of cells (Rabinovich and Toscano 2009). Additionally, and despite the absence of a classical secretory signal, galectins are released into the extracellular compartment and mediate extracellular matrix (ECM) assembly and remodelling through binding to ECM components (laminin, fibronectin and vitronectin) (Camby et al. 2006).

Key conserved amino acids in the CRDs across different galectins are responsible for the specific binding to β -galactoside-containing glycans. Despite these similarities, each galectin type reserves specificity for particular branched glycan's and glycan motifs attached to proteins and lipids alike (**Figure 2**) (Hirabayashi et al. 2002). For example, the presence of α 2,6-linked sialic acid prevents binding of galectin-1 to glycan chains, whilst the same motif enhances the affinity of galectin-8 for its ligand,

determining important interactions regulating inflammation (**Figure 2**) (Rabinovich and Toscano 2009). The structural determinants of galectin-glycan recognition have recently been reviewed in (Modenutti et al. 2019). The effects of glycan modification on galectin–glycan interactions have been reviewed elsewhere and are summarised in Figure 2 (Rabinovich and Toscano 2009; Nielsen et al. 2018). Whether or not structural differences contribute to distinct roles for individual galectin members is yet to be fully elucidated and since galectins are expressed by many cell types it is important to consider both the exogenous and endogenous function of galectins in the context of specific cell types and their physiological interactions.

Name	Classification	Glycan specificity
Galectin-1 	Prototype One CRD Can form homodimers	 <ul style="list-style-type: none"> • Binds terminal <i>N</i>-acetylglucosamine (LacNAc) units • α2,6 sialylation prevents Gal-1 binding • Binding not affected by α2,3 sialylation
Galectin-3 	Chimera One CRD Can form oligomers	 <ul style="list-style-type: none"> • Binds both terminal and internal LacNAc and affinity is increased with multiple units • Affinity enhanced by 3-O-sulfation • Binding not affected by α2,3 or α2,6-sialylation
Galectin-8 	Tandem-repeat Two distinct CRDs	 <ul style="list-style-type: none"> • Gal-8 N-terminal has increased affinity for α2,3 sialylated and 3-O-sulfated LacNAc • Preferential binding to some glycosphingolipids including GM3
Galectin-9 	Tandem-repeat Two distinct CRDs	 <ul style="list-style-type: none"> • Preferentially binds branched N-glycans and repeated LacNAc units • Preferential binding to some glycosphingolipids including GM1

Key:
 ● Glucose
 ■ N-acetylglucosamine
 ◆ Neu5Ac
 ● Galactose
 ■ N-acetylgalactosamine
 ▲ Fucose
 ● Mannose

Figure 2: Structure and specificity of human endothelial-expressed β -galactoside binding galectins.

The classification of galectins into prototype, tandem-repeat and chimera types is based on the number of carbohydrate recognition domains (CRDs) they contain. Each galectin type reserves high specificity for certain glycan motifs. Figure adapted from Lightfoot et al. 2021.

1.4.1 Regulation of galectin expression in inflammation

To play a role in leukocyte trafficking, galectins must be present at the site of inflammation where endothelial-leukocyte interactions occur. Expression of galectin-1, -3, -8 and -9 mRNA and protein have been detected in in vitro cultured human macro and microvascular ECs, with expression largely intracellular (Thijssen, Hulsmans, and Griffioen 2008). The release of soluble galectin-1 and -8 from human macro- or microvascular ECs respectively, has also been reported (He and Baum 2006; Cattaneo et al. 2014). Immunohistochemistry (IHC) on sections of human placenta, liver, kidney and colon tissue revealed that low levels of galectin-1 were consistently detected, whilst galectin-3, -8 and -9 expression was detected at variable levels in some but not all of the tissue sections (Thijssen, Hulsmans, and Griffioen 2008). Interestingly, the cellular localisation of endothelial galectin expression is highly variable between the different vascular tissue beds (Thijssen, Hulsmans, and Griffioen 2008; Baum et al. 1995). Specialised high endothelial venules (HEV) present in sections of human lymph node and tonsil tissue showed higher levels of galectin-9 expression than ECs in other vascular beds (Chakraborty et al. 2021). Conversely, galectin-3 was not detected, and galectin-1 expression was relatively low in HEV from healthy human lymph node sections (Stillman et al. 2006)(Baum et al. 1995). The variable expression of galectins reported in lymphoid tissues could be indicative of distinct immunoregulatory roles between the galectin types and highlight key considerations that must be made when comparing the cross-talk between endothelial cells and leukocytes since the HEV reside within close proximity to leukocytes within the tissue.

An additional consideration when studying ECs is that they possess a complex system of mechanosensitive proteins that respond to haemodynamic forces (Wragg et al. 2014). In response to physiological blood flow, ECs maintain an atheroprotective environment by suppressing gene expression of inflammatory, pro-apoptotic and proliferative pathways via mechanotransduction pathways (Zhang et al. 2009). The expression of integrins and adhesion molecules, including PECAM, are modulated via this mechanism. Perturbations in shear stress can disturb EC mechanosensitive protein signalling, contributing to the pathophysiological angiogenesis in tumour vasculature where low shear stress is experienced, and driving inflammation in atherosclerosis-prone vascular niches and flow-obstructing pathologies where shear stress is disturbed (Cunningham and Gotlieb 2005; Mura et al. 2012a). Deep sequencing of the transcriptome of HUVEC and human aortic EC (HAEC) in response to patterns of shear stress has identified changes in expression of galectins not only in response to specific flow patterns, but also across EC type (Maurya et al. 2021). Collectively, these findings suggest that expression of individual galectins is highly dependent on the tissue microenvironment and that a more in-depth comparison of the patterns of galectin expression across different vascular beds could be insightful for understanding galectin regulation and function in this context.

As is the case with many immunoregulatory proteins, galectin expression is modulated with EC activation in response to inflammatory mediators, pathogen exposure, and injury (Thijssen, Hulsmans, and Griffioen 2008; Ishikawa et al. 2004) (Imaizumi et al. 2002; Ayona et al. 2020). A concentration-dependent increase in expression of galectin-9 mRNA and protein was observed *in vitro* following treatment of primary HUVEC with double-stranded RNA viral mimetic, polyinosinic-polycytidylic acid [poly(I:C)], a TLR3 ligand (Ishikawa et al. 2004; Imaizumi et al. 2002). Similarly,

through the TLR4 pathway, lipopolysaccharide (LPS) stimulation up-regulated surface expression of galectin-8 in human microvascular EC (HMVEC), suggesting a specific role for galectins in viral and bacterial related infections (Cattaneo et al. 2014). More basic chemical mediators involved in acute and chronic immune responses have also been shown to differentially regulate endothelial galectin expression. Surface expression of galectin-3 on HUVEC is increased in response to treatment with IL-1 β (Rao et al. 2007b). Interestingly, stimulation of HUVEC with IFN- β/γ did not increase expression of galectin-3 (or galectin-1), though a significant increase in galectin-9 surface expression was observed (Chakraborty et al. 2021). More complex cocktails of soluble disease mediators, such as those released in the conditioned culture medium from colon carcinoma cell lines and in mixtures of oxidised low-density lipoproteins, a known driver of atherosclerosis and cardiovascular disease, stimulated galectin-1 translocation to the cell surface in HUVEC and HAEC (Thijssen, Hulsmans, and Griffioen 2008; Baum et al. 1995). The link between increased galectin expression and inflammation is well established, and elevated levels of galectin-3 in the serum and tissue of IMID patients is now recognised as a biomarker for detecting early stages of autoimmune and chronic inflammatory disease (Hara et al. 2020). Similarly, elevated serum levels of galectin-3 are detected in various cancers and even more so in metastatic disease, correlating with increased levels of metastasis-promoting cytokines released from vascular endothelial cells (Chen et al. 2013). The galectin expression profile within the tumour vasculature itself highlights a role for endothelial galectins in disease pathogenesis, where soluble factors secreted from tumour cells have been shown to induce galectin-1 expression and translocation to the EC surface to promote tumour angiogenesis and inhibit T-cell migration across the endothelium (Thijssen, Hulsmans, and Griffioen 2008; Thijssen et al. 2010; He and Baum 2006).

The link between galectins and tumour angiogenesis, metastasis, and immune suppression could make for an attractive immunotherapy target in combination with currently available cancer therapeutics. Blockade of vascular endothelial growth factor (VEGF) is the current standard of targeted anti-angiogenic therapy and offers variable treatment efficacy dependent on the cancer type (Vasudev and Reynolds 2014). Perhaps galectin-1 could be a more appropriate and effective target, even more so if used in combination with targeted therapy such as CAR-T cells to increase tumour infiltration. As has been confirmed with *in vitro* studies, galectin expression in leukocytes is also modulated in response to stimulation with various inflammatory mediators and could be a major influence on the differential expression observed in inflamed tissue and patient serum samples (Krautter et al. 2020). As such, soluble galectins released from immune cells can contribute to the differential levels of galectins observed in inflamed tissue and circulation, potentially counteracting endothelial cell-bound and/or expressed galectin functions. Distinguishing the specific effects of endothelial galectins on leukocyte trafficking and pathogenesis from the roles of alternative sources of galectins in the inflamed microenvironment is necessary to fully explore the potential for therapeutic intervention.

1.4.2 Leukocyte trafficking regulation by endothelial galectins

The interaction between glycans and glycan-binding proteins is crucial at all stages of leukocyte trafficking (Krautter and Iqbal 2021) and remains an active area of research. A large proportion of the literature investigating galectins in inflammation report pro- and anti-inflammatory functions of exogenous galectins. In the absence of inflammatory stimuli, galectin-1 has been reported to promote neutrophil migration *in vitro* via both chemotaxis and chemokinesis depending on the concentration used,

responsive to 25 nM and 250 nM respectively (Auvynet et al. 2012). Conversely, in the presence of acute inflammatory mediators IL-8 and TNF α , neutrophil chemotaxis was inhibited by galectin-1 (La et al. 2003; Cooper, Norling, and Perretti 2008). Similarly, the transmigration of modified T-lymphocyte cell lines across stimulated HUVEC was significantly inhibited by galectin-1 compared to unstimulated HUVEC (He and Baum 2006). Local injection of galectin-3 into the dorsal air pouch was shown to increase monocyte infiltration (Sano et al. 2000). More recently, galectin-3 was shown to directly dimerise with the chemokine CXCL-12 via an interface containing the GAG-binding motif, inducing anti-chemokine effects and inhibiting CXCL-12-induced migration of monocytic THP-1 cells and neutrophils *in vitro* (Eckardt et al. 2020). This latter finding could indicate an endothelial-specific galectin function whereby soluble galectin-3 released from ECs binds to the cell surface to mediate the interaction between leukocytes and CXCL-12. This concept is supported by the study from Yamamoto et al., which reported enhanced binding of T-cells, B-cells, neutrophils, eosinophils and monocytes to HUVEC following pre-incubation with increasing concentrations (0 - 2 μ M) of both galectin-8 and -9 (Yamamoto et al. 2007). Interestingly enhanced binding was not observed with galectin-1 or -3, although others have shown that oligomerisation of galectin-3 at the EC surface was observed by fluorescence resonance energy transfer (FRET) and facilitated leukocyte clustering at the tricellular corners of HUVEC monolayers where leukocytes preferentially transmigrate (Nieminen et al. 2007). Galectin-9 was originally identified as a potent chemoattractant and activator of eosinophils (Matsumoto et al. 1998) It has since also been shown to bind to protein disulfide isomerases on T-helper 2 cells (Th2), influencing their migration through recombinant galectin-9 coated matrigel by increasing the reduction of disulfide bonds on integrins (Bi et al. 2011). In the absence

of inflammatory stimuli, galectin-9 has been shown to significantly induce monocyte chemotaxis *in vitro* compared to control (O'Brien et al. 2018). This finding was also supported *in vivo*, with increased monocyte and macrophage infiltrate in isolated knee tissue from mice receiving galectin-9 via intra-articular knee injection (O'Brien et al. 2018). The earlier reports strongly suggest a positive role for galectin-9 in driving Th2-type immune responses that could be contributing to the development of diseases such as allergic asthma. However, the substantial increase in galectin-9 expression in ECs following stimulation with Poly:IC and IFN γ , and the increased monocyte and macrophage infiltrate observed in response to galectin-9 injection, suggests that galectin-9 mediated immune responses may be broader than Th2-type only. Together, these findings highlight a potential role for galectins as both pro- and anti-inflammatory molecules affecting leukocyte trafficking dependent on the mediators and cell types in the local microenvironment. It is also worth noting that the glycosylation patterns of leukocyte surface molecules change upon cell activation, and as such, are worth considering when studying the interactions between glycans and glycan-binding proteins to elucidate context specific roles and functions. With only a limited amount of research on the secretion of galectins from ECs, we cannot predict that the results observed in response to exogenous galectins would translate to such function *in vivo*. Thus, further investigation is required to understand the regulators of endothelial galectin secretion and the impact of this on leukocyte migration *in vivo*.

Galectin knockout mice and knock-down studies have been invaluable for studying the endogenous functions of galectins in a more physiological context. Galectin-1 appears to exhibit anti-inflammatory functions since extravasation to inflamed cremaster tissue was enhanced in galectin-1 knockout mice compared to wildtype (Cooper, Norling, and Perretti 2008). These mirrored *in vitro* results showing neutrophil

recruitment and rolling along TNF- α stimulated HUVEC was enhanced following galectin-1 knockdown in ECs (Cooper, Norling, and Perretti 2008). Similarly, endogenous galectin-1 appeared to inhibit T-lymphocyte capture, rolling and adhesion to stimulated HUVEC under physiological flow (Norling et al. 2008). Interestingly in an acute model of oedema, we found that the absence of galectin-1 did not exacerbate the inflammatory response and recruitment of leukocytes as predicted. This in part was due to redundancy amongst galectins, as we demonstrated galectin-9 levels were significantly elevated in these mice and could therefore potentially compensate for the absence of galectin-1 and promote resolution (Iqbal et al. 2011). Galectin-3 on the other hand, has been shown to promote leukocyte recruitment *in vivo*, as impaired slow rolling and emigration of leukocytes to IL-1 β stimulated cremasteric postcapillary venules of galectin-3 knockout mice were observed by intravital microscopy (Gittens et al. 2017). Interestingly, these galectin-3 null mouse ECs showed reduced surface expression of ICAM-1 and E-selectin following treatment with IL1- β and vehicle compared to wildtype, suggesting endothelial function might be impaired in the absence of endogenous galectin-3 (Gittens et al. 2017). There is limited research on the roles of galectin-8 and -9 on leukocyte trafficking, especially *in vivo*. The correlation between the results from *in vivo* studies using galectin knockout mouse models and *in vitro* studies using galectin-knockdown ECs support the endogenous galectin function on leukocyte trafficking and inflammation. Despite these convincing reports, an endothelial-specific galectin knockout mouse model is necessary to explore and understand mechanistic pathways and regulators of galectin function in the endothelium. Several endothelial-specific Cre and Cre/ERT2 mouse models have successfully been used in the vascular biology field and should be exploited to study endothelial galectin function.

Galectins have been shown to perform intra- and extracellular functions leading to inflammation and autoimmune pathologies. Galectins act as both pro- and anti-inflammatory mediators, involved in modulating leukocyte trafficking into tissue and clearance of inflammatory infiltrate. Activation of the endothelium and subsequent immune cell recruitment is a crucial event in the acute inflammatory response, though over exposure to pro-inflammatory factors including chemical mediators, LDL cholesterol and long-term changes in fluid shear stress may contribute to endothelial dysfunction and subsequent chronic disease. Endothelial galectin expression has been shown to be modulated in diseased tissue and in response to various inflammatory mediators. Despite this observation, very little research has investigated the regulators of- and the downstream consequences of endothelial galectin expression on the immune response and inflammation under physiological flow conditions. Therefore, we wish to study the roles of endothelial galectins in vascular inflammation and the mechanisms that underlie this.

1.5 Hypothesis and Aims

Glycan-binding proteins (GBPs) are key facilitators of leukocyte trafficking from the bloodstream into tissue as part of the inflammatory response. Galectins, a class of GBP, have key endogenous and exogenous functions within leukocyte populations that promotes their recruitment to the site of inflammation and drives the development of plaques within atherosclerosis. Despite the endothelium being a major source of galectins, there is very little research on the function of endothelial-galectin interactions driving leukocyte trafficking. We hypothesise that endothelial galectins are key drivers of immune cell recruitment to the site of injury, making them an attractive therapeutic target for treating chronic vascular inflammation. To challenge this hypothesis, the following aims were addressed:

1. Investigate the expression of endothelial galectins in response to shear stress and pro-inflammatory mediators.
2. Examine the role of endothelial galectins in leukocyte trafficking using a combination of *in vivo* and *in vitro* methods under physiological flow.
3. Uncover novel protein interactors of exogenous galectin-3 on the surface of endothelial cells.

CHAPTER 2: MATERIALS AND METHODS

2.1 Ethics

2.1.1 Human ethics

Human umbilical vein endothelial cells (HUVEC) were acquired from umbilical cords from women undergoing elective caesarean section at Sandwell & West Birmingham Hospitals (15/NE/0285). Neutrophils were isolated from the blood of one healthy donor under study number 12/EE/0122.

Human liver sections were kindly provided by Dr Daniel Pattern and Prof Shishir Shetty of the Centre for Liver and Gastrointestinal Research, Institute of Immunology and Immunotherapy, University of Birmingham. Normal liver tissue was obtained from rejected organ donors deemed unsuitable for transplantation under study numbers 06/Q2702/61 and 18/WA/0214. Diseased liver tissue was obtained from liver explants from patients undergoing transplantation at the Queen Elizabeth Hospital Birmingham, under study numbers 06/Q2702/61 and 18/WA/0214.

All tissue samples were obtained with prior written, informed consent and approval from the West Midlands and Black Country Research Ethics Committee Northeast Research Ethics Committee, or University of Birmingham Local Ethical Review Committee in compliance with the Declaration of Helsinki.

2.1.2 Mouse ethics

All mouse experiments were carried out under procedural guidelines, severity protocols and within the United Kingdom with ethical permission from the Animal Welfare and Ethical Review Body (AWERB) and the Home Office. Unless otherwise stated, all experimental animals were fed standard chow diet and water *ad libitum* and

maintained on a 12-hour light-dark cycle under pathogen-free conditions. Unless otherwise stated, all experiments were performed with mice weighing between 21 and 32 g, aged between 6- and 13-weeks.

2.2 Human endothelial cell isolation and culture

Unless otherwise stated, all cultures of human endothelial cells were maintained at 37 °C and 5% CO₂ conditions.

2.2.1 Isolation of human umbilical vein endothelial cell (HUVEC) for cell culture

In preparation for cell seeding, 25cm² culture flasks (T25 flasks; BD Falcon, UK) were pre-coated with 1% bovine skin gelatin (Type B G1393, Sigma-Aldrich, UK) solution (2% stock diluted 1:1 in phosphate buffered saline PBS with magnesium and calcium [PBS +/+]) for 30 minutes at room temperature (RT) before gelatin was aspirated and the flask was ready for cell seeding. Human umbilical vein endothelial cells (HUVEC) were isolated from cords as previously reported (Munir et al. 2015). Briefly, umbilical cords were sprayed liberally with 70% ethanol and glass cannula were inserted into the vein and secured with cable ties. The vein was flushed through with PBS, modified without magnesium and calcium (PBS [-/-]), followed by air to remove residual liquid.

The vein was filled with 1 mg/ml collagenase type 1a (Sigma type IA, C2674; Sigma-Aldrich) diluted in PBS (-/-) and incubated at 37 °C and 5% CO₂ for 15 minutes. Once removed from the incubator, cords were gently massaged for 45 seconds using the back of the knuckles. The cord was flushed through with PBS (-/-) followed by air for recovery of cell suspension into a 50 ml collection tube before centrifuging at 300 xg for 5 minutes. The cell pellet was resuspended in 4 ml HUVEC isolation media (**Table 1**), before seeding onto the gelatin coated T25 flasks. After a minimum of two hours and up to 18 hours the media was replaced, and cells were grown to desired confluency for passaging (Section 2.2.4) freezing (Section 2.2.5) or seeding (Section 2.2.6) for further experiments.

Table 1: Media and constituents used for human tissue cell culture.

Component				
	HUVEC isolation media	HUVEC treatment media	pHUVEC	pHAEC
Basal medium	Medium M199 (Gibco, 31150022)	Medium M199 (Gibco, 31150022)	Endothelial cell growth medium (Promocell, C-22210)	Endothelial cell growth medium MV (Promocell, C-22220)
Fetal calf serum	20 % (Sigma-Aldrich)	20 %	20 ug/ml	50 ug/ml
rhEGF, ng/ml	10 (Sigma-Aldrich)	10	0.1	10
rhBFGF, ng/ml	-	-	1	-
Hydrocortisone, µg/ml	1 (Sigma-Aldrich)	-	1	1
Heparin, µg/ml	-	-	90	90
Endothelial cell growth supplement, µg/ml	-	-	4	-
Penicillin-Streptomycin, U/mL	100 (Gibco)	100	-	-
Gentamycin, µg/ml	-	-	-	-
Amphotericin, µg/ml	2.5 (Thermo Fisher)	2.5	-	-

2.2.2 Expansion of cryopreserved endothelial cells

Commercial cryopreserved HUVEC and human aortic endothelial cells (HAEC) from single donors (Promocell, Heidelberg, Germany) were recovered under sterile conditions at passage 1 or 2 respectively, following the manufactures recommendation. Briefly, cells were defrosted using a water bath by warming the vial at 37 °C for two minutes, before recovering the contents in 1 ml of warmed complete media ([pHUVEC and pHAEC, respectively] Promocell, Table 1). Cells were added to a T25 flask and cultured for two hours before replacing the media. At 80-90% cell confluency, cells were passaged 1:3 for a total of four or five passages for HUVEC and HAEC respectively, following the protocol detailed in Section 2.2.4.

2.2.3 Washing and detachment of primary endothelial cells

At desired confluency, endothelial cells were washed with EDTA solution ((Sigma-Aldrich): E8008; 0.02%) for 30 seconds before replacing with 2 mL of 1X 0.05% Trypsin-EDTA (Gibco, Cat: 25300). HUVEC were incubated with room temperature trypsin until cells began to detach (~ 2 min), followed by a firm tap to fully detach the cells from the flask. Neutralisation of the trypsin was achieved by adding two volumes of HUVEC isolation media followed by centrifugation at 300 xg for 5 minutes. Media was aspirated and cell pellet reconstituted for passaging (Section 2.2.4), freezing (Section 2.2.5) or seeding for experiments (Section 2.2.6).

2.2.4 Passaging of primary endothelial cells

Following washing and detachment (Section 2.2.3) of cells, cell pellets were reconstituted in appropriate media before being placed into a new tissue culture flask. Cells were evenly distributed across the flask by gently moving the flask from side to

side and back and forth before returning the flask to the incubator until desired confluency for freezing (Section 2.2.5) or seeding of cells for experiments (Section 2.2.6).

2.2.5 Freezing of primary endothelial cells

At 85 – 90% confluency, endothelial cells were washed and detached (Section 2.2.3) and the cell pellet frozen in 10% DMSO in FBS; one T25 flask per cryovial [Greiner Bio-One Ltd, Gloucestershire, UK] for in-house isolated HUVEC, or 1×10^6 cells/mL for Promocell endothelial cells. Cryovials were placed into a Mr. Frosty™ Freezing Container (Thermo Fisher), for 24 hours in the -80°C , before being transferred to liquid nitrogen for long term storage.

2.2.6 Seeding of endothelial cells for experimental assays

For seeding of cryopreserved cells, vials were removed from the -80°C freezer and warmed in a waterbath set to 37°C for 2 minutes. Cells were recovered in 8 mL of their respective media, placed in a 15 mL Falcon tube and centrifuged at 300 xg for 5 minutes before removing media. Cells in culture were first washed and detached as detailed in (Section 2.2.3).

Each T25 of cells was divided into either four wells of 6-well plates; ten wells of 12-well plates; twenty wells of 24-well plates (Falcon); or resuspended in 1.5 mL culture media and adding 100 μL to each channel of the ibiTreat 0.4 mm μ -Slide I Luer or 30 μL in ibiTreat 0.4 mm μ -Slide VI Luer (ibidi, Germany) channels. For cells stored in 1×10^6 aliquots, these were seeded into three wells of 6-well plates; eight wells of 12-well plates; sixteen wells of 24-well plates; or resuspended to 1.6×10^6 cells/ml for seeding into ibiTreat 0.4 mm μ -Slide channels.

Cells were placed back in the incubator until required. For μ -Slides, media was topped up in the reservoirs after two hours, and a complete media change was performed every 24 hours. This was done by repeated three rounds of aspirating supernatants and replacing with fresh media.

2.2.7 *SiRNA knockdown of HUVEC*

HUVEC were seeded directly from culture or frozen aliquots, into either 24-well plates for optimisation and validation experiments, or ibiTreat 0.4 mm μ -Slide VI Luer channels (ibidi-AN03 2022) for use in flow adhesion assays (Section 2.2.6). The following day, culture media was aspirated, and the cells washed with PBS (-/-). As per manufacturers protocol, HUVEC were treated with between 5 nM – 50 nM of FlexiTube GeneSolution (Qiagen) siRNA against either *LGALS3* (GS3958), *LGALS9* (GS3965), in combination for knockdown of both *LGALS3* and *LGALS9* genes, or AllStars Negative Control siRNA (Qiagen).

To prepare the gene knockdown solutions, 5 – 50 nM of siRNA against *LGALS3* (Gal-3 KD), *LGALS9* (Gal-9 KD) or a combination of both (Gal-3/Gal-9 KD) were used for knockdown of specific galectin genes alongside non-specific scrambled control (sc-siRNA), diluted in 25 μ l of OptiMEM (Gibco). To prepare the transfection reagent, 1.5 μ l of LipofectamineTM RNAiMAX (Invitrogen) was diluted in 25 μ l of OptiMEM and added to each of the siRNA mixtures for five minutes incubation. Following this, warmed OptiMEM was added to the reagent mixture to total 500 μ l before adding solution to one well of a 24-well plate or applying 150 μ l to a single channel of the μ -Slide. Lipofectamine and media only controls were also prepared and added to cells. The siRNA knockdown solution was incubated with cells for four hours before the

mixture was aspirated and replaced with fresh media with hydrocortisone omitted. Cells were cytokine stimulated the following day (Section 2.2.8).

2.2.8 Cytokine stimulation of HUVEC

Supernatant was aspirated from cells and replaced with media +/- either: TNF α (R&D, 100 U/ml), IFN γ (Peprotech, 20 ng/ml), IFN β (Proteintech, 0.1 – 5 ng/ml), IFN- α 2 (Proteintech, 0.1 – 5 ng/ml), PolyI:C (Tocris, 20 μ g/ml), or TNF α + IFN γ combination (10 ng/ml and 20 ng/ml, respectively) in pre-warmed pHUVEC, pHAEC, or HUVEC treatment medium with hydrocortisone omitted (37 °C). Following 24- or 48-hour cytokine stimulation or negative control, supernatants were either discarded or collected in Eppendorfs and frozen at -80°C until required for protein expression analysis by ELISA (Section 2.5.5). HUVEC were washed three times with PBS (-/-) through repeat addition of PBS, followed by aspiration. After the final wash, HUVEC were processed for extraction of RNA and analysis of gene expression (Section 2.3), RNA sequencing (Section 2.4), analysis of protein expression (Section 2.5) or for use in flow adhesion assays (Section 2.7).

2.2.9 Orbital shaking culture of HUVEC

Cryopreserved promocell HUVEC were defrosted and seeded directly into wells of a 6-well tissue-culture plate and grown until 90% confluent. Media was exchanged with 2 mL fresh pre-warmed pHUVEC media containing 100 U/ML penstrep (Gibco). Cells were then placed in a plastic box with a loose-fitting lid and placed either in a static, or 125 rpm orbital shaking incubator (Innova 44R, Eppendorf) set to 37°C, maintained at 5% CO₂. Following 24 or 72 hours in culture, cells were prepared either for ELISA

(Section 2.5.5), extraction of RNA and analysis of gene expression (Section 2.3), or for immunofluorescence staining (Section 2.5.6).

2.2.10 Endothelial cell culture under flow using Ibidi Pump System

HUVEC were seeded into μ -Slide I Leur Ibidi (Ibidi, Cat: 80176) channels in a volume of 100 μ L and left to adhere for a minimum of 2 hours at 37 °C with 5% CO₂, before washing the cells by replacing the media through successive aspiration and addition of 100 μ L of pre-warmed media three times (ibidi-AN03 2022). Cells were placed back into the incubator until they reached 90% confluent. Media was replaced once more, before connecting the slides to the Ibidi Pump system for cell culture under shear stress.

Using the ibidi Pump System Quad, laminar and/or oscillatory shear stress of 0.05 Pa (0.5 dynes/cm²), 0.3 Pa (3.0 dynes/cm²), 1 Pa (10 dynes/cm²) and 2 Pa (20 dynes/cm²) was applied to HUVEC for up to 48 hours (ibidi-AN13 2022). For investigating 0.05 and 0.3 Pa low shear stress, the White Perfusion Set (Ibidi Cat no: 10963) was used. The Yellow-Green Perfusion set (Ibidi Cat no: 10964) was used for culturing cells with 1 Pa and 2 Pa high shear stress. Where oscillatory flow was used, the system was set to oscillate every second (1 Hz) and was run alongside laminar and static control. Media was replaced every 24 hours on the static controls. At the end of the experiment, cells were washed three times by replacing media in the channel with PBS (-/-). PBS was removed from the slide chambers before proceeding to mRNA extraction.

2.3 Extraction of RNA and analysis of gene expression

2.3.1 mRNA extraction

Messenger ribonucleic acid (mRNA) from cells was isolated using RNeasy Mini Kit (Qiagen, Manchester, UK) and according to the manufacturer's instructions. All centrifugation steps were performed at ≥ 8000 xg. Briefly, cells were washed with PBS (-/-), lysed in 350 μ l RLT buffer and stored at -80°C until required. Lysed samples were thawed on ice and homogenised by transferring samples to a Qias shredder column in a 2 ml collection tube and centrifuged for 2 minutes. The flow-through was mixed with an equal volume of ice-cold 70% ethanol and transferred to a RNeasy spin column placed in a 2 ml collection tube and centrifuged for 1 minute.

Samples were prepared differently depending on whether they were intended for RNA sequencing or cDNA synthesis. For RNA sequencing, the column was first washed with 350 μ l Buffer RW1 and centrifuged for 1 min. Then, DNase I, prepared by diluting 10 μ l of DNase I stock solution into 70 μ l of Buffer RDD, was added to the column and incubated for 15 minutes. The column was washed again with 350 μ l Buffer RW1 and centrifuged for 1 min. For cDNA synthesis, the column is simply washed with 700 μ l Buffer RW1 and centrifuged for 1 min.

For all sample processing, the flow-through was discarded and 700 μ l of buffer RW1 was applied to the spin column and centrifuged for 1 minute. The flow-through was discarded and 500 μ l of wash buffer RPE (with added ethanol) was applied to the spin column and centrifuged for 1 minute, this step was repeated one more time. The flow-through was discarded and the spin column was centrifuged for a further 5 minutes to remove residual wash buffer. Finally, 14 μ l of RNase-free water was applied directly

to the spin column filter and incubated for 5 minutes before centrifuging the sample for 2 minutes. Final eluate underwent RNA quality control.

2.3.2 RNA Quality control

The concentration of the eluted mRNA was measured in ng/μl from the absorbance at 260 nm (A₂₆₀), obtained using a Nanodrop ND-1000 Spectrophotometer (Thermo Fisher). mRNA was stored at -80°C or used immediately for synthesis of complementary DNA (cDNA).

Prior to sequencing, the RNA integrity number (RIN) was measured by Genomics Birmingham (University of Birmingham, UK) using the High Sensitivity RNA

ScreenTape® (Agilent Technologies, Stockport, UK). The RIN scores ranged between 9.2 – 9.6, suggesting high quality RNA for sequencing.

2.3.3 cDNA synthesis

Following extraction and quantification, each mRNA sample was standardised to 800 ng in a total of 10 μl of RNase-free water. cDNA synthesis was carried out using random primers supplied in the High-Capacity cDNA Reverse Transcription Kit (Thermo Fisher, #4368814). A 1X master mix was prepared in RNase-free water using 10X Reverse transcription buffer, 10X RT random primers, 25X dNTP mix, 40 units of RNaseOUT ribonuclease inhibitor (Invitrogen, #10777019) and 100 units of Multiscribe™ Reverse Transcriptase to a final volume of 10 μl per RNA sample. The master mix was combined and mixed thoroughly with the diluted mRNA sample to a final reaction volume of 20 μl in 0.5 mL microcentrifuge tubes. Samples underwent a thermo-cycle of 25 °C for 10 minutes, 37 °C for 120 minutes and 85 °C for 5 minutes

using the Veriti Thermocycler (Applied Bioscience). cDNA was stored at -20°C or used immediately in quantitative polymerase chain reaction (qPCR).

2.3.4 Quantitative PCR (qPCR)

qPCR was carried out using TaqMan Gene Expressions Assays according to the manufacturer's instructions in 384-well PCR reaction plates (Applied Biosystems). For each gene being analysed, a 1X reaction master mix made using 2X TaqMan Master Mix, and 20X FAM-labelled TaqMan gene expression assay on demand primer-probe conjugates (Applied Biosystems, **Table 2**) was prepared in RNase-free water for a final volume of 10 µl per sample. To 10 µl of reaction master mix, 0.5 µl of each sample cDNA was added and run in replicates of two or three in the reaction plate. The plate was centrifuged at 500 xg for 5 minutes and processed on the QuantStudio 5 qPCR System (Applied Biosystems) for 40-cycles and analysed using ThermoFisher Connect™ (Thermo Fisher). The average C_T value from triplicates were used and data was processed using the $2^{-\Delta\Delta C_t}$ method, normalising each sample to the 18S housekeeping gene and displaying as relative fold change to either unstimulated or static control, depending on the experiment (Livak and Schmittgen 2001).

Table 2: List of FAM-labelled Taqman probes used for qPCR.

Primer name	Protein Name	Cat number
LGALS1	Galectin-1	Hs00355202_m1 LGALS1
LGALS3	Galectin-3	Hs00173587_m1 LGALS3
LGALS8	Galectin-8	HS01057135_m1 LGALS8
LGALS9	Galectin-9	Hs04190742_mH LGALS9
VCAM1	Cellular adhesion molecule	Hs01003372_m1 VCAM1
ICAM1	Cellular adhesion molecule	Hs00164932_m1 ICAM1
KLF2	Kruppel-like factor 2	Hs00360439_g1 KLF2
KDR	Kinase Insert Domain Receptor (VEGFR2)	Hs00911700_m1 KDR
SELE	E-selectin	Hs00174057_m1 SELE
18S	Ribosomal subunit 18	Hs03003631_g1 18S

2.4 RNA Sequencing

2.4.1 Library Preparation

Library preparation was performed by University of Birmingham Genomics Service (Birmingham, UK) using the QuantSeq 3' mRNA Seq Library Prep Kit FWD (Lexogen, Vienna, Austria) (LexogenGmbH 2023) and the Illumina NextSeq 500 (Illumina:Sequencing 2015). All sequences were provided in.fastq format as provided from Illumina, and used for further RNA sequencing analysis (Section 2.4.2).

2.4.2 RNA sequencing analysis

FastQC software was used to assess adapter content and quality scores of the sequencing output and were confirmed as passing the quality check before moving onto sequence trimming (Section 2.4.2). Although the FastQC analysis determined that no trimming was required, a script to remove poly-AAA tails and adapter sequence contamination from the fastq files was run before aligning sequences to the genome.

To align sequences to the human genome, genome indexes were generated using the 'Homo_sapiens.GRCh38.dna Subread.primary_assembly' human genome file and corresponding gene transfer format (GTF) annotation file, downloaded from the ensemble website (Ensembl 2023). STARalign was then used to align sequences to the human genome. Finally, FeatureCounts from the Subread package was used to generate a table of ensemble IDs for each of the HUVEC samples.

iDEP was used for downstream analysis of RNAsequencing output (South Dakota State University 2023; Ge, Son, and Yao 2018). Transformation, normalisation and differential gene expression were all run through iDEP using the DESeq2 functionality.

For heatmaps and principal component analysis (PCA), read counts were first transformed using variance stabilising transformation (VST). Visualisation of data was performed using GraphPad Prism.

2.5 Analysis of Protein Expression and Binding

2.5.1 Total protein isolation and quantification from adhered cells

For lysis of cells from a 24-well plate, 50 µl of radioimmunoprecipitation assay buffer (RIPA, Sigma-Aldrich #R0278) supplemented with 1X protease inhibitor cocktail (Sigma-Aldrich, #P8340) was added to each well and incubated on ice for 30 minutes. Lysis was ensured by vigorous up and down pipetting of each sample before transferring 25 µl of lysate to a 1.5 ml microcentrifuge tube for quantification of protein (Section 2.5.2) and the rest stored at -80°C until required for SDS-PAGE (Section 2.5.3).

2.5.2 Quantification of protein from lysates

Protein quantification was performed using Pierce™ BCA Protein Assay Kit and protocol (Thermo Fisher). Briefly, bovine serum albumin (BSA, Sigma-Aldrich) standards in the range of 25 – 2000 µg/ml were diluted in RIPA buffer. A protein-free, RIPA buffer-only 'blank' was also prepared. Twenty-five microliters of each the standards, and unknown samples were added to a 96-well microplate (Falcon). A dilution of working reagent was prepared by mixing BCA reagents A and B, 50:1. Two-hundred microliters of working reagent was added to each sample, mixed thoroughly, and incubated for 30 minutes at 37°C or until blue colour was visible in the second to last most diluted standard sample. The plate was cooled to room temperature and the absorbance was measured at or near 562 nm on the GloMax Discover plate reader (Promega). The average optical density at 562 nm absorbance measurement of the Blank standard was subtracted from the average of the standards and unknown sample replicates. The standard curve was plotted using the absorbance blank-

corrected measurement of each BSA standard, with its known concentration in $\mu\text{g/ml}$, from which the protein concentration of unknown samples was derived. Samples were then run on SDS-PAGE gels prior to Western blotting (Section 2.5.3).

2.5.3 Sodium dodecyl sulphate-polyacrylamide gel electrophoresis (SDS-PAGE)

SDS-PAGE electrophoresis was used to resolve proteins according to molecular weight, and for the confirmation of single protein species in purified protein solutions. Following protein quantification of cell lysates by BCA assay, 20 – 30 µg of lysate, or 1.5 µg of purified protein was recovered in RIPA buffer to a total volume of 20 µl. Total volume was brought to 25 µl with the addition of 4x Laemmli sample buffer (containing 1:10 β-mercaptoethanol) before denaturing samples by placing at 95 °C for 10 minutes. For preparation of the XCell SureLock Mini-Cell (Invitrogen, #EI0001) electrophoresis tank, NuPAGE™ 4 to 12%, Bis-Tris, 1.0mm, Mini Protein Gel was placed within the buffer core and the locked in place using the gel tension wedge. The upper buffer chamber was filled with ~200 ml of 1X NuPAGE™ MOPS SDS Running Buffer (Invitrogen, # NP0001) and the lower buffer chamber filled with ~600 ml 1x running buffer. Sample was loaded onto the gel alongside four microliters of PageRuler™ Prestained Protein Ladder (Invitrogen #26616). Protein gels were run at 125V for ~90 minutes, or until loading dye had reached the end of the gel. Gels were removed from the plastic casing and either added directly to Coomassie Brilliant Blue R-250 (Bio-rad) for two hours, for rapid visualisation of protein bands, or transferred onto membranes for Western blotting (Section 2.5.4). Following Coomassie blue staining, gels were washed for five minutes, three times in destaining solution (H₂O, methanol, and acetic acid in a ratio of 50/40/10 [v/v/v]) until the background was less dark.

2.5.4 Western Blot

Proteins were transferred from SDS-PAGE gels using the Trans Blot Turbo Midi 0.2mm transfer (BioRad). Briefly, the gel was assembled onto the PVDF membrane

and flanked by two stacks of sponges. A roller was used to ensure that all bubbles were removed from the sandwiched stack before it was placed into the cassette and into the Trans-Blot Turbo system (BioRad). The machine was set to run 1.5mm mini gel, for 10 minutes. After the transfer process, the membrane was removed and blocked in 10% milk (Marvel, St. Albans, UK) in PBS (+/+) containing 0.1% Tween20 (PBST 0.1%) on a shaking platform at room temperature for 1.5-2 hours, followed by three 10-minute washes with PBST to remove residual blocking buffer.

Primary antibodies to the protein of interest were prepared in 5% BSA in PBST and incubated with the membrane at 4 °C overnight (Table 3). The membrane was washed three times with PBST for 10 minutes each before incubation with the appropriate HRP-conjugated secondary antibody for 1.5 hours at room temperature (Table 3). A further three, 10-minute washes with PBST were performed before the membrane transferred to cling film and incubated in the dark for 1 minute at room temperature with Pierce ECL blotting substrate mix (1:1, Thermo Fisher). In a dark developing room, the PVDF membrane was transferred to a piece of Amersham Hyperfilm ECL (Cytiva, Marlborough, MA) for up to 30 minutes before being processed in developer.

For membrane-reuse, blots were placed in stripping buffer (Thermo Fisher, #21059) for 20 minutes at 37°C, followed by washing with PBST three times and re-blocking of the membrane and re-probing as described above.

Resulting images were scanned into a digital format using a digital scanner before performing semi-quantitative analysis using Fiji software as described in the User manual (imagej.net 2012; Schindelin et al. 2012). Resulting measurements were then normalised to actin-beta housekeeping bands and shown relative to control.

2.5.5 Enzyme-linked immunosorbent assay (ELISA)

R&D Quantikine ELISA kits were used for detection and quantification of soluble Gal-3 (DGAL30) and Galectin-9 (DGAL90) in cell culture supernatants. Briefly, 100 µl of assay diluent was added to each well of the provided, pre-coated ELISA plate. Standards were prepared according to the kit-specific instructions, using serial dilutions made up in calibrator diluent, plus a blank no-protein control. Duplicates of each standard and the unknown samples were added to the assay plate at 100 µl per well and incubated at room temperature for two hours. Wells were aspirated and washed a total of four times, each time adding 400 µl of wash buffer followed by aspiration. After the final wash, plates were blotted against a clean paper towel to ensure dryness. Assay-specific conjugate for either Gal-3, or Gal-9 were added to each well at 200 µl and incubated at room temperature for two hours. Liquid was aspirated from the wells and four wash steps were performed. After blotting the plate dry, 200 µl of substrate solution (equal parts reagent A and B) was added to wells and left for 20 minutes away from light. Stop solution was added at 50 µl per well, turning liquid from a blue to yellow colour. The absorbance was measured at 450 nm and corrected using 540 nm or 570 nm wavelength reading.

The standard curve was plotted using the blank-corrected absorbance measurement of each assay standard with its known concentration in ng/ml, from which the protein concentration of unknown samples was derived.

2.5.6 Immunofluorescence staining of HUVEC

Cells were washed three times with PBS (-/-), aspirating in between each wash. Cells were fixed using 4% PFA to cover the cell layer and left on ice for 10 minutes. Fixative

was aspirated and cells washed three times with PBS (-/-) to remove residual PFA. All further incubation stages were carried out for one hour on a shaking platform at room temperature unless otherwise stated. Incubation with blocking buffer containing 5% BSA in PBS (-/-) was carried out, followed by aspiration and addition of primary antibodies made up in PBS (-/-) [Table 3]. Primary antibodies were aspirated from the wells before three 10-minute washes in PBST 0.1% were carried out. Fluorescently conjugated secondary antibodies were diluted 1:200 in PBS (-/-) and added to each well for incubation, followed by aspiration and three washes with PBST. Nuclear staining was performed using Hoechst or DAPI in PBS ([/-], 1:1000), followed by three washes with PBS (-/-). Finally, PBS (-/-) was added to the wells and imaged using either the Fluorescence microscope Zeiss AxioObserver.Z1 Apotome.2 or EVOS M5000 Imaging System, Thermo Fisher AMF5000.

For quantification of images, mean fluorescence was measured in all images and background fluorescence in secondary only control was subtracted from values.

Table 3: Antibodies used for protein expression and binding assays.

Antibody	Application and dilution	Manufacturer and Cat number	Secondary antibody
Anti-galectin-3	Western Blot 1:1000 Immunofluorescence 1:75 Immunohistochemistry 1:75 Flow cytometry 1:50 ELISA 1:1000	R&D AF1154	Mouse anti-Goat IgG-HRP Donkey anti-Goat IgG AF647
Anti-galectin-9	Western Blot 1:1000 Immunofluorescence 1:75 Immunohistochemistry 1:75	R&D AF2045	Mouse anti-Goat IgG-HRP Donkey anti-Goat IgG AF647
Secondary antibodies			
Mouse anti-Goat IgG-HRP	Western blot 1:5000 ELISA 1:1000 Immunohistochemistry 1:200	Santa Cruz Biotech, sc-2354	N/A
Donkey anti-Goat IgG (H+L) AF647	Immunofluorescence 1:200 Flow cytometry 1:200	(Invitrogen A21447)	N/A

2.5.7 Immunohistochemistry on frozen human tissue sections

Sections were removed from the freezer and thawed for five minutes at room temperature prior to washing the slides in PBST (0.1%) for five minutes on a rocking platform. To block endogenous peroxidases, the PBST was removed, and the slides were placed into a solution of 0.3% hydrogen peroxide in methanol for 30 minutes. Slides were washed in PBST for 5 minutes on a rocking platform. Blocking buffer of 1x casein in PBS (-/-) was added to tissue sections and incubated for 20 minutes in a humidifying chamber at room temperature to prevent non-specific staining. Tissue sections were washed in PBST for 5 minutes before adding 150 µl of anti-galectin-9 antibody made up at 1:75 in PBS (-/-), or just PBS for secondary only control, to each tissue section and incubating in the humidifying chamber on a rocking platform for 60 minutes.

Primary antibodies were removed from the tissue sections prior to two 5-minute washes in PBST. Peroxidase conjugated secondary antibodies were prepared in PBS (-/-) and applied to each tissue section for 30 minutes incubation on a rocking platform. Sections were washed twice in PBST, each for 5 minutes before DAB substrate (brand) was added for a further 5 minutes. DAB substrate was removed with tap water and sections were counterstained with haematoxylin for 30 seconds. Sections were placed into cold water that was slowly replaced with warm water and left for two minutes to change colour. To dehydrate sections, sequential washes with 70%, 80%, 90% and 100% ethanol was performed, each for two minutes. Similarly, sequential washes in xylene (from 70% - 100%) were performed to clear tissue sections before slides were mounted with DPX (brand) and stored at room temperature prior to image acquisition. Images were acquired from slides using the Zeiss Axio Scan.Z1 (ZEISS

Oberkochen, Germany). Fields of view for presentation were selected using Zen Blue software (Zeiss).

2.6 Human Blood Leukocyte Isolation

Whole blood was collected from healthy donors aged 25-29 years into EDTA-coated VACUETTE® tubes (Greiner, 4550360) and layered onto Histopaque 1119 and 1077 (Sigma-Aldrich) in a 15 mL Falcon tube (**Figure 3**). Following centrifugation at 800 xg for 40 minutes, the neutrophil layer was isolated using a Pasteur pipette and transferred to a new Falcon tube. The cells were then resuspended to a final volume of 12 ml in PBSA (PBS [+/+] + 0.15% BSA), followed by centrifugation at 300 xg for 6 minutes (Sigma-Aldrich 2020). After removing the supernatant, the cells were counted and resuspended in PBSA to a final concentration of 1×10^6 cells/ml. Neutrophils were stored at room temperature for up to 1.5 hours before use in the flow adhesion assay (Section 2.7).

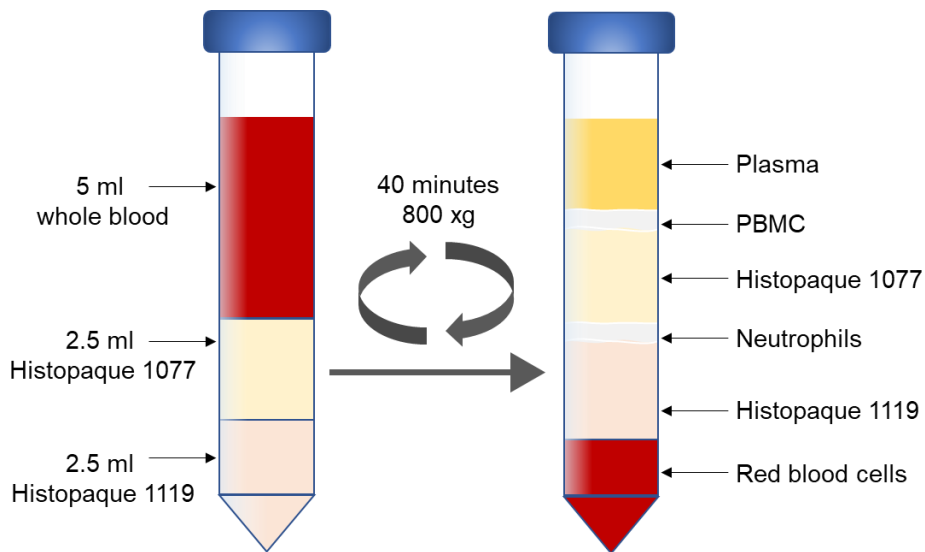


Figure 3: Schematic showing method for isolation of neutrophils from whole blood

To separate out neutrophils, 5 ml of whole blood was layered onto an equal volume of 1077- and 1119-density Histopaque layers. Following centrifugation, a clear band of neutrophils was visible and picked for use in experimental assays.

2.7 Flow Adhesion Assay

HUVEC in Ibidi μ -Slide VI 0.4 slides were treated with siRNA targeting *LGALS3*, *LGALS9*, a combination of both, or a scrambled-siRNA control one day after seeding. The following day, 150 μ l of media containing TNF α (10ng/ml) and IFN γ (20 ng/ml) was added to the cells for 24 hours.

On the day of the experiment and at least four hours prior to running the experiment, the flow assay chamber box was set-up and prepared according to **Figure 4** and following the protocol published (Yang, Chang, and Wei 2016). Falcon tubes of 0.15% BSA in PBS ([+/+] PBSA) were placed inside the chamber and the box was preheated to 37°C. The flow system was primed to remove bubbles by passing PBSA through the system using the wash syringe.

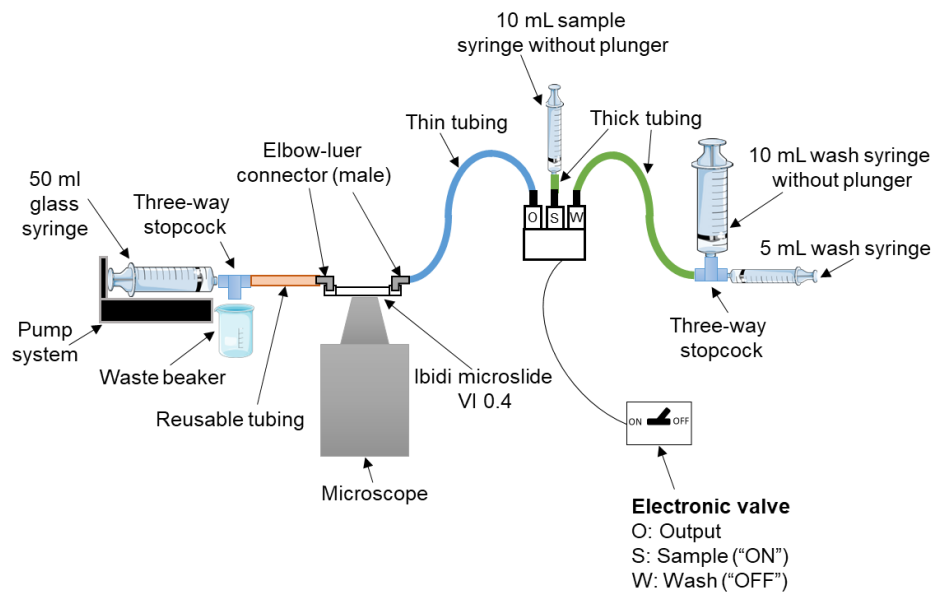


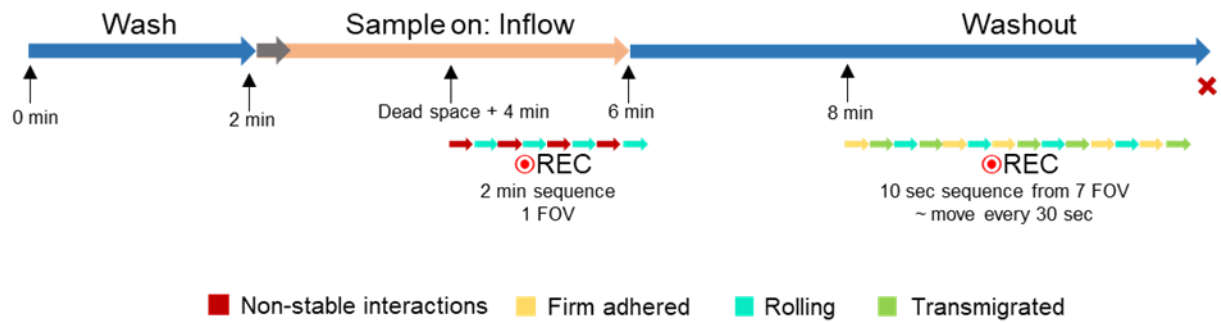
Figure 4: Flow adhesion assay set up.

Ibidi μ -slides were placed onto the microscope imaging stage and connected to the flow system via elbow-luer connectors for analysis of leukocyte trafficking under flow, *in vitro*.

Cells were placed on the viewing platform and a single channel connected to the flow system via the tubing. A final concentration of 1×10^6 cells/ml in 2 ml of neutrophils were added to the sample syringe for 1-minute, before the pump was set to infuse at 0.4 ml/min (0.05 Pa/0.5 dyn/cm²), priming the HUVEC. After two minutes, the electronic valve was switched to 'ON', beginning a four-minute perfusion or 'inflow' of neutrophils across the HUVEC. After this, the electronic valve was switched back to 'OFF' and a two-minute perfusion of PBSA, or 'washout' began. One continuous video recording was performed throughout the experiment using phase contrast microscopy, stored onto VCR.

Analysis of adherent and non-stable interactions were counted from 2-minute videos capturing the neutrophil inflow (226 images captured at intervals of 400 ms) within one field of view (FOV) in the centre of the slide (**Figure 5A**). Cells adhered to the endothelium for the entire recording were marked as 'adherent' and cells that stuck for at least one second before leaving the endothelium were recorded as 'touch and go' interactions (**Figure 5**). Analysis of firm adhered and transmigrated cells within the washout stage were recorded from seven FOVs within 20 images captured at intervals of 400 ms across 10 seconds. Neutrophils exhibiting 'phase bright' and 'phase dark' features were reported as adherent and transmigrated respectively (**Figure 5B**).

A



B

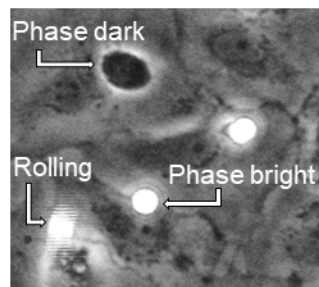


Figure 5: In vitro analysis of the role of endothelial galectins in leukocyte trafficking under flow.

A) Overview of workflow for flow assay experiment. $\text{TNF}\alpha$ + $\text{IFN-}\gamma$ (10 ng/ml, 20 ng/ml) stimulated HUVEC were washed for 2 minutes with PBSA at a rate of 0.4 ml/min. Neutrophils were flowed over the HUVEC monolayer for 4 minutes, with image sequence recording (REC) after 2 minutes for the duration of 2 minutes. HUVEC were washed for 2 minutes with PBSA before recording 10 second sequences across 8 fields of view were acquired. **B)** Images were analysed for phase bright (non-stable interactions, firm adhered, rolling), phase-grey (firm adhered) and phase dark (transmigrated) neutrophils.

2.8 Proximity Labelling of Galectin Interactors On Endothelial Cells

This work was conducted using a recombinant protein called PX-Gal3, containing the protein full length galectin-3 sequence fused to ascorbate peroxidase (APEX2) enzyme via flexible serine-glycine linker. This was used for enzymatic labelling of galectin-3 interactors on the surface of cells. Access to reagents and protocols for proximity labelling of galectin interactors on endothelial cells was possible through collaborative work with the Huang group at Scripps Research, San Diego, CA, USA.

2.8.1 Validation and optimisation

2.8.1.1 Preparation of cells for proximity labelling and Gal-3 binding

Initial validation was performed either on HUVEC and peripheral blood mononuclear cells (PBMCs) in suspension; or HUVEC *in situ*. For labelling *in situ*, HUVEC were seeded into 24-well plates, grown to 90% confluency, and washed two times in PBS (-/-) by discarding supernatant and replacing with PBS. All liquid was aspirated before proceeding to small-scale proximity labelling and validation by immunofluorescence (Section 2.8.1.2).

For labelling in suspension, HUVEC were grown to 90% confluency in a T25 flask (Section 2.2.6). Media was discarded before washing the cells with PBS (-/-) and replacing liquid with 2 mL of StemPro Accutase (Thermo Fisher). Cells were incubated for 2-7 minutes at 37°C, until rounded and dissociated from plastic. HUVEC were recovered in 8 mL of 37°C warmed HUVEC growth media. As a positive control, a vial of frozen PBMCs (Panda 2013) was defrosted in a 37 °C water bath and cells recovered with 8 mL of 2% FBS in M199. PBMCs were transferred to a 15 mL falcon tube for incubation at 37 °C for 10 minutes. PBMCs and HUVEC in suspension were

centrifuged for 5 minutes at 300 xg, and the supernatant discarded. Cells were resuspended in culture medium, either HUVEC treatment media, or 2% FBS in M199 for HUVEC and PBMCs respectively, counted and 4×10^5 cells placed into five U-bottom 96-well plates. Plates were centrifuged for 2 minutes at 300 xg and either fixed with 4% PFA solution for 10 minutes or used directly in proximity labelling (Section 2.8.1) or in validation for flow cytometry (Section 2.8.1.3).

2.8.1.2 *Small-scale proximity labelling*

Cells were treated according to the protocol published by Joeh et al (Joeh et al. 2020). In brief, DMEM containing either 25 – 200 nM of PXGal3; 100 nM PXGal3 with 100 mM Lactose; or with no additives, was incubated with cells, at 37°C, 5% CO₂ for 30 mins. Adherent cells were washed by discarding supernatant and replacing with PBS (-/-), repeated three times. For cells in suspension, centrifugation steps, performed for two minutes at 300 xg was required before each aspiration step.

After aspirating PBS, DMEM supplemented with 2% FBS and 500 µM of biotin tyramide (APExBIO, TX, USA) was added to cells before replacing them in the incubator for 30 mins. Whilst carefully agitating the liquid by swirling the plate, 100 mM of H₂O₂ was added to the solution for a final concentration of 1 mM, for one minute at room temperature. Quencher solution was prepared using 100 x stocks of sodium ascorbate (1M in water), sodium azide (1M in water), and Trolox (0.5 M in DMSO) diluted in PBS (-/-). Liquid was aspirated and replaced with quencher solution, repeated three times. For cells in suspension, centrifugation for two minutes at 300 xg was required before each aspiration step. From this point, HUVEC labelled *in situ* were prepared for immunofluorescence microscopy, using fluorescently conjugated

streptavidin (Section 2.5.6); and cells in suspension used flow cytometry validation of proximity labelling (Section 2.8.1.3).

2.8.1.3 *Validation of proximity labelling by flow cytometry*

Cells in 96-well U-bottom plates were centrifuged at 300 xg for 2 minutes, liquid was replaced with PBS (-/-), and cells were pelleted again. For cells that did not undergo prior proximity-labelling, 0-100 nM of rGal3 or PX-Gal3 in PBS (-/-) was incubated for 30 minutes, followed by centrifugation at 400 xg for two minutes, discarding the supernatant. Cells were washed by resuspending in PBS (-/-) and centrifuging for a further two minutes before discarding supernatant.

Cells were resuspended in PBS (-/-) containing either polyclonal anti-Gal-3 antibody (R&D Systems Cat#) followed by anti-goat PE conjugated secondary antibody or for cells having undergone proximity labelling, PE-conjugated streptavidin for 30 minutes in PBS (-/-) (**Table 3**). Each incubation was performed in the dark and on ice for 20 minutes, followed by centrifugation for two minutes at 300 xg, discarding liquid and replacing with PBS (-/-). For analysis of live/dead cells, Zombie Aqua (Biolegend. Cat #423101) in PBS (-/-) was added 1:1000 and incubated in the dark at room temperature for 15 minutes. Cells were washed twice, by centrifugating samples, discarding liquid and replacing with PBS (-/-). One final centrifugation step, followed by aspirating PBS was followed by resuspension of cell in 300 µl of PBS (-/-) for acquisition of data using the CyAn ADP flow cytometer (Beckman Coulter).

Cells were gated using scatter plots showing forward (FSC) and side scatter (SSC) linear and singlets identified through pulse width to FSC plot. Dead cells were detected

using the Violet Laser (405 nm). The flow cytometry results were analysed using FlowJo™ v7.6 Software (BD Life Sciences).

2.8.2 Proximity labelling HUVEC in-situ for enriched proteomics analysis

2.8.2.1 Proximity labelling of Galectin-3 interactors on live HUVEC

Cryopreserved pooled HUVEC (Promocell Cat: C-12203, Lot: 466Z022) were cultured according to the methods detailed in 2.3.3. All cell vials were recovered in pHUVEC media and grown to passage five before splitting across sixteen 15 cm tissue-culture dishes (Corning). The following day, HUVEC growth medium was replaced with 20 mL of pHUVEC (PenStrep [100 U/ml]) media +/- TNF α (10 ng/ml) and IFN γ (20 ng/ml). Following 24-hour treatment, medium was aspirated and replaced with PBS (-/-) to remove liquid. For each of the stimulated and unstimulated conditions, plates were allocated into the follow conditions for proximity labelling: triplicates of PXGal3 and PXGal3+Lac, and duplicated Neg background control.

The following experiment was performed at room temperature. HUVEC were incubated for 1 minute with 7 mL of DMEM containing either: (i) 75 nM of PXGAL3 for 'PXGal3'; (ii) 100 mM lactose with 75 nM PXGAL3 for 'PXGal3+Lac; or (iii) DMEM only for 'Neg' controls. Media was aspirated and HUVEC were washed three times with PBS (-/-). Biotin phenol was diluted 1:1000, to a final concentration of 500 μ m in 7 mL of 2% FBS in DMEM and added to each plate for 1 minute incubation. The plate was gently swirled whilst adding 70 μ L of 100 mM H₂O₂ for 1 minute. Liquid was aspirated from plates and replaced with 7 mL of Quencher solution, repeated three times, aspirating between each addition. On ice, cells were scraped in 4 mL quencher

solution and collected into 15 mL falcon tubes. Cells were centrifuged at 500 xg for 3 minutes at 4°C and washed by replacing the liquid with cold PBS (-/-) before repeat centrifugation and aspiration of the liquid. Cell pellets were frozen at -80°C until required for enriched proteomics preparation (Section 2.8.2.2).

2.8.2.2 Cell lysis and protein precipitation

Cell pellets were recovered in 300 µl of cold PBS (-/-) and lysed by two rounds of sonication using a Branson SFX250 sonicator as follows: 15 ms ON and 40 ms OFF Total ON time: 1 s Amplitude: 15%. Quantification of protein from lysates was performed (Section 2.5.2) and normalised to 1.6 mg/ml into 500 µL PBS (-/-) across all samples.

For protein precipitation, 2 mL of cold MS-grade methanol was added to each sample and placed at -20°C overnight. Tubes were centrifuged for 10 minutes at 4000 xg, 4°C to create a protein pellet. Liquid was aspirated and replaced with 2 mL of cold methanol, sonicating as described above to ensure complete resuspension. One final 10-minute centrifugation was performed at 4000 xg and the supernatant discarded.

2.8.2.3 Denature, reduce and alkylate proteins

Proteins were denatured by adding 500 µl of 6 M urea (Millipore) in PBS (-/-), and 10 µl of 10% (w/v) sodium dodecyl sulfate (SDS, Sigma-Aldrich, CAS no. 151-21-3) in PBS (-/-) directly to the protein pellet. A mixture of equal parts 200 mM tris(2-carboxyethyl)phosphine (TCEP, in PBS) and K₂CO₃ (600 mM in PBS [-/-]) was used to reduce disulphide bonds by adding 50 µl to the protein samples for 30 minutes at 37°C.

Protein alkylation was performed by adding 70 µl of 400 mM iodoacetamide in PBS (-/-) and incubated in the dark at room temperature for 30 minutes. To each sample, a further 130 µl of 10% SDS in PBS (-/-) was added and the sample was diluted with 5.5 mL of PBS (-/-).

2.8.2.4 Perform streptavidin enrichment and trypsinisation

Biotin-tagged proteins were enriched using streptavidin beads (Thermo Fisher. cat #20353). Using 100 µl/sample, beads were washed once in 10 mL PBS (-/-) and centrifuged for 2 minutes at 400 xg, before removing liquid. Beads were resuspended in 100 µl PBS (-/-) per sample and split equally between each sample, for 1.5 hours at room temperature on a rotating platform. Following incubation, beads were washed with 5 mL of each 0.2% SDS in PSB (-/-), PBS (-/-) and 100 mM triethylammonium bicarbonate (TEAB, pH 8.5, Thermo Fisher. cat #90114; in water), centrifuging at 400 xg for two minutes and discarding liquid between each wash. After this, each sample was resuspended in 500 µl of 100 mM TEAB and transferred to low-bind Eppendorfs. A further 500 µl TEAB was used to rinse the original tube and transferred to the low-bind Eppendorf (total 1 mL). Beads were pelleted by centrifugation (two minutes at 400 xg) and the supernatant removed. Sequencing-grade porcine trypsin (Promega) was prepared by reconstituting 20 µg vials in 2 mL of 100 mM TEAB with 20 µl 100 mM CaCl₂ in dH₂O, and 200 µl of this was added to each sample. Beads were incubated with trypsin at 37°C overnight on a shaking platform.

2.8.2.5 Perform TMT labelling

Digested peptides contained within the supernatant were transferred to a new low-bind Eppendorf following centrifugation of samples for 5 minutes at 400 xg. Beads

were washed with 100 μ l of 100 mM TEAB to remove any remaining peptides, centrifuged for 5 minutes at 400 xg, and the supernatant transferred to the harvested peptide mix (total ~300 μ l).

For 16-plex TMT labelling (TMT16Plex, Thermo Fisher. cat #90406) of peptides, samples were centrifuged for 5 minutes at 400 xg and ~200 μ l of supernatant containing the peptides of interest were each transferred to a new low-bind Eppendorf (Eppendorf LoBind, cat. no. 022431081). Beads were washed with 100 μ l of 100 mM TEAB, centrifuged again, and 100 μ l of supernatant transferred to the same low-bind Eppendorf (total ~300 μ l).

2.8.2.6 *Combine samples*

Optima LC/MS-grade acetonitrile (AcN; Fisher Scientific) was added to the sample peptides to a final concentration of 30%, before 100 μ l of this mix was added to the respective 16-plex unique TMT tag tube (Stored in 8 μ l aliquots at -80°C, Thermo Fisher. cat #A44521). Samples were mixed well before transferring back to the low-bind Eppendorf to ensure all complete tagging. Peptide mix was incubated with the TMT tag for 1 hour at room temperature. To quench the reaction, 6 μ l of 5% MS-grade hydroxylamine (Sigma-Aldrich) in water was added to each sample and incubated for 15 minutes. Four microliters of Optima LC/MS-grade formic acid (Fisher Scientific) was added to acidify each sample and dried to near completion in a vacuum-centrifuge (Savant Speedvac). TMT-tagged samples were combined by adding 200 μ l of 0.1% Trifluoroacetic acid solution (TFA, in water; Sigma-Aldrich) into one sample tube, vortexing and burst microcentrifugation (~5s), before transferring solution to the second sample tube. Repeat vortex, centrifuge and transfer until all samples have

been resuspended together. A further 100 µl of 0.1% TFA solution was added to the first tube to recover any remaining tagged peptides and transferred through the sixteen tubes as was done previously.

2.8.2.7 *Desalt sample*

To desalt the TMT-tagged peptide mix, C18 columns were first conditioned with one column volume (1 mL) of each of the following: 100% AcN; 80% AcN, 0.5% formic acid; 0.1% TFA before the sample was added to the column and the vacuum was applied ensuring the column did not dry out. The column was washed with 5 mL of 0.1% TFA solution, followed by 1 mL of 0.5% formic acid. All liquid was allowed to pass through the column before the vacuum was stopped and pressure was released. To elute the peptides, 500 µl of 40% AcN, 0.5% formic acid solution was applied to the column using a pipette to form pressure within the column to force the elution through the column and into a new low-bind Eppendorf. A second elution with 500 µl of 80% AcN, 0.5% formic acid was performed and collected in the same Eppendorf. Samples were spun one final time in the vacuum centrifuge until dry, and frozen at -80°C before handing over to the Scripps Mass Spectrometry Core Facility for sample injection.

2.8.2.8 *Mass-spectrometry proteomics data analysis*

Processing of the mass-spectrometry proteomics data was done as described in (Joeh et al. 2021), using Proteome Discoverer 2.4 software (Thermo Fisher) and peptide sequences determined by matching protein databases of *Homo sapiens* with fragmentation patterns using SEQUEST HT algorithm, specifying TMT-tags modifications. All keratins were removed, and the dataset was filtered for unique

peptides ≥ 2 . Any samples returning missing values within one of the replicate samples were replaced with the value of '1' for further analysis. The raw TMT abundance values were averaged between the triplicates and transformed to their \log_2 values. Multiple t-tests with unpaired experimental design were performed on the data, with significance determined as $P < 0.05$. The ratio of PX-Gal3 to Neg were taken as 'Enrichment' and filtered >10 to determine enriched proteins. The arbitrary cutoff for 'Competition' was decided as proteins with a ratio >4 between PX-Gal3 and PX-Gal-3+Lac. Correlation between enriched and competed proteins were compared. Proteins were compared between the $\text{TNF}\alpha + \text{INF}\gamma$ treated and untreated HUVEC by finding the ratio of the two and filtered from highest to lowest.

2.8.3 Glycomics

2.8.3.1 Sample preparation

Cryopreserved HUVEC were seeded into six 10 cm tissue-culture dishes (Corning) in pHUVEC growth medium (Section 2.3.4). Upon reaching 90% confluency, HUVEC medium was replaced for cytokine stimulation in 10 mL treatment medium, with or without $\text{TNF}\alpha + \text{INF}\gamma$ in pHUVEC medium. Triplicate samples were prepared for both treated and untreated control.

After 24-hour stimulation, medium was aspirated and HUVEC were washed once with PBS (-/-) before harvesting cells into 15 mL Falcon tube using a cell scraper. HUVEC were pelleted by 4°C centrifugation at 800 xg for 5 minutes. Cell pellets were washed four times by aspirating liquid, resuspending cells in cold PBS (-/-) and centrifuging the cell suspension.

2.8.3.2 *Isolation and purification of N-glycans for glycomics analysis*

To remove cell surface peptides, 500 µl of 2.5 mg/ml trypsin (diluted in PBS [-/-]) was added to each sample and transferred to a microcentrifuge tube. Trypsin was also added to an empty tube to provide a control for background glycan contamination in the porcine-derived trypsin. After shaking incubation for 15 minutes at 37°C, 150 rpm, cells were centrifuged at 14,000 xg for 15 minutes at 4°C, and the supernatant was transferred to a new microcentrifuge tube. Trypsin was heat-inactivated for 5 minutes at 100°C. After cooling on ice, 2 µl of PNGase F (Recombinantly expressed by T. O'Leary at Scripps Research Institute) was added to each sample and the control tube for digestion of N-glycans overnight shaking at 180 rpm at 37 °C.

Samples were acidified to a final concentration of 5% acetic acid (AcOH) for column purification. C-18 columns (Pierce, Thermo Scientific, cat. no. 89873) were conditioned before use, using one column volume (3 mL) of each of the following: 100% MeOH; 5% AcOH; 100% isopropanol; and 5% AcOH. The sample was then applied to the column and the flow-through collected into a clean tube, before adding 2 mL 5% AcOH. A hole was punched through the lid of the tube before being placed at -80°C for 30 minutes and performing lyophilisation overnight.

To prevent the separation of anomeric forms of glycans during mass spectrometry, N-glycans were reduced using 250 µl of 10 mg/ml sodium borohydride in 1 M ammonium hydroxide at 60 °C for one hour. Samples were purified using a G10 column, conditioned with 12 mL water. The sample (~250 µl) was applied to the column followed by 350 µl of water. A clean Eppendorf was placed underneath the column to collect the flow-through after adding 600 µl of water to the column. The sample was frozen and lyophilised overnight as described above.

For permethylation, a NaOH/DMSO gel prepared by Tim O’Leary was used. Glycomics samples were dissolved in 200 µL DMSO and vortexed for 15 minutes. After adding 350 µL of the NaOH/DMSO gel, glycans were vortexed for an additional 10 minutes. Iodomethane (100 µL) was added to the samples to permethylate glycans for 10 minutes. Samples were then transferred to a glass vial containing 1 mL of water.

After nitrogen bubbling to remove iodomethane, dichloromethane (2mL) was added, causing separation of the sample into layers. The water layer from the top of the sample was removed and the remaining organic layer was washed three times in water, each time using nitrogen bubbling to dry the samples. Finally, acetonitrile (75 µL) was used to rinse the vial wall before samples were frozen at -80°C and lyophilized overnight. Samples were re-dissolved in 8:2 water/acetonitrile (20 µL) and injected into LTQ XL ion trap Mass Spectrometer (Thermo Fisher).

2.8.3.3 Mass-spectrometry glycomics analysis

Data was processed using XCalibur 2.1 (Thermo Scientific). Relative proportions of N-glycans were calculated using the area of the extracted ion chromatogram (EIC) for all adducts and charge states for a particular glycan. Glycan compositions and structures were identified using GlycoWorkbench (Ceroni et al. 2008).

2.8.4 In silico modelling of PXGal-3 interactions

2.8.4.1 Retrieval of target and template protein sequences

The primary amino acid sequences of the following proteins: human CD38 (entry identifier: P28907); human CADM3 (entry identifier: Q8N126); human TLR2 (entry identifier: O60603); and human MMRN2 (entry identifier: Q9H8L6) were downloaded from the UniProt database in FASTA format.

2.8.5 Utilising ColabFold to model PXGal3-protein interactions

ColabFold is an initiative from Google Colab and AlphaFold2 for use in protein structure prediction using deep learning system developed by DeepMind (Jumper et al. 2021). ColabFold was used in the prediction of PXGal-3 folding and in modelling interactions with either CD38, TLR2 or MMRN2. Molecular graphics and analyses were performed using ChimeraX (Meng et al. 2023).

2.8.6 Direct ELISA for Gal-3 binding to recombinant CD38 and MMRN2

Recombinant CD38 (Sino Biologicals, 10818-H08H) or MMRN2-6xHis (The Protein Expression Facility, University of Birmingham, using HEK293T expression system) was prepared in PBS (+/+) at 3 µg/ml, and 100 µl was added to wells within LUMITRAC medium-binding microplates (Nunc, GN655075), and stored overnight at 4°C. The next morning, solution was aspirated, and wells washed four times, each wash consisting of adding 300 µl PBST ([+/+] 0.1% tween) followed by aspiration. To block the plate, 300 µl of 1% BSA in PBST was added to the well for 2 hr at room temperature with rocking. Blocking solution was aspirated and each well washed four times as previously described. Either PX-Gal3 or rGal-3 protein was prepared in 1% BSA in PBS (+/+) at concentrations 0 - 3000 nM, +/- 100 mM sucrose or lactose in 200 µl and added to each well for 1 hour at room temperature. Liquid was aspirated and wells washed four times as previously described. Anti-Gal-3 (R&D) antibody was diluted 1:1000 in PBS (+/+) and 100 µl added per well for 1 hour incubation, followed by aspiration and four washes with PBST. Peroxidase-conjugated anti-goat secondary IgG was prepared in 1% BSA in PBS (+/+) at a final dilution of 1:1000, before adding 100 µl to each well for one hour at room temperature before repeating aspiration and wash steps. Finally, 100 µl of TMB was added to each well and left until blue colour

appeared stable (1-30 minutes), before adding 100 µl of stop solution per well, causing a shift in colour from blue to yellow. The absorbance was measured at 450 nm and corrected using 540 nm or 570 nm wavelength reading.

For determination of EC₅₀ values, all data points were transformed using GraphPad Prism, to the log of dose/concentration (nM). The “Nonlinear regression (curve fit)” function was used to determine “log(agonist) versus response—Variable slope (four parameters)” for EC₅₀.

2.8.7 Co-Immunoprecipitation of PX-Gal3 interactors

Reagents including Hek293 cells, full-length MMRN2 (MMRN2-FL), truncated His-tagged MMRN2 (Trunc MMRN2) and empty vector were kindly provided by A Baber (Institute of Cardiovascular Science, University of Birmingham). HEK293 cells were seeded at 1×10^6 cells in 6 cm TC-coated dishes (Corning) in 10 mL of 5% FBS in DMEM and cultured overnight at 37 °C and 5% CO₂ the day before transfection. Transfections were performed using 3 µg of either vector, diluted in 300 µl OptiMEM and 12 µl polyethylenimine (PEI) for 10 minutes before adding to the cells and mixing by gentle rocking of the plate back and forth and returning cells to the incubator.

After overnight incubation, cell supernatants were discarded and cells washed with 3 mL of PBS (-/-). The PBS was aspirated and replaced with 1 mL of fresh PBS (-/-) and cells harvested into an Eppendorf by using a cell scraper to detach cells from the plate. Cells were centrifuged for 2 minutes at 5,000 rpm. Supernatant was discarded and the cell pellet was thoroughly resuspended in 300 µl of NP40 lysis buffer (1:1 NP40 in dH₂O, 1 X protease inhibitor and 1 X phosphatase inhibitor) and left on ice for 15 minutes. The lysed cells were centrifuged for 15 minutes at full speed, before the

supernatants were collected into clean Eppendorf's ready for co-immunoprecipitation (co-IP). Equal volumes of IP binding buffer (50 mM Tris pH 8, 20 mM KCl, 1mg/mL BSA 2.5% (v/v) Glycerol, 14mM 2-Mercaptoethanol, 1% protease inhibitor and 1x phosphatase inhibitor) were added to the cell lysates. For whole cell lysate controls, 20 µl was collected and mixed with equal volumes of 2x sample buffer (50 mM Tris Ph 6.8, 10% β-ME, 2% SDS, 2 mg Bromophenol blue stock, 10% glycerol made up in dH₂O to 20 mL total volume) were added to the whole cell lysate control and the rest of the lysate was split equally between two new tubes. To MMRN2-FL transfected cells, 1 ug of PX-Gal3 +/- 25 nM lactose was added; or to Trunc MMRN2-transfected cell lysates, 1 ug of rGal-3 (Peprotech) +/- 25 nM of lactose was added and incubated overnight with rotation.

Immunoprecipitations were performed using 25 µl nickel beads per samples, which were first washed with PBS (-/-), before incubating with samples for 1.5 hours. Samples were centrifuged for four minutes at 10,000 rpm, the liquid discarded and replaced with IP wash buffer (100 mM Tris pH 7.5, 200 mM NaCl and 0.5% v/v NP40), repeated four times to remove unbound proteins. After the final wash, 60 µl of 2x sample buffer was added to the beads ready for running SDS-Page gel (Section 2.5.3) and Western blot.

Table 4: Co-immunoprecipitation conditions for analysis of Gal-3-MMRN2 interactions

Expression vector	Pull-down	Bead capture
MMRN2	PX-Gal3 +/- Lactose	Nickel
Empty vector	PXGal-3 +/- Lactose	Nickel
MMRN2-His	rGal-3 +/- Lactose	Nickel
Empty vector	rGal-3 +/- Lactose	Nickel

2.9 Mice used for experimental studies

Global Gal-3^{-/-}, Gal-9^{-/-} and Gal-3/Gal-9^{-/-} knockout mice were on a homogenous C57BL/6 background. In all experiments age and sex-matched controls (wildtype (WT) C57BL/6) were purchased from Charles River.

2.9.1 Complete blood count analysis

For basal blood count analysis, samples were collected by exsanguination from mice anaesthetised using 4% isoflurane in 100% O₂. For post-IVM analysis, blood was collected from the inferior vena cava (IVC). Blood was diluted 1:9 with acid citrate dextrose anticoagulant (ACD, 100 mL made using citric acid monohydrate 0.8 g; dextrose monohydrate 2.45 g; sodium citrate dihydrate 2.2 g; in water. Complete blood counting (CBC) was carried out using the Pentra ES 60 automated haematology analyser (HORIBA ABX SAS).

2.10 Intravital Microscopy (IVM) Based Studies

2.10.1 Cytokine-induced Inflammation

To assess the role of galectins in the inflammatory response, mice were given intrascrotal (I.S) injection of either TNF α (500 ng) or IL-1 β (50 ng) in a total volume of 200 μ l PBS (-/-), two hours prior to surgery and between four and six hours before imaging post-capillary venules in the cremaster (Section 2.10) (**Figure 6**). These

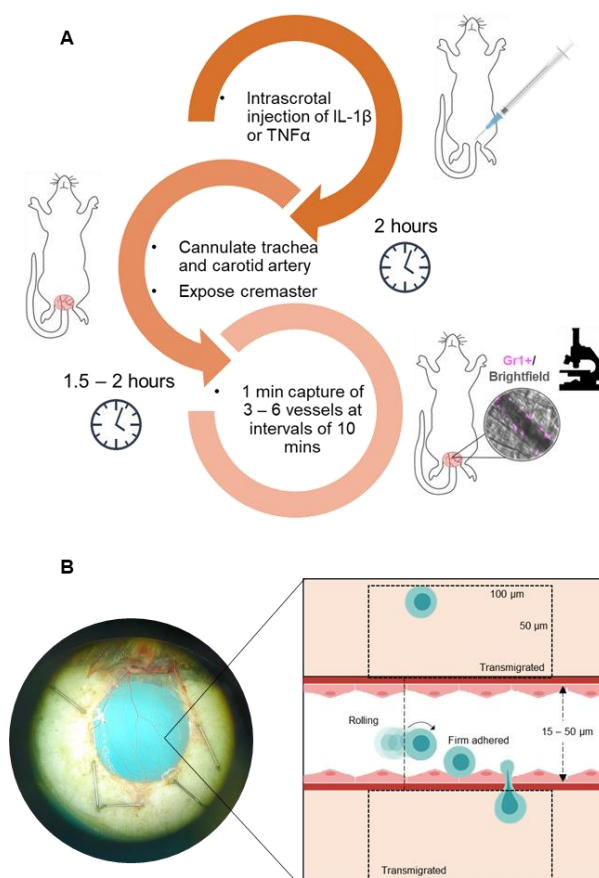


Figure 6 (A-B): Intravital microscopy was used to investigate leukocyte trafficking events in vivo.

(A) Mice received 200 μ l intrascrotal injections of either 50 ng IL-1 β or 500 ng TNF α in PBS two hours prior to surgery. Following anaesthesia of the mice, the trachea was exposed and cannulated to ensure maintained breathing before the carotid artery was cannulated for delivery of fluorescently labelled antibodies to detect Gr1+ cells. An incision was made in the scrotum to expose the testicle. (B) The cremaster muscle was cauterised straight down the middle and spread flat across the transparent viewing platform and held taut using sterile staples pinning the cremaster to the sponge board. After a 30-minute resting period, 3–6 blood vessels each of 15–50 μ m in diameter were selected and recorded for 1-minute for analysis of Gr1+ cells using fluorescence, and unlabelled leukocytes by brightfield imaging. Analysis of rolling flux, firm adhesion (>30 s) and transmigration was performed within 100 μ m lengths of each vessel.

conditions were decided based on previously reported protocols (Woodfin et al. 2009; Gittens et al. 2017).

2.10.2 Pre-surgical Preparation

All equipment to be used during surgical procedures were sterilised either by autoclaving (e.g. surgical instruments), or by disinfecting with Sterillium (e.g. downdraft surgical table, imaging stage). The surgical board was pre-heated to 39°C prior to surgery and covered with a surgical drape. An induction dose of ketamine/medetomidine (Ket/Med) (10 µl/g body weight) was administered to the mouse via intraperitoneal (I.P) injection, followed by confirmation of complete anaesthesia by pedal reflex. Maintenance anaesthesia was delivered in 50 µl doses by I.P when necessary. Prior to surgery, hair was removed from the operating areas using Veet hair removal cream, and the underlying skin was disinfected using Sterillium. With the mouse on its back, a small piece of surgical thread was hooked around the front two teeth and taped back to the surgical board to keep the neck exposed. Forelimbs were spread and taped apart to expose the cervical area. Installation of a tracheal tube was necessary to ensure proper ventilation during surgery and imaging. This was performed by exposing the area of trachea in the cervical region of the mouse and making a small incision in the annular ligament between two cartilage rings of the trachea. A small metal tracheal cannulae was inserted into the hole and secured in place using a double knotted suture.

Following insertion of the tracheal cannula, the left carotid artery was exposed and separated from the vagus nerve. A knotted suture was placed onto the carotid artery at the end closest to the head of the animal, and a microvascular clamp was placed as far back on the artery as possible to restrict blood flow. A small incision was made

in the artery before insertion of a cannula attached to a 1 ml syringe of PBS (-/-) required for injection of maintenance fluids and fluorescently labelled antibodies. The cannula was held securely in place using a double knotted suture (Kunkel and Ley 1996).

2.10.3 Exteriorisation of Cremaster Muscle

The cremaster muscle was used to observe leukocyte trafficking events *in vivo* (Kunkel and Ley 1996). To prepare for this, the mouse was moved from the surgical preparation mat and onto an imaging stage, comprised of a raised Perspex cylinder with a sponge ring around a permanently fixed glass coverslip where the mouse's hind legs were taped apart and against the raised cylinder. PBS (+/+) was placed onto the imaging window and on to the scrotum before a small cut was made at the distal end of the scrotum. Using forceps, the cremaster muscle was exteriorised and pinned onto the sponge board using needles bent into a 2-pronged shape. To prevent the cremaster muscle from drying, PBS (+/+) was applied throughout the preparation. The skin surrounding the cremaster was gently pulled away and excess fatty tissue was cleared using forceps. The cremaster muscle was cauterized down the middle, spread flat against the viewing stage and held firmly in place with sterile staples into the sponge ring. Finally, the tissue and vessel connecting the testes to the cremaster was cauterized to separate the two, and the testes were pushed back into the scrotum. The viewing stage was moved to the Zeiss Axio Upright Confocal microscope set up with a water immersion lens to allow for continuous superfusion with warmed PBS (+/+). A 30-minute stabilisation period was initiated prior to capturing images or videos, in which the delivery of fluorescent antibodies (PE conjugate anti-mouse Ly-6G/Ly-6C

[Gr-1], Clone: RB6-8C5, Bio-Rad; and APC anti-mouse CD3 Antibody, Clone: 17A2, Biolegend) via the I.V cannula was performed.

Post-capillary venules with a diameter between 16 – 50 μm were selected and imaged using brightfield and fluorescence acquisition on the Zeiss Axio Upright Confocal microscope fitted with a 40 X objective lens. All videos were captured using Slidebook software from Intelligent Imaging TTL and analysed with SlideBook Reader and Fiji software (Schindelin et al. 2012).

2.10.4 Analysis of IVM Images and Recordings

Leukocyte rolling flux, firm adhesion and transmigration were measured in 100 μm segments taken from recordings of 3-6 vessels per mouse, from 7-9 mice per group (Kunkel and Ley 1996).

Cell flux was analysed by counting cells that pass a perpendicular line drawn through the vessel within the 60 second capture. Firm adhered cells were defined as cells remaining stationary on the vessel wall for more than 30 seconds per recording, and transmigrated cells as those within the area 100 μm length by 50 μm width, on both sides of the vessel (**Figure 6**).

2.11 Statistical analysis

GraphPad Prism software (GraphPad Software) was used for all statistical analysis. Normal distribution was tested using Shapiro-Wilk test. Analysis of differences between two groups were performed by t-test. For comparison of two or more groups, one- and two-way Analysis of variance (ANOVA) with appropriate post hoc testing were performed. For data which was not normally distributed, a Kruskal-Wallis test was performed. Correlation analysis was performed using Spearman's rank correlation coefficient. A p value ≤ 0.05 was considered significant.

CHAPTER 3: CHARACTERISING THE REGULATORS OF ENDOGENOUS ENDOTHELIAL GALECTIN EXPRESSION

3.1 Introduction

The endothelium is a crucial component in immune regulation and maintaining homeostasis. Dysfunctional endothelium has been linked to pathogenesis of inflammatory diseases, including atherosclerosis, diabetes, and rheumatoid arthritis (Gimbrone and Garcia-Cardena 2016; Hadi and Suwaidi 2007; Yang, Chang, and Wei 2016). In these instances, the endothelium's response to microenvironmental changes is controlled by physical, mechanical, and biochemical mechanisms which become dysregulated in disease.

Mechanotransduction, the process by which cells convert mechanical stimuli into biochemical signals, allows endothelial cells to adapt to changing microenvironments. For instance, endothelial cells lining arteries and veins respond differently to shear stress, reflecting their distinct roles. Low shear stress in veins facilitates leukocyte trafficking, while high shear stress in arteries promotes oxygen delivery and can be characterised by greater expression of adhesion molecules such as *ICAM1* and *VCAM1*, and *KLF2* and *NOS3* genes in the low and high shear environments, respectively (Chien 2007; Harrison et al. 2006; Huang et al. 2023). Unpublished microarray expression profiling results from departmental colleagues; S. Durant, H.M.McGettrick and R. Bicknell, showed that *LGALS9* and *LGALS8* are both upregulated in HUVEC cultured for 24 hours under 1.5 Pa (15 dynes/cm²) laminar shear stress, whilst *LGALS1* transcription was downregulated compared to static control [methods detailed in (Wragg et al. 2014)]. This prompted our investigation into the shear regulation of endothelial galectins in this chapter.

Endothelial cells express galectin-1, -3, -8 and -9 under basal conditions (Thijssen, Hulsmans, and Griffioen 2008). Research from our lab reports that *LGALS9*

transcription is upregulated in HUVEC in response to pro-inflammatory mediators including Poly:IC and TNF α + IFN γ (Krautter et al. 2022). There is limited data on the regulators of galectin-1, -3 and -8 expression in HUVEC, and no reports on the shear regulation of galectins have been published to date. As such, within this chapter we aimed to investigate regulators of endothelial galectin expression, with a particular focus on exploring shear regulation and responses to pro-inflammatory mediators. We next combined the two themes through the study of galectin expression in liver sinusoidal endothelial cells (LSEC) in normal and diseased liver sections, which are exposed to low shear stress and undefined inflammatory cytokines *in situ*.

3.2 Shear regulation of endothelial galectins

3.2.1 *Orbital shaking culture of endothelial cells upregulates galectin transcription in vitro.*

To validate the results identified in public RNA sequencing and microarray datasets, we cultured both HUVEC and HAEC under orbital shaking conditions of 125 rpm for either 24 or 72 hours and looked at changes in galectin expression by qPCR, ELISA and immunofluorescence. Within shaking cultures, cells are exposed to ‘atheroprotective’ laminar flow in the periphery of the well, whilst the cells at the centre are subject to ‘atherogenic’, disturbed and multidirectional patterns of flow (**Figure 7A**). HUVEC cultured for 24 and 72 hours under orbital shaking conditions had increased *LGALS3* and *LGALS9* transcription compared to static control (**Figure 7B**). This finding was consistent with the upregulation of *KLF2*, a shear regulated control gene, under the same conditions (**Figure 7B**). Both *LGALS3* and *LGALS9* were similarly upregulated in HAEC following 24- and 72-hour culture with orbital shaking (**Figure 7C**). Notably, *LGALS1* transcription was significantly downregulated in response to 72 hours of orbital shaking culture in HAEC only, and not in the HUVEC (**Figure 7B & C**). We observed no changes in *LGALS8* transcription in the orbital shaking compared to static culture. Due to the comparable trends observed between HUVEC and HAEC, we opted to continue using only HUVEC throughout our studies, as we were able to access them more readily through our collaborative partnership with Sandwell and West Birmingham Hospitals. In addition to this, it was reported that differentially expressed genes (DEGs) were most prominent when comparing P0 cells to both the early and late passaged HUVEC (P2-3 and P7-8, respectively), suggesting

that any *ex vivo* culture and/or expanding of the cells has a significant effect on the HUVEC transcriptional responses to environmental changes.

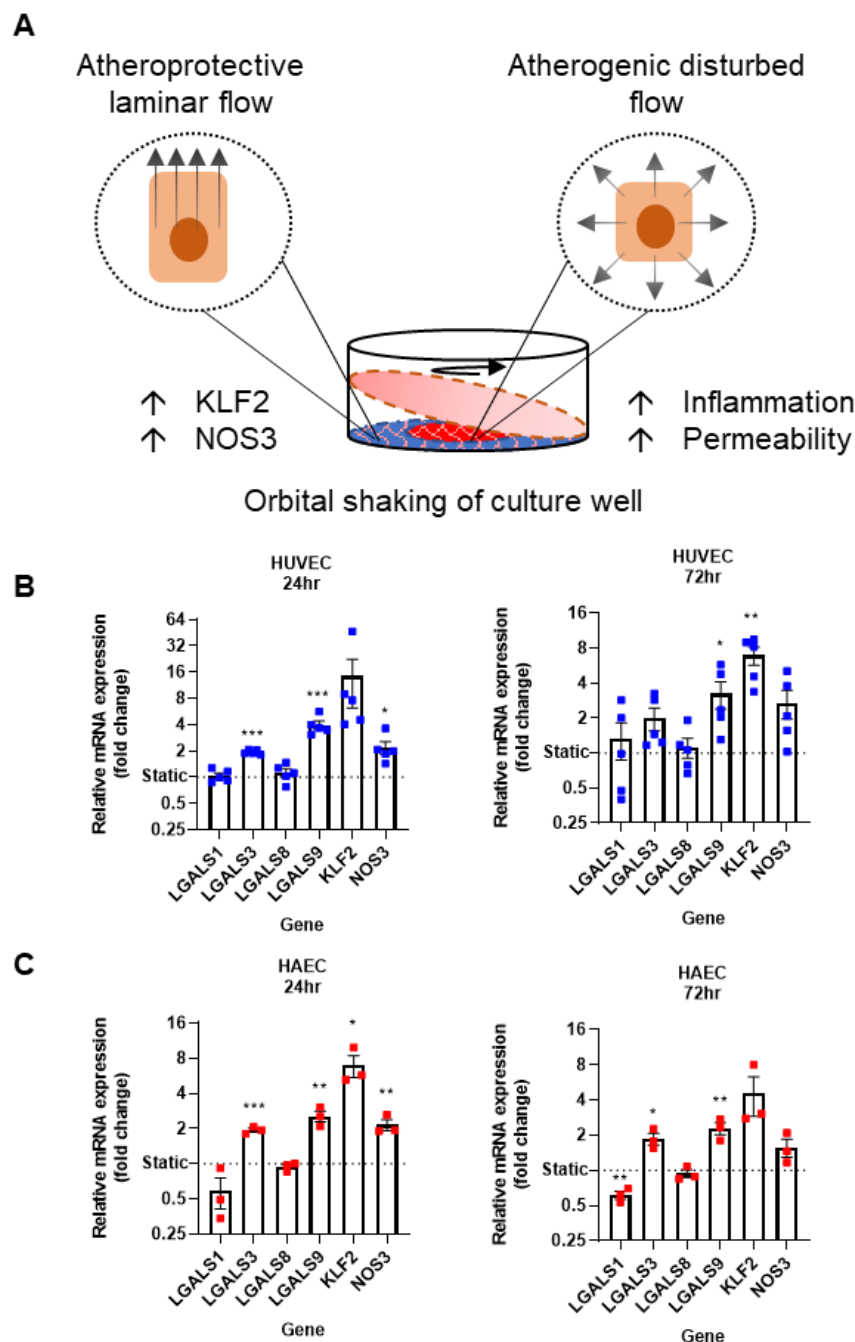


Figure 7: Endogenous endothelial galectin-3 and -9 expression is shear regulated.

(A) Endothelial cells grown under orbital shaking conditions (125 rpm) exposes the cells to both atheroprotective laminar and atherogenic disturbed shear stress. (B) Human umbilical vein endothelial cells (HUVEC) and (C) human aortic endothelial cells (HAEC) show increased galectin-3 (*LGALS3*) and galectin-9 (*LGALS9*) transcription following culture for 24 and 72 hours with orbital shaking compared to static control. Statistical analysis was performed for each gene, against static control, using unpaired t-test of orbital shaking and static control groups. Data are presented mean \pm SEM (biological repeats HUVEC $n=5$, HAEC $n=3$). p -value < 0.05 (*), < 0.01 (**), < 0.001 (***).

Our results show that culturing HUVEC with orbital shaking conditions modulates *LGALS3* and *LGALS9* gene transcription through overexpression. We determined *LGALS8* to be unaffected by shaking culture, whilst *LGALS1* transcription was downregulated only in the HAEC after 72 hours culture with orbital shaking (**Figure 7B & C**). Overall, these results suggest that endothelial galectin transcription is regulated by shear stress. Subsequently, we sought to determine whether the changes in transcription induced by orbital shaking culture were also reflected in protein expression levels.

We used ELISAs to measure the amount of soluble Gal-3 and -9 in the supernatants of HUVEC cultured with orbital shaking conditions compared to static. We saw greater amounts of both Gal-3 (**Figure 8A**), and Gal-9 (**Figure 8B**) in the supernatants at 72 hours compared to 24 hours. On comparing the effects of orbital shaking culture to static control, we saw that levels of Gal-3 were reduced at both timepoints, and that this reduction was statistically significant after 72 hours of orbital shaking culture (**Figure 8A**). Soluble Gal-9 was detected in all culture conditions, though not to the same extent as expected based on the qPCR data showing that *LGALS9* transcription is increased 2-fold following orbital shaking culture, compared to static control (**Figure 7**). The discrepancy between the fold-differences observed between static and shaking culture in the qPCR and ELISA data might be due to protein expression being restricted to within the cell, on the cell membrane, or within extracellular vesicles, making them undetectable via ELISA (Bänfer and Jacob 2020).

No significant differences in the concentration of soluble Gal-9 was observed between the culture conditions or between the hours spent in culture (**Figure 8B**). Overall, we saw greater amounts of Gal-9 than Gal-3 in HUVEC supernatants, although the concentrations only ranged 1-4 ng/ml (**Figure 8**). This is relatively low, at least compared to levels of Gal-9 in supernatant following HUVEC stimulation with TNF α and IFN γ , which increased to 10 ng/ml after 24 hr (Krautter et al. 2022). The general trend in this data suggests that expression and secretion of Gal-3 and Gal-9 is maintained over time, in-line with upregulated transcription. Due to the heterogeneity and complexity of shear rates and patterns within the wells of culture plates undergoing orbital shaking, we are unable to draw firm conclusions on the specific shear regulation of galectins from qPCR and ELISA alone. Instead, we sought to use immunofluorescence microscopy to quantify the mean fluorescence intensity of

galectin expression at specific regions of the well that have previously been mapped for their shear stress values (Velasco et al. 2016).

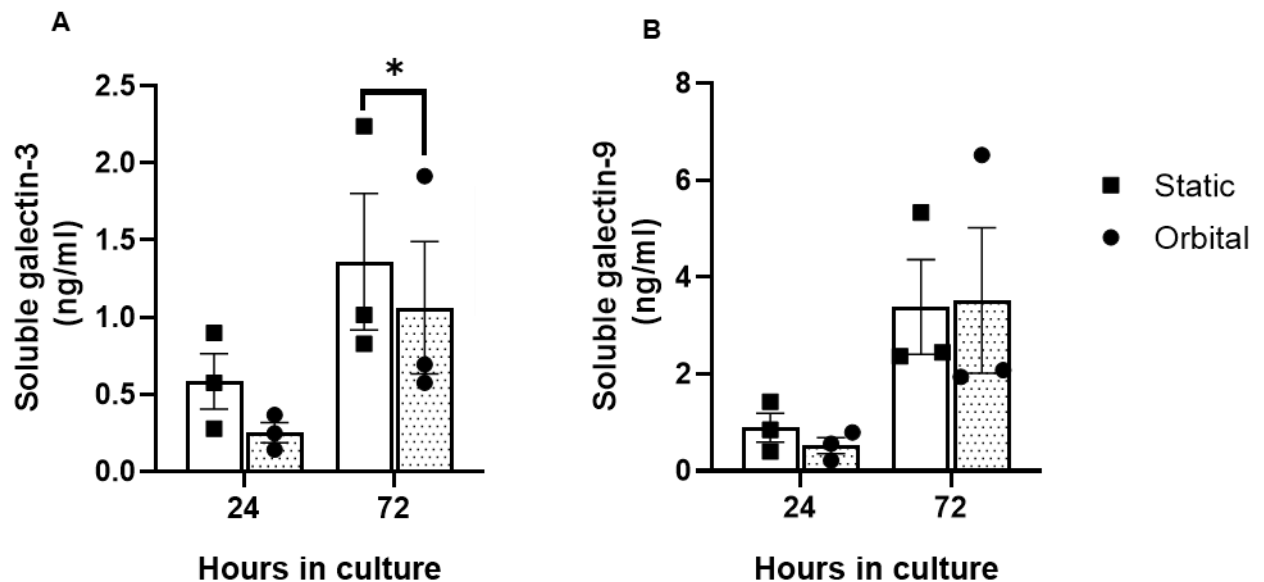


Figure 8: Concentration of soluble galectin decreases following culture with orbital shaking.

HUVEC were cultured for 24 and 72 hours under orbital shaking conditions (125 rpm). The concentration of (A) soluble galectin-3 and (B) galectin-9 in the supernatants was measured by ELISA. A two-way ANOVA was conducted to test the effects of culturing HUVEC under orbital shaking and time in culture on the expression of soluble galectin-3 (A) and galectin-9 (B), as detected by ELISA. The effect of culturing HUVEC under orbital shaking was significant on Gal-3 expression ($p < 0.05$) but not Gal-9. Post-hoc comparison using Tukey's test revealed that there was a significant reduction in soluble Gal-3 in the supernatants of HUVEC grown under orbital shaking conditions compared to static control (p -value < 0.05 (*). Data are presented mean \pm SEM (biological repeats $n=3$).

Since we aimed to detect proteins either within or on the cell surface of HUVEC, and not the secreted proteins, we chose to perform immunofluorescence microscopy on cells following 24 hours of culture. We opted to perform immunofluorescence staining on HUVEC after 24 hours in orbital or static culture, since we observed both gene transcription to be upregulated, as well as secreted protein at this timepoint. To do this, the relative mean fluorescence intensity from images taken across 10 – 14 positions within each well and biological replicate, was compared between orbital

shaking and static control. We observed that the average relative mean fluorescence of Gal-3 (**Figure 9A**) and Gal-9 (**Figure 9B**) expression was greater in HUVEC cultured under orbital shaking conditions compared to static control. This observed difference was only significant for galectin-9 immunofluorescence (**Figure 9B**).

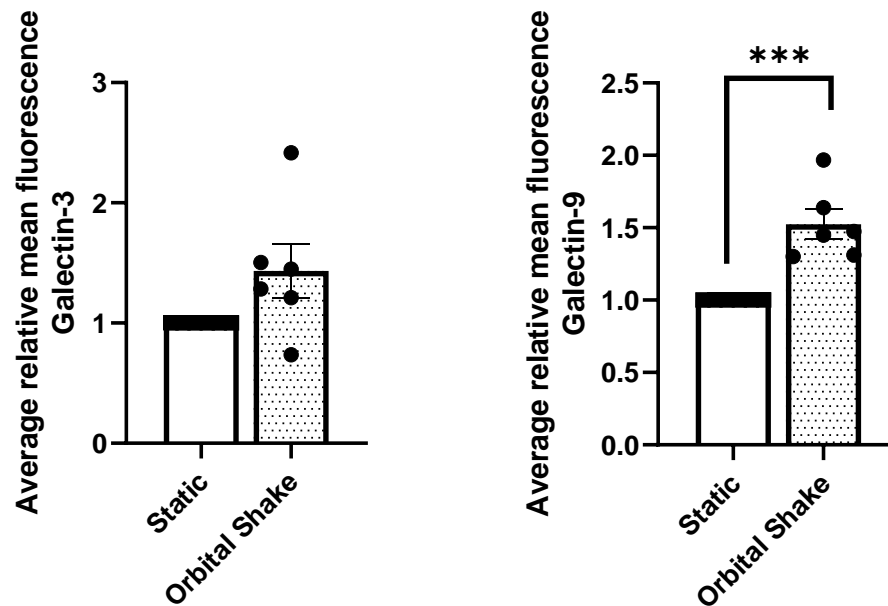


Figure 9: Immunofluorescence staining of HUVEC grown in culture with orbital shaking show greater levels of galectin-3 and -9 positive staining.

Galectin-3 and -9 expression was measured by immunofluorescence staining in HUVEC cultured for 24 hours with 125 rpm of orbital shaking. Greater mean fluorescence in Gal-3 and Gal-9 probed cells above isotype control, was observed in orbital shaking culture conditions relative to static control. Images were taken at 10 – 14 locations within tissue culture wells and the relative mean fluorescence from all locations within each well was then averaged to represent one biological replicate. Statistical analysis was performed using unpaired t-tests. Data are presented mean \pm SEM (biological repeats n=6). p-value \leq 0.01 (**).

To investigate whether specific regions within the well exhibited greater galectin-positive staining, we divided images based on their location within the periphery or centre of the wells, which correspond to laminar high-shear stress (periphery) and disturbed lower-shear stress zones (centre), respectively, as established and reported elsewhere **(Figure 10A)** (Velasco et al. 2016). Although our findings were not significant by statistical testing, we saw more even Gal-3 positive staining in all areas of the well relative to static control images **(Figure 10B)**. For Gal-9 staining we observed greater average relative mean fluorescence in the periphery of the well **(Figure 10C)**. These data might suggest that Gal-3 is bound onto the surface of the HUVEC, since the conditioned medium will contact all areas of the well through shaking culture. Meanwhile, greater fluorescence of Gal-9 in the periphery of wells undergoing shaking culture suggests intracellular expression of Gal-9 is regulated by laminar shear stress. Thus, specific conditions of shear stress are responsible for the up- and down- regulation of galectin-3 and -9 expression in HUVEC compared to static culture.

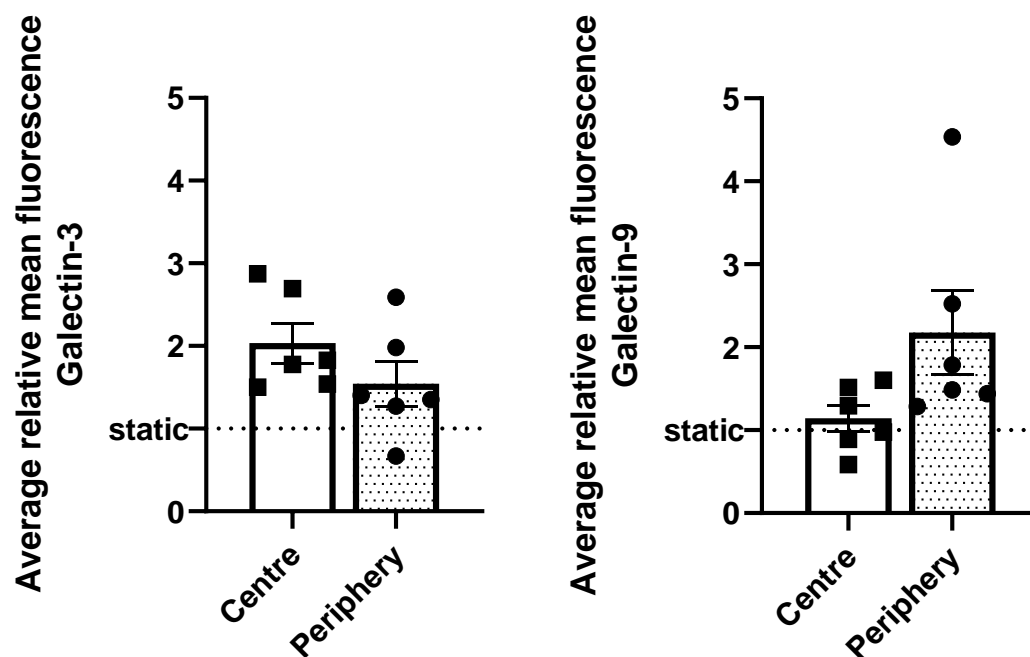


Figure 10: Immunofluorescence staining of HUVEC cultured under static conditions and 125 rpm orbital shaking show differential galectin-3 and -9 expression depending on shear stress.

(A) Ten to fourteen images were taken across each well, distinguishing between regions of high laminar shear stress (periphery) and disturbed and lower shear stress (centre), as mapped and reported in (Velasco et al. 2016). Galectin-3 and -9 expression was quantified by averaging the mean fluorescence of images taken from the periphery and centre of each well from the orbital shaking conditions relative to static control. Statistical analysis was performed using unpaired t-tests. Data are presented mean \pm SEM (biological repeats n=6).

Overall, our results presented within this section suggests that transcription and subsequent expression of galectins, namely Gal-3 and Gal-9 from endothelial cells is regulated by shear stress. The heterogeneity of flow rates and patterns inflicted on cells within the orbital shaking model does not allow us to draw firm conclusions on the specific shear regulation taking place. Instead, we used the Ibidi Pump System as a more robust model that allows us to define shear stress rates, mimicking physiological conditions including continuous unidirectional and oscillating patterns of flow to understand the shear regulation of galectins.

3.2.2 Investigating defined and complex shear stress patterns on galectin transcription in HUVEC using the ibidi culture system.

To better understand which flow rates and/or flow patterns are regulating galectin-3 and -9 expression *in vitro*, we cultured HUVEC under either high (2 Pa) or low (0.05 Pa) shear stress using the Ibidi pump culture system. We looked at changes in gene transcription of galectins and control genes by qPCR, relative to static control over 4 – 48 hours. The difference in relative transcription of *LGALS1* (**Figure 11A**), *LGALS3* (**Figure 11B**) and *LGALS8* (**Figure 11C**) between the two shear stress rates and to static control was not significant across any of the timepoints in culture. Despite this, we observed an increase in the relative expression of *LGALS3*, by ~1.5 fold at the 24- and 48-hour time points in HUVEC cultured under 2 Pa laminar flow compared to static control (**Figure 11B**). Transcription of *LGALS9* was statistically lower in HUVEC after 48-hour culture with low shear stress compared to static control (**Figure 11D**). Our shear-regulated control genes, *CLEC14A* (**Figure 11E**) and *KLF2* (**Figure 11F**) were significantly down- and upregulated, respectively, following four hours of culture with high shear stress compared to static control (Wu et al. 2022). Previous reports have

shown that *CLEC14A* expression is reduced by ~90% after 24 hours in HUVEC cultured with 2 Pa of shear stress compared to static control (Mura et al. 2012b). Meanwhile, we observed a reduction of only ~50% in *CLEC14A* transcription which was consistent across all timepoints (**Figure 11E**). We also observed a significant difference in the expression of *CLEC14A* between 2 Pa and 0.05 Pa experiments at the 12-hour timepoint only (**Figure 11E, denoted by #**). Compared to the results obtained using the orbital shaking model, we observed a more reserved difference in the fold change in galectin gene responses, for which we saw very few changes in the relative transcription of in HUVEC cultured at both 2 Pa and 0.05 Pa over time. Since we only tested 0.05 and 2 Pa, we might have observed greater differences at the higher shear stress rates, perhaps mimicking the arterial flow which is greater than 2 Pa (Mishani et al. 2021). We next aimed to determine whether flow patterns, particularly oscillatory and laminar shear stress affect galectin gene transcription compared to static control.

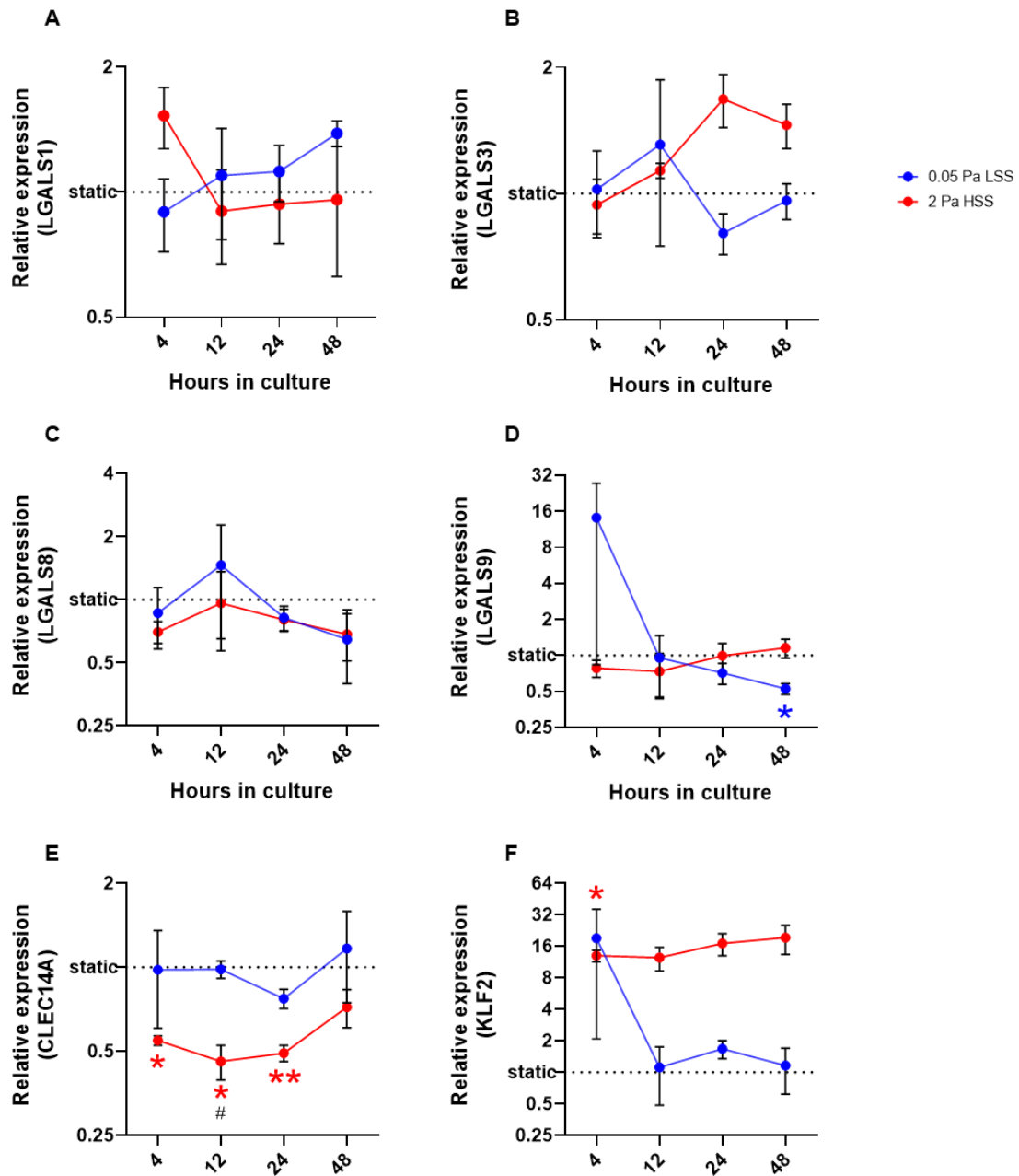


Figure 11: Galectin transcription in HUVEC following culture with low and high laminar shear stress over time relative to static control.

(A-F) HUVEC were cultured for 4, 12, 24 and 48 hours with either low shear stress (LSS, 0.05 Pa), high shear stress (HSS, 2 Pa) laminar flow, or no laminar flow (static, dashed line) and analysed for gene transcription by qPCR. Culture with both laminar HSS and LSS appeared to have little effect on endothelial galectin (A-D) gene transcription over time. CLEC14A (E) and KLF2 (F) control genes were down- and upregulated, respectively in response to HSS over time. A two-way ANOVA was conducted to test the effects of shear stress and time in culture on gene transcription, revealing a significant effect of shear stress on gene transcription in KLF2 and CLEC14A only (p -values < 0.05). Post-hoc comparisons using Tukey's test revealed that the mean fold change in transcription of *LGALS9*, *CLEC14A* and *KLF2*, following culture with HSS (red) or LSS (blue) shear stress was significantly different from static (*) or between shear stress rates (#) at the different time points. p -value < 0.05 (*)/(#), < 0.01 (**). Data are presented mean \pm SEM ($n=3$).

qPCR was used to assess gene transcription in HUVEC cultured for 24 hours under laminar or oscillatory shear stress at 0.3 Pa, 1 Pa, or 2 Pa compared to static controls, based on previously reported experimental conditions (Sheikh et al. 2003). We first confirmed the efficacy of this model through the observation of morphological changes; elongation and alignment of HUVEC in the direction of flow at 0.3 and 2 Pa. We observed more prominent elongation and alignment in the HUVEC cultured with 2 Pa of laminar shear stress compared to 0.3 Pa (**Figure 12**). Of note, we see a white halo around the HUVEC that have undergone culturing with 2 Pa laminar flow which is not observable in the other conditions and may be due to changes in the cell cytoplasm arrangement that affects the 3D shape of the HUVEC.

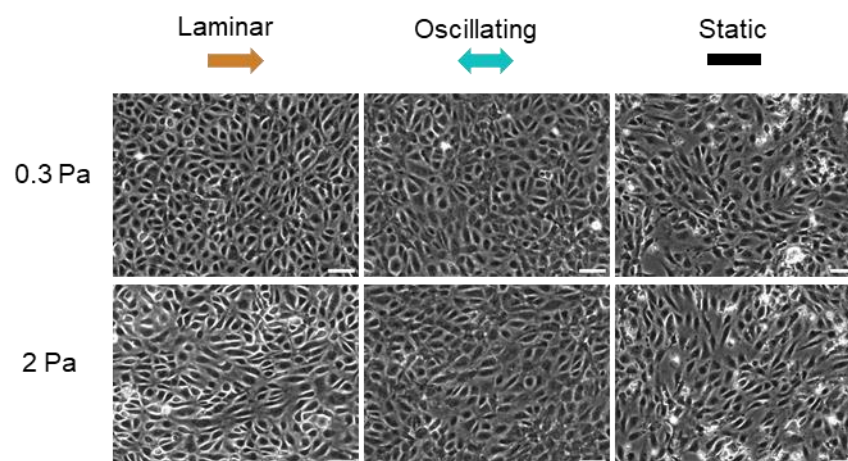


Figure 12: Endothelial cell morphology appeared directional with high laminar shear stress and less so with oscillating culture.

HUVEC morphology was changed through culture with high laminar shear stress (2 Pa), and less so with the oscillating culture or lower shear stress (0.3 Pa). Images representative of repeat experiments (n=4). Scale bar bottom right 15 μ m.

Our qPCR results show that the relative transcription of *LGALS1* was significantly lower in HUVEC cultured with oscillatory flow compared to laminar flow at 0.3 Pa, and not with increased shear stress of 2 Pa (**Figure 13A**). We saw a similar trend in *LGALS3* transcription, where the relative expression was lower in HUVEC cultured with oscillating compared to laminar flow at both 0.3 Pa and 1 Pa shear stress, although this difference was not statistically significant (**Figure 13B**). The trends in

LGALS8 transcription were inconsistent as we saw a large spread in our repeat samples (**Figure 13C**). We saw a significant decrease in *LGALS9* transcription following culture with oscillatory flow at all shear stress rates, relative to static control (**Figure 13D**). Meanwhile, *LGALS9* transcription was significantly upregulated following culture with 1 Pa of laminar flow (**Figure 13D**). With this experiment, we no longer saw significant reductions in *CLEC14A* transcription in response to culture with high laminar shear stress as was observed in our previous experiment (**Figure 13E**). Though we observe a cluster of datapoints suggesting that *CLEC14A* transcription is overall reduced with increasing levels of laminar shear stress, particularly following culturing at 2 Pa, though may require repeat experiments using higher shear stress to confirm (**Figure 13E**). With oscillatory flow, we observed a 2-fold increase in *CLEC14A* transcription in both 1 Pa and 2 Pa conditions relative to static control (**Figure 13E**). The observation that *CLEC14A* transcription is upregulated with disturbed high shear stress has previously been reported in H-type vessels within the bone. In contrast, L-type vessels, which display lower but still disturbed shear stress rate show lesser *CLEC14A* transcription (Neag 2022). As expected, *KLF2* was upregulated with increasing rates of laminar shear stress and suppressed with prolonged exposure to oscillatory flow (**Figure 13F**) (Wu et al. 2022; Wang et al. 2006). From this experiment we identified *LGALS9* to be upregulated in response to increasing rates of laminar flow and downregulated in response to culture with oscillatory flow, thus identifying distinct galectin gene responses to both the rate and patterns of shear stress in HUVEC cultured over 24 hours. Meanwhile, *LGALS3* transcription appears to be stable following culture with both laminar and oscillatory flow at 0.3, 1 and 2 Pa shear stress.

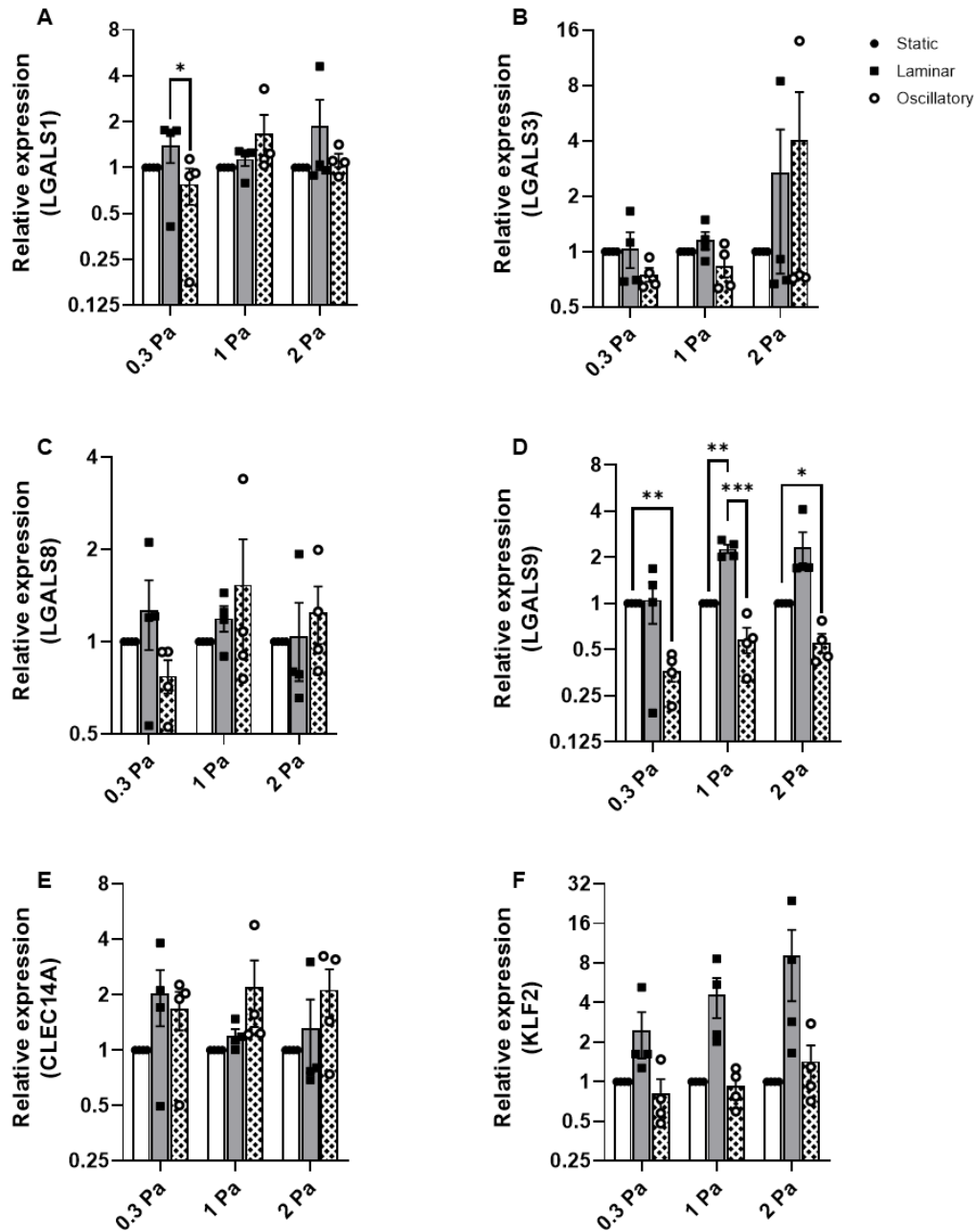


Figure 13: qPCR analysis of transcription of galectin genes in HUVEC following culture with low, medium, and high laminar or oscillatory shear stress over time relative to static control.

(A-F) qPCR gene transcription analysis was performed on HUVEC cultured for 24 hours under either laminar or oscillatory flow conditions of 0.3, 1 or 2 Pa shear stress and shown relative to static control. A two-way ANOVA was conducted to test the effects of flow patterns and shear stress rates on gene transcription, revealing a significant effect of shear pattern on gene transcription in *KLF2*, *CLEC14A* (p-values < 0.05) and *LGALS9* (p < 0.001). Post-hoc comparison using Tukey's test revealed that the mean fold change in transcription of *LGALS1* and *LGALS9* was significant between flow patterns. p-value ≤ 0.05 (*), ≤ 0.01 (**), $p \leq 0.001$ (***). Data are presented mean \pm SEM (n=4).

Overall, the results presented within this section show that there is very little effect of both low and high laminar shear on the transcription of *LGALS1*, *LGALS3* and *LGALS8* in HUVEC over time. We do, however, identify differences in the transcription of *LGALS9* in response to laminar and oscillatory flow with increasing rates of shear stress. Since *KLF2* plays an atheroprotective role in endothelial cells exposed to prolonged laminar shear stress, the trends we observe in Gal-9 expression may suggest an anti-inflammatory or protective role for endothelial galectin-9, though the context in which this might be the case is still to be elucidated. Indeed, it is evident that there are limitations in the orbital shaking and Ibidi pump models used to study shear stress that makes it difficult to draw firm conclusions from our data. The lack of robustness in either of these experiments also highlights that results from publicly available datasets should be interpreted with caution before drawing any firm conclusions.

3.3 Endogenous galectin expression is modulated in response to inflammatory mediators.

Having identified Gal-9 as being regulated by shear stress, we next wanted to confirm the results from previous reports of pro-inflammatory stimuli as mediators of endothelial galectin expression (Krautter et al. 2022). Published data from our lab shows that soluble and cell surface Gal-9 was significantly increased, as well as *LGALS9* mRNA, in response to stimulation with TNF α + IFN γ , and PolyI:C, compared to untreated control (Krautter et al. 2022). We mimicked this study using the same stimuli with HUVEC to investigate whether expression of the other endothelial galectins was also regulated by pro-inflammatory mediators.

Amongst all treatment conditions, *LGALS9* transcription was the most differentially modulated gene in HUVEC (**Figure 14A**), and HAEC (**Figure 14C**). We observed the greatest log fold increase in transcription for *LGALS9*, compared to any of the other *LGALS* genes (**Figure 14A**). This was of a similar degree to our positive control gene, *VCAM1*, which is upregulated following endothelial activation to carry out its function as an adhesion molecule for leukocyte trafficking (**Figure 14A & C**). On further interrogation of the transcriptional changes in *LGALS9*, we observed ~32-fold increase in gene transcription following IFN γ and PolyI:C treatment, and approximately a 64-fold increase in response to TNF α + IFN γ combined treatment at both 24- and 48 hours (**Figure 14B**). Of note, these mediators are associated with viral immunity, compared to TNF α which is a mediator more broadly associated with inflammation. The trends observed in *LGALS9* transcription in HUVEC were also seen in the HAEC, though TNF α had a greater effect on gene upregulation at 24 hours in HAEC (**Figure 14D**). Our HAEC sample size was too small to perform any meaningful statistics but has

been included to show that similar trends are evident between the two cell sources. The extent to which *LGALS9* was modulated in HUVEC following treatment with inflammatory stimuli was similar to the response observed for *VCAM1*, which is highly suggestive that Gal-9 also plays a crucial role in the inflammatory response. We next wanted to determine whether the differences in expression were apparent also at the protein level.

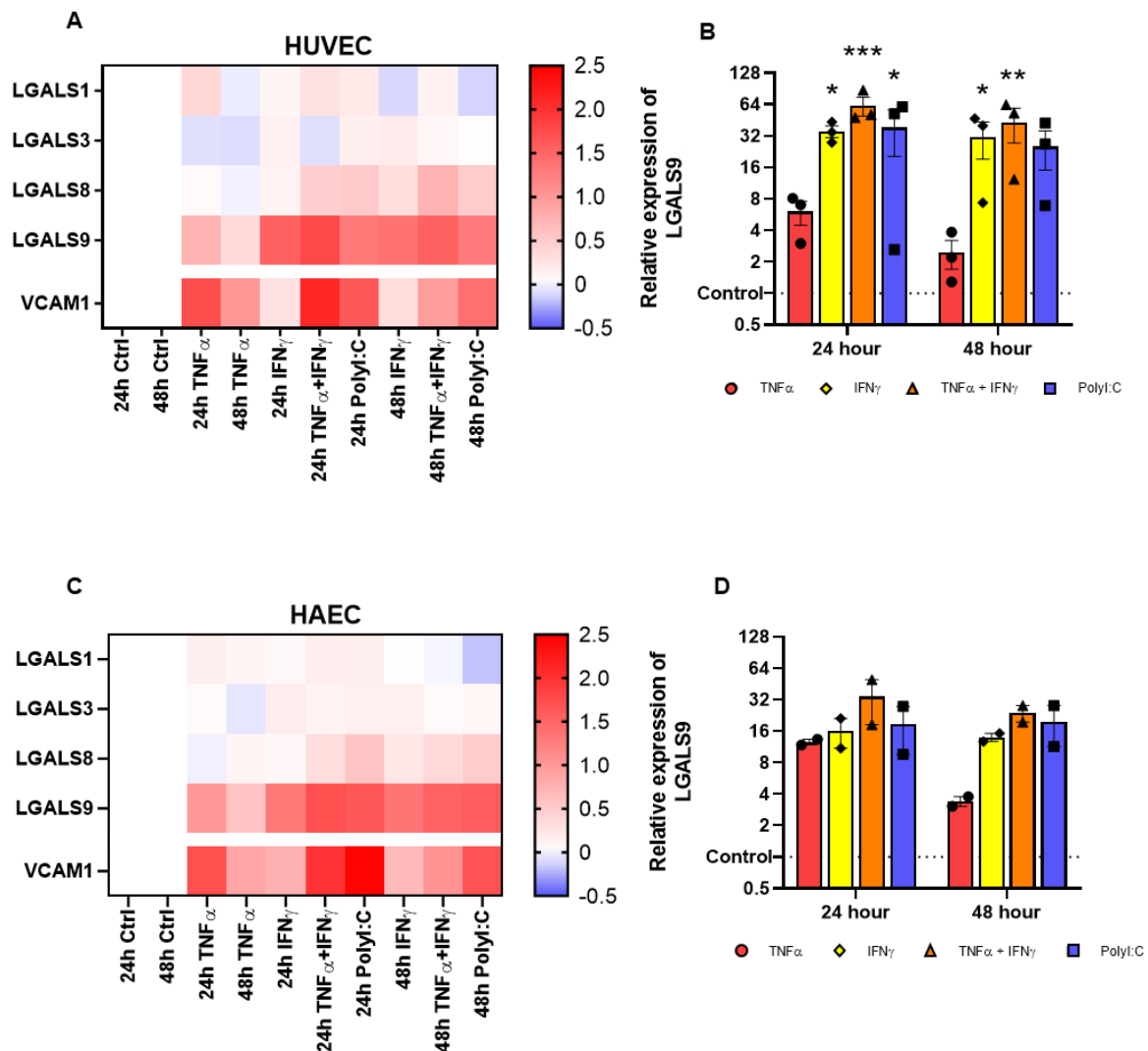


Figure 14 (A-D): Transcription of endogenous galectins is modulated in endothelial cells following stimulation with pro-inflammatory mediators.

qPCR gene transcription analysis was performed on HUVEC (A&B) and HAEC (C&D) cultured for 24 or 48 hours with either TNF α (10 ng/ml), IFN- γ (20 ng/ml), polyinosinic-polycytidylic acid (Poly:IC, 20 μ g/ml) or TNF α + IFN- γ (10 ng/ml, 20 ng/ml). Heat maps show log fold change in gene expression of galectins and VCAM1 positive control in HUVEC (A) and HAEC (C) relative to untreated control. A two-way ANOVA was conducted to test the effects of treatment stimulus and time on *LGALS9* gene transcription, revealing a significant effect of treatment on gene transcription ($p < 0.05$). Post-hoc comparison using Dunnett's test revealed that the mean fold change in transcription of *LGALS9* relative to untreated control was significant in IFN- γ , TNF α + IFN- γ and Poly:IC treated HUVEC at 24 hours. p -value ≤ 0.05 (*), ≤ 0.01 (**), $p \leq 0.001$ (***). Data are presented mean \pm SEM ($n=3$ HUVEC, $n=2$ HAEC). Similar trends were observed in HAEC, though this was not tested using statistical tests (D).

To further interrogate the changes in *LGALS9* transcription, we performed Western blot analysis on whole cell lysates from HUVEC treated with TNF α + IFN γ compared to untreated control. We were unable to suitably determine Gal-9 protein levels due to poor resolution of bands on the Western blot. We were able to detect Gal-3 within cell lysates and observed ~25% decrease in protein levels in HUVEC treated with TNF α + IFN γ for 24 hours, compared to unstimulated control (**Figure 15**). Although we were unable to get meaningful results from the Gal-9 Western blot, previously published results from our lab confirm that total Gal-9 protein is increased in HUVEC following 24-hour treatment with TNF α + IFN γ compared to untreated control, as detected by western blot, flow cytometry and ELISA (Krautter et al. 2022).

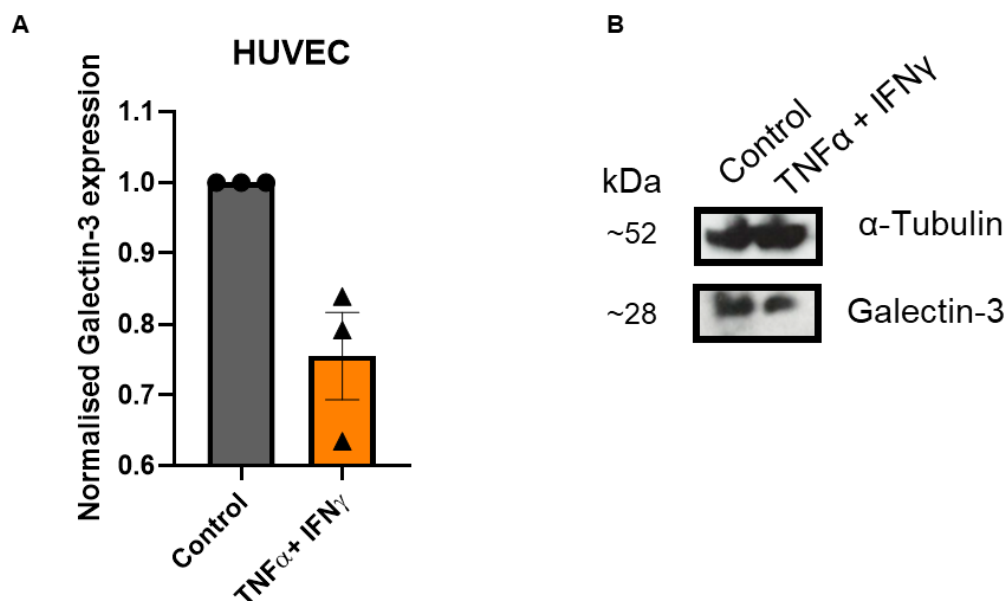


Figure 15 (A-B): Expression of endogenous galectin-3 is modulated in endothelial cells following stimulation with inflammatory mediators.

(A) Effect of inflammatory mediators on the expression of galectin protein in endothelial cells. Western blots showing Gal-3 total protein expression in HUVEC following 24-hour treatment with TNF α + IFN γ (10 ng/ml, 20 ng/ml). A Wilcoxon matched-pairs signed rank test was conducted to test the effects of TNF α + IFN γ treatment on Gal-3 protein expression compared to untreated control and was deemed not significant. Data are presented mean \pm SEM (n=3). **(B)** Representative Western blot shows reduced intensity of Gal-3 protein in lysates from treated cells compared to untreated control.

IFN γ is a type II IFN which interacts with the interferon-gamma receptor complex (IFNGR) on the cell surface to induce STAT signalling through GAS elements, resulting in pro-inflammatory phenotypes. Poly:IC on the other hand, targets TLR3 receptors on ECs and induces transcription of type I IFN stimulated genes (Platanias 2005). We wanted to test whether type I IFNs; IFN α 2 and IFN β , could also regulate *LGALS9* gene transcription through direct mechanisms with interferon- α/β receptors. We found that *LGALS9* transcription was upregulated in a dose-dependent manner for both IFNs, more so in IFN β than IFN α 2 (**Figure 16**).

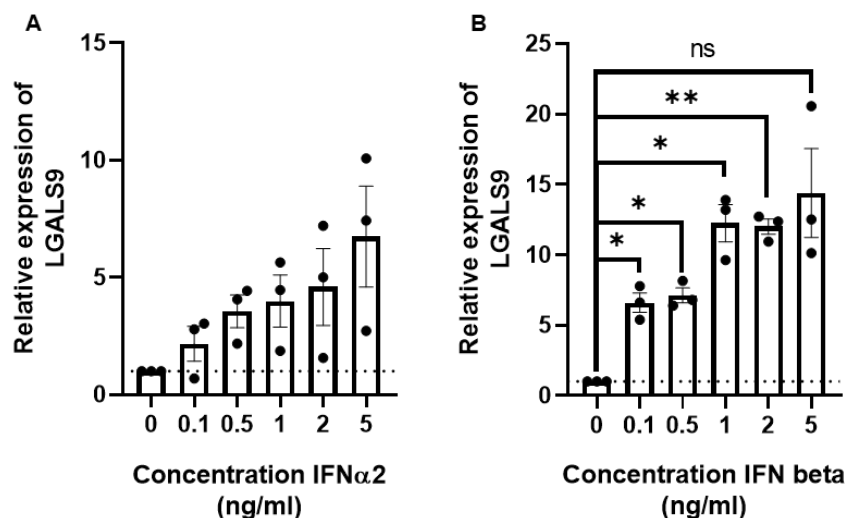


Figure 16: Galectin-9 gene transcription is modulated by IFN α 2 and IFN β treatment.

qPCR analysis of *LGALS9* gene transcription was performed on HUVEC stimulated with increasing concentrations of IFN α 2 (**A**) and IFN β (**B**) for 24 hours. Statistical analysis was performed using one-way ANOVA with Dunnett's multiple comparisons follow up test. A repeated measures one-way ANOVA was conducted to compare the mean of treated conditions to untreated control and deemed not significant. Post-hoc comparison using Dunnett's test revealed that the mean fold change in transcription of *LGALS9* relative to untreated control was significant in HUVEC treated with 0.1 – 2 ng/ml of INF- β only. p-value ≤ 0.05 (*), ≤ 0.01 (**). Data are presented mean \pm SEM (n=3 HUVEC).

Overall, this response is less so than observed in cells treated with IFN γ , where we see a 32-fold increase in *LGALS9* transcription, compared to ~15-fold with IFN β (**Figure 14**). The transcriptional regulation of galectin genes in response to pro-inflammatory mediators, supports a role for endothelial *LGALS9* in the inflammatory response. We therefore aimed to further investigate the transcriptional effects of viral-associated mediators on HUVEC to elucidate Gal-9 roles in inflammation and immune responses.

3.4 Characterisation of Galectin expression in human liver

We were kindly given cDNA and tissue sections from Dr Daniel Pattern and Prof Shishir Shetty (Institute of Immunology and Immunotherapy, University of Birmingham) so that we could investigate galectin expression in the liver. The liver is a tissue prone to viral infection and damage from lifestyle choices. It is also unique in that it is a highly vascularised area that contains many vessels throughout, called sinusoids. These sinusoids are exposed to low shear stress *in situ* and are the site for leukocyte trafficking in the liver (Wilkinson, Qurashi, and Shetty 2020). Since we have shown that galectin expression is modulated with non-static culture conditions, this research combines the themes of shear stress and inflammation to provide additional context to determine galectin function *ex vivo*.

We measured galectin gene transcription in liver sinusoidal endothelial cells (LSEC) and found no significant changes in *LGALS1* transcription in response to either TNF α , IFN γ or with the combination of both TNF α + IFN γ (**Figure 17A**). Meanwhile, *LGALS3* was significantly downregulated by ~3-fold following the combination treatment and compared to unstimulated control (**Figure 17B**). *LGALS9* was significantly upregulated by ~32-fold in response to TNF α + IFN γ combination treatment, and ~5- and ~20-fold with each individual component, respectively (**Figure 17**). We confirmed LSEC activation through the upregulation of *ICAM1* (**Figure 29D**). Our observations in LSEC are similar to the trends seen in HUVEC, where the combination treatment of TNF α + IFN γ is most potent in regulating *LGALS3* and *LGALS9* gene transcription compared to treatment with each individual component alone (**Figure 17B and C**).

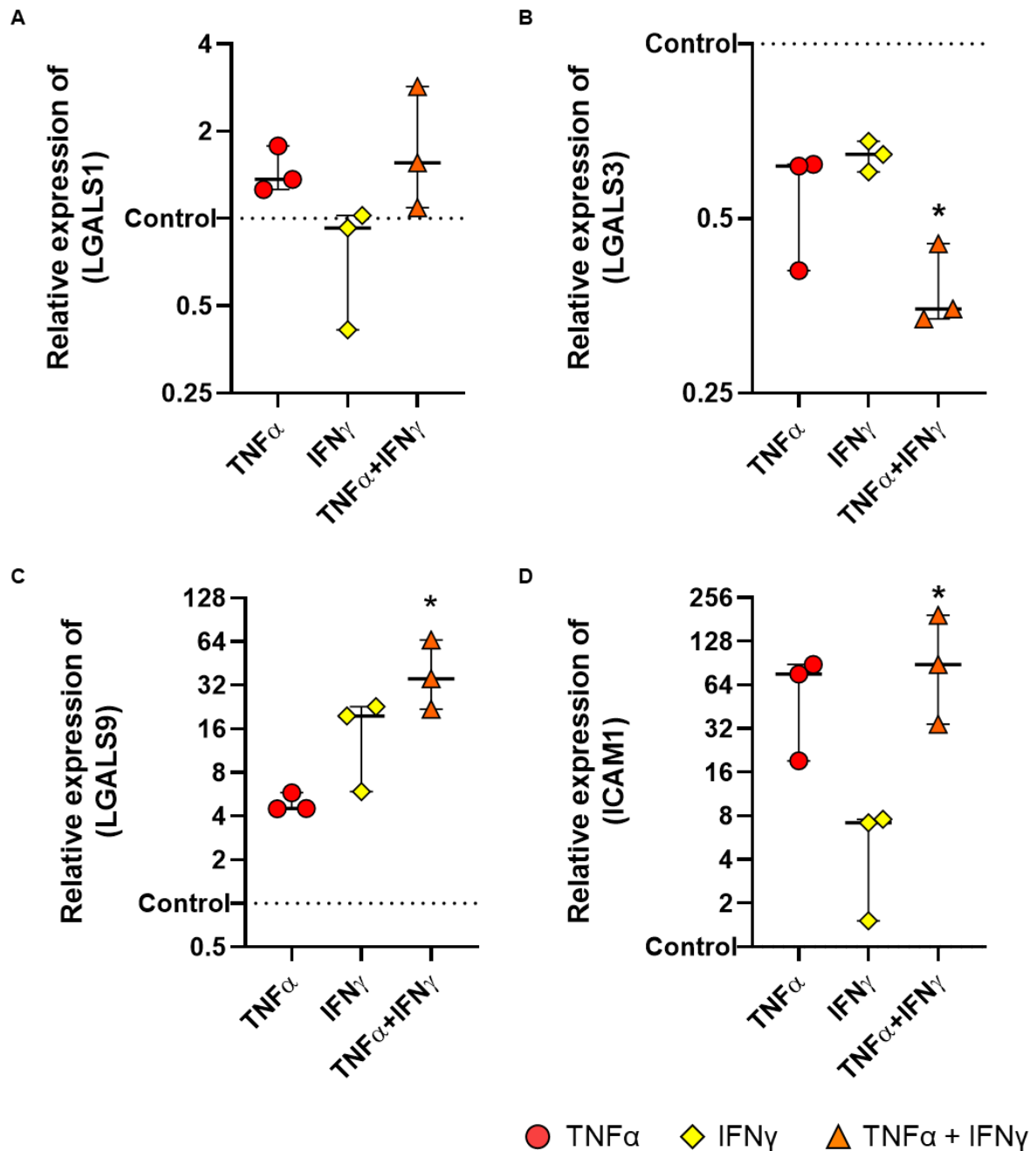


Figure 17: Galectin genes are differentially transcribed in liver sinusoidal endothelial cells in response to pro-inflammatory stimuli.

mRNA transcription of A) Galectin-1 (*LGALS1*), B) Galectin-3 (*LGALS3*), C) Galectin-9 (*LGALS9*), and D) Intercellular Adhesion Molecule 1 (*ICAM1*) in response to TNF α , IFN- γ , or TNF α + IFN- γ treatment were examined in liver sinusoidal endothelial cells (LSEC) cDNA by qPCR and shown as fold change relative to untreated control (dotted line). Samples were kindly provided by Dr Daniel Pattern, University of Birmingham. Statistical analysis was performed using Kruskal-Wallis test with Dunn's post hoc test. p-value < 0.05 (*). Data are presented as median \pm IQR of n=3 biological repeats.

We next looked at the expression profile of Gal-3 and -9 in the liver, using tissue sections taken from diseased and non-diseased patients. We sourced sections from non-diagnosed (normal), primary sclerosing cholangitis (PSC), alcoholic liver disease (ALD) and primary biliary cholangitis (PBC) patients for IHC staining. Gal-3 expression was minimal across all disease types, with the strongest positive staining observed in areas of fibrotic scarring (dashed line) on liver sections from patients with ALD, and some sinusoidal patterns of expression indicated by the arrowheads in PBC and ALD patient tissue (**Figure 18**). Gal-9 expression was observed throughout all sections, including the normal control (**Figure 18**). Sections from patients with diagnosed ALD and PSC were also positive for Gal-9 expression but was most strongly expressed in PBC. Expression of Gal-9 was largely located to sinusoids (arrowhead) in the PBC sections, and across all sections we observed positive staining within the sinusoids in what looked to be liver-resident macrophages, the Kupffer cells (arrows) (**Figure 18**). These data highlight that differential galectin expression, particularly Gal-9, may be determined by differences in the pathology of disease, at least within the liver.

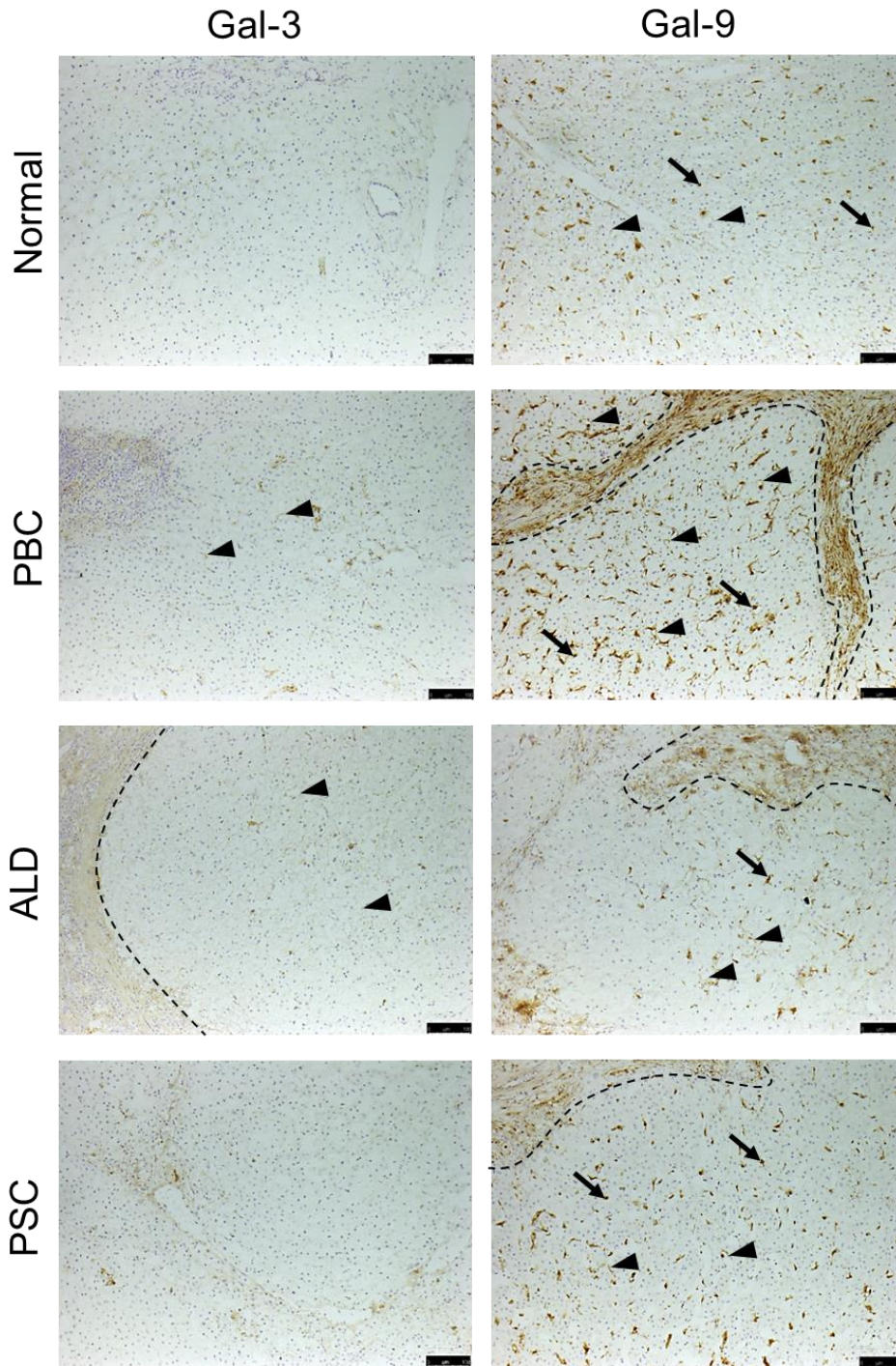


Figure 18: Galectin-9 (Gal-9) was expressed highly in liver tissue sections from primary biliary cholangitis (PBC) patients.

Gal-9 (brown, right column) expression appeared localised to sinusoids (arrowheads), within sinusoids in what resemble Kupffer cells (arrows), and in areas of fibrotic scar tissues (inside dashed lines) within liver tissue sections from non-diagnosed (normal), primary sclerosing cholangitis (PSC), alcoholic liver disease (ALD) and primary biliary cholangitis (PBC) patients. Less galectin-3 (Gal-3) expression was observed in liver tissue sections. Hepatocytes appeared negative for Gal-9 expression. Samples were counterstained with haematoxylin for nuclear staining. Hepatocytes were negative for galectin expression. Images were selected using Zen Blue software (Zeiss) after acquisition of entire tissue sections using a Zeiss Axio Scan.Z1 with 20x objective. Images shown are representative of 3-4 patient samples for each disease for galectin-9 and only two patients per condition for galectin-3. Scale bars represent 100 μ m.

We next looked at Gal-9 expression in sections of liver from patients diagnosed with Hepatitis C (HepC), based on our observation that Gal-9 transcription was upregulated in response to viral-associated mediators *in vitro*, and that PBC has been linked to viral infection (Xu et al. 2003; Tanaka, Leung, and Gershwin 2019). We observed a large amount of positive staining for Gal-9 within HepC positive liver sections, particularly on the luminal side of the sinusoids, similar to the pattern we observed in the PBC sections (**Figure 19**). We also saw positive staining for Gal-9 in Kupffer-cell like structures inside the sinusoids (**Figure 19**). Our results from *ex vivo* staining of liver sections strongly supports our *in vitro* findings that Gal-9 expression is highly regulated by viral-associated mediators and requires further investigation to confirm.

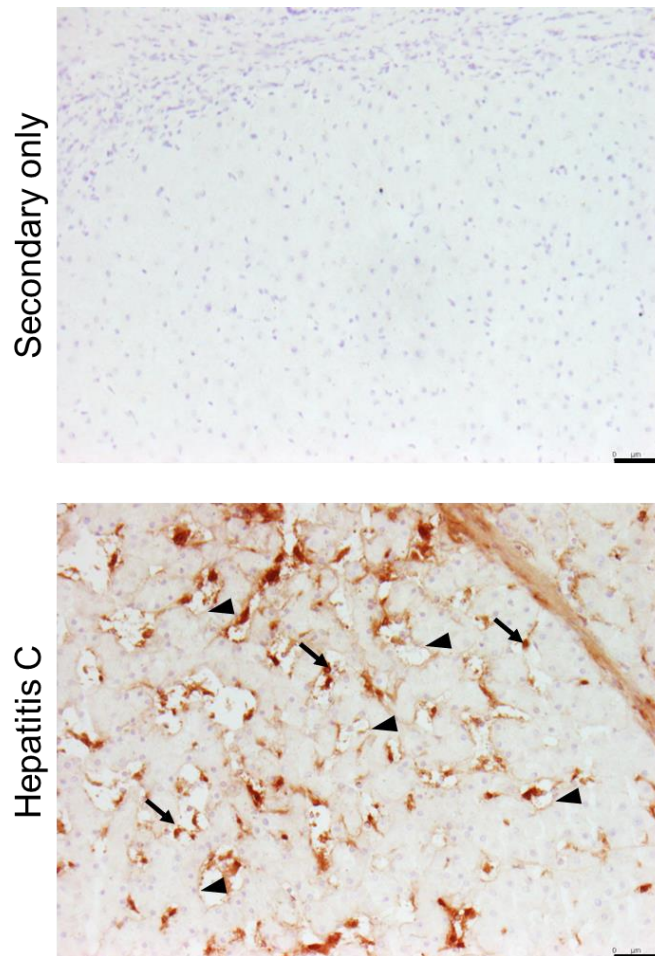


Figure 19: Galectin-9 (Gal-9) was expressed highly in liver tissue sections from Hepatitis C (HepC) patients.

Secondary only control showed no Gal-9 (brown) positive staining, whilst expression appeared localised to sinusoids (arrowheads) and within sinusoids in what resemble Kupffer cells (arrows) in tissue sections from livers acquired from Hepatitis C patients. Hepatocytes appeared negative for Gal-9 expression. Samples were counterstained with haematoxylin for nuclear staining. Hepatocytes were negative for galectin expression. Images were selected using Zen Blue software (Zeiss) after acquisition of entire tissue sections using a Zeiss Axio Scan.Z1 with 20x objective. Images shown are representative of 3-4 patient samples. Scale bars represent 50 μ m.

3.5 Summary and Discussion

The primary aim of this experimental chapter was to characterise regulators of endothelial galectin expression. To do this, we explored the effects of shear stress and inflammatory mediators on endothelial cells *in vitro*. Finally, we combined all themes to investigate galectin expression patterns in normal and diseased liver sections. Our main findings show that: a) Gal-9 is highly upregulated in HUVEC in response to virus-associated inflammatory mediators; b) Gal-3 and -9 expression appears to be positively regulated by shear stress; and c) Gal-9 expression is highly associated with liver sinusoidal endothelial cells in PBC and HepC disease. These data highlight a strong link between immune-response and shear regulation of galectin expression that may be used to understand the importance of galectins in liver disease pathology.

3.5.1 Shear stress and pro-inflammatory mediators as regulators of galectin expression

We report that Gal-3 and -9 genes are significantly upregulated in response to culture under orbital shaking conditions. Although this has been included in published datasets using bulk RNAsequencing (Maurya et al. 2021; Afshar et al. 2023; Ajami et al. 2017), this finding has not yet been specifically validated nor published. The orbital shaking method is a heterogenous and closed system whereby the patterns of shear stress differ in the centre and periphery of the wells. As such, it is not a useful method for determining the specific mechanosensitive responses of genes. The nature of this experimental setup means that soluble mediators that get released from the cells will have confounding effects on our results. In response to disturbed flow, HUVEC become misaligned and mechanosensitive genes become variably activated (Baeriswyl et al. 2019). Disturbed flow causes NFkB signalling to become activated,

leading to overexpression of adhesion molecules *ICAM1* and *VCAM1*, and *IL-6* (Go et al. 2014; Watson et al. 1996). Stimulation of ECs with IL-6 activated Janus kinase-mediated STAT3 (JAK-STAT) phosphorylation leading to reduced endothelial barrier function as well as transcription of further inflammatory cytokines (Alsaffar et al. 2018). Since we also confirm reports that soluble mediators upregulate Gal-9 expression, we might be seeing increased galectin transcription due to the combination of cytokines and other soluble mediators within the supernatant, rather than effects of the shear stress. *In situ*, endothelial cells are under constant exposure from circulating blood, and cytokines get filtered out or catabolised by the liver and kidneys (Bocci 1991). As such, this model only gives us limited insight into shear stress as a regulator of endothelial galectin expression. Of note, we see that protein expression is increased with gene transcription following orbital shaking culture, for both Gal-3 and Gal-9. We saw this to be significantly different between the Gal-3 and Gal-9 conditions, suggesting that the mode of expression may differ between the galectins.

We used the Ibidi Flow culture system to better understand the effects of shear stress and rates on galectin expression, as well as reducing the confounding variable of soluble mediator effects. Our results suggest that endothelial galectins are more responsive to different patterns of fluid shear stress, rather than the rate of fluid flow, since we report that transcription of *LGALS9* is significantly downregulated following culture with oscillatory flow, compared to static control. The link between disturbed shear stress and modulation of endothelial galectin expression could be a key predictor of disease. In a model of atherosclerosis, plaque size was reduced in the abdominal aorta section from Gal-9^{-/-}/ApoE^{-/-} KO mice after 12 weeks on high fat diet (Krautter et al. 2022). Due to the straightness of this area of the aorta, it is most likely to be an area exposed to laminar high shear stress, which we associated with

upregulation of Gal-9 in HUVEC (**Figure 13**). In areas of disturbed shear stress, such as in the aortic arch, plaque burden was not significantly reduced in Gal-9 KO mice (Krautter et al. 2022). Our data suggests that this may be because Gal-9 expression is already low in this area of low shear stress. Since our data alludes to the shear responsiveness of Gal-9, alongside rapid upregulation in response to inflammatory stimuli, we determine Gal-9 to be a uniquely selective molecule within the endothelium.

We confirmed that Gal-9 expression was highly upregulated in endothelial cells in response to pro-inflammatory mediators, most specifically to those associated with viral infection, including IFN γ , α , β and PolyI:C (Krautter et al. 2022; Chakraborty et al. 2021). Interestingly, we observed that fewer differentially transcribed genes were found in HUVEC responding to IFN- β and PolyI:C compared to TNF α + IFN γ . To decipher the crucial genes involved in the *LGALS9* inflammatory response, we need to knockdown the *LGALS9* gene from HUVEC, followed by stimulation with each of the inflammatory mediators, before finally measuring the changes in some of the top differentially expressed genes to determine pathways affected by Gal-9 function.

3.5.2 Galectin expression in liver disease

Although currently considered an autoimmune disease, PBC has been remarked and reviewed several times for potential aetiologies similar to infectious disease (Haydon and Neuberger 2000; Mason 2018). Since we see strong positive staining for Gal-9 in HepC sections and evidence in our cytokine stimulation data that strongly suggests viral-associated mediators in driving Gal-9 expression in ECs, we might find that presence of Gal-9 is a telling sign that some instances of PBC are driven by viral infection. One study reports that blood serum from PBC patients is reactive to retroviral proteins, more so than patients' with PSC (Mason et al. 1998). Similarities in the

reoccurring onsets of PBC after diagnosis and transplantation can be observed in HepC re-infections (Asthana et al. 2011) (Mason 2018). The link between viral infection and autoimmunity has been bridged in the context of HIV infection, where the virus incorporates host-plasma membrane and proteins when budding from the cell, triggering autoantibody responses and could be a similar suggestion for PSC aetiology (Wasilenko, Mason, and Mason 2009). Either way, we speculate that the presence of Gal-9 in the PBC sections is pertinent to the potential viral-link in PBC aetiology.

Our observation that Gal-9 expression is downregulated in low shear stress conditions compared to static control, suggests that under physiological conditions in the liver, Gal-9 expression is required to be low (**Figure 11**). This is further supported by our observation of low levels of Gal-9 positive staining following IHC on normal liver sections (**Figure 18**). The low shear environment of the liver, which we observed to downregulate Gal-9 expression *in vitro*, suggests that under homeostatic conditions, Gal-9 levels are required to be low. Reports of ~60-fold increase in *LGALS9* transcription in response to $\text{TNF}\alpha$ + $\text{IFN}\gamma$ and PolyI:C for example, is modulated in as few as four hours, with the majority of protein being localised intracellularly (Krautter et al. 2022). This suggests that Gal-9 is crucial in the initial stage of the immune response.

With all the evidence within this chapter, we might hypothesise that Gal-9 is necessary in aiding a pro-inflammatory response to viral infection. The regulation of Gal-9 under different patterns and rates of shear stress might be necessary homeostatic adaptations of the endothelial cell to the bifurcations, curvature, and valves of the blood vessels dependent on the tissue microenvironment. Whilst the responsiveness of EC's to express Gal-9 following $\text{TNF}\alpha$ + $\text{IFN}\gamma$, for example, is necessary for aiding

immune-responses and leukocyte trafficking. The persistence of Gal-9 expression, in the case of positive staining in liver sections from HepC and PBC patients, suggests that either the mechanism of Gal-9 expression may be faulty in patients, or that the binding of Gal-9 to its natural ligand is also contributing to chronic disease.

CHAPTER 4: EXAMINING THE FUNCTION OF ENDOGENOUS ENDOTHELIAL GALECTINS IN LEUKOCYTE TRAFFICKING

4.1 Introduction

We describe in the previous chapter that endothelial galectins are regulated by inflammatory mediators and shear stress, which is conducive to an immunoregulatory role for these proteins. This data highlights the importance of studying endothelial galectins as close to physiologically relevant conditions as possible. One such way is by using intravital microscopy (IVM) to study inflammation in the microcirculation using galectin-knockout mice. IVM data published from Gittens et al. report that mechanisms mediating leukocyte slow rolling and migration are impaired in Gal-3^{-/-} mice (Gittens et al. 2017), whilst our lab reports that neutrophil and monocyte recruitment was significantly reduced in Gal-9 knockout mice (Iqbal et al. 2022). Our lab has previously reported reduced neutrophil adhesion to HUVEC following siRNA knockdown of endothelial Gal-9 in a model of leukocyte trafficking under flow (Krautter et al. 2022). Aside from this, very little research has been published on the specific effects of endothelial galectins on leukocyte trafficking and inflammation.

As such, the aim of this section is to characterise the novel Gal-3^{-/-}/Gal-9^{-/-} knockout mice alongside single knockout mice in IVM studies to elucidate galectin function in leukocyte trafficking. Additionally, we aim to explore whether galectin function in leukocyte trafficking is a result of endothelial-sourced galectins, by using siRNA knockdown to eliminate galectin expression in HUVEC and study neutrophil adhesion and migration under physiological flow. We hypothesise that the combined function of Gal-3 and -9 is crucial in the regulation of leukocyte trafficking events, particularly within the endothelium as the source of galectins.

4.2 Characterisation of global galectin knockout mice under resting conditions

Our objective was to characterise galectin-knockout mice under resting conditions. We determined whether there were any differences in the leukocyte populations within whole blood from non-inflamed galectin-3 null (Gal-3^{-/-}), galectin-9 null (Gal-9^{-/-}), and galectin-3/galectin-9 (Gal-3^{-/-}/Gal-9^{-/-}) double knockout mice by performing complete blood count (CBC) analysis. This analysis was performed after our IVM experiments using mice that were surplus to the maintenance breeding pairs. To align with the NC3Rs principles for humane experimental animal use, we opted to reduce mice samples by excluding analysis of matched WT mice. We did observe however, that cell subpopulations within the whole blood of all mice fell within the normal ranges of C57BL/6 mice as reported by Charles River (Charles River Laboratories International 2012). Red blood cell, platelet, and monocyte counts between groups of knockout mice were determined statistically different by one-way ANOVA testing (**Figure Error! Reference source not found.20A**). No significant differences were observed between groups in white blood cells, neutrophils, and lymphocyte counts (**Figure 20A**). We also looked at whether there were any significant differences between groups in the correlation of age and weight but observed none across the genotypes (**Figure 20B**). These data suggests that no inherent relationship between galectin expression, age, weight, or baseline blood counts is present and as such, is unlikely to be a confounding factor in our study of galectin function in leukocyte trafficking.

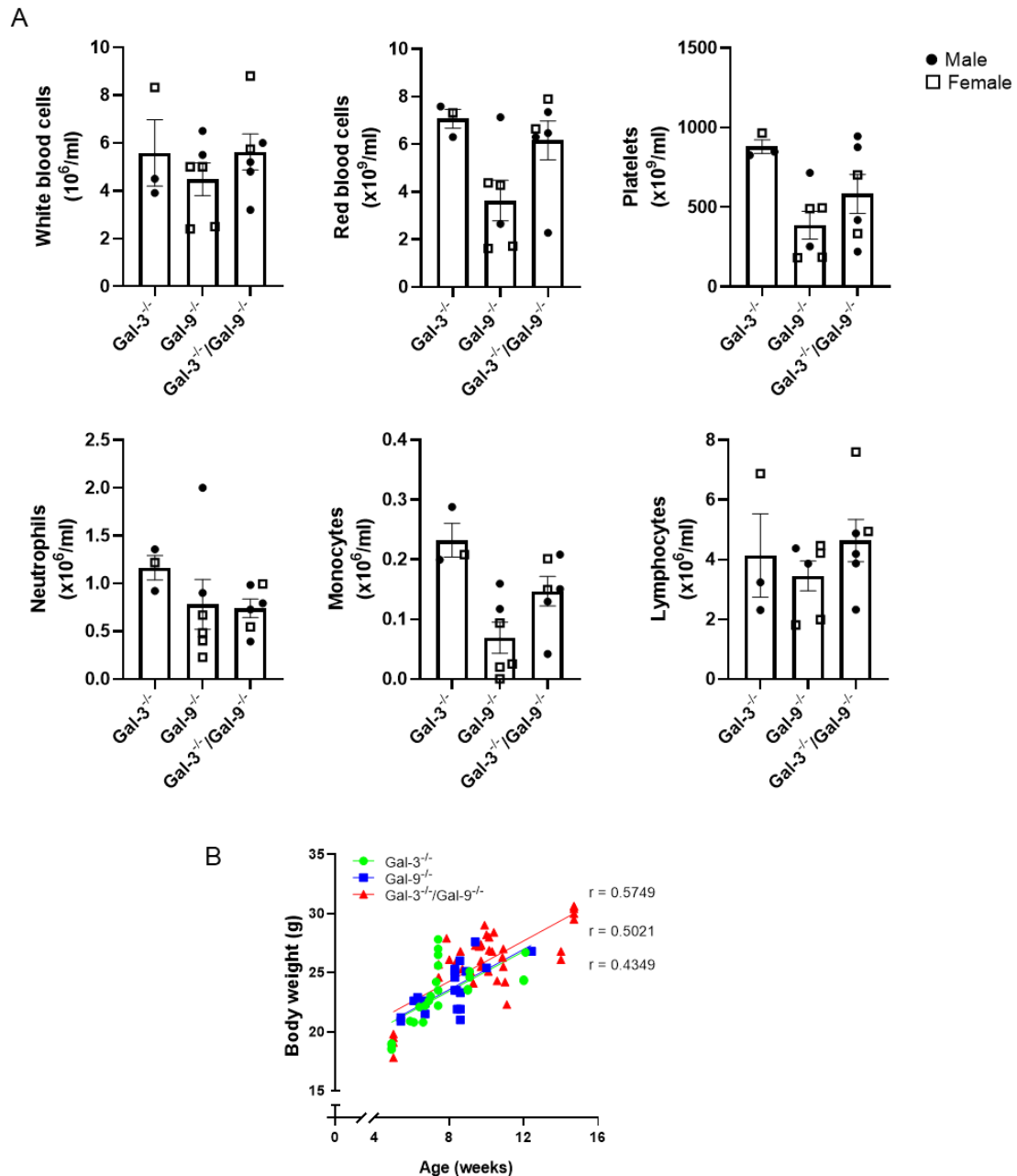


Figure 20 (A-B): Characterisation of galectin-knockout mice.

A) Statistically significant differences in baseline complete blood counts across groups of galectin-knockout mice were observed in total red blood cells ($P=0.0395$), platelets ($P=0.0403$), and monocytes ($P=0.0071$) by one-way ANOVA but not in multiple comparisons follow up test ($n = 3-6$ male and female). **B)** Correlation between age and body weight was measured between galectin-knockout genotypes and the coefficient (r) displayed for each group in order of lines as observed. No statistical difference was observed between the slope of regression lines of each group as determined by ANCOVA (Analysis of covariance). Graphs displaying CBC data shows the mean \pm SEM of 3-6 mice per group. Correlation graph shows data point for each mouse per group, $n = 25$ for Gal-3^{-/-} (green), $n = 21$ for Gal-9^{-/-} (blue), and $n = 40$ for Gal-3^{-/-}/Gal-9^{-/-} (red), all male mice aged 6-12 weeks old.

4.2.1 Endogenous Gal-3 and -9 are both required for controlled leukocyte rolling in the IL-1 β inflamed post-capillary venules of the cremaster

We used intravital microscopy (IVM) to study the function of galectins in leukocyte trafficking within the cremaster muscle. We chose the cremaster model due to its ease of accessibility, high transparency, vascularity, and responsiveness to inflammatory stimuli. This model has also been used in the characterisation of Gal-3^{-/-} mice, in response to TNF α and IL-1 β stimuli, meaning we can compare our results directly to those previously reported by Gittens et al (Kunkel and Ley 1996; Gittens et al. 2017).

Statistical analysis was based on the mean number of cells counted across 6-8 vessels per mouse. Data is displayed using unique symbols to represent data from each mouse, highlighting the variation across individual vessels.

Recruitment behaviours within the post-capillary venules of IL-1 β inflamed cremaster were visualised by immunofluorescence and brightfield microscopy to analyse Gr1+ and total leukocyte populations, respectively (**Figure 21A**). No significant differences between Gal-KO mice and WT were found across any of the parameters by Dunn's multiple comparisons test. Rolling flux of Gr1+ (**Figure 21B**) and all leukocytes (**Figure 21E**) were significantly different across groups by ANOVA ($p=0.0065$ and $p=0.0178$, respectively) as we observed greater rolling in the Gal-3^{-/-} and Gal-3^{-/-}/Gal-9^{-/-} mice groups. We also saw that the average total # of cells were greater in the Gal-3^{-/-} group compared to WT and Gal-9^{-/-} group, although this was not significant (**Figure 21H and I**). No significant differences in either firm adhered (**Figure 21C & F**) or transmigrated cells (**Figure 21D & G**) was observed in either galectin-knockout mice groups compared to wildtype. We report that the total number of Gr1+ cells (**Figure 21H**) recruited to the inflamed cremaster was significantly different between groups by ANOVA with $p=0.0464$, most probably due to increased Gr1+ cell flux in the vessel. We did not observe this within the unlabelled cell population (**Figure 21I**), most probably due to difficulties in observing unlabelled leukocytes within brightfield videos. We saw very few transmigrated Gr1+ cells (**Figure 21D**) in our analysis, fewer than in the brightfield videos (**Figure 21G**).

To eliminate the possibility of these unlabelled cells being due to an increase in lymphocytes, we administered a fluorescently labelled anti-CD3 antibody and detected no positively labelled cells across the groups of mice. Instead, the discrepancy between the number of transmigrated Gr1+ and unlabelled leukocytes may be due to transmigration events taking place prior to the administration of the fluorescently labelled antibody. Poor antibody penetration into the surrounding tissue may lead to inefficient labelling of transmigrated leukocytes.

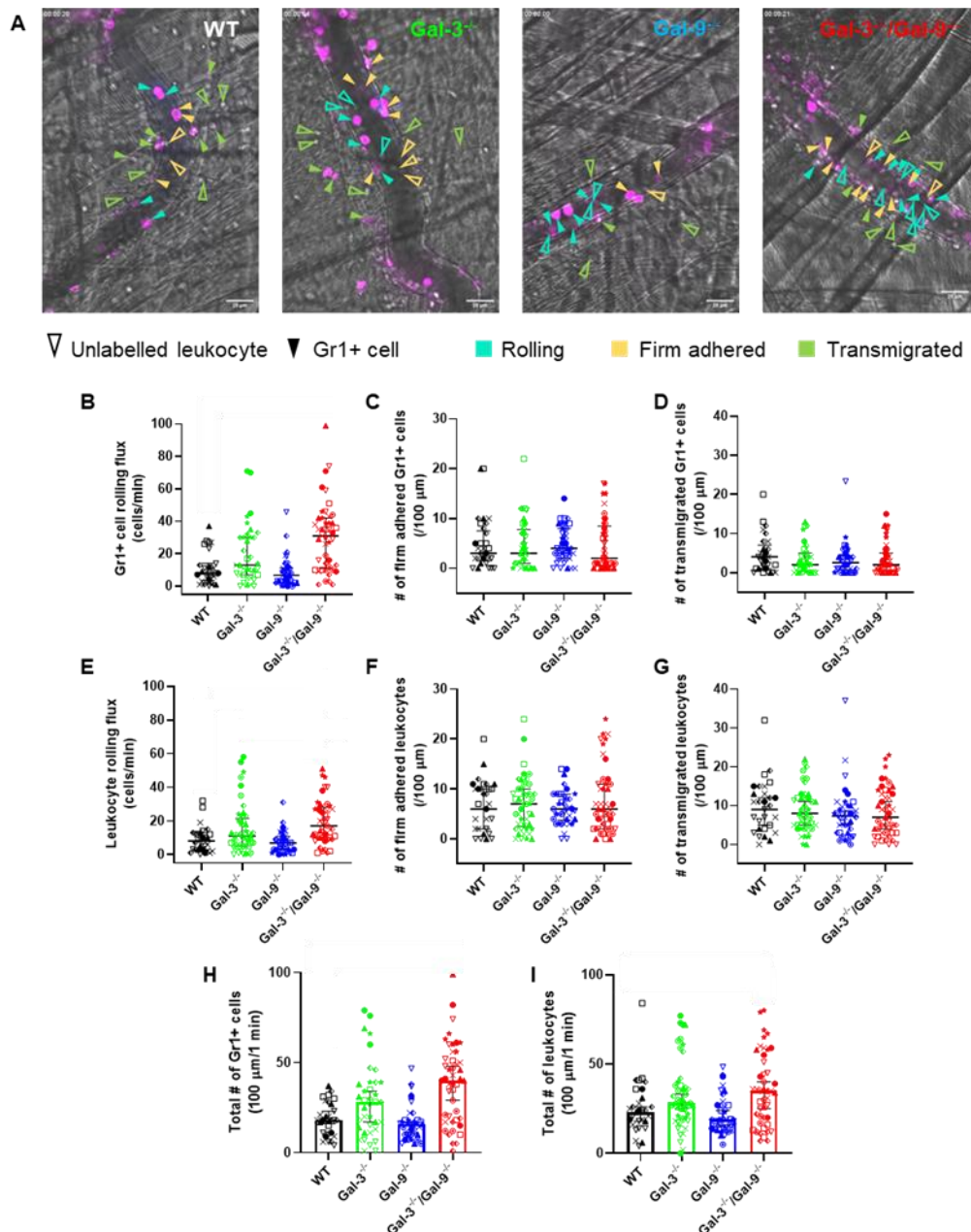


Figure 21 (A-I): Gr1+ leukocyte rolling flux and overall leukocyte numbers in post-capillary venules of IL-1 β stimulated cremaster were significantly different across galectin-knockout and wildtype mice.

Intravital microscopy was used to image post-capillary venules in the inflamed cremaster of Gal-3^{-/-}, Gal-9^{-/-} and Gal-3^{-/-}/Gal-9^{-/-} double knockout mice and C57BL/6 wildtype control mice, four hours following intrascrotal injection with 50 ng of recombinant murine IL-1 β (in 200 μ l PBS). **(A)** Rolling flux, **(B)** firm adherence and **(C)** transmigration of Gr1+ cells (using fluorescently labelled anti-Ly6C/Ly6G antibody delivered intravenously) detected using fluorescence, and **(E, F and G)** unlabelled leukocytes detected by brightfield imaging from 100 μ m segments of 3-6 vessels per mouse captured in one-minute recordings. **(H)** Total number of Gr1+ and **(I)** unlabelled leukocytes are also reported. Individual mice were designated a unique shape to denote spread of data from each blood vessel. Plots display the median with the IQR of 7-9 mice per group. Statistical significance was assessed by Kruskal-Wallis and Dunn's multiple comparisons test.

We assembled correlation matrices to compare the results within each parameter across the brightfield and fluorescence analysis methods. We found strong correlation (Pearson $r > 0.75$) between 'Gr1⁺' and 'all' cells counted in brightfield in the rolling flux, adhered, and total cells parameters (**Figure 22A**). This observation suggests that both methods, fluorescent and brightfield microscopy, are representative of these leukocyte behaviours *in vivo*. Correlation between the number of transmigrated cells from both analysis methods was lower (Pearson $r < 0.65$) in comparison (**Figure 22A**). This discrepancy may be due to inefficient labelling of Gr1⁺ cells that have already transmigrated through the tissue prior to delivery of the fluorescent antibody (Lu et al. 2020). The correlation analysis between the two imaging methods was determined significant (blue) across all parameters, except for rolling (yellow) (**Figure 22B**). One observation made during this experiment, and evident in our analysis is that capturing data from the rolling flux parameter was more efficient using the fluorescent microscopy analysis. This is because we were able to increase the contrast between the labelled cells and the dark background – meaning we could more easily observe cells in different slices along the horizontal plane of the vessel. As such, we see benefits of using both analysis types to obtain an overall better understanding of leukocyte trafficking behaviours *in vivo*.

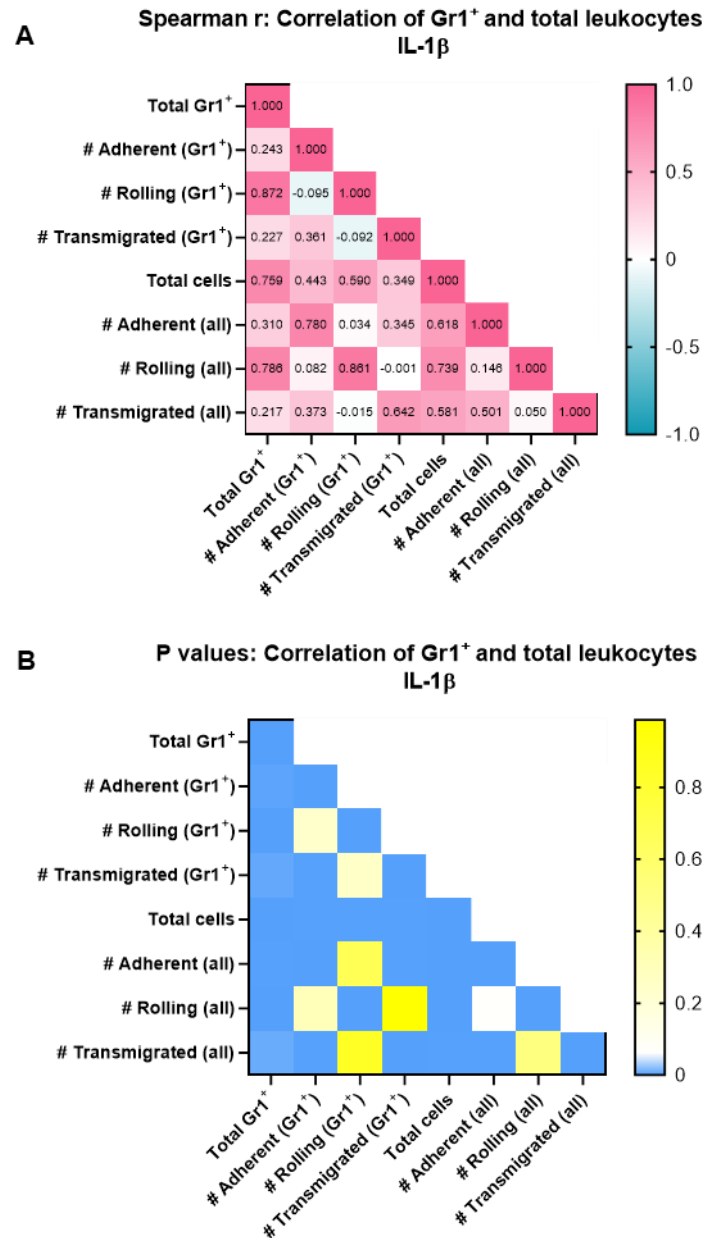


Figure 22 (A-B): Correlation matrix of IL-1 β intravital microscopy data shows strong positive relationship between the leukocyte trafficking events of Gr⁺ cells and total leukocytes observed by brightfield.

A) The strength of the Spearman's rank correlation coefficient (r) is great between the Gr1⁺ cells and total leukocyte (all) numbers within each parameter analysed (adherent, rolling, transmigrated) where the baseline value of zero is shown in white and values greater in pink and lesser in blue. **B)** p values of the Spearman's r values are denoted as ≤ 0.05 in white, zero in blue, and non-significant values > 0.05 shown in yellow.

Prior to termination of the IVM experiment, we collected blood samples from the inferior vena cava (IVC) for CBC analysis. Although we're unable to directly compare, we observe 3-4 million cells/ml in CBC from mice under resting conditions (Error! Reference source not found.**23**), compared to just 1.25 – 1.75 million/ml following IVM (**Figure 23**). This difference could be due to migration of lymphocytes from the blood into the inflamed tissue, either due to inflammatory challenge, or from the invasive surgery. We observed significant differences in neutrophil numbers across genotypes (**Figure 23**). Although not significant, a similar trend was observed in white blood cell (WBC) numbers, where Gal-3^{-/-} and Gal-3^{-/-}/Gal-9^{-/-} mice groups had greater (~1 million cells/ml) WBC numbers compared to WT and Gal-9^{-/-} groups (**Figure 23**). Overall, this fits with our IVM data in which we identified a significant increase in leukocyte rolling flux in the blood vessels of Gal-3^{-/-}/Gal-9^{-/-} mice, and a trend for greater rolling flux in Gal-3^{-/-} mice (**Figure 21B and E**). Since we observed differences in the endothelial response to different pro-inflammatory stimuli *in vitro*, we repeated our IVM studies on galectin-knockout mice using TNF α as the inflammatory mediator.

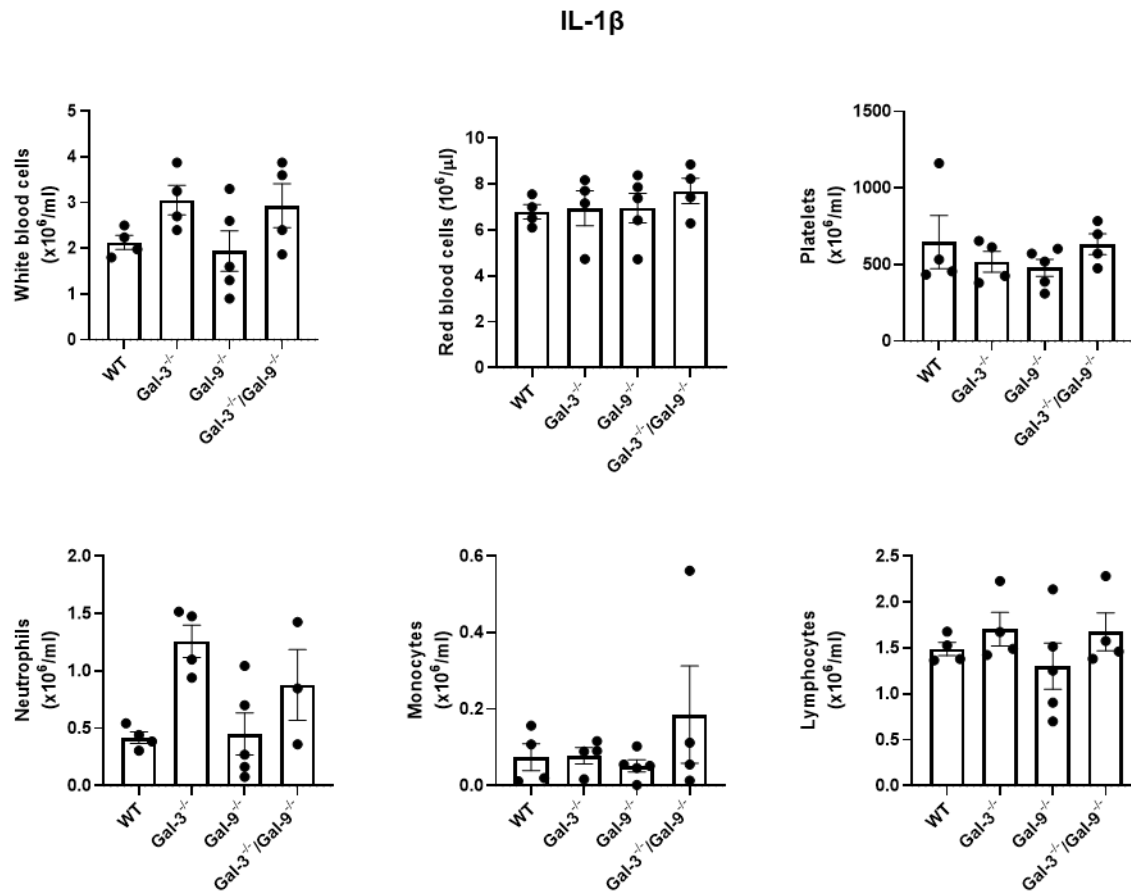


Figure 23: Complete blood counts from mice following treatment with IL-1 β and surgery for intravital microscopy.

Mice were treated with 50 ng of IL-1 β four hours prior to undergoing surgery for intravital microscopy. Following this, blood was taken from the inferior vena cava and analysed for complete blood counts using the Pentra ES 60 automated haematology analyser. Statistically significant differences in were observed between galectin-knockout mice groups in neutrophil numbers ($P=0.0395$) by Kruskal-Wallis test. No significant differences were observed between groups compared to wildtype (WT) control following Kruskal-Wallis test with Dunn's multiple comparison ($n = 3-5$). Data displayed as average \pm SEM.

4.2.2 Endogenous Gal-3 and -9 are both required for controlled leukocyte rolling in the TNF- α inflamed post-capillary venules of the cremaster

We replicated the technique described in the previous section, substituting IL-1 β for TNF α injection, and analysed leukocyte trafficking events using fluorescence and brightfield imaging (**Figure 24A**). Although not statistically significant, we did observe a small increase in rolling flux of Gr1+ and total leukocytes in the Gal-3^{-/-}/Gal-9^{-/-} mice group compared to others (**Figure 24B and E**). No significant differences in the number of adhered leukocytes between mice groups were observed (**Figure 24C and F**). Surprisingly, we saw a significant decrease in the number of transmigrated Gr1+ cells in the double knockout group compared to WT control (**Figure 24D**). This difference was not observed in the brightfield image analysis, and the overall number of transmigrated cells was actually greater in the double knockout group (**Figure 24G**). Conversely to what was observed in mice following IL-1 β treatment, we saw no significant differences in the total number of cells counted between groups (**Figure 24D**). Overall, our data shows that there is no great difference in leukocyte trafficking events between genotypes in response to TNF α challenge. Statistical analysis was based on the mean number of cells counted across 6-8 vessels per mouse. Data is displayed using unique symbols to represent data from the vessels from each mouse, highlighting the variation across individual vessels.

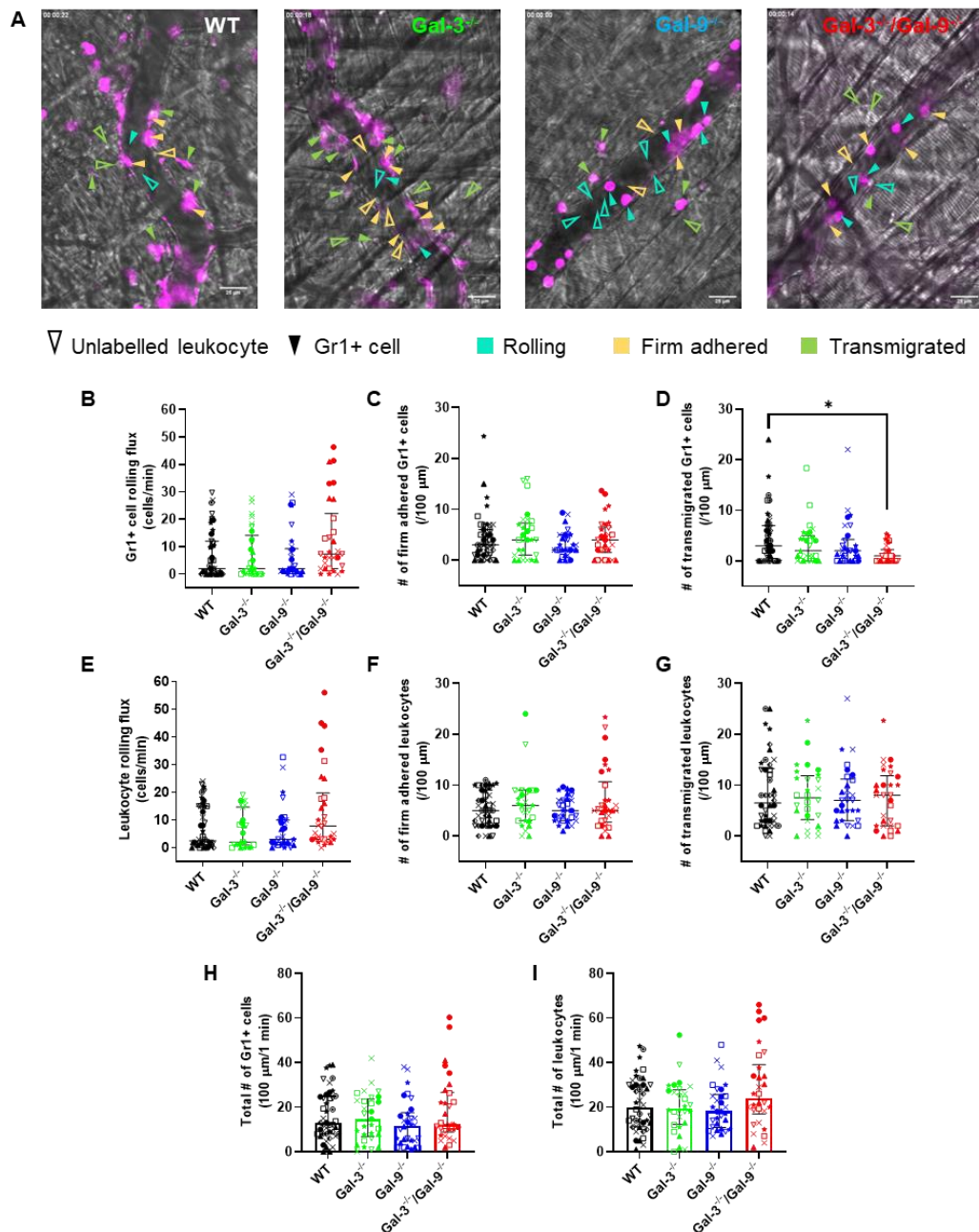


Figure 24 (A-I): Mice deficient in both the Gal-3 and -9 genes show reduced transmigrated Gr1+ cells in post-capillary venules of TNF α stimulated cremaster.

Intravital microscopy was used to image post-capillary venules in the inflamed cremaster of Gal-3^{-/-}, Gal-9^{-/-} and Gal-3^{-/-}/Gal-9^{-/-} double knockout mice and C57BL/6 wildtype control mice, four hours following intrascrotal injection with 500 ng of recombinant murine TNF α (in 200 μ l PBS). **(A)** Rolling flux, **(B)** firm adherence and **(C)** transmigration of Gr1+ cells (using fluorescently labelled anti-Ly6C/Ly6G antibody delivered intravenously) detected using fluorescence, and **(E, F and G)** unlabelled leukocytes detected by brightfield imaging from 100 μ m segments of 3-6 vessels per mouse captured in one-minute recordings. **(H)** Total number of Gr1+ and **(I)** unlabelled leukocytes are also reported. Individual mice were designated a unique shape to denote spread of data from each blood vessel. Plots display the median with the IQR of 7-9 mice per group. Statistical significance was assessed by Kruskal-Wallis and Dunn's multiple comparisons test denoted by asterisks * $p \leq 0.05$.

The correlation matrix indicates a strong positive relationship between the data obtained from labelled (Gr1+) and brightfield counted leukocytes (all) across rolling flux, adhered and in total (#) of cells in the blood vessels, with an r value of >0.69 **(Figure 25A)**. This was less so in the transmigrated cells, with an r value of 0.598 **(Figure 25A)**. As was also observed in the other IVM experiment, the correlation between the two analysis methods to be significant (blue) across all parameters except for rolling (yellow) **(Figure 25B)**. Again, we highlight here the benefit and value of using both brightfield and fluorescent microscopy in the analysis of leukocyte trafficking behaviours *in vivo*.

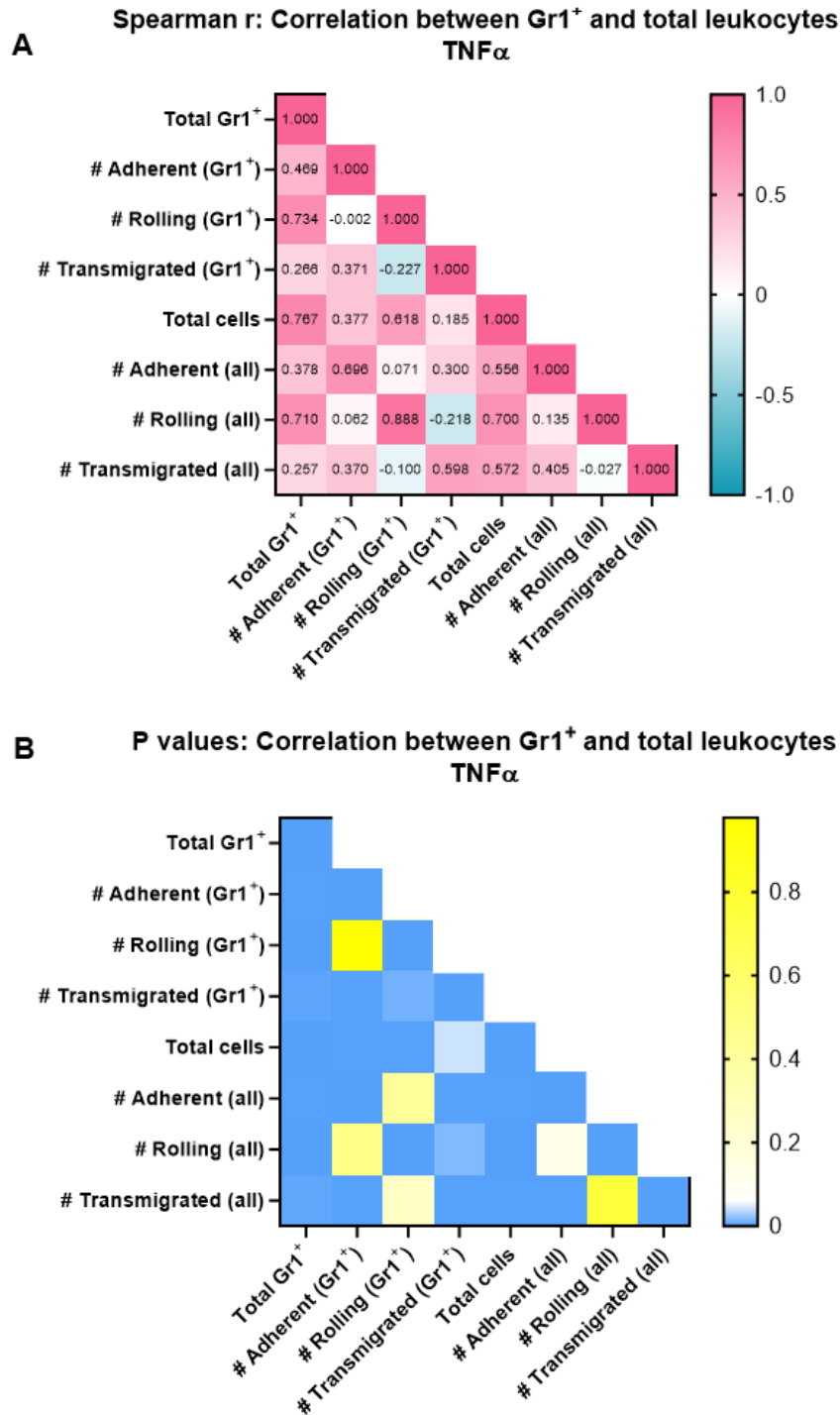


Figure 25 (A-B): Correlation matrix of TNF α intravital microscopy data shows strong positive relationship between the leukocyte trafficking events of Gr⁺ cells and total leukocytes observed by brightfield.

A) The strength of the Spearman's rank correlation coefficient (r) is great between the Gr1⁺ cells and total leukocyte (all) numbers within each parameter analysed (adherent, rolling, transmigrated) where the baseline value of zero is shown in white and values greater in pink and lesser in blue. **B)** p values of the Spearman's r values are denoted as ≤ 0.05 in white, zero in blue, and non-significant values > 0.05 shown in yellow.

Analysis of complete blood counts following IVM identified no significant differences across groups of mice, in any of the cell leukocyte populations (**Figure 26**). Compared to the baseline blood counts of non-inflamed animals, we identify a reduction in lymphocyte numbers of ~2.5 million per millilitre, more like the numbers observed following IL-1 β IVM (**Figure 23A**). Overall, we observed similar trends in leukocyte trafficking between mouse groups, but to a lesser extent than we did in the IL-1 β IVM. Increased rolling flux was most notable in the double knockout mice compared to all other genotypes (**Figure 21B and E**). Since we saw this to a much greater extent in the double knockout mice compared to either of the single knockout mouse, our findings support the notion of a synergistic relationship between galectin-3 and galectin-9 that drives their function in inflammation.

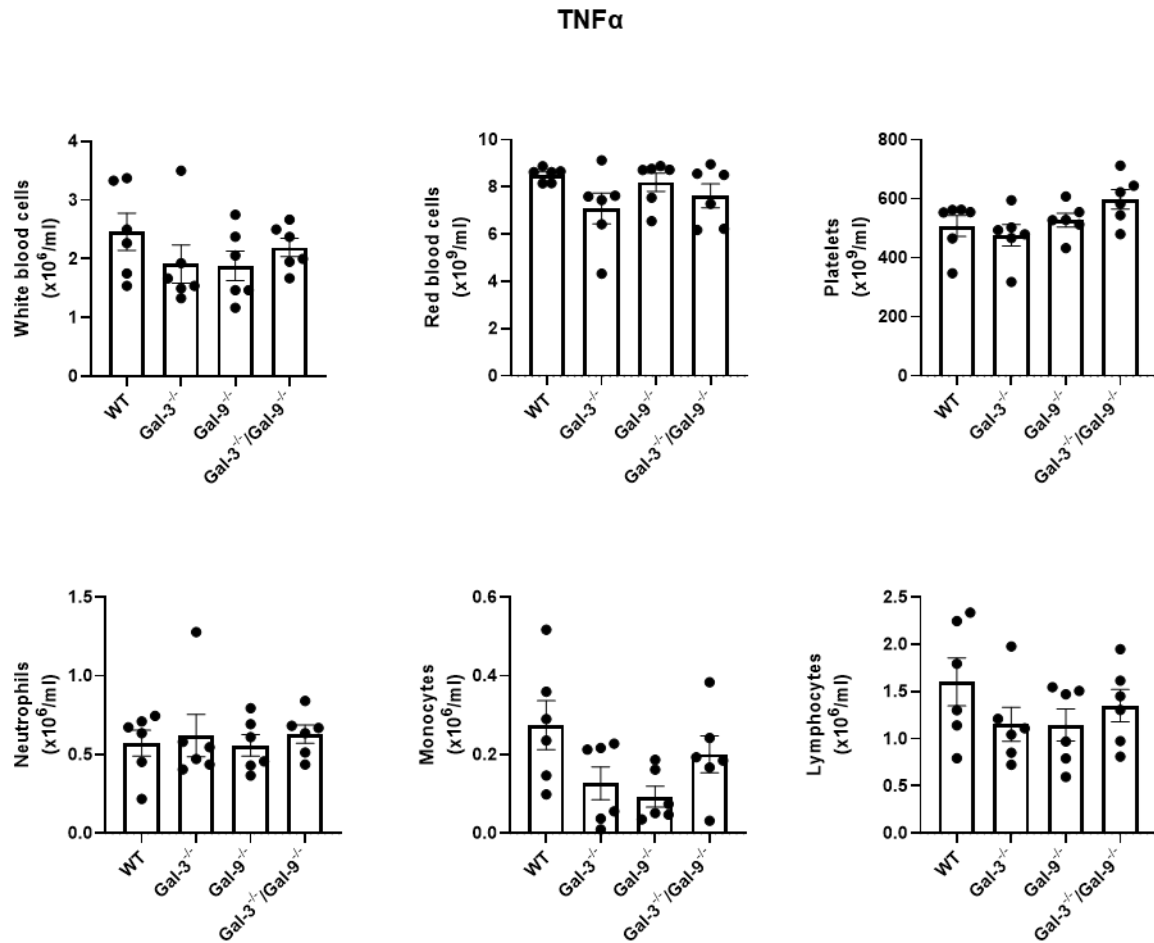


Figure 26 (A-B): Complete blood counts from mice following treatment with TNF α and surgery for intravital microscopy.

No statistically significant differences in complete blood counts between groups of galectin-knockout mice were observed by Kruskal-Wallis test with Dunn's multiple comparison against wildtype control (n = 6). Data displayed as average \pm SEM.

Overall, we find that the leukocyte trafficking response within the inflamed cremaster is dependent on the inflammatory stimuli used in the model. We observed fewer differences in leukocyte trafficking events between galectin-null mice treated with TNF α compared to IL-1 β . Although our use of global-knockout mice sheds insight on the role of endogenous galectins in acute inflammation, we were interested in understanding the role of endothelial-derived galectins specifically. Since we do not have access to endothelial-specific galectin knockout mouse models, we turned to *in vitro* techniques to further investigate the function of endothelial galectins in leukocyte trafficking.

4.3 *In vitro* analysis of endothelial galectins under physiological shear stress

As we previously reported shear stress as a regulator of endothelial galectin-expression (Section 3.2), we aimed to study galectin function under physiological flow. To do this, we used siRNA knockdown to inhibit galectin gene function in HUVEC, before using a modified version of the flow adhesion assay to study leukocyte trafficking events in the absence of endothelial galectins (Cooke et al. 1993).

4.3.1 *Optimisation and validation of siRNA knockdown in HUVEC*

To mimic our experimental groups used in the *in vivo* studies, we aimed to use siRNA to knockdown galectin genes in HUVEC and assess galectin function in a model of inflammation. We assessed siRNA efficacy in HUVEC following knockdown and subsequent treatment with media +/- TNF α + IFN γ . We tested 25 nM of each of the four gene-specific probes in the Qiagen FlexiTube GeneSolution against both *LGALS3* and *LGALS9* to determine which was most efficient in reducing gene transcription. We observed over 70% reduction (dashed line) in *LGALS3* transcription in both TNF α + IFN γ stimulated, and untreated HUVEC from all probes, compared to non-transfected media only control (**Figure 27A**). *LGALS9* knockdown was overall less successful, with only *LGALS9-1* probe able to reduce gene transcription by 70% compared to untransfected control, and only in TNF α + IFN γ -stimulated HUVEC (**Figure 27B**). We observed limited cross-reactivity from most of the siRNA probes against non-specific galectin genes, including *LGALS1* (**Figure 27C**). Of the QIAGEN supplied siRNA probes, we determined *LGALS3-1* (#SI04250799) and *LGALS9-1* (#SI03188409) as the most efficient and specific probes for reducing *LGALS3* (**Figure 27A**) and *LGALS9* (**Figure 27B**) gene transcription, respectively.

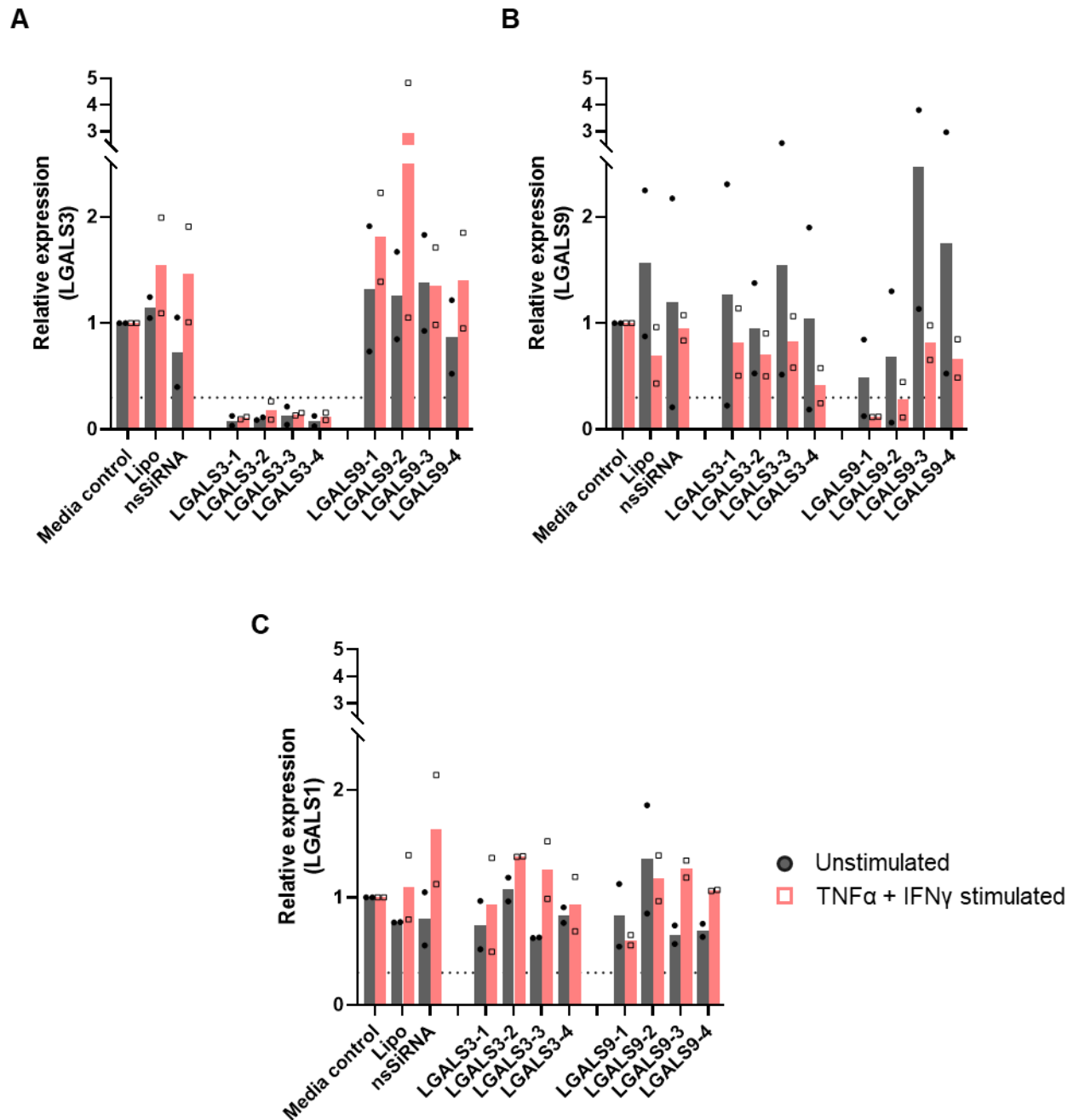


Figure 27: Optimisation of siRNA knockdown of galectin-genes in HUVEC.

siRNA knockdown was performed in HUVEC using 25 nM of four separate probes specific to *LGALS3*, and *LGALS9* genes in OptiMEM, before replacing with fresh media in the presence or absence of TNFα + IFN-γ (10 ng/ml, 20 ng/ml) for 24 hours. Efficient gene knockdown was determined by qPCR analysis of **A)** *LGALS3* and **B)** *LGALS9* gene transcription by at least 70% (dashed line) in HUVEC. To minimise off-target effects, **C)** *LGALS1* gene transcription was also analysed and confirm limited cross-reactivity between gene knockdowns. Bar graph displays the average of two repeats (n=2).

We next wanted to determine the optimal concentration of siRNA for maximum transfection efficacy and for least cross-reactivity to non-specific galectin genes. We determined all concentrations of *LGALS3*-specific probe to be efficient at reducing *LGALS3* transcription in TNF α + IFN γ -stimulated and unstimulated HUVEC, whilst having limited effects on *LGALS1* and *LGALS9* transcription (**Figure 28A**). We determined 10 nM of *LGALS9*-specific siRNA to be most efficient at reducing gene transcription, with the least off-target effects compared to other concentrations (**Figure 28B**). We saw no major changes in *LGALS1* or *LGALS3* transcription with all concentrations of scrambled-control siRNA (**Figure 28C**). There was a limited amount of change in *LGALS9* transcription in scrambled siRNA (sc-siRNA) control, though this was more varied with concentrations greater than 10 nM (**Figure 28C**). From these results, we determined 10 nM to be the optimal concentration for all siRNA treatment conditions since gene-specific transcription was reduced by at least 70% (dashed line) and had limited off-target effects on non-specific galectin genes.

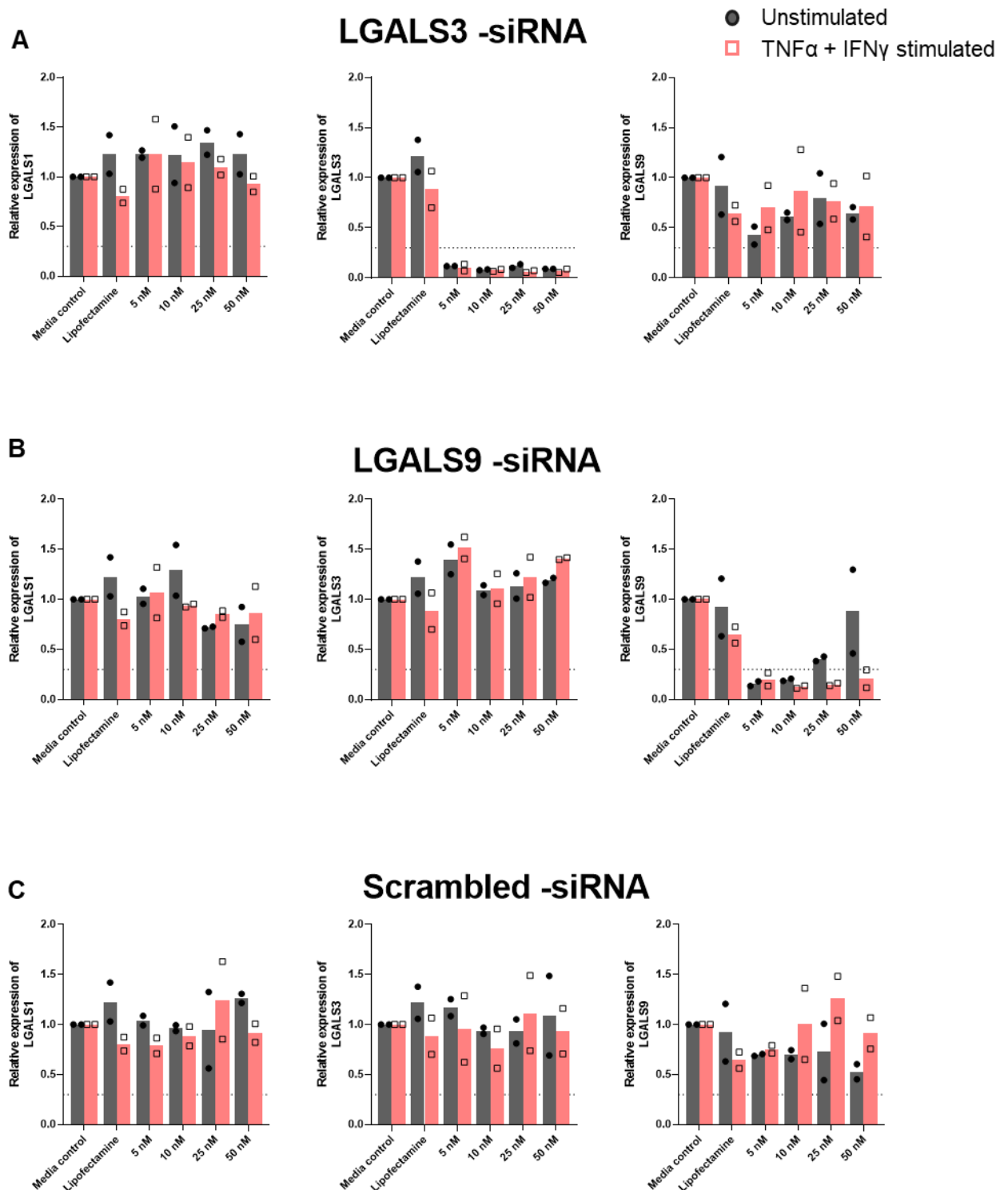


Figure 28 (A-C): Optimisation of probe concentration for *LGALS* knockdown.

Transcription of *LGALS1*, *LGALS3* and *LGALS9* genes in treated and untreated HUVEC were quantified by qPCR following gene knockdown with either 5 nM, 10 nM, 25 nM or 50 nM of siRNA probe specific to **A) *LGALS3***, **B) *LGALS9*** and **C) scrambled control**, shown as relative expression compared to media only control. Validated siRNAs for knocking down each gene were defined as showing at least 70% knockdown as indicated by dashed line on the graph. Bar graph displays the average of two repeats (n=2).

To replicate our *in vivo* experiments using Gal-3 and Gal-9 single and double knockout mice in a model of inflammation, we validated siRNA knockdown (KD) effectiveness under our optimised conditions for Gal-3, Gal-9 and combined Gal-3/Gal-9 knockdown and compared to sc-siRNA control. This time, we increased our replicates and performed TNF α + IFN γ -stimulation the day following siRNA treatment. *LGALS3* transcription was significantly lower in gene-specific single and double knockdown conditions, and not in controls (**Figure 29A**). Similarly, *LGALS9* transcripts were reduced in HUVEC following single-gene and double Gal-3/Gal-9 KD compared to sc-siRNA control (**Figure 29B**), thus confirming successful and specific knockdown of galectins in HUVEC.

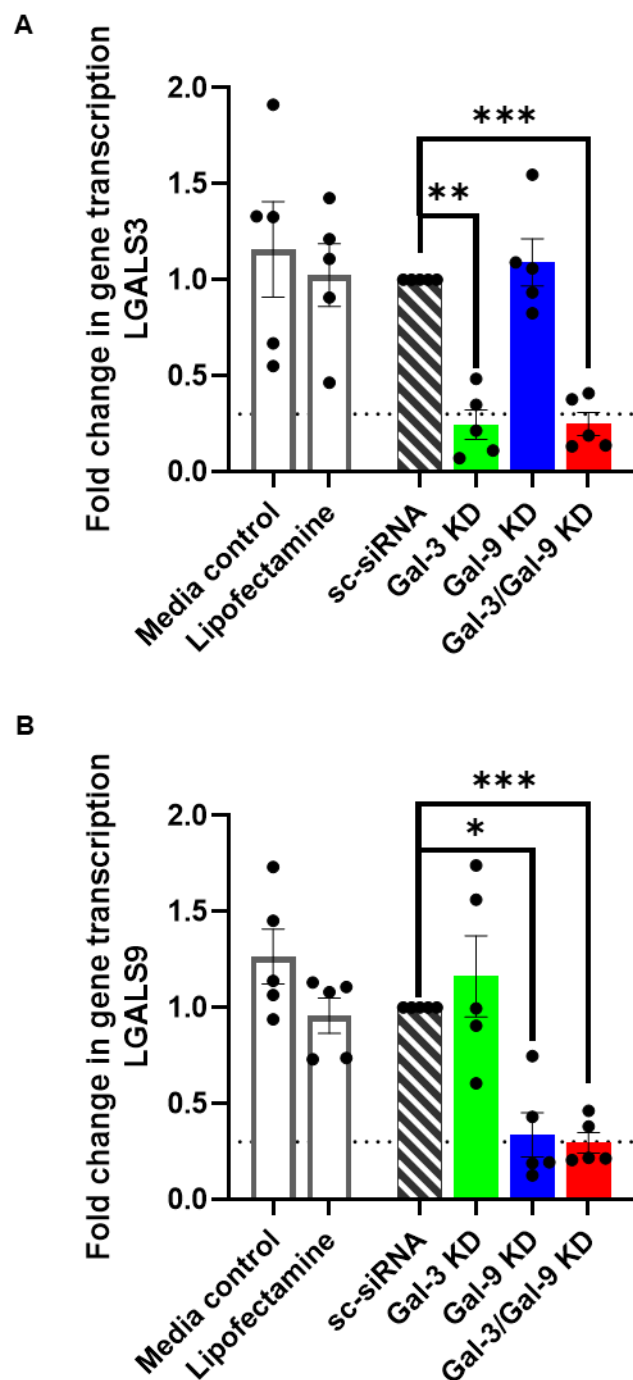


Figure 29: Optimised knockdown of galectin gene transcription in HUVEC by siRNA.

Efficient knockdown of **A)** *LGALS3* and **B)** *LGALS9* genes using 10 nM of gene-specific siRNA was confirmed by qPCR (70% denoted by dashed line) relative to scrambled control in HUVEC treated with TNF α + IFN- γ (10 ng/ml, 20 ng/ml) for 24-hours following siRNA knockdown. Statistical analysis was performed using repeated measures one-way ANOVA with Dunnett's multiple comparison test to untreated control. Data are presented mean \pm SEM (n=5). p-value ≤ 0.05 (*), ≤ 0.01 (**), ≤ 0.001 (***)

To test whether total protein was reduced because of gene silencing, we use Western blot to detect Gal-3 and Gal-9 protein in our samples. siRNA gene knockdown significantly reduced total Gal-3 protein by more than 70% (dotted line) (**Figure 30A**). This was observed in both the single, and double *LGALS3*-specific siRNA treated HUVEC (**Figure 30A**). We did not observe the same reduction in the Gal-9 protein in HUVEC treated with *LGALS9*-specific siRNA probes (**Figure 30B**). We saw two protein bands in the Gal-9 Western blot, which were smudged and of varied intensity within each lane, leading to huge variation in the results between replicates (**Figure 30B**). These results may be inconclusive, at least for measuring galectin-9 protein levels due to the high variation observed (**Figure 30B**). Despite this, and since we were able to show efficient knockdown of both *LGALS3* and 9 by qPCR, we proceeded to use the finalised protocol to knockdown galectin genes in stimulated HUVEC for *in vitro* analysis of leukocyte trafficking under flow.

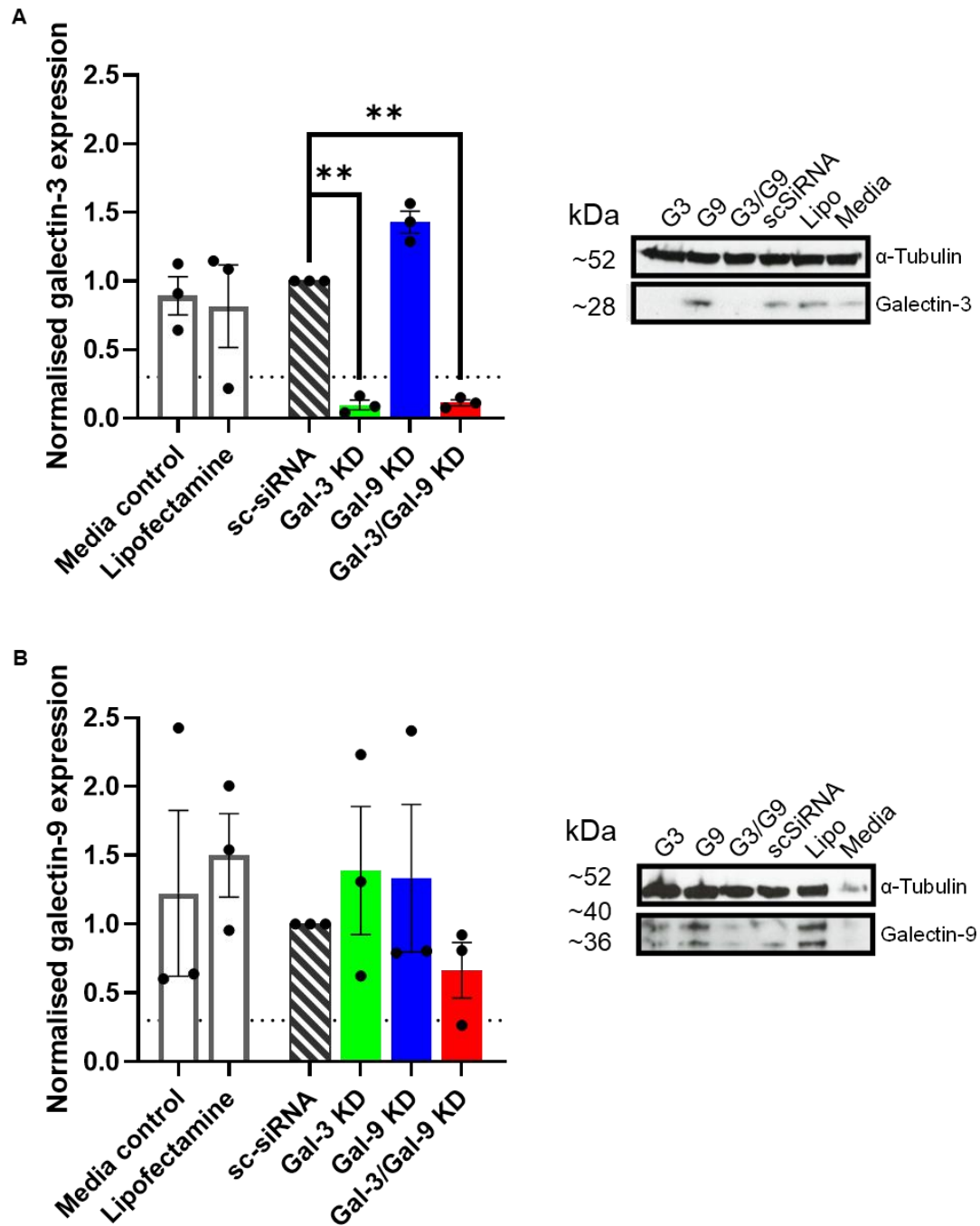


Figure 30: Protein expression analysis following galectin gene knockdown by siRNA.

Protein expression of **A)** Galectin-3 and **B)** Galectin-9 was assessed by Western blot using lysates from cells treated with 10 nM of gene-specific siRNA, control scrambled siRNA, lipofectamine only or no treatment media control, prior to 24-hour stimulation with TNF α + IFN- γ (10 ng/ml, 20 ng/ml). Successful knockdown was determined by a 70% reduction (dashed line) in protein amount. Statistical analysis was performed using RM-one way ANOVA with Dunnett's multiple comparison test to untreated control. Data are presented mean \pm SEM (n=3). p-value \leq 0.01 (**).

4.3.2 *Leukocyte trafficking is modulated in the absence of endothelial LGALS3 and LGALS9 function.*

We seeded HUVEC into ibidi 6-well μ -Slides the day prior to performing knockdowns with siRNA. The following day, cells were stimulated with $\text{TNF}\alpha$ + $\text{IFN}\gamma$ for 24-hours. On the day of the flow adhesion assay, we isolated neutrophils from fresh whole blood for the *in vitro* assay. We used neutrophils since these greater numbers were observed in the CBC of Gal-3^{-/-} and Gal-3^{-/-}/Gal-9^{-/-} knockout mice after our IVM experiments (**Figure 23**). We also know that neutrophils are first responders in the inflammatory response and readily respond to EC activation (Fine et al. 2020). Flow rates were performed at post-capillary shear stress (0.4 ml/min, equivalent to 0.05 Pa) to facilitate leukocyte trafficking. We chose to use multiple HUVEC donors throughout our experiment so that we could capture biological variation in endothelial galectins, whilst limiting variation in our leukocyte responses by keeping our blood donor consistent throughout.

We observed no significant differences in the number of neutrophils that adhered to HUVEC in the inflow across any of the experimental groups compared to scSiRNA control (**Figure 31A**). Of the cells that adhered in the inflow, we observed significantly fewer non-stable ‘touch and go’ interactions in the Gal-3/Gal-9 KD HUVEC group (**Figure 31B**). Within the washout stage, we saw no significant differences between HUVEC groups in the total number of adherent neutrophils (**Figure 31C**), or in the percentage of transmigrated cells (**Figure 31D**) compared to control. The percentage of transmigrated neutrophils was overall low across all HUVEC groups (**Figure 31C**). Our data suggests that although neutrophils are not more likely to engage with Gal-3/Gal-9 KD HUVEC, but once engaged, they are more likely to remain adhered

compared to control. Again, this effect is more prominent within the double knockdown group compared to *LGALS3* and *LGALS9*-silenced single knockdown HUVEC.

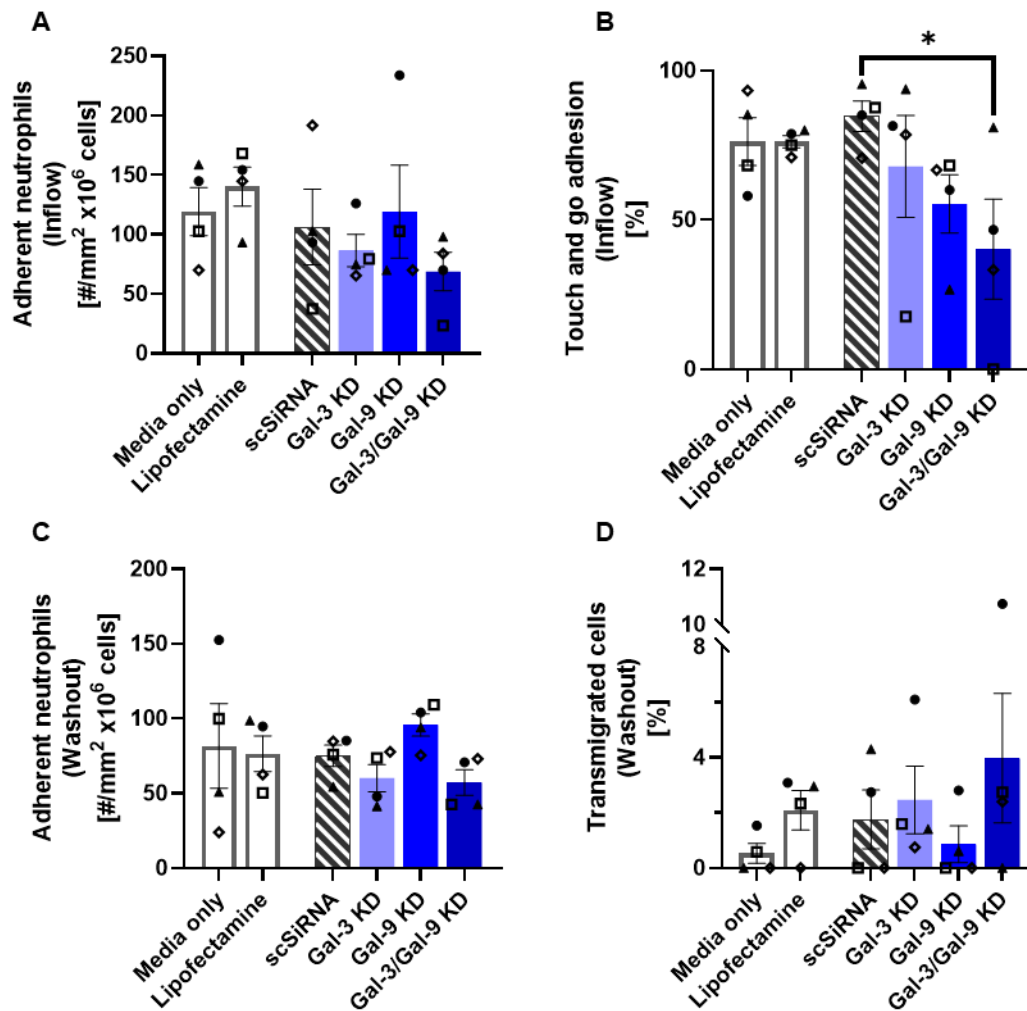


Figure 31: Neutrophils show decreased ‘touch and go’, or non-stable interactions with inflamed HUVEC deficient in both the Gal-3 and -9 genes.

Neutrophil interactions with HUVEC deficient in both Gal-3 and Gal-9 genes, under $\text{TNF}\alpha$ and $\text{IFN}\gamma$ stimulation were analysed with a flow rate of 0.4 ml/min (0.05 Pa). No statistical differences between groups were observed in the **A)** total number of neutrophils adhering to the HUVEC in the inflow, though **B)** a lower percentage of ‘touch and go’ interactions amongst the adhered neutrophils was observed in the HUVEC treated with siRNA for both Gal-3 and Gal-9. No differences were observed for neutrophil behaviour in the washout, as **C)** adherent neutrophils, and **D)** percentage of transmigrated neutrophils did not differ between groups of siRNA treated endothelium. Statistical analysis was performed using Friedman test with Dunn’s multiple comparison test to scrambled siRNA control (scSiRNA). Data are presented mean \pm SEM ($n=4$). p -value ≤ 0.05 (*), ≤ 0.01 (**), ≤ 0.001 (***), with each experimental repeat denoted by a unique shape.

Overall, we observe that the loss-of-function effects of exogenous galectins is greater with the combination of both Gal-3/Gal-9 compared to removal of each single gene. Much like our IVM data in which we observed increased cell flux through the blood vessel, our *in vitro* assay confirms that neutrophils are still rolling across the Gal-depleted endothelium, but that fewer non-stable, or 'touch and go' interactions are taking place. Gittens et al reported increased cell velocity in leukocytes in Gal-3 knockout mice, which may be the parameter necessary to explain the increased cell flux and reduced 'touch and go' interactions *in vitro* (Gittens et al. 2017). This would also explain why once the neutrophil establishes firm interaction with the Gal-3/Gal-9 null endothelium, it remains stable throughout the experiment (**Figure 21 and Figure 24**).

4.4 Discussion

The primary aim of this experimental chapter was to elucidate the function of endogenous galectins in the context of inflammation. To do this, we used a combination of *in vivo* experiments, using IVM to characterise leukocyte trafficking in the inflamed cremaster of galectin-global knockout mice; and *in vitro* experiments mimicking blood vessels to specifically study endothelial galectins. Our main findings show that: a) there are differences between galectin-knockout mice in the numbers of leukocyte subpopulations within the peripheral blood; b) leukocyte rolling flux within the inflamed cremaster microcirculation is increased in the absence of both Gal-3 and Gal-9, though this is dependent on the inflammatory stimuli used; and c) in the absence of both endothelial Gal-3 and -9, fewer non-stable interactions take place between neutrophils and HUVEC. These data demonstrate that endothelial galectins may work synergistically to regulate immune functions in leukocyte trafficking, particularly since the effect observed in double knockout mice is greater than in their single-knockout counterpart.

4.4.1 Characterisation of galectin knockout mice

We report that rolling flux in the IL-1 β inflamed cremaster is significantly increased in Gal-3^{-/-}/Gal-9^{-/-} mice compared to wildtype control. This is a novel observation and has not previously been reported. Gittens et al. have previously characterised the Gal-3 knockout mice with the same parameters and stimuli with which our studies were designed. In this report, they observed that the average cell flux was greater in Gal-3 KO mice compared to WT, though not significantly (Gittens 2014). We report the same observation in the Gal-3^{-/-} mice within our own data, and in the absence of Gal-9 this increase in flux is even greater (**Figure 21**). Gittens et al. report that Gal-3^{-/-} mice

displayed increased rolling velocities compared to WT control (Gittens et al. 2017). Whilst we didn't directly measure the cell rolling velocities, we might speculate that increased cell rolling flux through the vessel would positively correlate with increased cell velocity, as fewer cells participate in slow rolling. However, several reports using IVM to study genetically modified mice report the opposite of this, showing that as flux increases, cell velocity decreases (Perez-Del-Pulgar et al. 2001) (Sperandio et al. 2001). Of course, these reports could be due to genotype effect. As such, we determine that our data requires additional analysis to interpret cell rolling velocities for direct comparison to the reports on differences in leukocyte trafficking between Gal-3^{-/-} mice compared to wildtype *in vivo*.

We observed significant differences between mice groups in the overall neutrophil counts within the blood following IVM (**Figure 23**). Although this was only determined significant by Kruskal-Wallis test, and not in our post hoc test comparing knockout groups to WT control, it might be the reason we see increased cell flux in Gal-3^{-/-}/Gal-9^{-/-} mice compared to WT (**Figure 21**). Then again, we report a similar number of neutrophils in the CBC of the Gal-3^{-/-} group, for which we did not observe the same increase in cell flux compared to WT (**Figure 23 and Figure 21**). As such, this may be the only determining factor for the differences we observe *in vivo*. Ideally, we would perform CBC analysis from each mouse using blood pre- and post- IVM. We were unable to take blood samples prior to IVM, due to limitations in access to the animal housing unit, and some mice were excluded from post-IVM CBC analysis due to lack of proficiency in executing blood collection from IVC.

Our data suggests that Gal-3 and Gal-9 are required for leukocyte tethering and rolling. Whilst leukocyte rolling is mediated by selectins found on both endothelial cells and

leukocytes, we later-on identify Gal-3 as a ligand for E-selectin (SELE) which might be a key interaction that regulates leukocyte tethering and rolling (**Table 5**). Gittens et al report that membrane expression of SELE on lung EC's is lower in Gal-3^{-/-} mice (Gittens 2014). Since SELE is only synthesised in response to endothelial activation, endogenous Gal-3 may be necessary for the synthesis and/or translocation of SELE to the cell surface (Bevilacqua et al. 1987). Additionally, since α 4-integrin-like CD44 and Vascular adhesion protein-1 (VAP-1) work independently of selectins (Salmi et al. 2001), Gal-9 might be targeting this pathway alongside Gal-3 targeting SELE, hence we observe greater phenotypic effects in the double knockout mice compared to the single galectin knockouts. We could study this in the first instance, by using confocal microscopy to track the localisation of SELE and VAP-1 for example, in galectin-null ECs.

We observed no significant differences in the number of transmigrated leukocytes in the IL-1 β inflamed cremaster between galectin-knockout mice. This contradicts reports from Gittens et al. who observed ~50% fewer transmigrated cells in the Gal-3^{-/-} mice group, compared to <10% reduction we saw compared to wildtype control (Gittens et al. 2017). Within our data alone, we observe great variation in the number of transmigrated cells across different vessels in the same mouse. The disparity between these results is perplexing, though may be explained by confounding factors in the IVM methodology. Since the cremaster is a delicate and highly vascularised muscle, it is prone to damage from handling. The necessary cauterisation of blood vessels can cause changes in shear stress and blood velocity within the occluded and collateral vessels, which may not be apparent at the time of imaging (Meisner et al. 2012). Despite the standardisation of vessel diameter between groups, shear stress within blood vessels can be highly variable and could influence the trafficking parameters

being analysed (Meisner et al. 2012). Reduced shear stress increases leukocyte tendency to migrate across the endothelium (Moazzam et al. 1997), and redirection or reperfusion of blood flow in the occluded and collateral vessels can also lead to increased leukocyte trafficking that might explain the variation in the reported data (Granger 1999). Considering the role for Galectin-3 in neovascularisation (Nangia-Makker et al. 2002), there may also be differences in the branching and looping of vessels within the cremaster that makes Gal-3 null mice less susceptible to vessel damage during surgery (Meisner et al. 2012). Thus, it may be dependent on the researcher analysing a representative selection of blood vessels to report accurate data. We reported data from each individual blood vessel for transparency on the variation observed within each mouse. Overall, we found no differences in the number of adhered and transmigrated cells between galectin-knockout mice and WT control, following stimulation with IL-1 β .

We observed different trends between mice in leukocyte trafficking behaviours dependent on the stimuli used. We report significantly fewer transmigrated Gr1⁺ cells in the inflamed cremaster of Gal-3^{-/-}/Gal-9^{-/-} mice compared to WT, following stimulation with TNF α (**Figure 24**). Meanwhile Gittens et al report significantly fewer transmigrated cells in the Gal-3 KO groups compared to WT, only in response to IL-1 β injection and not TNF α (Gittens et al. 2017). Whilst other studies report that Gal-3^{-/-} mice have reduced leukocyte infiltration compared to wildtype, such as in bronchoalveolar lavage fluid following ovalbumin-challenge (Ge et al. 2010), and in the central nervous system in a model of experimental autoimmune encephalomyelitis (Jiang et al. 2009). Meanwhile, Galectin-3 has been reported to play a protective role in infection, as one study reports that Gal-3^{-/-} mice used in a DSS model of colitis displayed increased immune cell infiltration compared to wildtype (Tsai et al. 2016).

Another study found that in the absence of Gal-3, mRNA for TNF α , IL-1 β were significantly upregulated, and IL-10 downregulated in the liver and spleen following LPS stimulation (Fernandez-Martin et al. 2022). These highlight differential mechanisms of Gal-3 dependent on the stimuli. As for the function of Gal-9, one study found that following injection of Gal-9 into the cremaster, leukocytes were recruited to the site of inflammation as evidenced by greater numbers of adhered and emigrated Ly6G cells (Iqbal et al. 2022). We observed no significant differences in cell behaviours in the absence of Gal-9 with either stimulus. Based on our data from Chapter 3, we should investigate leukocyte trafficking events in Galectin knockout mice in a model of viral infection of the liver, since we predict a strong link between galectin-9 function in response to viral immunity.

Several studies that use IVM to investigate leukocyte trafficking behaviours *in vivo*, report similar numbers within each measured parameter in response to both IL-1 β and TNF α in their C57BL6 wildtype groups (Gittens et al. 2017) (Young, Thompson, and Nourshargh 2002). Meanwhile, we saw ~28% fewer transmigrated cells in our TNF α analysis, compared to IL-1 β . Interestingly, one study reports that the peak of leukocyte accumulation to the site of inflammation is 30-60 minutes for TNF α , followed by a second peak at 90-135 minutes (Chandrasekharan et al. 2007), and 3-4 hours for IL-1 β (Young, Thompson, and Nourshargh 2002; Rampart et al. 1989). This suggests that our intravital microscopy observations are within the resolution stage, supported also by the lack of differences between mouse groups in the CBC analysis post-IVM. Alternatively, the potency of the TNF α used may not have been sufficient in generating an immune response.

To summarise this section, we report that rolling flux was significantly increased in Gal-3^{-/-}/Gal-9^{-/-} mice compared to WT control, following IL-1 β stimulation. One study observed by flow cytometry that TNF α , but not IL-1 β , directly stimulated L-selectin shedding and β 2 integrin expression on mouse neutrophils (Young, Thompson, and Nourshargh 2002). Gal-8 has previously been reported to interact with β 2 integrin, *LFA-1*, to displace *ICAM1* binding (Vicuna et al. 2013). Unsurprisingly, endothelial Gal-9 was also recently proposed as a binding partner of β 2 integrin, which facilitates monocyte capture under flow (Krautter et al. 2022). Meanwhile, Gal-3 binding to β 1 integrins was reported across several studies (Sedlar et al. 2021). As such, our observation of differences in leukocyte rolling flux in the double-knockout mice could be due to inhibited galectin-integrin interactions. We hypothesised that this observation was due to the lack of endogenous endothelial galectins, rather than a result of inhibited galectin expression in leukocytes and used *in vitro* assays to determine this.

4.4.2 Flow adhesion assay

Since we did not have access to endothelial-specific galectin knockout mice, we instead performed siRNA knockdown of endothelial galectins in HUVEC and performed flow adhesion assays to mimic our *in vivo* experimental design. Following siRNA knockdown of *LGALS3* and *LGALS9*, we saw a significant reduction in transcription of both genes of around 70%, compared to scrambled control. Interestingly, we observed a similar efficacy of knockdown in the protein expression of Gal-3, but not for Gal-9. Several other members of our group have reported 30-75% reduction in intracellular expression, and ~25% reduction in extracellular Gal-9 protein following siRNA knockdown, as measured by flow cytometry (Mansour et al. 2022),

(Krautter et al. 2022). We used Western blot for quantification in this instance and observed smearing in our blots that made quantification highly variable between repeats. Paralogs of *LGALS9* encoded by distinct genes have similar protein sequences, size and folding to Gal-9 but may be less susceptible to the siRNA knockdown but still detected by anti-Gal-9 antibodies. This could explain why we observe multiple intense bands for Gal-9 by Western blot, and the discrepancy between results observed by qPCR.

Functionally, we observed a reduction in the percentage of neutrophils performing 'touch and go', or non-stable interactions with Gal-3^{-/-}/Gal-9^{-/-} HUVEC. This was not accompanied by an increase in the number of firm adhered neutrophils, suggesting that interactions were not necessarily more stable, but rather that there were less non-stable interactions taking place. Since the flow rate and number of neutrophils were standardised across all conditions, our results may indicate increased cell rolling flux, similar to what was observed *in vivo*. In which case, we might apply the same hypothesis that neutrophil tethering and slow rolling could be inhibited in the absence of both galectins, and to a much greater extent than the single genes alone. We only performed this experiment with HUVEC stimulated with TNF α and IFN γ and will require repeat experiments using different inflammatory stimuli to determine whether these effects are stimulus-specific like the responses observed *in vivo*.

4.4.3 Limitations

Crucially, some of our results within each parameter studied by IVM, differed depending on our analysis method, either using fluorescence or brightfield analysis. We speculate brightfield is most representative and inclusive of leukocyte behaviours in transmigration, since labelling might be less efficient on cells that have

transmigrated prior to administration of the fluorescently labelled antibody and thus might be excluded from counting in the fluorescence analysis. Indeed, it may be possible that the unlabelled cells are not positive for Gr1, although we determined that these cells were not of lymphocyte origin, so instead may be lowly expressing Ly-6G and/or Ly-6C (Rose, Misharin, and Perlman 2012). On the other hand, fluorescently labelled cells are much easier to count when analysing adherent cells and rolling flux, since the contrast between the fluorescence and background makes cells easily distinguishable across several planes of the vessel. Instead, delivery of a fluorescent antibody cocktail specific to Gr-1 and CD11b, for example, might be a more accurate and inclusive marker for analysing leukocyte behaviours *in vivo* (Rose, Misharin, and Perlman 2012). Contrary to this, the lack of normal distribution within our results highlights a potential lack of stratification of cells, and oversimplification of 'leukocyte' behaviours *in vivo*. Crainiciuc et al, characterised the behavioural landscape of leukocytes observed *in vivo* during inflammation via IVM, and identified three distinct clusters, based on 73 morpho-kinetic parameters which closely linked with changes in genetic and signalling networks as identified by single-cell RNA sequencing (Crainiciuc et al. 2022). Taking this top-down approach, they identified key molecular switches, namely the *FGR* gene, as a driver of pathogenic neutrophil state and vascular inflammation (Crainiciuc et al. 2022). As such, the nuances of endogenous galectin function may be better understood through greater interrogation of leukocyte behaviours *in vivo*.

Although we observed significant differences between groups in one parameter observed by flow adhesion assay, we would expect to observe ~50% transmigration under flow, which was not reached in our experiment (Sheikh et al. 2005). We observed less than 4% transmigration overall (**Figure 31**). This may have been a result

of TNF α degradation over time, resulting in reduced TNF α potency. We used the same TNF α stocks throughout all experiments to maintain consistency. However, the flow adhesion assays should be repeated using a new batch of TNF α so that we can observe any differences between groups to a larger effect.

In summary, we are the first to characterise leukocyte trafficking within the TNF α and IL-1 β inflamed cremaster of Gal-3^{-/-}/Gal-9^{-/-} mice. We showed similar results in our flow-based adhesion assay, suggesting that endothelial galectins are the key driver of this phenotype. Overall, this suggests that expression of both Gal-3 and Gal-9 in endothelial cells is crucial for regulating early stages of the leukocyte adhesion cascade.

CHAPTER 5: INVESTIGATING INTERACTIONS BETWEEN EXOGENOUS GALECTINS AND ENDOTHELIAL CELLS

5.1 Introduction

We have previously described virus-associated inflammatory mediators and shear stress as potent regulators of endogenous endothelial galectin expression. Additionally, we have linked the expression of endogenous endothelial galectins to their function in facilitating leukocyte trafficking in the inflamed blood vessels, using both *in vivo* and *in vitro* techniques. Although sometimes anchored within the cell membrane, galectins are inherently soluble proteins which exert their function through binding to glycan ligands on the surface of cells or within the extracellular matrix. Despite being broad glycan-binding proteins, each galectin type displays preferential specificity for certain branched glycan's and glycan motifs attached to proteins and lipids alike. These interactions vary in their strength and as such, the weaker but physiologically relevant interactions between galectins and their ligands may go undetected and remain insufficiently described in the literature.

We worked collaboratively with Dr Mia Huang and Dr Geno Joeh at Scripps Research, to identify interactors of galectin-3 on the surface of endothelial cells, to elucidate galectin functions in the inflammatory response. To do this, we used a fusion protein comprised of ascorbate peroxidase enzyme and galectin-3, to tag proteins within a 20 nm radius of PX-Gal3 bound on the surface of HUVEC. We aimed to compare protein interactors on TNF α + IFN γ stimulated and unstimulated HUVEC, to further elucidate galectin function in inflammation. We hypothesise that this technique will allow us to identify novel binding partners of galectin-3 and explore their potential as functional interactions that might be regulating the inflammatory immune response.

5.2 Optimisation of proximity labelling galectin interactors on live cells

To validate the fusion protein in HUVEC and to determine the optimal concentration for labelling, increasing concentrations of PX-Gal3 fusion protein were added to fixed HUVEC, alongside PBMCs as a positive control (Joeh et al. 2021). Using flow cytometry, we observed an increase in the side scatter profile (SSC) in both HUVEC and PBMCs with increasing concentrations of PX-Gal3. Cell populations went from 57.2% and 75.3% in untreated conditions, to 6.52% and 3.66% following labelling with 200 nM PX-Gal3 in HUVEC and PBMCs respectively (**Figure 32A**). Since the cells were fixed prior to labelling, the increase in SSC was unlikely to be due to cells undergoing apoptosis or necrosis (Vermes, Haanen, and Reutelingsperger 2000). Notably, precipitates formed in solution following incubation with PX-Gal3 and biotin-phenol (**Figure 32B, left**) which appeared to further aggregate after the quenching step, as precipitates appeared to clump together more in the absence of PX-Gal3 than in its presence (**Figure 32B, right**). This phenomenon was not due to aggregation or degradation of the PX-Gal3 protein, since only one single band was observed on the SDS PAGE gel (**Figure 32C**). We next considered the effect of fixing the cells prior to labelling, and whether this was responsible for causing the shift in the SSC.

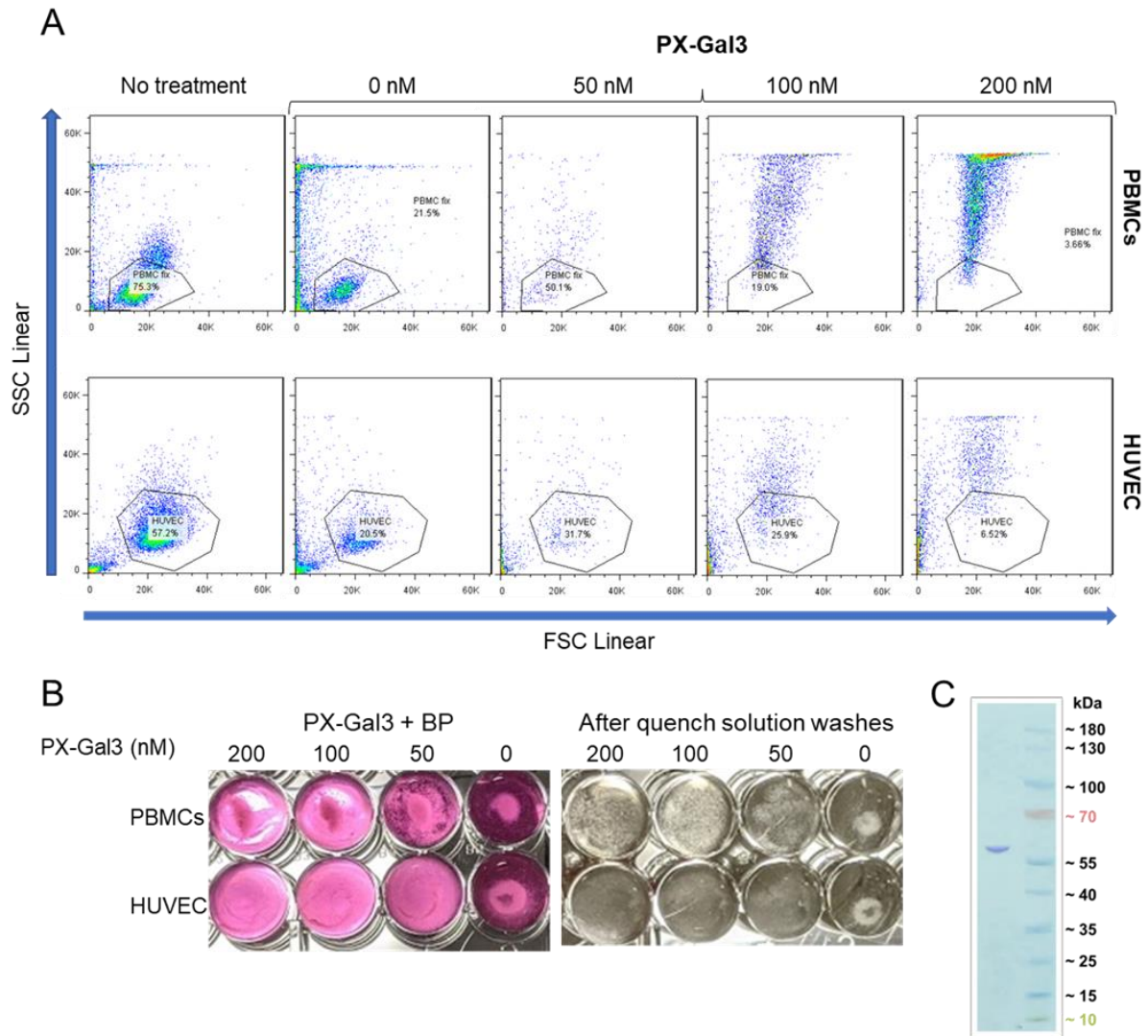


Figure 32: Proximity labelling of PFA-fixed PBMCs and HUVEC with PX-Gal3 in solution leads to a shift in side scatter, associated with aggregates.

PBMCs and HUVEC were fixed with 4% PFA prior to incubation with increasing concentrations of PX-Gal3 for 30 minutes. Cells were washed in PBS before undergoing 30-minute incubation with 500 μ M biotin-phenol in DMEM and adding 100 mM hydrogen peroxide for one minute. The reaction was stopped through three washes of the cells with quench solution. A) Cell populations were gated by forward (FSC) and side scatter (SCC) and showed a shift in SSC with increasing concentrations of PX-Gal3, as determined by flow cytometry. B) Aggregates were observed in solution following the incubation with biotin-phenol (left) and remained until the end of the experiment (right). C) A single band of PX-Gal3 protein was observed by SDS-PAGE gel.

Since PFA is known to precipitate out of solution and can be highly reactive to certain chemicals, the labelling was repeated in live PBMCs without prior fixing. The population of PBMCs went from 80% in the untreated PBMCs to 65 – 66% in the 50 nM and 100 nM treatments respectively (**Figure 33**). A larger shift in the population

SSC was observed only at the highest concentrations of PX-Gal3 labelling, where the population of PBMCs reduced to 28% (**Figure 33**). Overall, the observed shift in SSC was less prominent, but still present in the live cells versus fixed, suggesting that the PFA was interfering with the assay.

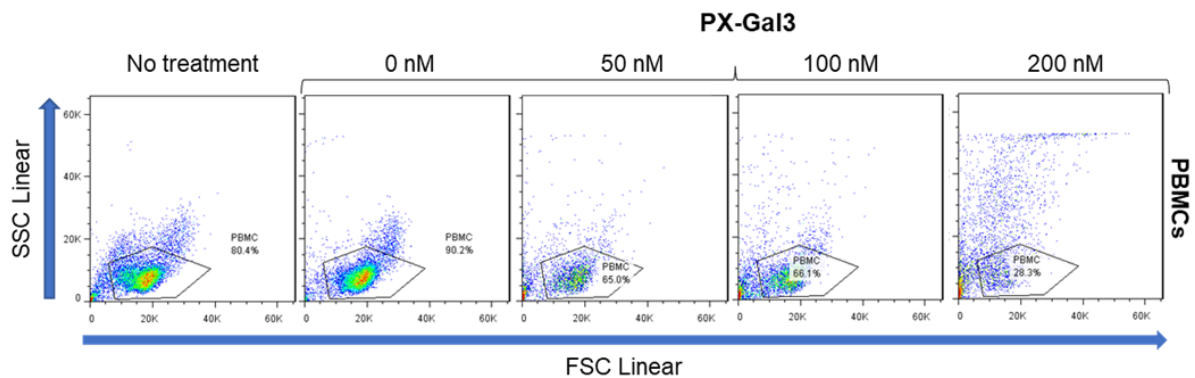


Figure 33: PX-Gal3 binding to live PBMCs causes a shift in the side scatter plot with increasing concentrations.

Live PBMCs were treated with increasing concentrations of PX-Gal3 and subsequent biotin-phenol, hydrogen peroxide and quench solution to perform the labelling experiment. Cell population as measured by forward (FSC) and side scatter (SSC) shifted with increasing concentrations of PX-Gal3.

We next sought to determine whether the increase in SSC was a phenomenon of exogenous Gal-3 interactions with the cells or was only being observed following incubation with the Gal-3 fusion protein. First, we treated live PBMCs and HUVEC with increasing concentrations of recombinant human Gal-3 (rGal3, carbohydrate recognition domain only). The PBMC population remained between 76 and 78% regardless of the concentration of rGal3 (**Figure 34A**). Gating on the PBMC population and looking only at the single, live cells, a concentration dependent increase in fluorescence intensity was observed, thus confirming the binding of rGal3 to PBMCs (**Figure 34B**).

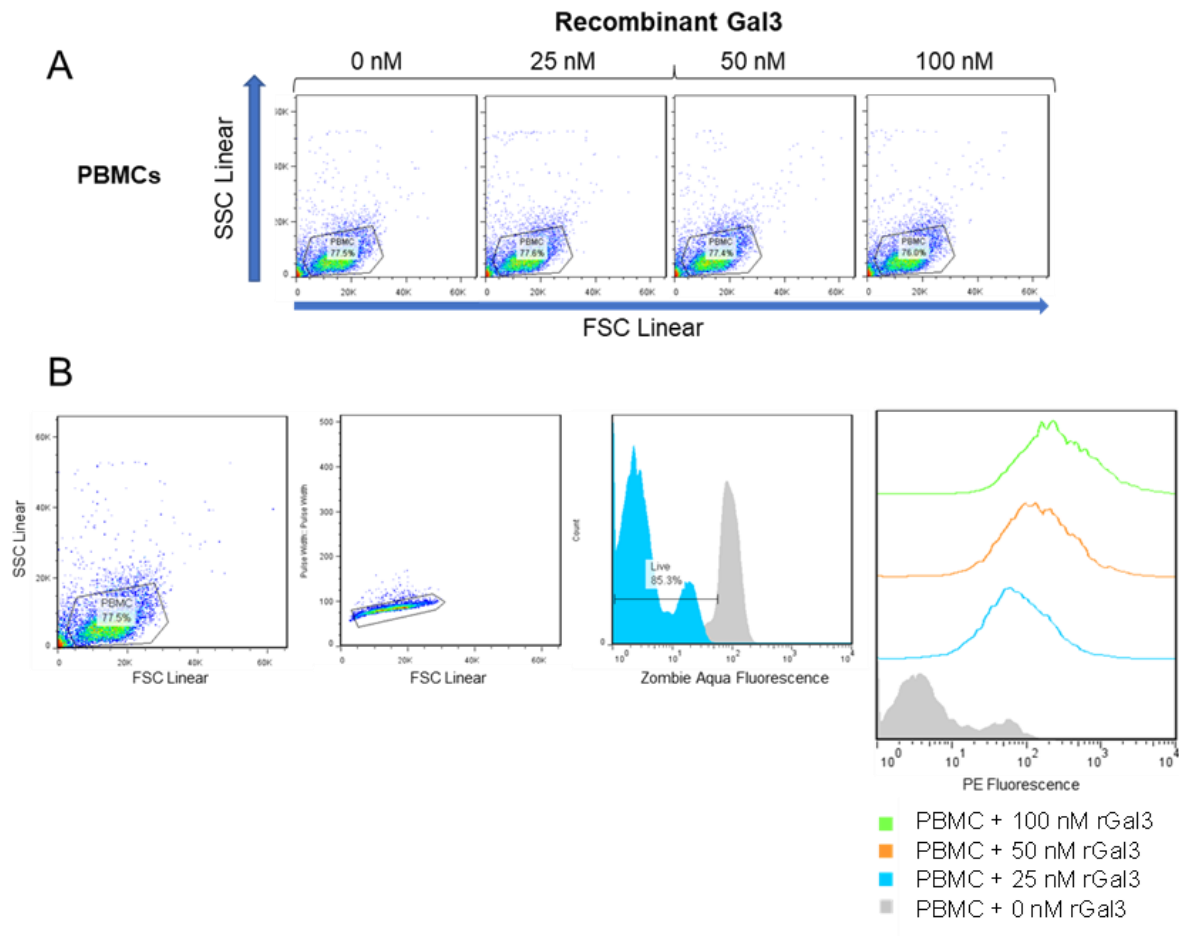


Figure 34: rGal3 binding to live PBMCs does not cause a shift in side scatter plot with increasing concentrations.

A) Percentage population of PBMCs following incubation with increasing concentrations of rGal3 was determined by forward (FSC) and side scatter (SSC) profile by flow cytometry. B) Binding of rGal3 on the single-cell population of live PBMCs was determined by mean fluorescence of bound PE-conjugated anti-Gal3 antibody.

A similar observation was found in HUVEC, with the population ranging between 39-45% following treatment with increasing concentrations of rGal3 (**Figure 35A**). As with the PBMCs, the increase in fluorescence intensity confirmed Gal-3 binding to HUVEC in a concentration dependent manner (**Figure 35B**). These results confirm that the CRD of rGal3 alone, was not causing a shift in SSC of PBMCs and HUVEC, and that binding of rGal3 to the surface of the cells could be detected.

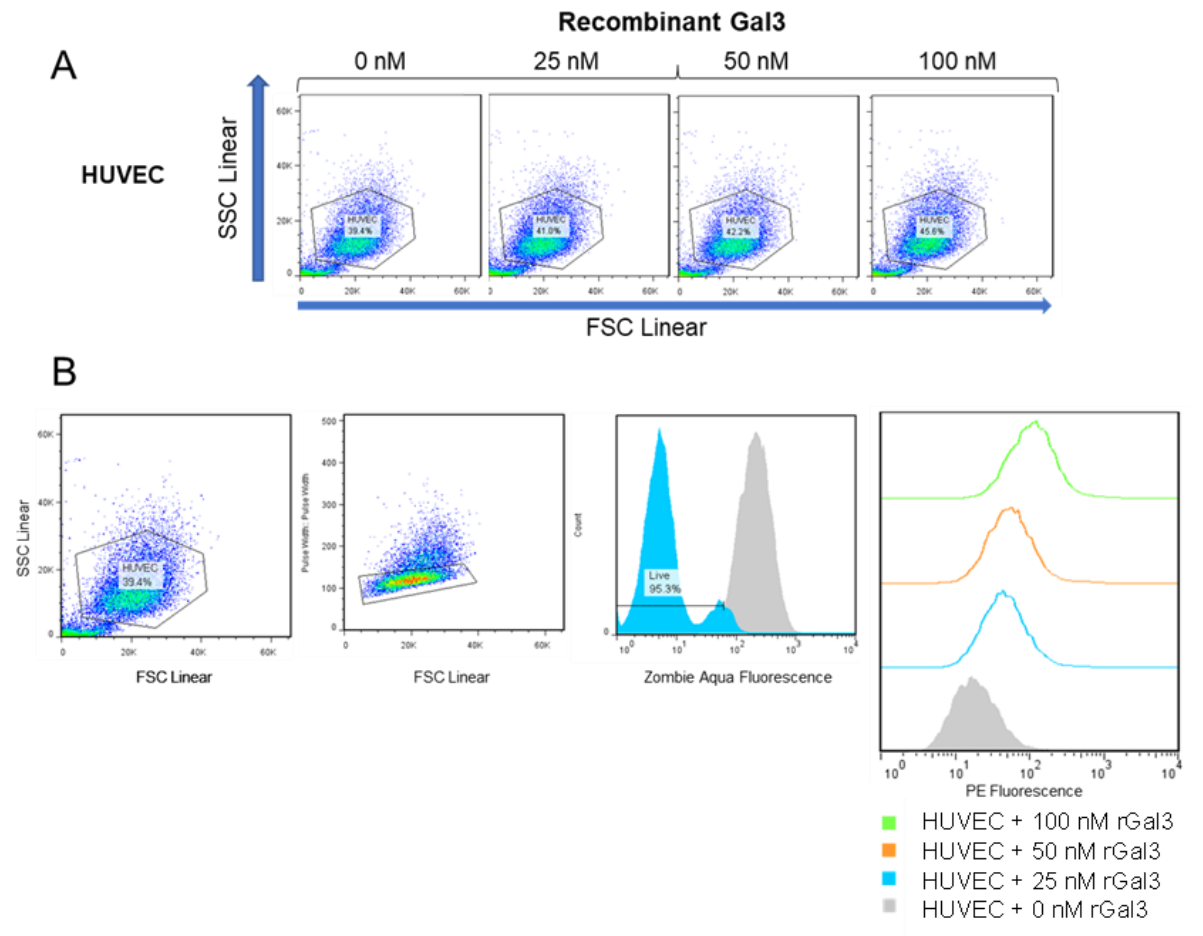


Figure 35: rGal3 binding to live HUVEC does not cause a shift in side scatter plot with increasing concentrations.

A) Percentage population of HUVEC following incubation with increasing concentrations of rGal3 was determined by forward (FSC) and side scatter (SSC) profile by flow cytometry. B) Binding of rGal3 on the single-cell population of live HUVEC was determined by mean fluorescence of bound PE-conjugated anti-Gal3 antibody.

When the same cells were incubated with PX-Gal3, the population of PBMCs was reduced from 77.6% in the negative control to 33% following treatment with 100 nM PX-Gal3, due to a shift in the SSC (**Figure 36A**). Surprisingly, we did not observe a concentration dependent shift in fluorescence intensity following incubation with PX-Gal3 (**Figure 36B**).

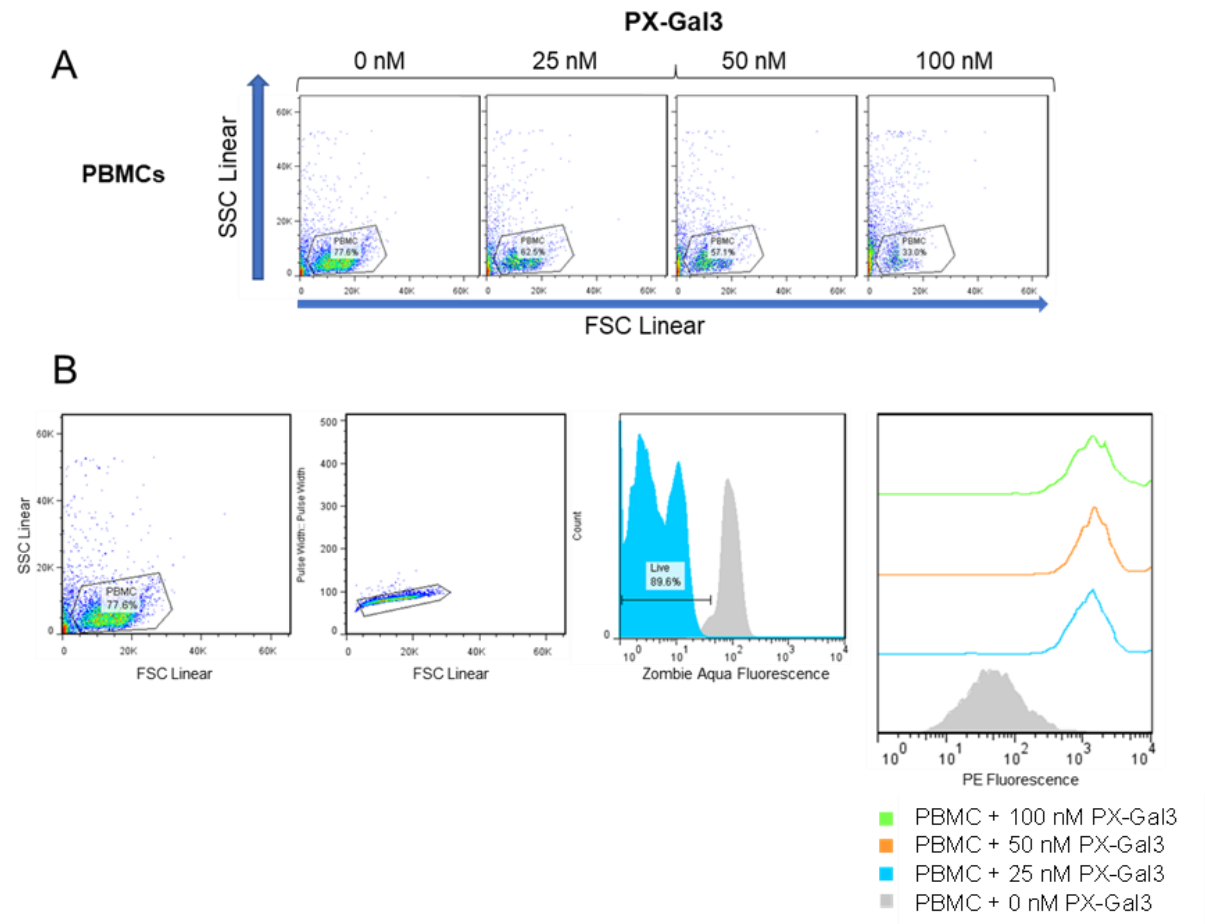


Figure 36: PX-Gal3 binding to live PBMCs causes a shift in side scatter plot with increasing concentrations.

A) Percentage population of PBMC following incubation with increasing concentrations of PX-Gal3 was determined by forward (FSC) and side scatter (SSC) profile by flow cytometry. B) Binding of PX-Gal3 on the single-cell population of live PBMC was determined by mean fluorescence of bound PE-conjugated anti-Gal3 antibody.

There was no observed shift in the SSC in HUVEC following incubation with PX-Gal3 since the starting cell population was unexpectedly small, meaning the variation between 11.5% and 19.5% in population size had no relation to concentration (**Figure 37A**). As with the PBMC population, PX-Gal3 binding to HUVEC was independent of concentration (**Figure 37B**). Since SSC is a measure of internal complexity of each cell, it's possible that the PX-Gal-3 is penetrating the cell membrane, causing the concentration dependent shift in SSC whilst leaving the fluorescence intensity unaffected. This may be since surface bound PX-Gal3 is likely to be saturated. Overall,

we have shown that the PX-Gal3 is successfully binding to HUVEC alongside the PBMC control.

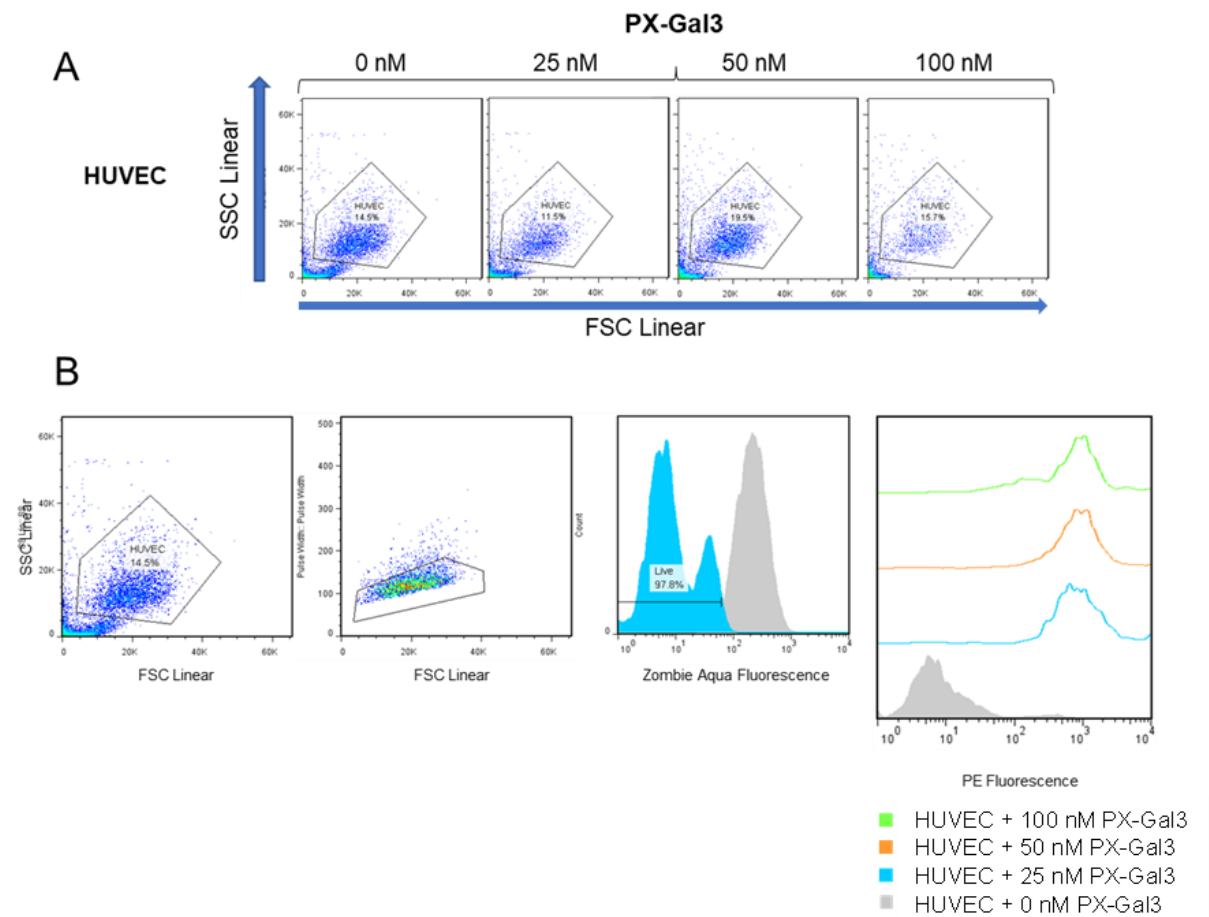


Figure 37: No shift was observed in HUVEC scatter plot following incubation with increasing concentrations of PX-Gal3.

A) Percentage population of HUVEC following incubation with increasing concentrations of PX-Gal3 was determined by forward (FSC) and side scatter (SSC) profile by flow cytometry. B) Binding of PX-Gal3 on the single-cell population of live HUVEC was determined by mean fluorescence of bound PE-conjugated anti-Gal3 antibody.

The next stages of optimisation were performed at Scripps, FL, USA, using pooled Promocell HUVEC made up of three donors of mixed genders. We wanted to test proximity labelling on adherent HUVEC *in situ*, using immunofluorescence to determine successful biotinylation of proteins. We chose to include an intermediate concentration of 75 nM PX-Gal3 within our optimisation test since we aimed to find a balance between minimising disruption to cell morphology whilst obtaining the

maximum amount of tagging possible. We chose to use the intermediate concentration of 75 nM to ensure saturated surface binding whilst limiting the shift/aggregation observed with 100 nM concentrations of PX-Gal3 by flow cytometry (**Figure 37**).

We observed successful biotinylation of HUVEC following incubation with all conditions containing PX-Gal3, with similar staining observed in the 75 nM and 50 nM, whilst appearing to be less intense at the highest concentration of 100 nM PX-Gal3 (**Figure 38A**). Of note, we observed disruption to the endothelial monolayer following the labelling protocol with all concentrations of PX-Gal3 (**Figure 38B**). We attributed this to the absence of supplements in the PX-Gal3/DMEM incubation step since we also observed HUVEC detachment and monolayer disturbance in HUVEC after incubation with DMEM only for 20 minutes (**Figure 38C**). We therefore aimed to adjust the incubation times within the labelling protocol to minimise monolayer disruption. We performed all optimisation steps using 75 nM of PX-Gal3, since this concentration showed sufficient labelling in the original protocol.

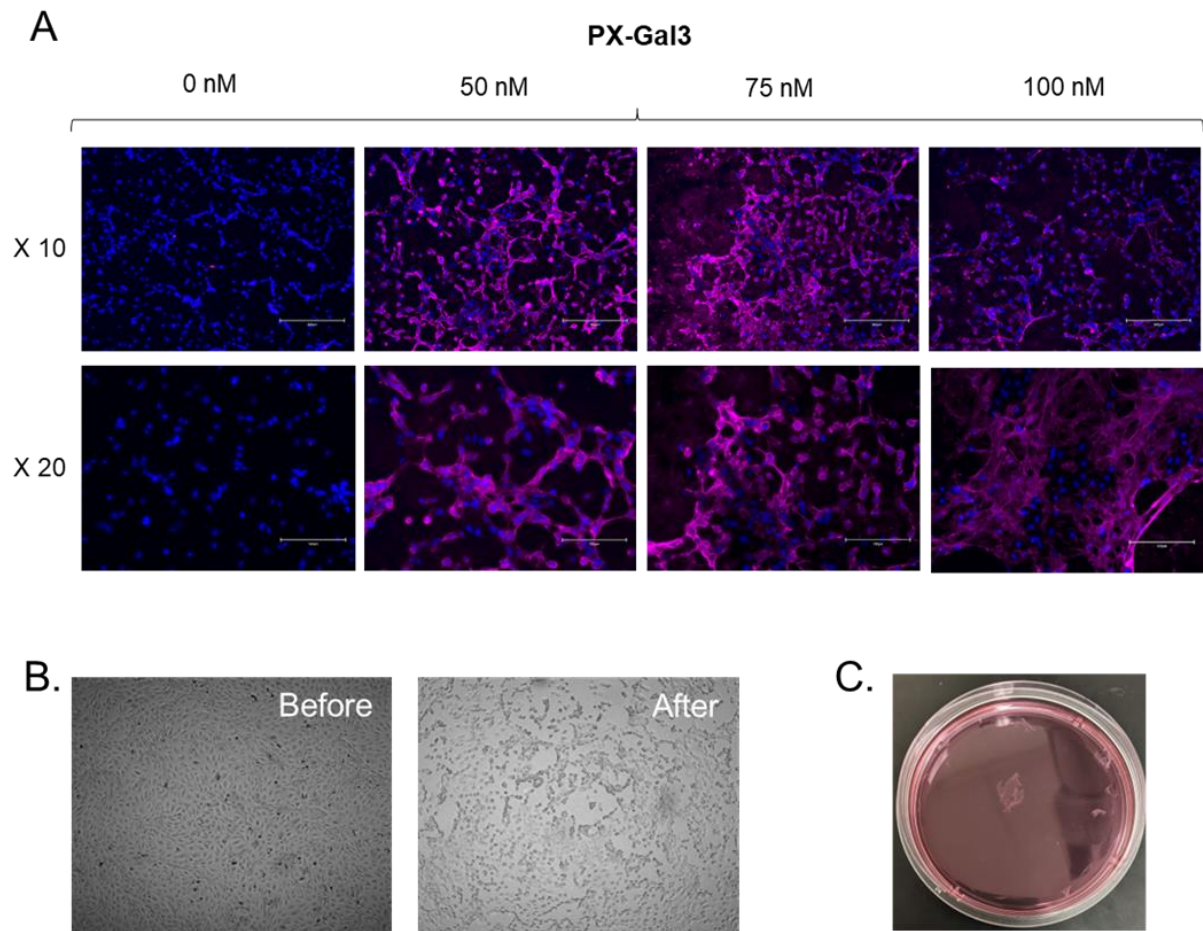


Figure 38: Proximity labelling technique damaged HUVEC monolayer.

A) Proximity labelling was performed with 0 – 100 nM of PX-Gal3 and validated using immunofluorescence at 10X and 20X magnification. **B)** HUVEC monolayer (left) was damaged (right) following the proximity labelling with PX-Gal3 protocol, observed at 4X magnification. **C)** HUVEC monolayer became detached after 20 minutes incubation in serum-free DMEM, in the absence of PX-Gal3. Scale bar (A, top) 300 μ m and (A, bottom) 150 μ m.

Through reducing the incubation times with PX-Gal3/DMEM, we were still able to detect biotinylation in all positive conditions and to a much greater extent following 1-5 minutes incubation with PX-Gal3 (**Figure 39**).

Subsequently, we investigated whether we could also reduce the biotin-phenol incubation time to improve labelling efficiency. Successful labelling was achieved at all incubation times, and to a similar intensity in all conditions (**Figure 40**). One final small-scale experiment was conducted using the optimised conditions to mimic the labelling of untreated and TNF α + IFN γ treated HUVEC for downstream proteomics.

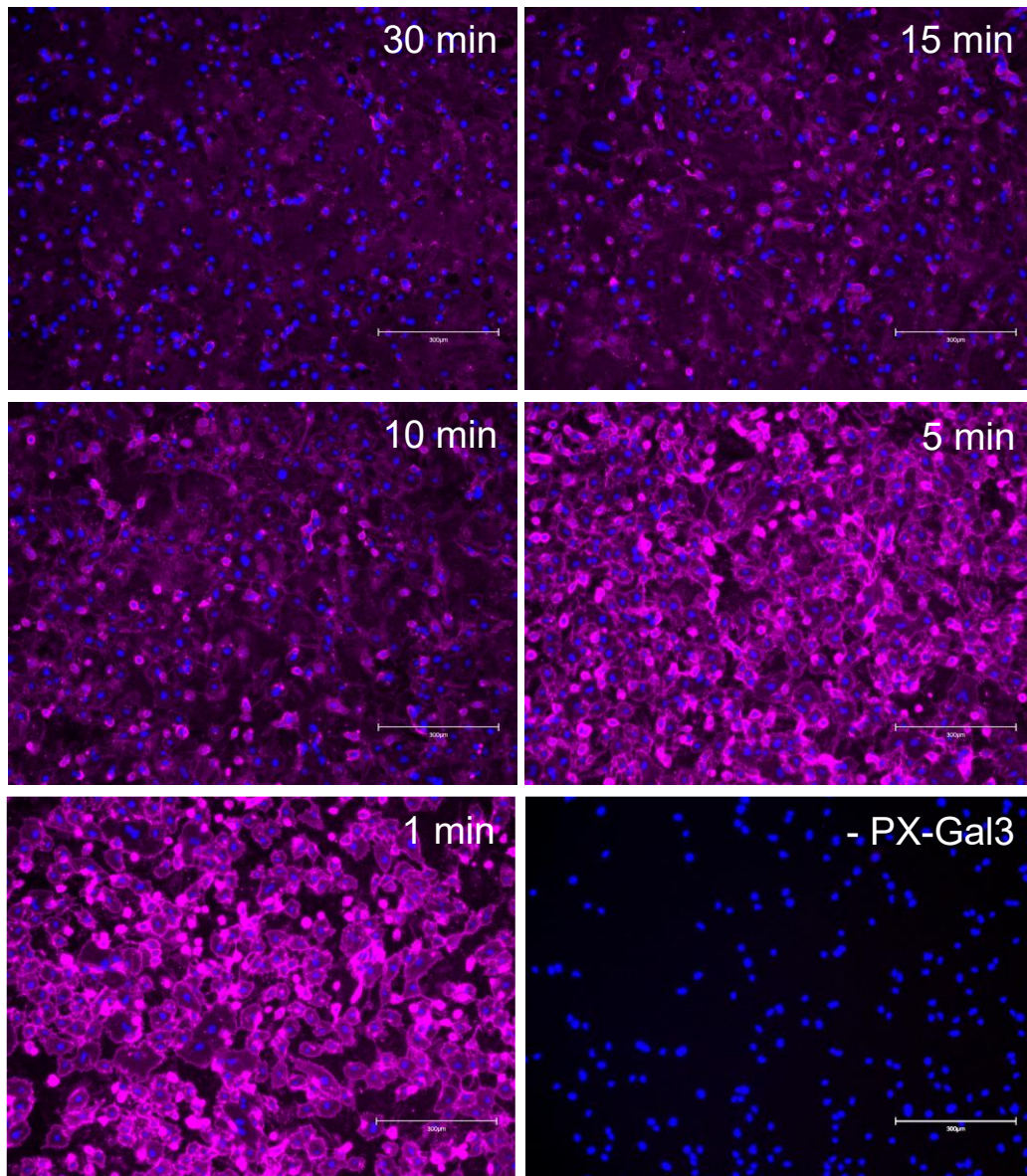


Figure 39: Improved biotin labelling was observed in HUVEC with reduced incubation times with PX-Gal3.

Serum free DMEM with 75 nM PX-Gal3, or without PX-Gal3 (-PX-Gal3) was added to confluent HUVEC for 30 minutes (including -PX-Gal3), 15 min, 10 min or 1 min. Cells were washed with PBS and replaced with 500 μ M biotin-phenol in DMEM for 30 minutes, before adding 100 mM hydrogen peroxide for one minute. The reaction was stopped through three washes of the cells with quench solution, before fixing the cells and staining using fluorescently conjugated streptavidin (magenta) and DAPI (blue) for subsequent microscopy. Scale bar 300 μ m.

Our results confirmed successful labelling of both the treated and untreated HUVEC, whilst the absence of fluorescence in the conditions containing lactose suggests that interactors of galectin-3 bound in an almost entirely glycan-dependent manner

(Figure 41). Overall, our findings confirm that one-minute incubation with 75 nM of PX-Gal3 followed by one-minute incubation with biotin-phenol was sufficient for labelling Gal-3 interactors of HUVEC, whilst limiting the amount of monolayer disruption obtained from following the original protocol. These optimised conditions were used in the large-scale experiment for mass spectrometry analysis.

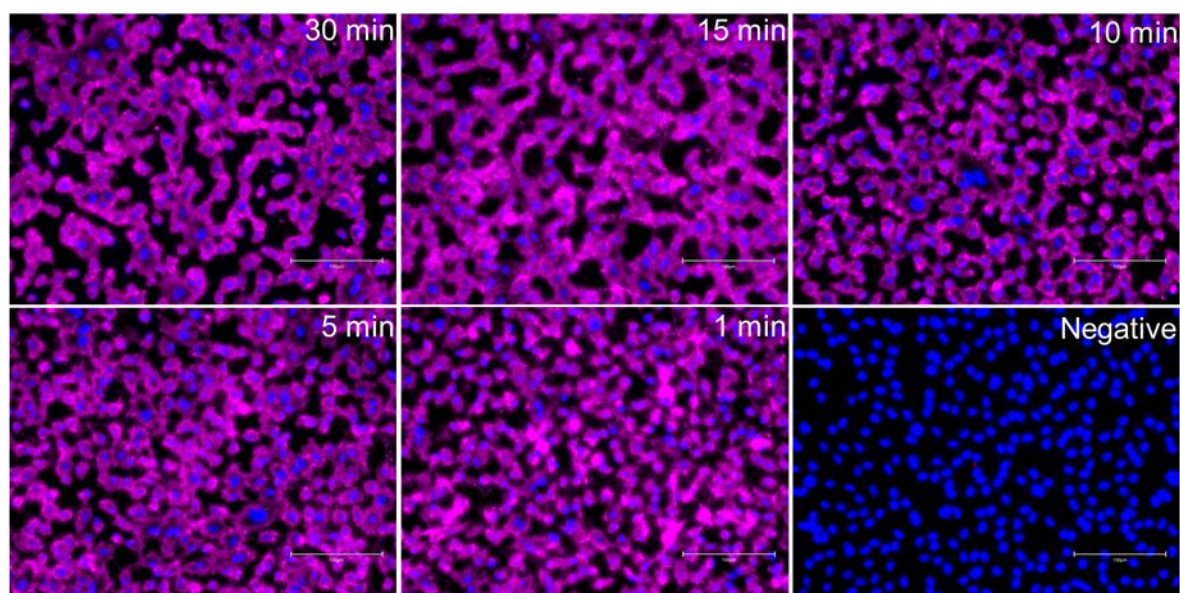


Figure 40: Sufficient biotin labelling was observed in HUVEC with reduced incubation times with biotin phenol.

Serum free DMEM with 75 nM PX-Gal3, or without PX-Gal3 (Negative) was added to confluent HUVEC for one minute. Cells were washed with PBS and replaced with 500 μ M biotin-phenol in DMEM for either 30 minutes (including Negative), 15 min, 10 min, 5 min or 1 min, before adding 100 mM hydrogen peroxide for one minute. The reaction was stopped through three washes of the cells with quench solution, before fixing the cells and staining using fluorescently conjugated streptavidin (magenta) and DAPI (blue) for subsequent microscopy. Scale bar 150 μ m.

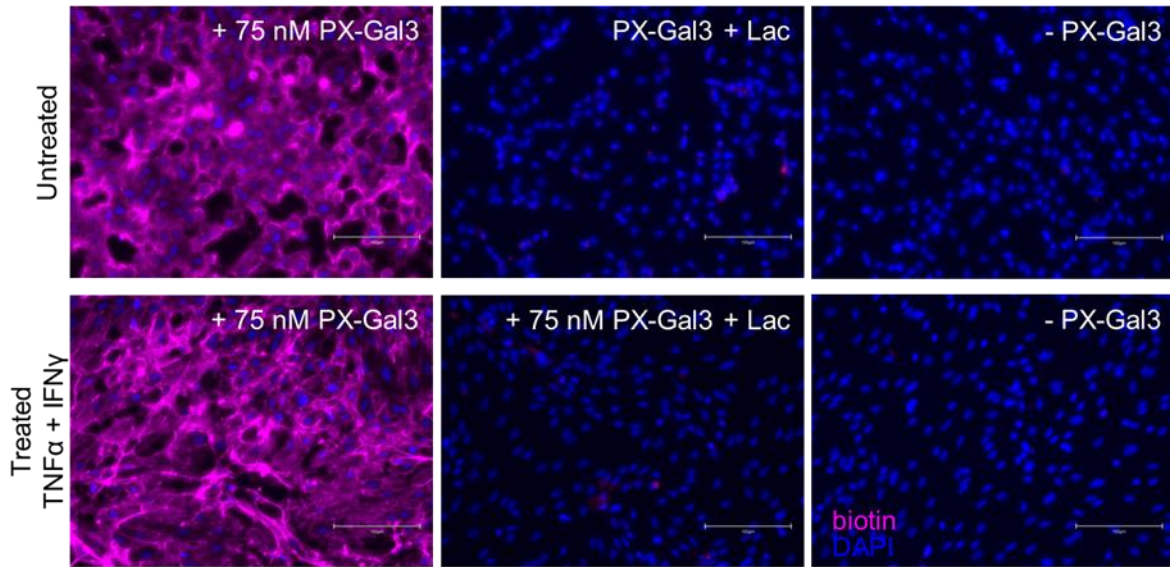


Figure 41: Immunofluorescence validation of optimised proximity labelling conditions on HUVEC.

Confluent HUVEC were incubated for 24 hours in media \pm TNF α and IFN γ (10 μ g/ml and 20 μ g/ml) prior to proximity labelling. Cells were first washed with PBS, before incubation for one minute in serum free DMEM containing either 75 nM PX-Gal3 \pm 100 mM lactose (Lac), or without PX-Gal3 as negative control (- PX-Gal3). Cells were washed with PBS and replaced with 500 μ M biotin-phenol in DMEM for one minute, before adding 100 mM hydrogen peroxide for one minute. The reaction was stopped through three washes of the cells with quench solution, before fixing the cells and staining using fluorescently conjugated streptavidin (magenta) and DAPI (blue) for subsequent microscopy. Scale bar 150 μ m.

5.3 Identification of PX-Gal3 interactors by mass spectrometry

With downstream tandem-mass-tagging (TMT), biotinylated proteins were isolated and identified by mass spectrometry to generate an extensive list of galectin-3 interactors on HUVEC. PX-Gal3 was used to identify exogenous galectin-3 interactors expressed in both unstimulated and TNF α + IFN γ stimulated HUVEC. In the untreated HUVEC samples, 383 proteins were significantly enriched above the PX-Gal3 negative control (**Figure 42A**), whilst 390 proteins were identified to be outcompeted by lactose (**Figure 42B**). In total, 342 proteins were both significantly enriched and outcompeted for binding in the presence of lactose, with an R^2 value of 0.8645 to suggest strong correlation between the two factors (**Figure 42C**). Additional hits were identified in the competition conditions containing lactose, suggesting that protein complexes and/or conformational changes induced by lactose may be required for Gal-3 binding (Yin et al. 2006). We replaced missing values in our mass spectrometry data with a nominal value of '1' to allow us to perform comparative analysis without excluding potential hits that were not identified by mass-spec due to complete competition by lactose and/or absence in the negative control.

Of the stimulated HUVEC datasets, 389 proteins were found to be significantly enriched above background (**Figure 43A**), with 391 proteins exhibiting competition by lactose (**Figure 43B**). In total, 340 proteins were significant in both the enriched and competition parameters, with an R^2 value of 0.8259 suggesting strong correlation between the two factors (**Figure 43C**). We next input each of our datasets into the Contaminant Repository for Affinity Purification (CRAPome) database for removal of contaminating and common proteins obtained from mass spectrometry. Overall, we

were able to generate a list of unique, potential interactors of PX-Gal3 for both untreated and TNF α + IFN γ stimulated HUVEC for further investigation and analysis.

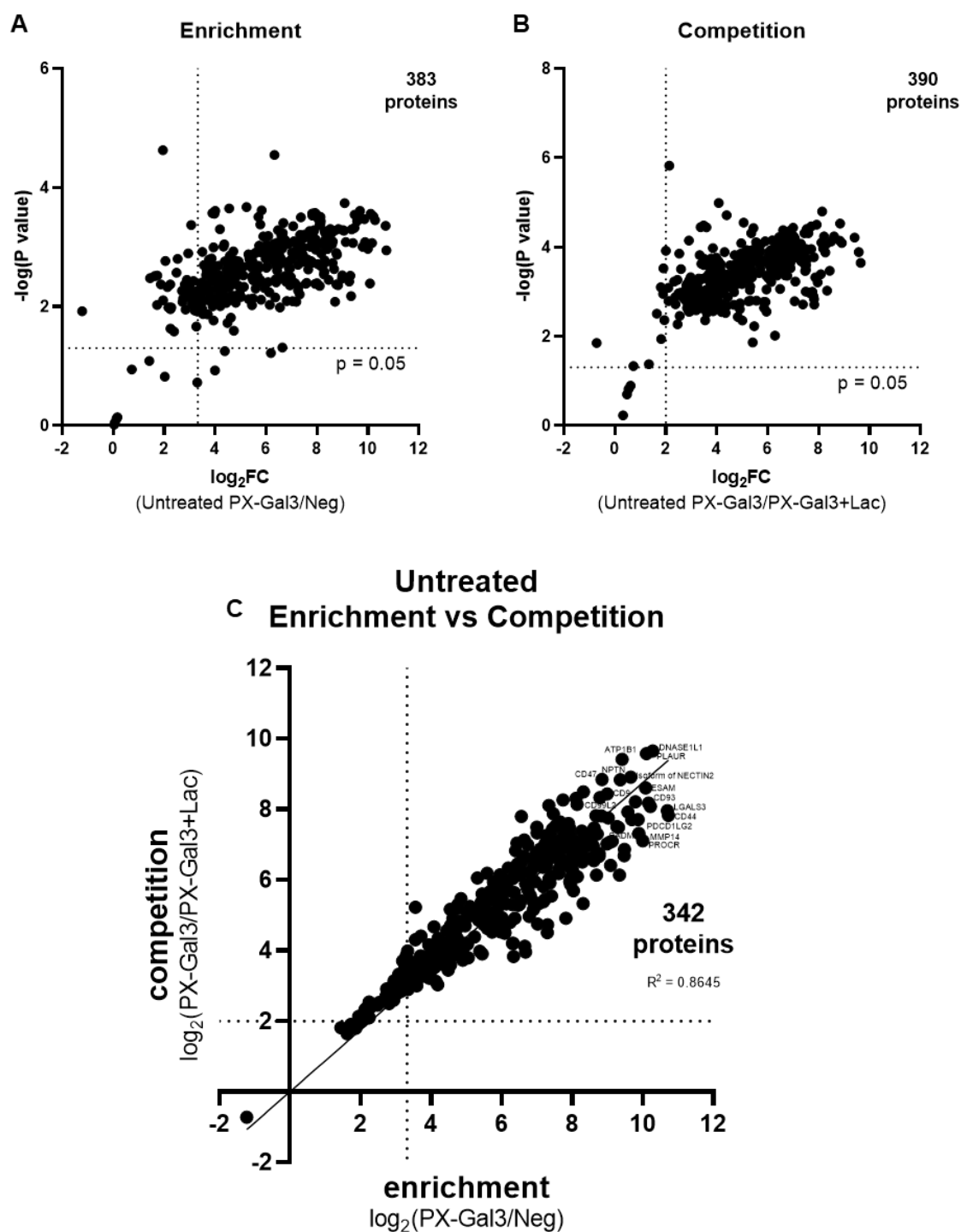


Figure 42: Mass spectrometry results from proximity labelling unstimulated HUVEC with PX-Gal3.

A) Correlation of statistically significant and highly enriched proteins from PX-Gal3 over negative treatment. B) Correlation of significant proteins and highly competed proteins from PX-Gal3 over PX-Gal3 with lactose. C) Correlation of proteins between competition and enrichment ratio. Significance threshold set to adjusted $\log_2 p > 1.5$ and arbitrary value of \log_2 ratio of 2 and 3.36 for enrichment and competition, respectively.

We mined our RNA sequencing data to explore transcriptomic differences within TNF α + IFN γ stimulated HUVEC for comparison against the mass-spec data obtained through streptavidin enrichment. We were able to identify and link transcriptional changes in response to treatment, to protein enrichment in one treatment condition over the other. Examples of this are CD38, ICAM1 and VCAM1, which were enriched in the TNF α + IFN γ treated HUVEC in both the proteomics and transcriptomics datasets (highlighted in green, **Figure 44**). Interestingly, multiple hits including TLR2, CADM3 and MMRN2 were identified to be enriched in one of the treatments conditions at the protein level but not transcriptionally (highlighted in orange **Figure 44**). Most noticeably, TLR2 protein had a 6.74 log₂ fold enrichment in the treated versus untreated HUVEC, whilst at the transcriptional level, only 0.37 log₂ fold change was observed (**Table 5**). Since we established that binding of PX-Gal3 could be out competed by lactose, the discrepancy between the proteomics and transcriptomic datasets could well be due to changes in glycosylation patterns on the proteins in response to treatment.

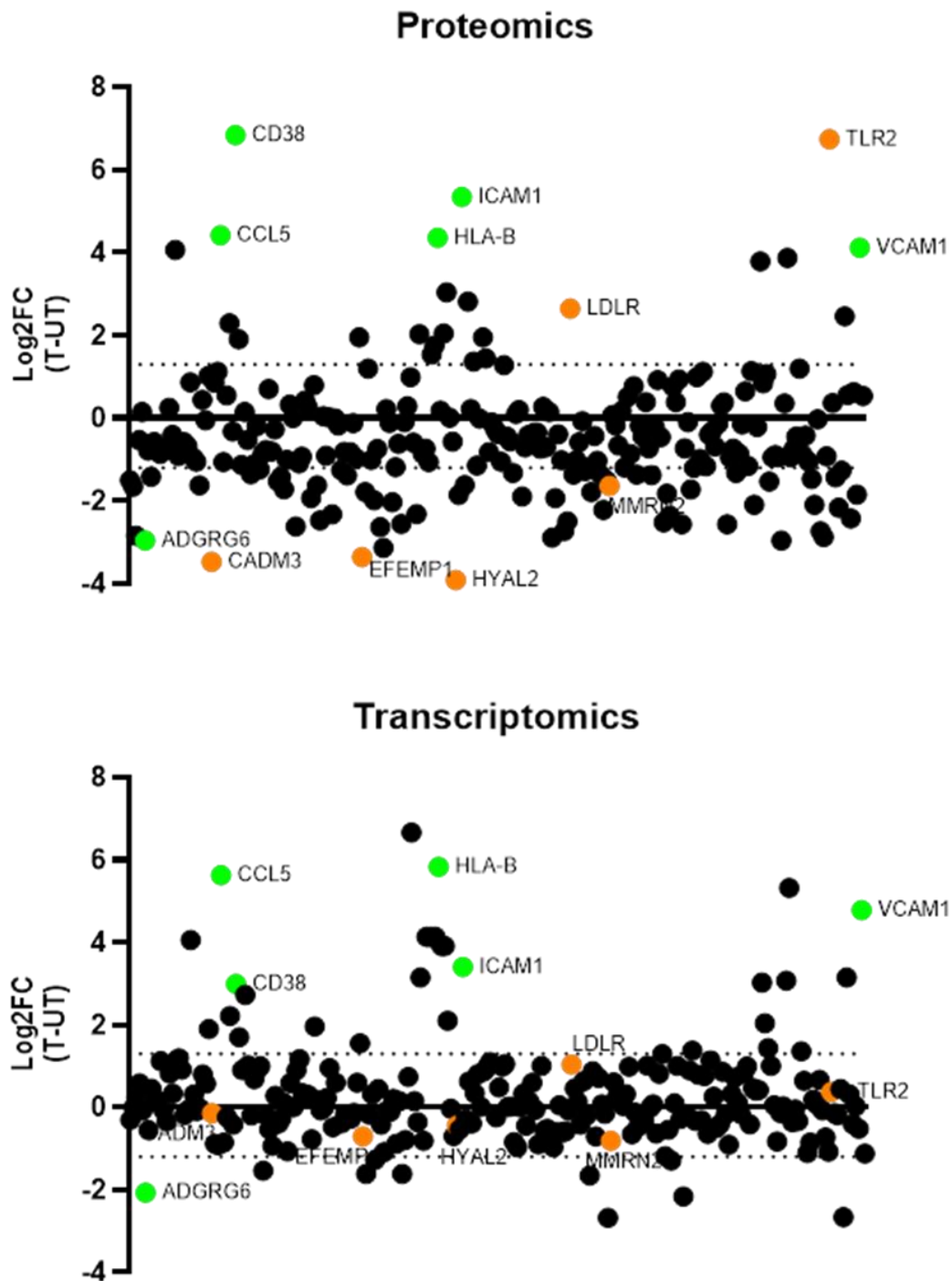


Figure 44: Comparison of proteomics and transcriptomics dataset identifies differences between TNF α and IFN γ stimulated and untreated HUVEC that may be due to changes in glycosylation patterns.

Proteins highlighted in green were observed to have similar trends in their fold change differences between treated and untreated conditions within the proteomics (top) and transcriptomic (bottom) datasets, as expected. Proteins highlighted in orange showed significant fold change (outside dashed line) differences in the mass spectrometry datasets, but not in the transcriptomics dataset.

Table 5: Table of PX-Gal3 interactors with significant fold change difference in enrichment between treated and untreated HUVEC.

		Mass spec								RNAseq	
		P value	an of T en	rin of UT en	Difference	of differer	t ratio	df	usted P Value	Difference	usted P Value
P28907	CD38	<0.000001	6.877	0.0343	6.843	0.4341	15.76	988	<0.000001	2.991	<0.000001 Yes
O60603	TLR2	<0.000001	7.461	0.722	6.739	0.4341	15.52	988	<0.000001	0.3723	>0.999999 No
P05362	ICAM1	<0.000001	7.294	1.946	5.348	0.4341	12.32	988	<0.000001	3.401	<0.000001 Yes
P13501	CCL5	<0.000001	6.942	2.524	4.419	0.4341	10.18	988	<0.000001	5.629	<0.000001 Yes
P30481	HLA-B	<0.000001	7.916	3.558	4.358	0.4341	10.04	988	<0.000001	5.827	<0.000001 Yes
P19320	VCAM1	<0.000001	8.964	4.842	4.123	0.4341	9.496	988	<0.000001	4.785	<0.000001 Yes
Q13508	ART3	<0.000001	6.185	2.121	4.064	0.4341	9.362	988	<0.000001	1.123	0.110874 No
Q12891	HYAL2	<0.000001	5.564	9.476	-3.913	0.4341	9.012	988	<0.000001	-0.4455	>0.999999 No
P04179	SOD2	<0.000001	5.317	1.444	3.872	0.4341	8.919	988	<0.000001	5.323	<0.000001 Yes
P16581	SELE	<0.000001	7.346	3.556	3.79	0.4341	8.729	988	<0.000001	3.025	<0.000001 Yes
Q8N126	CADM3	<0.000001	5.83	9.305	-3.475	0.4341	8.004	988	<0.000001	-0.1452	>0.999999 No
Q12805	EFEMP1	<0.000001	2.752	6.105	-3.353	0.4341	7.723	988	<0.000001	-0.7071	0.998596 No
Q96AP7	ESAM	<0.000001	6.942	10.08	-3.135	0.4341	7.222	988	<0.000001	-1.081	0.173111 No
P13747	HLA-E	<0.000001	8.053	5.012	3.042	0.4341	7.006	988	<0.000001	2.101	<0.000001 Yes
Q8IWA5	SLC44A2	<0.000001	6.901	9.86	-2.959	0.4341	6.816	988	<0.000001	0.02452	>0.999999 No
Q86SQ4	ADGRG6	<0.000001	5.309	8.265	-2.956	0.4341	6.81	988	<0.000001	-2.066	<0.000001 Yes
Q9Y219	JAG2	<0.000001	5.048	7.931	-2.883	0.4341	6.64	988	<0.000001	-0.971	0.466652 No
P35590	TIE1	<0.000001	5.449	8.316	-2.868	0.4341	6.606	988	<0.000001	-0.7286	0.996362 No
Q13444	ADAM15	<0.000001	4.43	7.267	-2.837	0.4341	6.536	988	<0.000001	0.2386	>0.999999 No
O75144	ICOSLG	<0.000001	6.315	3.496	2.818	0.4341	6.492	988	<0.000001	0.6252	0.999993 No
P07996	THBS1	<0.000001	4.163	6.896	-2.733	0.4341	6.295	988	<0.000001	-0.07198	>0.999999 No
P07942	LAMB1	<0.000001	5.243	7.97	-2.728	0.4341	6.283	988	<0.000001	-0.5786	>0.999999 No
P01130	LDLR	<0.000001	7.191	4.541	2.651	0.4341	6.105	988	<0.000001	1.036	0.270106 No
P54760	EPHB4	<0.000001	5.374	8.004	-2.629	0.4341	6.057	988	<0.000001	-0.4236	>0.999999 No
P02462	COL4A1	<0.000001	5.199	7.814	-2.615	0.4341	6.024	988	<0.000001	0.9004	0.716202 No
P23470	PTPRG	<0.000001	5.572	8.136	-2.564	0.4341	5.907	988	0.000001	-0.9093	0.686019 No
P16284	PECAM1	<0.000001	5.328	7.888	-2.559	0.4341	5.895	988	0.000001	-2.162	<0.000001 Yes
Q43155	FLRT2	<0.000001	5.58	8.135	-2.555	0.4341	5.884	988	0.000001	-1.613	0.000098 Yes
Q9HB63	NTN4	<0.000001	4.647	7.165	-2.518	0.4341	5.799	988	0.000002	-1.182	0.055244 No
P11047	LAMC1	<0.000001	5.309	7.806	-2.497	0.4341	5.752	988	0.000003	-0.08218	>0.999999 No
P35221	CTNNA1	<0.000001	4.898	7.365	-2.467	0.4341	5.682	988	0.000004	-0.07262	>0.999999 No
P50591	TNFSF10	<0.000001	4.706	2.242	2.464	0.4341	5.676	988	0.000004	3.152	<0.000001 Yes
Q8NG11	TSPAN14	<0.000001	5.359	7.784	-2.424	0.4341	5.584	988	0.000007	-0.4029	>0.999999 No
Q9P2E7	PCDH10	<0.000001	4.982	7.335	-2.353	0.4341	5.421	988	0.000016	-1.291	0.013449 Yes
P78310	CXADR	<0.000001	4.863	7.185	-2.322	0.4341	5.349	988	0.000023	-0.4804	>0.999999 No
P48060	GLIPR1	<0.000001	6.946	9.261	-2.315	0.4341	5.332	988	0.000025	-0.3597	>0.999999 No
Q9NZQ7	CD274	<0.000001	8.926	6.632	2.293	0.4341	5.282	988	0.000033	2.218	<0.000001 Yes
P50281	MMP14	<0.000001	7.668	9.881	-2.212	0.4341	5.096	988	0.000087	-0.1547	>0.999999 No
O14763	TNFRSF10	<0.000001	3.255	5.415	-2.16	0.4341	4.975	988	0.00016	0.4455	>0.999999 No
P61812	TGFB2	0.000002	5.197	7.293	-2.096	0.4341	4.828	988	0.000332	0.07898	>0.999999 No
Q969E2	SCAMP4	0.000002	4.693	6.787	-2.094	0.4341	4.823	988	0.000339	0.4041	>0.999999 No
P10321	HLA-C	0.000003	6.176	4.132	2.044	0.4341	4.707	988	0.000591	3.912	<0.000001 Yes
Q96S86	HAPLN3	0.000003	5.962	3.929	2.033	0.4341	4.683	988	0.000661	3.15	<0.000001 Yes
Q5VUB5	FAM171A	0.000003	6.797	8.825	-2.027	0.4341	4.67	988	0.000699	0.2075	>0.999999 No
P49961	ENTPD1	0.000005	5.191	7.176	-1.985	0.4341	4.573	988	0.0011	-1.273	0.017024 Yes
O43854	EDIL3	0.000007	6.713	4.756	1.957	0.4341	4.507	988	0.001486	1.556	0.000252 Yes
Q13478	IL18R1	0.000008	5.888	3.935	1.953	0.4341	4.499	988	0.001533	0.8783	0.784863 No
O75718	CRTAP	0.000009	1.507	3.441	-1.934	0.4341	4.454	988	0.001878	-0.7726	0.980001 No
Q9BX67	JAM3	0.00001	5.531	7.462	-1.931	0.4341	4.449	988	0.001914	-0.6073	0.999999 No
P25942	CD40	0.000012	9.348	7.438	1.911	0.4341	4.401	988	0.002363	1.702	0.000021 Yes
O60449-2	LY75	0.000015	5.726	7.616	-1.89	0.4341	4.353	988	0.002919	0.3389	>0.999999 No
Q9Y4L1	HYOU1	0.000021	2.073	3.93	-1.857	0.4341	4.278	988	0.004055	-0.5344	>0.999999 No
Q9BZM4	ULBP3	0.000023	5.187	7.036	-1.849	0.4341	4.259	988	0.004379	-0.5225	>0.999999 No
Q16625	OCLN	0.00003	4.96	6.779	-1.819	0.4341	4.19	988	0.005881	-0.5464	>0.999999 No
P36941	LTBR	0.000043	7.899	9.683	-1.784	0.4341	4.109	988	0.008272	0.8773	0.78697 No
P52799	EFNB2	0.000044	3.678	5.46	-1.782	0.4341	4.106	988	0.00835	-1.617	0.000092 Yes
P30456	HLA-A	0.000058	8.199	6.446	1.753	0.4341	4.038	988	0.011055	4.134	<0.000001 Yes
O00469	PLOD2	0.000076	2.099	3.825	-1.726	0.4341	3.975	988	0.014258	1.372	0.00429 Yes
O00501	CLDN5	0.000087	6.877	8.588	-1.711	0.4341	3.941	988	0.01628	0.0958	>0.999999 No
O14672	ADAM10	0.000146	4.905	6.561	-1.656	0.4341	3.813	988	0.026987	-0.0034	>0.999999 No
Q9H8L6	MMRN2	0.00017	5.656	7.295	-1.638	0.4341	3.774	988	0.031329	-0.8154	0.933314 No
P29279	CTGF	0.000193	5.554	7.179	-1.625	0.4341	3.742	988	0.035269	0.168	>0.999999 No
P35613	BSG	0.000195	5.776	7.399	-1.623	0.4341	3.739	988	0.035522	-0.02494	>0.999999 No
P13598	ICAM2	0.000212	7.006	8.62	-1.614	0.4341	3.718	988	0.038252	-0.2865	>0.999999 No

5.4 HUVEC N-Glycome profile changes in response to TNF α + IFN γ treatment

To understand whether the glycosylation profile of the cells changed with TNF α + IFN γ treatment, N-glycomics mass-spectrometry was performed on stimulated and unstimulated HUVEC. Within the treated cells, there were increased levels of FA2G2S2 and FA3G3S3, making up around ~22% of the N-glycan population (**Figure 45**). Most noticeably within this dataset, glycans with one or fewer sialic acid units, including FA2G2S1, FA3G3S1, A2G2S1, FA2G2 and A3G3S1 were all found to be more abundant within the untreated HUVEC, whilst glycans containing more complex patterns of sialic acid tended to be more abundant within the treated samples (**Figure 45**). This is noteworthy since Gal-3 has been reported to have specificity for LacNAc (Gal-GlcNAc) extensions on tri- and tetra-antennary N-glycans, with little tolerance for sialic acid (Nielsen et al. 2018). These glycan characteristics are most abundant within the untreated glycomics dataset (**Figure 45**), suggesting that it could be due to changes in the glycosylation patterns rather than the expression of proteins that is influencing the binding of PX-Gal3 and thus enrichment of interactors in one treatment condition over the other. Of the proteins identified within the proteomics datasets, ~82% (53 of 64) are reported to have N-glycosylation sites, whilst the remaining have potential or are reported as bearing O-linked glycans.

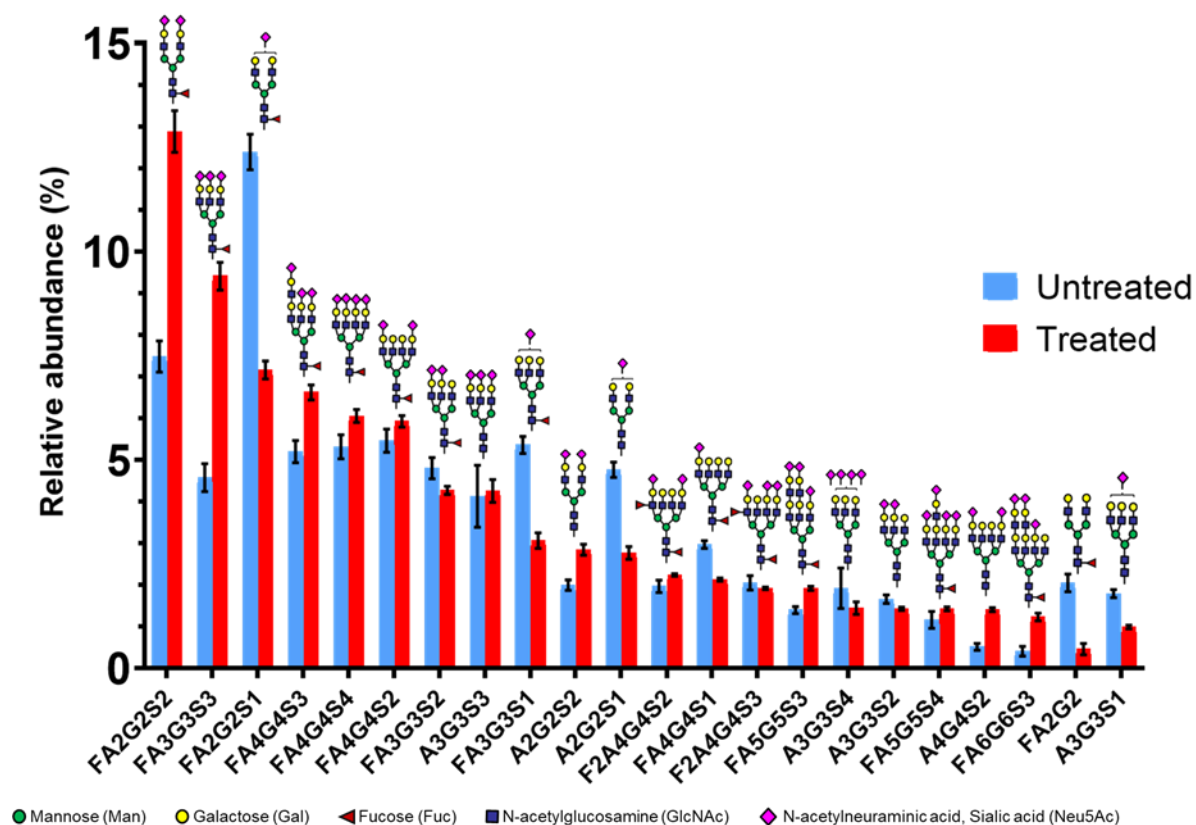


Figure 45: N-glycomics profile differs between untreated and TNF α and IFN γ stimulated HUVEC.

HUVEC were incubated in media +/- TNF α and IFN γ for 24 hours before purification of proteins and treatment with PNGase F for release of N-glycans for downstream mass spectrometry. Glycan compositions and structures were identified using GlycoWorkbench and the top 22 glycans across both datasets were plotted as % relative abundance.

5.5 Validation of Galectin-3 interactors by *in silico* techniques

To determine whether the proteins identified through mass spectrometry were already known binders of galectin-3, we input the list of significantly enriched proteins, as well as galectin-3 into the STRING database (Szklarczyk et al. 2019). BSG, PECAM1, SELE, ICAM1 and VCAM1 were shown to have direct protein-protein interactions with galectin-3 as previously reported (**Figure 46**) (Joeh et al. 2020; Colomb et al. 2017; Rao et al. 2007a). Moreover, the STRING analysis also identified novel interactors of galectin-3, including CD38, TLR2, MMRN2, LDLR, SCAMP4 and HYOU1 which have not yet been reported as interactors of Gal-3.

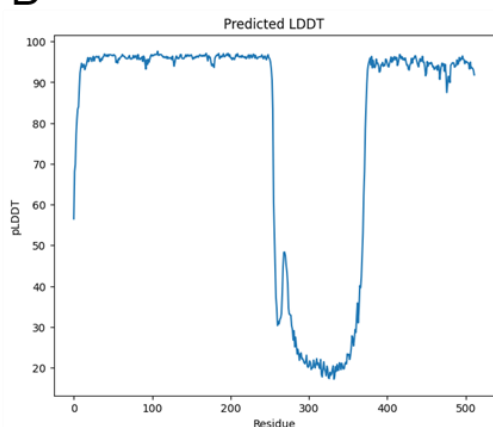
To better understand the interactions between PX-Gal3 and the proteins identified as potential binders by mass spectrometry, we used Alphafold to model the folding of PX-Gal3 *in silico*. PX-Gal3 consists of a His-tagged protein made up of APEX2 and full-length galectin-3, fused together by a short, flexible glycine-serine linker (**Figure 47A**). The predicted Local Distance Difference Test (pLDDT) score for the fusion protein averaged ~95, except at the linker like region that connects the N and C-term of the galectin-3 sequence, indicating a high-quality structure model (**Figure 47B**). The Predicted Aligned Error (PAE) indicates high confidence in the position of the APEX2 (AAs ~1-250) residues relative to each other, and the CRD portion of Galectin-3 (AAs ~370-510), but not within the engineered flexible linker region (AAs ~250-260) or non-CRD portion of Gal-3 (AAs ~260-510) as expected (**Figure 47C**). The PAE also suggests low confidence in the predicted position of each subunit (APEX2/N-Term/CRD) relative to another, due to the flexible linker necessary for unrestricted binding. The predicted model of PX-Gal3, colour coded according to the pLDDT score is shown in **Figure 47D**, with the top-most globular subunit being the CRD of galectin-

A

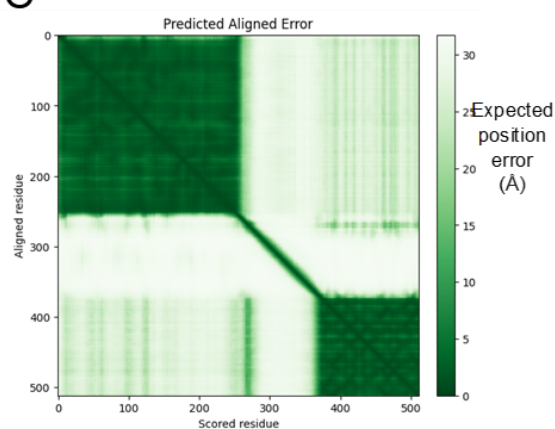
PX-(Gal3): Histag-APEX2-GSGGGGS-(Nterm-Linker-CRD)

MHHHHHHGKSYPTVSADYQDAVEKAKKKLRGFIAEKRCAPLMLRLAFHSAGTFDKGTK
TGGPFGTIKHPAELAHSANGLDIAVRLLEPLKAEPILSYADFYQLAGVVAVEVTGGPKV
PFHPGREDKPEPPPEGRLPDPTKGSDDLRLDVFVKAMGLTDQDIVALSGGHTIGAAHKE
RSGFEGPWTSNPLIFDNSYFTELLSGEKEGLQLPSDKALLSDPVFRPLVDKYAADEDAF
FADYAEAHQKLSELGFADAGSGGGGSADNFSLHDALSGSGNPNPQGWPGAWGNQPA
GAGGYPGASYPGAYPGQAPPAYPGQAPPAYPGAPGAYPGAPAGVYPGPPSGPG
AYPSSGQPSATGAYPATGPYGAAGPLIVPYNLPLPGGVPRMLITLGTVPKPNANRIALD
FQRGNDVAFHFNPRFNENRRVIVCNTKLDNNWGREERQSVFPFESGKPFQIVLVEP
DHFKVAVNDAHLLQYNHRVKKLNEISKLGISGDIDLTASYTMI

B



C



D

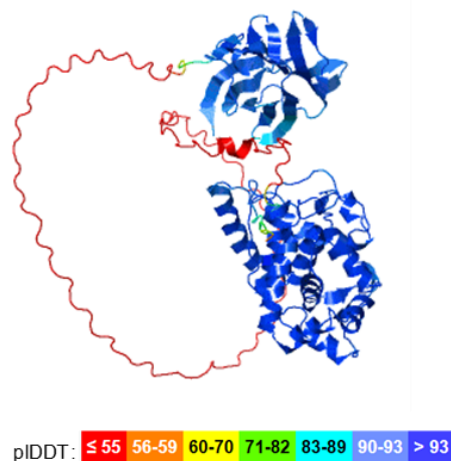


Figure 47: In silico modelling of PX-Gal3 using ColabFold.

(A) PX-Gal3 amino acid sequence, composed of APEX2 and Gal3 proteins fused together with a serine-glycine linker. **(B)** Predicted LDDT and **(C)** predicted aligned error (PAE) are used to display predicted model error. **(D)** 3D rotating model of PX-Gal3 designed using Pymol and coloured according to predicted error (pLDDT), where blue indicates high confidence in predicted folding and red is low confidence.

Using ColabFold, we were able to obtain predictions of the interactions between CD38 and TLR2, the two proteins with the greatest fold change enrichment in treated versus untreated conditions, plus CADM3 which was enriched by the greatest fold change in the untreated conditions. ColabFold was unable to make a prediction on HYAL2, the protein with the second greatest fold change in the untreated condition over treated, so this was not displayed. The other three proteins were run through the software and the PAE between each protein and PX-Gal3 was generated by ColabFold. The protein of interest is shown in quadrant one and the PX-Gal3 within quadrant four (Left to right across the top then bottom). Where white or blue is observed in quadrant two and three is indicative of increased proximity to the other protein (**Figure 48**). From this, we can see limited interaction between either of the proteins of interest and PX-Gal3 (**Figure 48**). In rank1 of the CD38 predictions, we see some binding to the APEX2 portion of PX-Gal3, indicated by the large sections of white within quadrant two and three, with limited proximity between the CRD region and CD38 at specific points indicated by faint white sections (**Figure 48**).

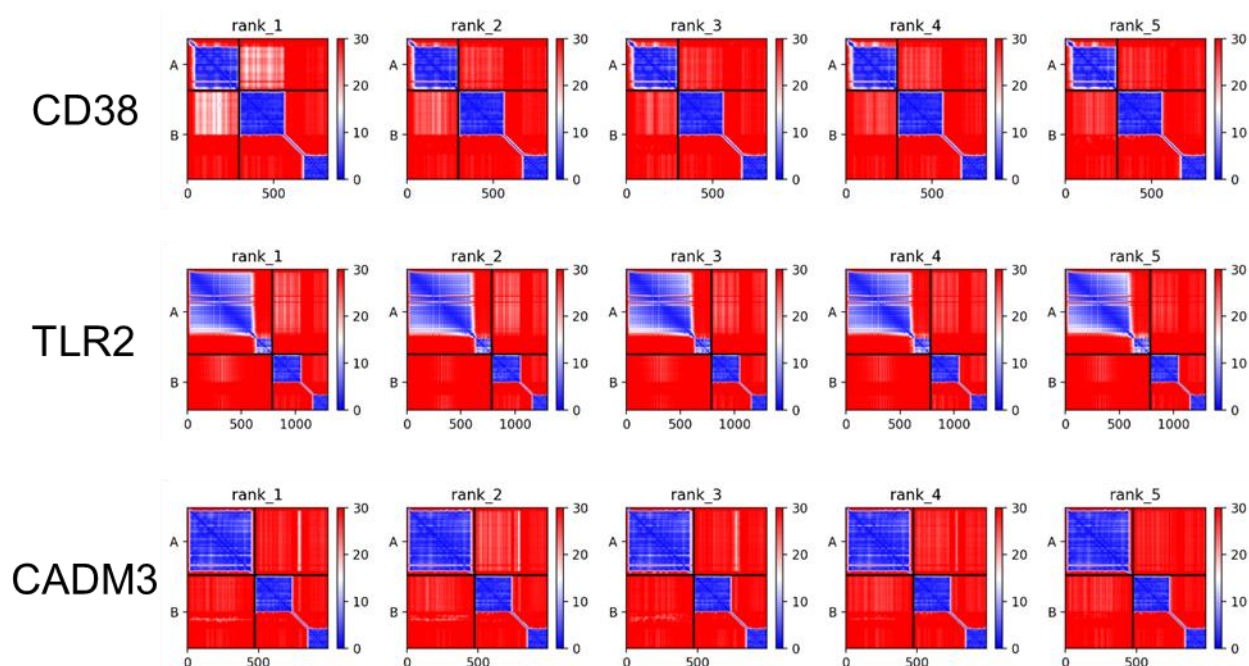


Figure 48: In silico modelling was used to predict interactions with PXGal3.

CD38, TLR2 and CADM3, all proteins identified as interactors of PXGal3 by proximity labelling were modelled using ColabFold for Predicted Aligned Error (PAE) scores, where red indicates high predicted error and blue is low. The top left quadrant displays PAE scores of the protein of interest and bottom right quadrant displays PAE for PXGal3. Quadrants on either side displays the PAE of residues from each of the two proteins interacting with each other.

We used ChimeraX to model the predicted protein structure and interactions between PX-Gal3 and CD38 with higher specificity (**Figure 49**) (Pettersen et al. 2021). When selecting for PAE of 4 ångströms (Å) or fewer, we can observe which amino acids are predicted to interact and form strong electrostatic salt bridges, displayed by the connecting red lines (**Figure 50**). Most predicted salt bridges are between the APEX2 (in grey) rather than the Gal-3 (magenta) portion of PX-Gal3 and CD38 (green) (**Figure 50**). Since Gal-3 is a glycan-binding protein, glycosylation may be necessary for improved affinity and predicted interactions between the two proteins, something that is not considered in *in silico* modelling. The potential sites for glycosylation on CD38 are labelled, at asparagine position 209 and 219, both relatively close to the CRD of the Gal3 portion of PX-Gal3 (**Figure 50**). These prediction models support the mass spectrometry data, suggesting high probability of PX-Gal3 binding to CD38.

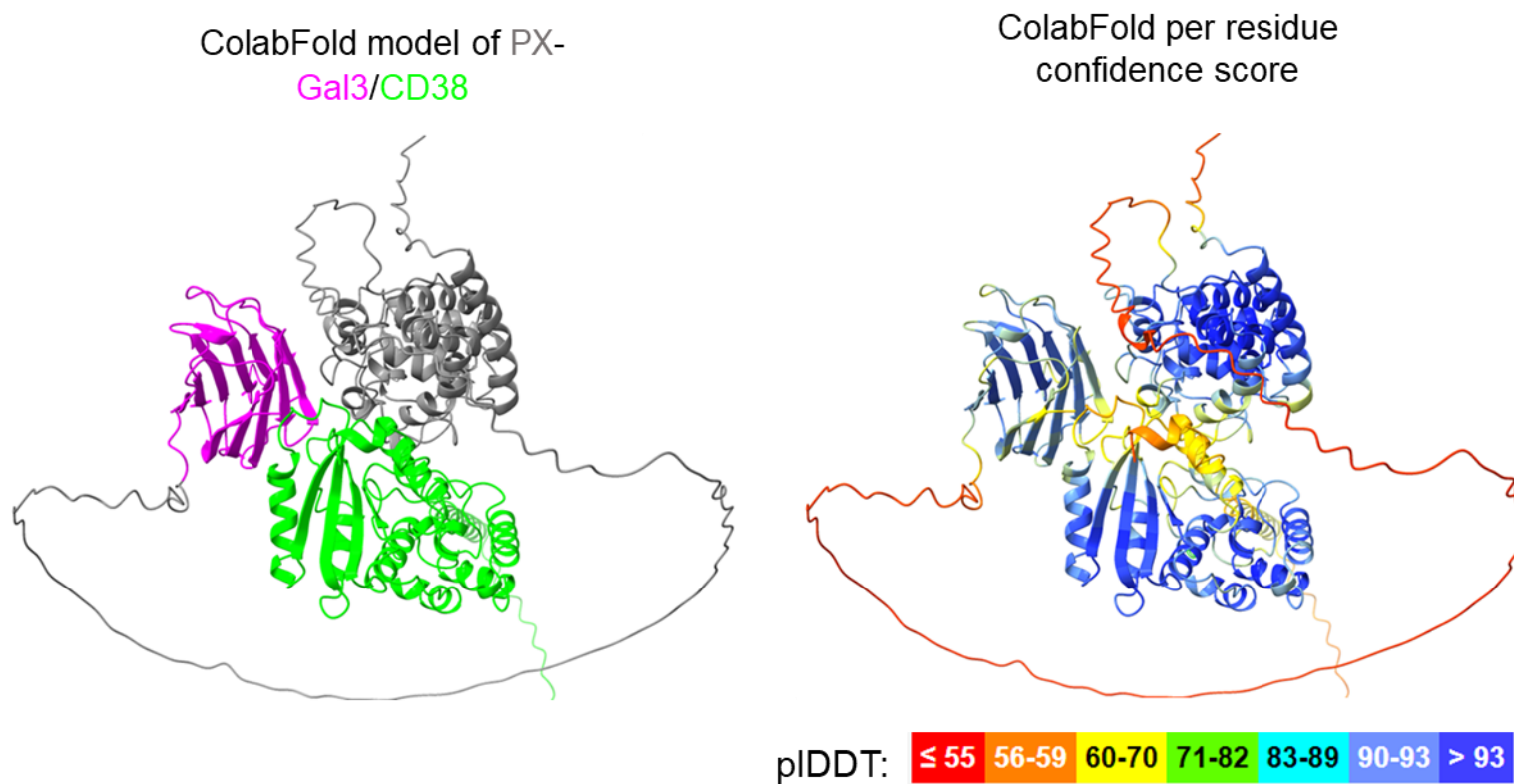


Figure 49: In silico model of PX-Gal3 interaction with CD38.

ColabFold was used to model and visualise the predicted interaction between PXGal3 and CD38. Left shows the structures coloured according to protein. Right shows model coloured based on predicted error in folding, where blue indicated high confidence in predicted folding and red is low confidence.

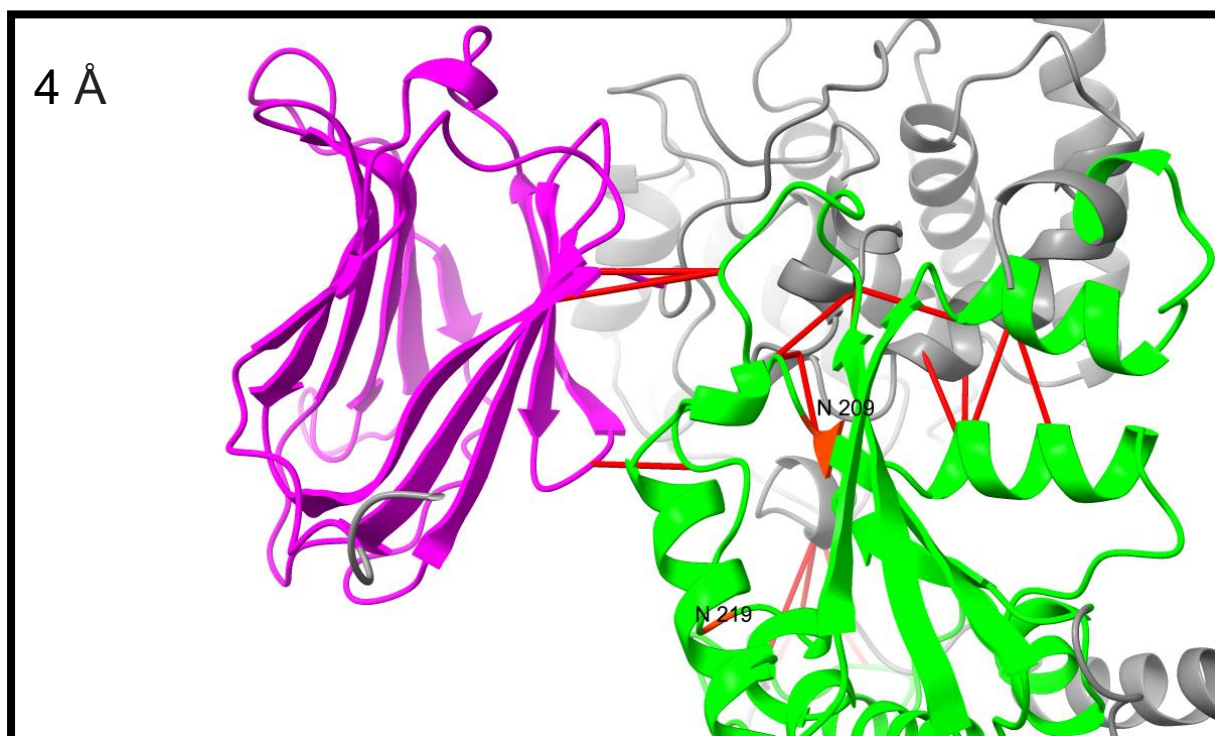


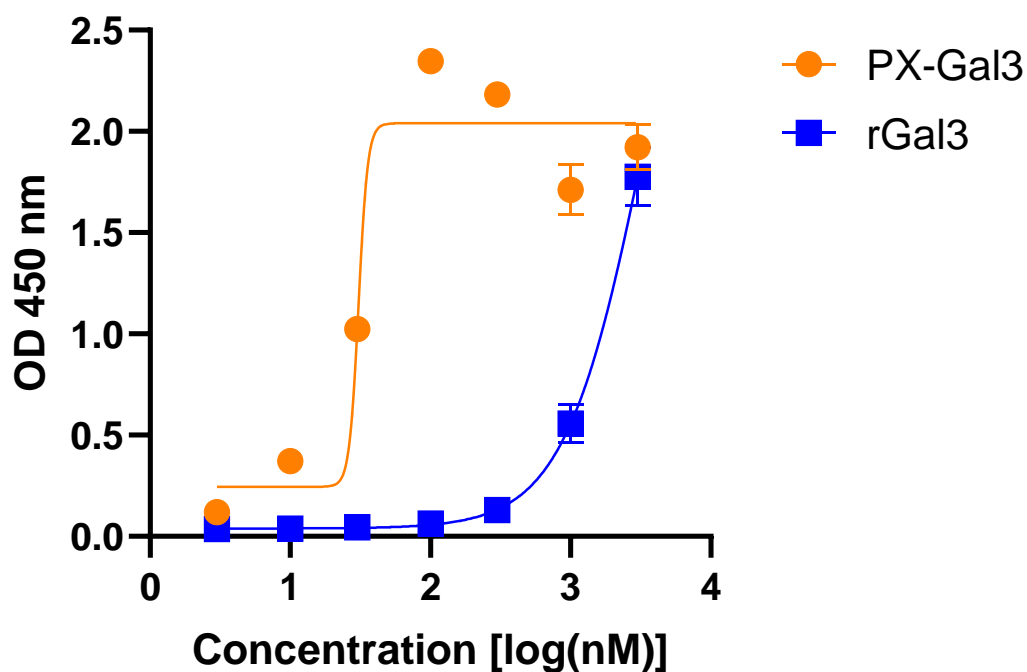
Figure 50: Predicted residues facilitating interactions between PX-Gal3 and CD38 were determined by in silico modelling.

ColabFold was used to model and visualise the predicted interaction between PXGal3 and CD38. Red bridges show predicted interactions between the Gal3 portion of PX-Gal3 (magenta) and the coils of CD38 (green) at 4 Å resolution. Asparagine positions on CD38 that are likely to be glycosylated *in vivo* are highlighted in red orange at N219 and N209, which are both within close proximity of the Gal-3/CD38 binding interface. Interactions between the APEX2 portion (grey) of PX-Gal3 and CD38 are also observed at 4 Å resolution.

5.6 *In vitro* validation of Gal3 binding to CD38

We next wanted to validate binding of Gal-3 to CD38 using an ELISA. We coated recombinant CD38 to 96 well high binding plates and titrated Gal-3, either PX-Gal3 or rGal-3 CRD only (rGal3) to determine specificity and the EC₅₀ for each protein. We observed binding to CD38 with both the PX-Gal3 and rGal3, observing a higher EC₅₀ value for PX-Gal3 compared to rGal3, of 0.031 μ M and 3.405 μ M respectively (**Figure 51**). This data confirms binding of Gal-3 to CD38, most likely through the CRD portion of Gal-3 since the commercial rGal3 lacks the linker and N-term portions of Gal-3. Although our *in-silico* model showed that APEX2 binding was likely, we expect that the discrepancy between the EC₅₀ values could be due to the peroxidase enzyme APEX2, amplifying the signal for binding through the catalytic reaction with TMB substrate.

To determine whether the interaction between Gal-3 and CD38 was glycan dependent, we performed another ELISA, either in the presence or absence of lactose or sucrose. Since, the affinity of Gal-3 towards galactose-containing glycan residues is much greater than other sugar motifs we could out-compete glycan binding using lactose. We observed that in the presence of lactose, binding to CD38 was reduced by over 90% for both the rGal3 and PX-Gal3, whilst sucrose had no effect on CD38 binding (**Figure 52**). These results provide further evidence to support Gal-3 binding to CD38 through the CRD, since lactose occupies the binding space within this region. It also suggests that any binding of the APEX2 to CD38 is minimal since the trends in binding were similar between the CRD only (rGal3) and PXGal3.



	CD38	
	PX-Gal3	rGal3
R squared	0.9402	0.9939
EC50 (μM)	~0.031	3.405

Figure 51: Confirmation of galectin-3 binding to CD38 by ELISA.

EC50 of PX-Gal3 (orange) and rGal-3 (blue) binding to immobilised CD38 was determined by ELISA. Increasing concentrations (shown as log nM) of rGal3 and PX-Gal3 were added to plate-bound CD38 for two hours. Wells were washed and anti-Galectin-3 peroxidase conjugate added to each well. Wells were washed and solution replaced with TMB substrate. Colour change in wells was measured at 450 nm and corrected using 540 nm or 570 nm wavelength. Data was plotted for the log nM concentration and curve fitted for determining EC50 values and shown as average \pm SD of triplicates. The R-squared value shows accurate line fitting.

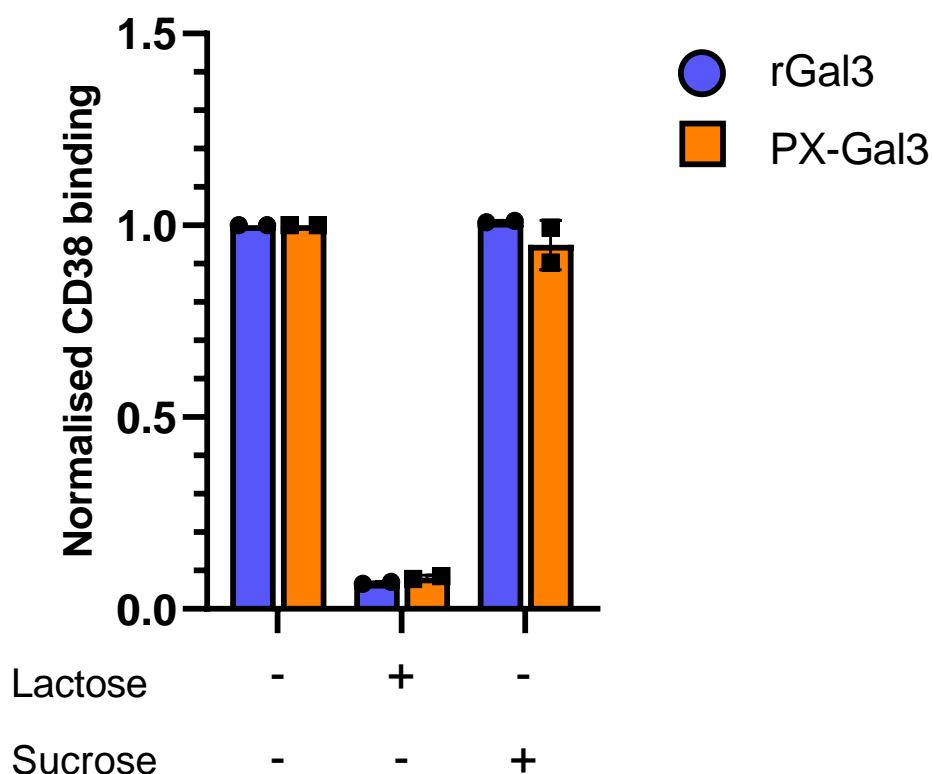


Figure 52: Galectin-3 binding to CD38 was outcompeted in the presence of lactose.

Binding of both PX-Gal3 (orange) and rGal-3 (blue) to immobilised CD38 (3 µg/ml) was determined using ELISA. Lactose was added to determine whether the interaction between CD38 and Gal-3 is likely to be glycan-dependent, compared to non-competing sucrose or in the absence of any sugars. Colour change in wells was measured at 450 nm and corrected using 540 nm or 570 nm wavelength. Data was normalised to non-sugar containing baseline to show changes in binding in the presence of sugar. Presented as average of two repeats (n = 2).

5.7 Validation of MMRN2 binding

Another protein highlighted as significant in the enriched mass spectrometry data (**Figure 15**), was Multimerrin-2. This protein is of particular interest within our research department as Professor Roy Bicknell has produced a significant amount of data relating to lectin-binding to MMRN2. As such, we were able to easily access a suite of reagents to perform validation assays, including co-immunoprecipitation experiments to determine Gal-3 binding to recombinant MMRN2.

Firstly, we predicted PX-Gal3 binding to MMRN2 using ColabFold v1.5.5, and observed low prediction scores on the overall folding of MMRN2, as indicated by the low pLDDT scores of 56-59 and even ≤ 55 in some regions (**Figure 53**) (Mirdita et al. 2022). Such low scores indicate flexibility and reduced confidence in the predicted folding, suggestive of intrinsically disordered protein regions. Focussing in on the space between the Gal3 portion (magenta) of PX-Gal3, we observe predicted interactions with MMRN2 of 4Å (**Figure 54**, connecting red lines). Of note, an N-linked glycosylation site at asparagine residue 439 (N439) is located near to the CRD of Gal3 (magenta) and might improve the affinity of Gal3 to MMRN2. Again, we observed strong predictions for APEX-2 (grey) binding to MMRN2 using *in silico* modelling (**Figure 54**).

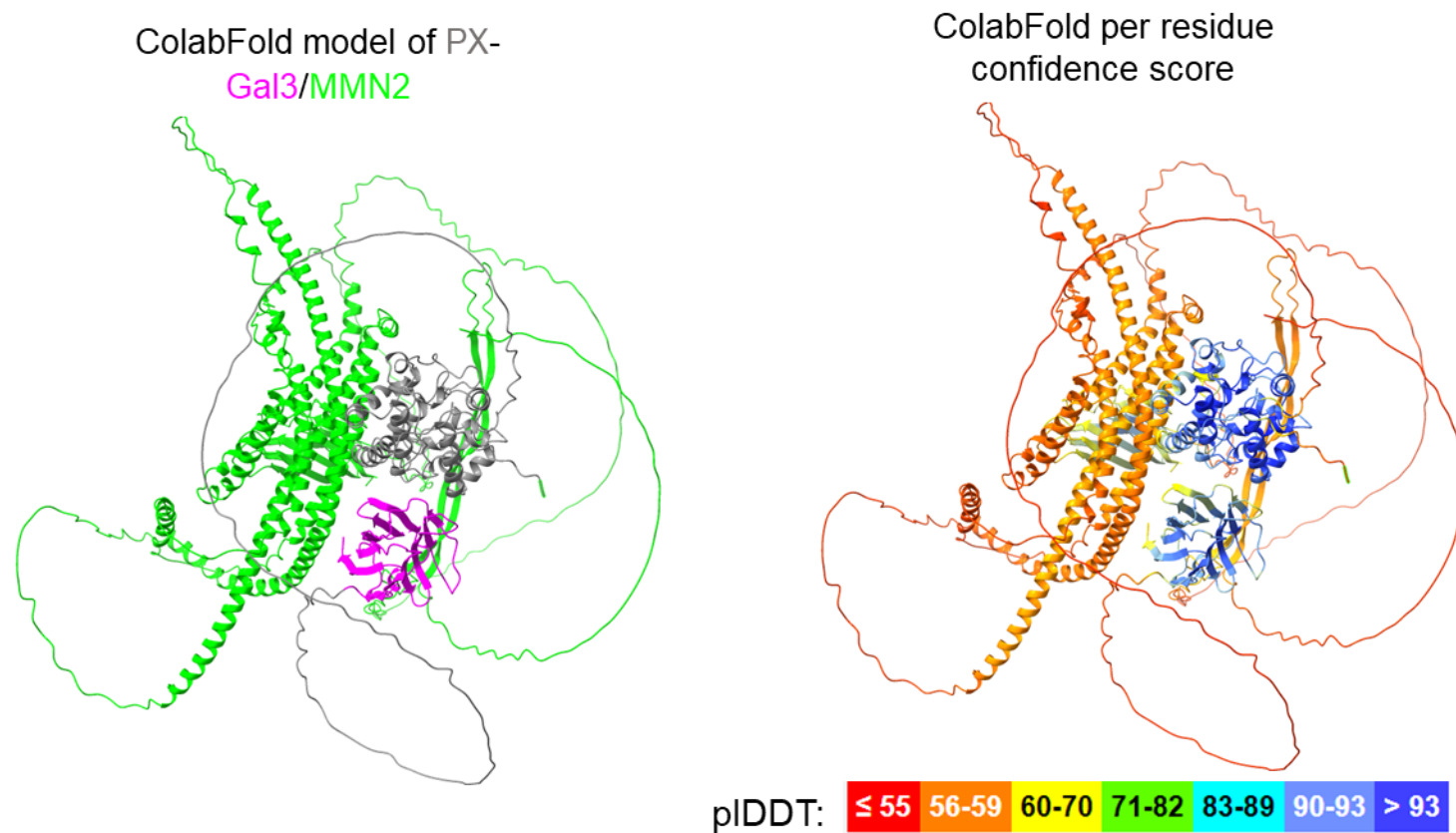


Figure 53: In silico model of PX-Gal3 interaction with Multimerin-2.

ColabFold was used to model and visualise the predicted interaction between PXGal3 and multimerin-2 (MMRN2). Left shows the structures coloured according to protein. Right shows model coloured based on predicted error in folding, where blue indicated high confidence in predicted folding and red is low confidence.

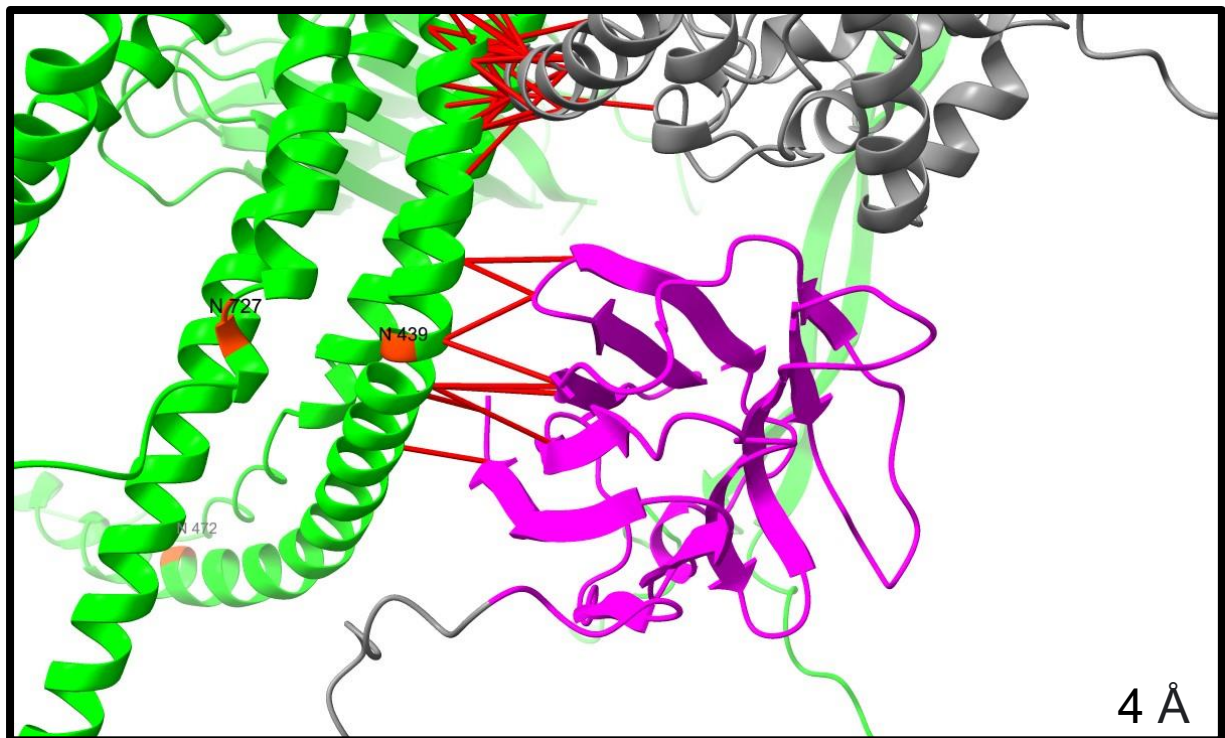


Figure 54: Predicted residues facilitating interactions between PX-Gal3 and MMRN2 were determined in silico.

ColabFold was used to model and visualise the predicted interaction between PXGal3 and multimerin-2 (MMRN2). Red bridges show predicted interactions between the Gal3 portion of PX-Gal3 (magenta) and the coils of MMRN2 (green) at 4 Å resolution. Asparagine positions on MMRN2 that are likely to be glycosylated in vivo are highlighted in red orange at multiple positions, including N439 which is within the centre of the Gal-3/MMRN2 binding interface. Interactions between the APEX2 portion (grey) of PX-Gal3 and MMRN2 are also observed at 4 Å resolution.

We confirmed by ELISA, that the CRD portion of Gal3 was binding to MMRN2 since we detected binding to both PX-Gal3 and rGal3 (**Figure 55**). We observed a 60% reduction in binding of either Gal-3 protein to MMRN2 in the presence of lactose, compared to negative control, and no changes in binding in the presence of sucrose (**Figure 55**). This partial reduction in binding confirms that the interaction between Gal-3 and MMRN2 is partially glycan-dependent since we still observed some degree of binding in the presence of lactose.

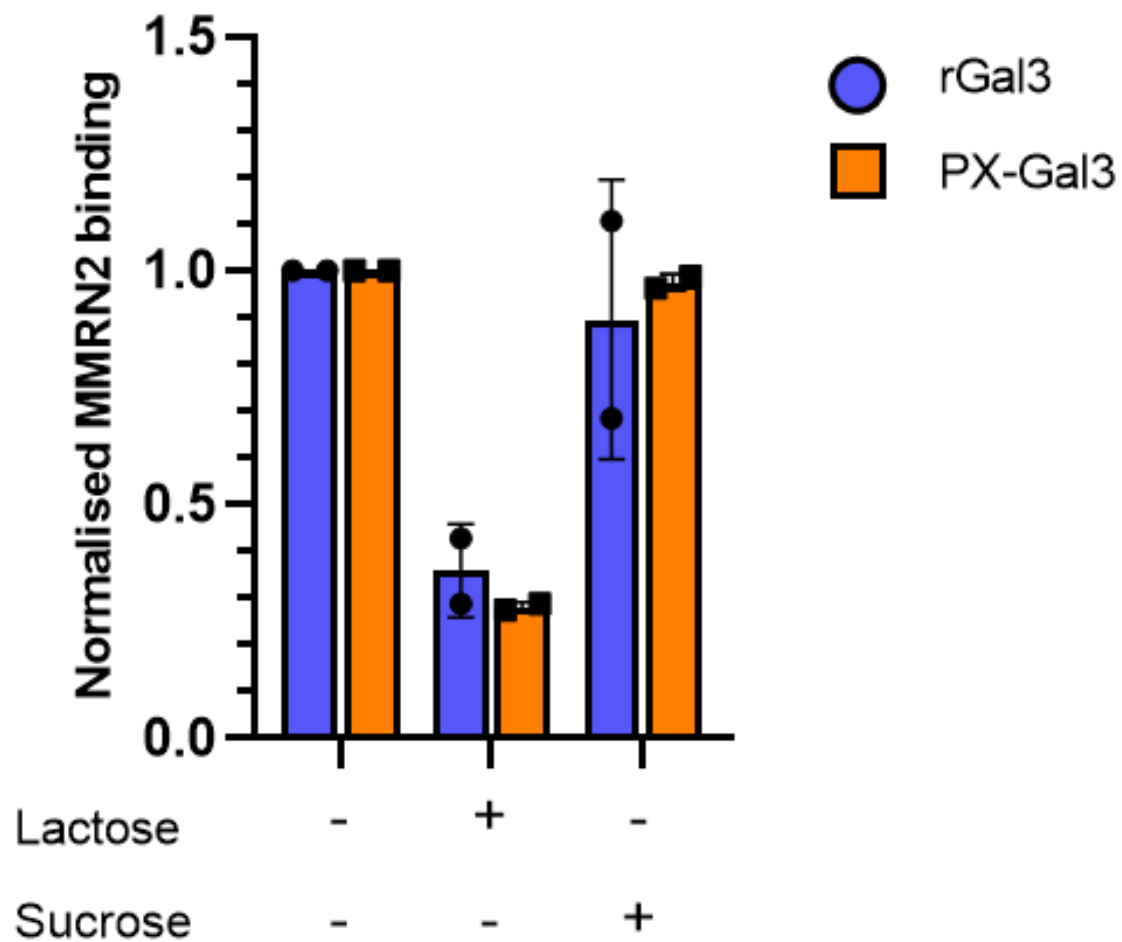


Figure 55: Galectin-3 binding to MMRN2 was not entirely glycan-dependent since binding was not fully inhibited in the presence of lactose.

rGal-3 (blue) and PX-Gal3 (orange) binding to immobilised CD38 was determined by ELISA. CD38 was coated onto plastic at 3 µg/ml overnight. Either PX-Gal3 or rGal3 +/- sucrose or lactose were added to the plate in replicates and incubated for 2 hours before washing. Anti-Galectin-3 peroxidase conjugate was added to each well, washed and replaced with TMB substrate. Colour change in wells was measured at 450 nm and corrected using 540 nm or 570 nm wavelength. Data was normalised to non-sugar containing baseline to show changes in binding in the presence of sugar.

Immobilisation of the recombinant MMRN2 to plastic can alter its shape and orientation, either preventing or facilitating specific interactions between MMRN2 and Gal-3. To overcome this, and to provide additional evidence supporting their interaction, we opted to use co-immunoprecipitation of recombinant MMRN2 and PX-Gal3 in solution. Following incubation with nickel beads to recover the PX-Gal3, we ran the immunoprecipitation eluate on Western blot and confirmed the presence of MMRN2 in solution, further supporting the binding interaction between the two proteins **(Figure 56)**. In the presence of lactose, we visualised very little difference in the band intensity for MMRN2, suggesting that the interaction between MMRN2 and PX-Gal3 is mediated by protein-protein interactions rather than being glycan-mediated **(Figure 56)**. We would have predicted to see ~40% reduction in band size based on our findings by ELISA. We observed a very faint band for MMRN2, if at all, in the whole cell lysate control in lane three, most probably due to the MMRN2 being too dilute in lysis buffer **(Figure 56)**. The presence of two Gal-3 bands was concerning, suggesting that the PX-Gal3 might have degraded in solution, as the lower band resides in the expected size of the CRD portion of Gal-3 (~35 kDa). Nickel beads were employed for PX-Gal3 pull-down. Depending on degradation timing, representative images may be affected, as the His-tag precedes the Gal-3 portion of PX-Gal3. To eliminate this issue, we replaced the PX-Gal3 with recombinant, CRD only, Gal-3. We used a truncated version of MMRN2, which contained a His-Tag, and nickel beads to pull down protein complexes.

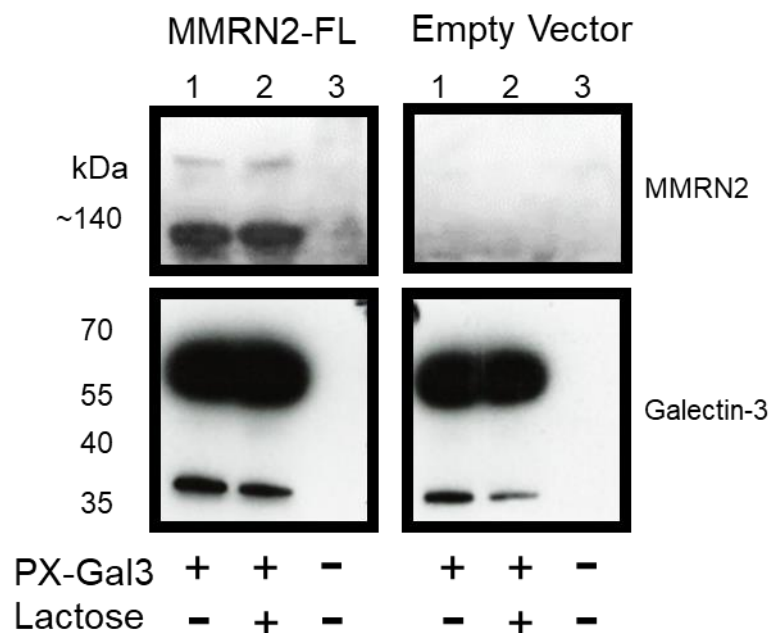


Figure 56: Western blot showing presence of Multimerin-2 bands following co-immunoprecipitation of PX-Gal3 in cell lysates.

HEK cells were transfected with multimerin-2 (MMRN2-FL) or control (Empty) vector for overexpression of full-length MMRN2 (MMRN2-FL) protein. Cells were lysed and either incubated with PX-Gal3, without lactose (1), with PX-Gal3 and lactose (100nM) (2), for two hours. Immunoprecipitation was performed using nickel beads to pull-down PX-Gal3 and associated complexes. Beads were washed before denaturing and running on SDS-gel, alongside whole lysate control (3). Western blotting was used to determine the presence of MMRN2 and Galectin-3 using specific antibodies.

We detected Gal-3 bands of ~35 kDa in all sample conditions, as confirmed by the band in our positive rGal-3 protein only control (**Figure 57**). Ni-NTA beads are notoriously 'sticky', as such they are likely to bind many endogenous proteins within the lysates. Given the promiscuity of Gal-3 binding, the exogenous rGal-3 is likely to bind to some of the proteins within the lysate which are then pulled down and detected by Western blot. Promisingly, we see a more intense band for Gal-3 in the Trunc-MMRN2 condition compared to the empty vector control (**Figure 57**). We also see that in the presence of lactose, the level of detected Gal-3 is lower. Although this is not sufficient evidence alone, it does strengthen our portfolio of evidence supporting the interaction Gal-3 to MMRN2 in a semi glycan-dependent manner.

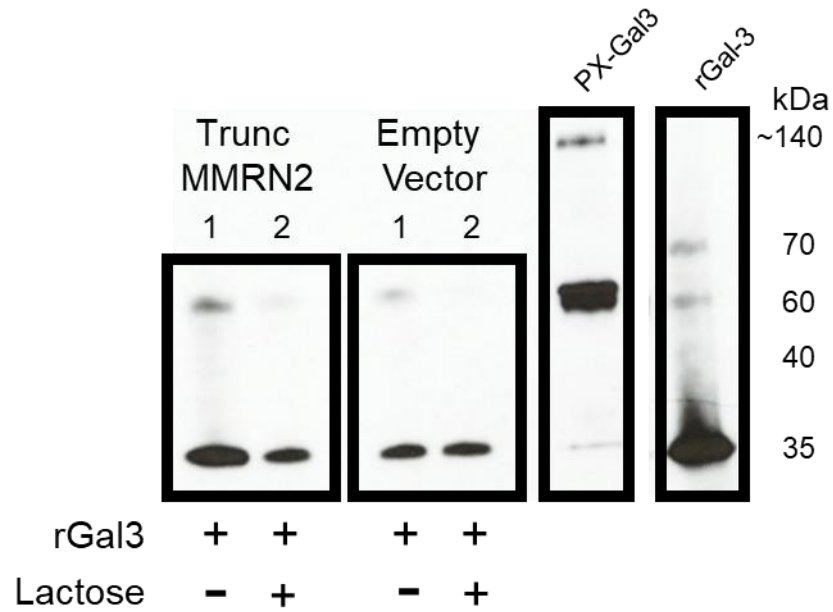


Figure 57: Western blot showing Galectin-3 bands following co-immunoprecipitation of MMRN2 using rGal3.

HEK293 cells overexpressing truncated-MMRN2, or empty vector were lysed and either incubated with rGal-3, without lactose (1), with rGal-3 and lactose (100nM) (2) overnight. Trunc-MMRN2 was pulled-out of solution using nickel beads, denatured, and run on SDS-PAGE gel, alongside PX-Gal3 and rGal-3 protein for detection and confirmation of Galectin-3 bands by Western blot.

5.8 Discussion

The rationale of this chapter was to elucidate the function of exogenous galectins in the context of endothelial cells and inflammation. To achieve this, our collaboration with Dr Mia Huang and Dr Geno Joeh, who provided the PX-Gal3 reagents, expertise, and access to proteomics and glycomics analysis, was instrumental. We have, a) identified a list of novel Gal-3 interactors on HUVEC and b) characterised proteins that may be important in the response to inflammatory stimuli to either promote or resolve inflammation. Moreover, we observed through competition studies with lactose, that many of these interactions were glycan dependent. Through the comparison of protein interactors enriched in response to $\text{TNF}\alpha$ + $\text{IFN}\gamma$ stimulated HUVEC or basal conditions, we were also able to identify several proteins that may be important in facilitating pro- and/or anti- inflammatory effects. Analysis of both proteomic and genomic datasets in parallel, highlights that differences in binding interactions between Gal-3 may be driven through changes in the protein-interactors' glycosylation state. This may be the case where differential enrichment across treatments groups is observed in the protein dataset but not at the transcriptional level.

5.8.1 Optimisation of proximity labelling of HUVEC

We established an optimised protocol for proximity labelling of HUVEC, involving 1-minute incubation with PX-Gal3 and subsequent 1-minute with biotin phenol. Joeh et al. published a list of potential Gal-3 interactors expressed in LX-2 cells, an immortalised hepatic stellate cell line, using 30-minute incubation steps (Joeh et al. 2020). We observed detachment of HUVEC from plastic following the original protocol, and after less than 10 minutes in DMEM containing no serum. Other studies have successfully cultured HUVEC in serum negative DMEM overnight and report no cell

detachment or death (Simoncini et al. 2002). Despite the tissue-culture plates being pre-treated for adherent cells, the lack of ECM pre-coating may also contribute to rapid cell detachment, since it has been shown that different ECM coatings can influence growth, adhesion, and morphology of adherent cells (Zhang et al. 2009). Our optimised protocol reduces the impact of these problems since cells were grown to full confluency before the labelling protocol and treated for only 1 minute without serum at the incubation stages.

Joeh et al report within their findings, the identification of intracellularly located proteins (Joeh et al. 2020). Following our modified and optimised protocol, we identified only extracellular, and membrane located proteins. Whilst the optimised protocol limits our ability to identify intracellular interactors of Gal-3, the reduced incubation times are likely to have aided in the recovery of intact membrane-bound, or ECM targets that are physiologically relevant. This is not only since cells remained adhered to the plastic with reduced incubation, but also that exogenous Gal-3 was reported to induce rapid MMP-9 expression and activity (Dange et al. 2014), which leads to cleavage of ECM components (Wang and Khalil 2018) and CAMs (Conant et al. 2010) in melanoma cells. Proteins cleaved in such a way might result in the loss of tagged proteins during the washing stages prior to mass spec analysis.

We identified a total of 342 and 340 potential interactors of galectin-3 on unstimulated and TNF α + IFN γ stimulated HUVEC, respectively. Positively, some of the proteins we identified were also present within the LX2 dataset, including *BSG*, *CD40*, *CD47* and *LGALS3* (Joeh et al. 2020). Joeh et al reported 248 proteins within the enrichment and competition LX2 datasets (Joeh et al. 2020). Given that galectin-3 is a promiscuous protein known for its binding to glycosylated proteins and lipids, which makes up 5 –

10 % of the total membrane mass (Cooper 2000), it is not surprising that we uncovered many enriched proteins by mass spectrometry. We identified unique proteins which were differentially enriched within the TNF α + IFN γ stimulated HUVEC, some of which we determined to be due to differential gene expression in response to treatment (**Table 5**). Amongst these were *ICAM1*, *VCAM1*, *SELE* and *PECAM1* which all have established roles within the leukocyte trafficking cascade (Herter and Zarbock 2013) (Ley et al. 1998). Interestingly, the crucial role of *SELE* in regulating leukocyte tethering and slow rolling appeared to be significantly inhibited in galectin-double-knockout mice, as seen by increased leukocyte flux, and to an extent but not significantly, within our Gal-3^{-/-} mice (**Figure 21 and 36**) (Chiu et al. 2007). Gittens et al show that lung endothelial cells from Gal-3^{-/-} mouse express reduced SELE on their cell surface (Gittens et al. 2017). Since we know that Gal-3 is also intracellularly expressed, a direct interaction between the two molecules, as supported by our data, might be driving the function of *SELE* within the leukocyte trafficking cascade.

Interestingly we identified some proteins that were more enriched within the mass spectrometry data, but which did not exhibit differential gene transcription. For example, *HYAL2*, a glycosylphosphatidylinositol-anchored hyaluronidase, showed almost 4-fold less enrichment within the treated conditions, despite displaying only a 0.5-fold reduction in transcription. Internalisation of *HYAL2* via endocytosis into lysosomes is required for its function in degrading hyaluronan (HA) - a major ECM component, into smaller functional fragments which stimulate synthesis of inflammatory cytokines (Ronny and Mark 2012) (Bourguignon et al. 2004). This could explain why we see less enrichment of *HYAL2* in the TNF α + IFN γ stimulated HUVEC.

TLR2 was amongst the most differentially enriched proteins within the stimulated HUVEC, though did not display significant differential gene transcription. *TLR2* is reported to translocate to the EC surface in response to IFN γ stimulation, which is supported by our observation of enrichment in the treated HUVEC mass spec data (Shuang et al. 2007). We also see that metalloprotease *ADAM10*, responsible for cleaving TNF α , is differentially enriched between the treatment groups in our mass spectrometry data, but not in the transcriptional dataset. Since *ADAM10*-mediated cleavage of TNF α is dependent on tetraspanins, we might hypothesise that *ADAM10* is undergoing conformational changes when bound to different tetraspanin ligands (Noy et al. 2016). Such a conformational change might 'mask' galectin-3 epitopes, thus *ADAM10* enrichment is greater in untreated HUVEC compared to TNF α + IFN γ stimulated HUVEC. Such intricacies of potential galectin-3 binding to its interactors, and the downstream functional consequence of this requires further reading and experimental work to validate and form hypothesis from our data. This might include confocal imaging of intact cells to determine exogenous gal-3 binding, localisation and potential trafficking within HUVEC.

We reported changes in the abundance of specific N-glycans, between stimulated and control HUVEC. Differences in the glycomic profile could affect the affinity for galectin binding to its natural ligands, since galectin-3 has an increased affinity for repeats of internal and terminal LacNAc units, with some tolerance for sialylation, of which we see more of in stimulated HUVEC (Patnaik et al. 2006). Changes in cell-surface glycans provide diagnostic and prognostic value in disease, particularly in cancer and rheumatoid arthritis (Ohtsubo and Marth 2006) (Axford et al. 1992) (Reily et al. 2019). Meanwhile, defects in the glycosylation patterns of cellular proteins have been reported to negatively influence recognition of self and non-self-antigens, resulting in

faulty or chronic inflammatory responses (Zhou et al. 2021). Therefore, it's possible that Gal-3 will preferentially bind proteins in one glycosylation state over another, explaining why we might see differential enrichment of one protein in one HUVEC condition and not the other. Further investigating into the different glycosylation states of the identified proteins would provide clarity on this as a potential factor influencing our results and whether this is a feasible explanation for the differences observed between HUVEC conditions.

5.8.2 *Gal-3 interactions with CD38*

We identified *CD38* as one of the most differentially enriched proteins between the two HUVEC datasets. *CD38* is ubiquitously expressed in several cell types, including T-cells, B cells, macrophages, monocytes, neutrophils and more, but was originally discovered for its role in inducing T-cell apoptosis via shared pathways with the *CD3*/T-cell receptor (Morra et al. 1998). The role of *CD38* as an immunomodulatory molecule in autoimmunity and inflammation has also been reviewed (Piedra-Quintero et al. 2020). Interestingly, *CD38* was not identified within the published list of enriched proteins in PBMCs following proximity labelling with PX-Gal3 (Joeh et al. 2020). One explanation for this may be due to the requirement of stimulation of PBMCs with pro-inflammatory cytokines, which was reported to upregulate *CD38* expression in macrophages and monocytes, as well as in HUVEC as confirmed in our dataset (Amici et al. 2018). It was recently reported that EC activation of *CD38* leads to accelerated degradation of nicotinamide adenine dinucleotide (NAD⁺), an important cofactor required for fundamental biological processes, linked to increased blood pressure and vascular damage associated with hypertension (Qiu et al. 2023). Membrane anchored *CD38* also interacts with *CD31* on endothelial cells, not only promoting leukocyte

adhesion, but triggering complex transmembrane signalling to induce pro-inflammatory responses (Deaglio et al. 2000). The localisation of CD38 into lipid-rafts is required for trafficking into the cell via endocytosis, to perform intracellular functions (Saeed et al. 2022). Interestingly, Gal-3 has previously been reported to trigger the ordering and subsequent bending of glycosphingolipids within the membrane to facilitate endocytosis of *CD44* in dendritic cells (Lakshminarayan et al. 2014). Together, these data suggest that Gal-3 could play a crucial role in facilitating the clustering of molecules into ordered membrane rafts to support signal transduction. This is particularly feasible since Gal-3 can oligomerise and broadly binds to glycans which are heavily present within the glycocalyx and on proteins and lipids embedded within the cell membrane. Further investigation into this hypothesis is required and would involve knocking down endogenous Gal-3 and adding in exogenous Gal-3 protein, measuring clustering events either by high-resolution microscopy or through western blotting for *CD38* in either ordered or non-ordered fractions.

5.8.3 *MMRN2* interaction with Galectin-3.

We identified *MMRN2* as a novel binding partner of Galectin-3. This has not previously been reported. *MMRN2* is a large surface-expressed molecule found mainly in endothelial cells and adipocytes (Atlas 2023). The expression of *MMRN2* is unaffected by inflammatory cytokines (Sanz-Moncasi et al. 1994), which we also confirm in our RNA sequencing dataset. Splenic, and hepatic sinusoids have reduced expression of *MMRN2* (Sanz-Moncasi et al. 1994; Pellicani et al. 2020), which incidentally are both areas of low shear stress, and where we would expect to see less Gal-3 expression in ECs based on our data (**Section 3.2**).

MMRN2 functions as an angiostatic molecule which inhibits *VEGFR2* signalling through its binding to *VEGFA* (Colladel et al. 2016). Contrary to this, Galectin-3 is a known angiogenic molecule through its role in facilitating clustering of integrin $\alpha\beta3$ through glycan-dependent interactions that promotes *VEGF* mediated angiogenesis (Nangia-Makker et al. 2000). *In silico* modelling predicts that the interaction between Gal-3 and *MMRN2* occurs at residues surrounding N439, which is a predicted glycosylation site. Since molecular modelling does not predict or display glycosylation sites or patterns, we speculate that the interaction and affinity of Gal-3 for *MMRN2* would improve in the presence of glycans, as the natural ligand for Gal-3. Our binding study suggests that the interaction between Gal-3 and *MMRN2* is not wholly glycan-dependent, since in the presence of lactose we still saw ~40% binding of rGal-3 to *rMMRN2*.

C-type lectin domain containing group 14 members; *CLEC14A*, *CD248* and *CD93*, have all been identified as cognate ligands for *MMRN2* (Khan et al. 2017). *CD248* is a molecule expressed in fibroblasts that has been found in complex with Gal-3 to promote inflammation and fibrosis through the induction of *CCL17* and collagen deposition in macrophages and myofibroblasts respectively (Pai et al. 2020). Deletion of *CD248* reduced the susceptibility of mice to liver fibrosis in one study, whilst another study report that capillary sprouting was dependent on *CD248* expression (Wilhelm et al. 2016) (Naylor et al. 2014). *CD248* binds to *MMRN2* between amino acids 133 and 486 which overlaps the predicted region for Gal-3 binding (Khan et al. 2017). Whilst the function of this interaction is yet to be determined, correlation between lowly expressed *MMRN2* within liver tissue, which is highly susceptible to fibrosis, suggests that Gal-3 and *MMRN2* interactions might be key in driving fibrosis. Given the promiscuity of Gal-3 binding, it is highly likely that Gal-3 may be facilitating multiple

simultaneous interactions between ECM components and requires careful design of functional assays to fully elucidate these functional relationships.

5.8.4 Therapeutic potential

The promiscuity of lectin binding and function as soluble protein makes them challenging molecules to target therapeutically. The use of lectin-fusion proteins to proximally tag and identify novel interactors offers an attractive method to understanding lectin-binding in the physiologically relevant context of specific cell states. In this case, we uncover novel interactors of exogenous galectin-3 on HUVEC in the context of inflammation through comparing enriched proteins within the TNF α + IFN γ stimulated HUVEC to unstimulated control. With further exploration of tissue-specific GBP-interactions, there is potential to uncover attractive therapeutic opportunities that limit cross-reactivity and off target effects to develop highly specific therapies.

One such example, could be in targeting the N-term of Gal-3, to prevent the formation of oligomers and thus lattice formation that may be responsible for downstream signalling and reprogramming of the endothelial extracellular environment that drives cancer and fibrosis (Marino et al. 2023). Alternatively, we might use proximity labelling to understand the mechanisms of the protective role of Gal-3 in microbial infection which is often accompanied by reduced neutrophil recruitment (Oliveira et al. 2021). Increased levels of serum Gal-3 are associated with cardiovascular disease and SARS-CoV-2 infections (Liu et al. 2022; Cervantes-Alvarez et al. 2022; Blanda et al. 2020). As such, we could try and target Gal-3 using bi- or tri-valent antibodies specific to the N-term, to recruit and redirect circulating serum Gal-3, towards its' ligands to facilitate protective or pro-resolving interactions to treat diseases. Alternatively, we

might wish to use fusion proteins containing Gal-3 to induce signal transduction in immune cells by facilitating the formation of lipid rafts that direct transduction towards a pro- or even anti-inflammatory response depending on the patients' needs (Demetriou et al. 2001) (Lagana et al. 2006) (Nangia-Makker et al. 2007; Nieminen et al. 2007).

5.8.5 Limitations

Our results are based on one round of proximity labelling performed in triplicate, on HUVEC samples made up of three cell donors pooled together. Ideally this experiment would have been repeated, to confirm the identification of proteins across multiple experiments, however, due to technical issues with the mass-spectrometry machine, we were unable to run the repeat samples. Since we used pooled HUVEC, our data should account for natural biological variation within our samples, and having run the experiment in triplicate, we should also account for sample variation in our data acquisition.

Galectin-3 and PX-Gal3 are both able to oligomerise in solution (Nieminen et al. 2007), which adds a layer of complexity in determining binding interactions and functions of protein interactions. We validated the binding between Gal-3 with CD38 and MMRN3 using immobilised rGal3 (CRD only) and PX-Gal3 to determine binding EC50s. In this format, we have no control over the orientation of the protein interactions, and therefore unable to determine whether oligomerisation is critical for these interactions.

In summary, we have identified a large list of novel protein interactors to PX-Gal3, of which several have been validated using *in silico* and *in vitro* techniques. Further work to establish functional impact of these interactions is required, but we hypothesise that

exogenous Gal-3 facilitates protein clustering within the membrane, to promote protein-protein interactions crucial for several cellular functions, including key mechanisms of inflammation and disease.

CHAPTER 6: CONCLUDING REMARKS AND FUTURE DIRECTIONS

6.1 Concluding Remarks

6.1.1 Concluding Remarks

In this thesis, we aimed to elucidate the function of endothelial galectins and their pivotal role in leukocyte trafficking, through research into the regulators of endogenous endothelial galectins, their functions in leukocyte trafficking *in vivo*, and in studying interactors between exogenous Gal-3 and stimulated HUVEC. Our approach involved characterising the regulators of endothelial galectin expression and elucidating their functions through *in vivo* and *in vitro* assays to uncover key molecular interactions. The findings presented here shed light on the nuanced roles of galectins in immune responses, presenting both intriguing revelations and avenues for further investigation.

6.1.2 Key Findings

Our results highlight several crucial insights: Firstly, we observed that endothelial Gal-9 expression is intricately regulated by viral-associated mediators (e.g.) IFN γ , IFN β , IFN α 2 and PolyI:C, suggesting its involvement in immune responses to infection. Secondly, our data indicate that endogenous Gal-3 and -9 operate through distinct mechanisms to regulate leukocyte trafficking events, as demonstrated by the increased leukocyte flux through the vessels of inflamed cremaster of Gal-3^{-/-}/Gal-9^{-/-} double knockout mice. We observe that endogenous Gal-3 expression is responsive to shear stress and less so to inflammatory mediators, whilst endogenous Gal-9 expression is highly regulated by both pro-inflammatory mediators and shear stress. Finally, we speculate that exogenous Gal-3 has a pivotal function in driving inflammatory responses as we report differences in the binding of exogenous Gal-3

with novel ligands, including *CD38* and *MMRN2*, on the surface of unstimulated and TNF α and IFN γ -stimulated HUVEC that alludes to a crucial and expansive role for exogenous Gal-3 on endothelial function in inflammation.

6.1.3 *Context-Dependent Functions*

The elusive role of galectins in regulating immune responses suggests their function is highly dependent on the context of the tissue environment. Previous studies from our lab report that Gal-9 is a key player in atherosclerosis, which we further support through our culture under flow studies, confirming shear stress as a regulator of Gal-9 expression (Krautter et al. 2022). This opens many avenues for investigating the function of galectins, particularly considering tissue context and disease. For example, we can contrast the environment of the aorta, a site of high laminar shear stress, to the vessels in the liver sinusoids, which experience low shear stress to elucidate the roles of endothelial Gal-9 more specifically in atherosclerosis and liver disease, respectively.

Similarly, we allude to Gal-3 having multifaceted functions, which are governed by its endogenous or exogenous interaction with endothelial cells. We confirm that endogenous endothelial Gal-3 is upregulated in response to shear stress, but not pro-inflammatory mediators. Our results suggest that Gal-3 may be expressed and secreted under high shear stress, where it then binds to protein interactors on the endothelial cell surface. We hypothesise that the state of the endothelial cell – and whether it is activated or not – is the key determinant of Gal-3 binding and function. Since we identified several novel protein interactors through proximity labelling, we predict that the glycocalyx will also be a key factor determining the function of Gal-3. In the context of inflammation, the glycocalyx becomes disturbed and damaged,

exposing the endothelium to opportunistic binding from exogenous Gal-3, for which leukocytes are a major source. It is in further understanding of this cause-and-effect relationship that we predict Gal-3 function is important. We predict that Gal-3 is responsible for facilitating key interactions that determine cell state and function – particularly since the oligomeric nature of Gal-3 allows it to do so.

6.1.4 Implications for Atherosclerosis

We report here that Gal-9 is particularly responsive to laminar shear stress, predominantly at increased rates. We observe increased *LGALS9* transcription in response to orbital shaking culture, which appears to be expressed intracellularly, as confirmed through our results showing that Gal-9 positive staining was significantly increased in cells cultured with orbital shaking compared to static. We did not see increased transcription in HUVEC cultured with 2Pa laminar flow, suggesting that the heterogenous nature of high shear stress within the shaking well format is indeed the driver of mechanotransductive Gal-9 expression. As such, further experiments are required to look at the effect of higher shear stress rates on EC Gal-9 expression. We might hypothesise that Gal-9 is stored intracellularly in ECs lining the aorta, with some soluble Gal-9 expressed from the ECs for homeostatic function through predicted interactions with the glycocalyx – which we know to be heavily comprised of β -galactose containing glycans. In early atherosclerosis, the glycocalyx undergoes destruction and remodelling, which exposes the ECs to inflammatory mediators – namely TNF α and IL-1 β – both inducers of *LGALS9* transcription in ECs (Mitra et al. 2017). We hypothesise that Gal-9 is then released from the cells in soluble form, where it enters the bloodstream, raising the serum Gal-9 levels as observed in disease and prompting leukocyte trafficking to the area with eventual accumulation of leukocytes

into the plaques that drive disease. As such, we report that endogenous Gal-9 is necessary for physiological function in ECs and that when stimulated within the pro-inflammatory context, Gal-9 is secreted into the blood stream where it facilitates endothelial-leukocyte interactions that drive leukocyte trafficking, inflammation and ultimately disease if not resolved.

6.1.5 Liver Pathogenesis and Beyond

In the context of the liver, our results hint at the role of endogenous endothelial Gal-9 as a key driver in virus-associated pathogenesis. Gal-9 expression in LSECs is low in healthy physiological conditions. Since the liver sinusoidal endothelial cells are specialised to withstand low shear stress, this appears to be of protective importance within this context. We observe that Gal-9 is overexpressed within the LSEC following their treatment with viral-associated inflammatory mediators – namely IFN γ . We observe a similar trend in our HUVEC and HAEC data whereby IFN α 2, IFN β and PolyI:C, drive overexpression of Gal-9. Our *ex vivo* IHC data using HepC and PBC tissue sections confirm that Gal-9 expression is upregulated in diseased tissue compared to healthy control. This observation is particularly interesting since PBC and HepC are both virus-associated pathologies (Haydon and Neuberger 2000; Mason 2018).

We observe that macrophages – more specifically Kupffer cells – express high levels of Gal-9 in all diseased sections, providing scope to explore the function of exogenous Gal-9 on endothelial cells, particularly in the context of disease. Perhaps it would be worthwhile performing similar proximity labelling experiments to elucidate Gal-9 function in this context. However further investigation is certainly required to understand the function of exogenous Gal-9 on ECs, particularly in the liver, and its

role in facilitating leukocyte trafficking in liver disease. Moreover, further investigation into the context of galectin expression patterns is necessary to understand the biological relevance of disease and tissue-specific galectin responses.

6.1.6 Future Directions

Moving forward, we will be continuing work to further understand the role of Gal-3 in the context of endothelial-leukocyte crosstalk. We observe interesting results alluding to soluble exogenous Gal-3 being a key molecule for determining endothelial cell fate and function. We observe that endogenous endothelial Gal-3 transcription remains stable in HUVEC following stimulation with pro-inflammatory mediators, and is significantly decreased in LSEC with TNF α and IFN γ treatment. As such, using the list of novel surface-expressed interactors that we discovered through proximity labelling of HUVEC treated with TNF α and IFN γ , and comparing this with the list of interactors we recovered from proximity labelling on untreated HUVEC, we wish to better understand the function of Gal-3 in the context of leukocyte trafficking. We hypothesise that exogenous Gal-3 functions through initiation of signal transduction by facilitating the formation of lipid rafts. Many reports have shown that Gal-3 is increased in the serum of patients suffering from various diseases, including cardiovascular and autoimmune diseases, neurodegenerative disorders, and cancer, which may provide the exogenous Gal-3 that initiates immune and inflammatory responses across the blood vessels.

Following the discovery of Gal-3 as a molecule expressed by activated macrophages, it appears to be a significant contributor to elevated serum levels. Our objective is to delve deeper into understanding the interplay between soluble Gal-3 and one of its identified interactors – CD38. We hypothesise that Gal-3 plays a pivotal role as a

mediator in this interaction. Our investigation will extend to the interaction between CD38 and its established ligand CD31, which we believe acts as a crucial catalyst for transmigration. We hypothesise that this process is facilitated by the initiation of lipid raft formation through which we believe Gal-3 interactions with phosphosphingolipids and CD38 to be crucial. To explore these dynamics, we plan to employ fluorescently labelled recombinant proteins and super-resolution microscopy techniques. This methodology will enable us to monitor the movement of CD38 and CD31 through the membrane in the presence of exogenous Gal-3. The significance of such research may uncover potential therapeutic opportunities that could be used to prevent chronic inflammation, and even alter the endothelial cell states towards homeostatic to promote disease resolution.

6.1.7 Conclusion

In conclusion, galectins emerge as complex glycan-binding proteins with diverse functions dependent on their context. The interplay between galectins, shear stress, and the vascular microenvironment presents a fascinating area for future exploration. As we delve deeper into the sophisticated family of galectins, we anticipate unravelling their intricate contributions to the cross talk among molecules and structures in the larger biological landscape. The dual nature of pro-inflammatory and pro-resolution responses suggests galectins as key players in maintaining immune homeostasis—a field ripe for further investigation.

LIST OF REFERENCES

- Afshar, Y., F. Ma, A. Quach, A. Jeong, H. L. Sunshine, V. Freitas, Y. Jami-Alahmadi, R. Helaers, X. Li, M. Pellegrini, J. A. Wohlschlegel, C. E. Romanoski, M. Vikkula, and M. L. Iruela-Arispe. 2023. 'Transcriptional drifts associated with environmental changes in endothelial cells', *Elife*, 12.
- Aird, William C. 2007. 'Phenotypic Heterogeneity of the Endothelium', *Circulation Research*, 100: 158-73.
- Ajami, N. E., S. Gupta, M. R. Maurya, P. Nguyen, J. Y. Li, J. Y. Shyy, Z. Chen, S. Chien, and S. Subramaniam. 2017. 'Systems biology analysis of longitudinal functional response of endothelial cells to shear stress', *Proc Natl Acad Sci U S A*, 114: 10990-95.
- Alsaffar, H., N. Martino, J. P. Garrett, and A. P. Adam. 2018. 'Interleukin-6 promotes a sustained loss of endothelial barrier function via Janus kinase-mediated STAT3 phosphorylation and de novo protein synthesis', *Am J Physiol Cell Physiol*, 314: C589-C602.
- Amici, S. A., N. A. Young, J. Narvaez-Miranda, K. A. Jablonski, J. Arcos, L. Rosas, T. L. Papenfuss, J. B. Torrelles, W. N. Jarjour, and M. Guerau-de-Arellano. 2018. 'CD38 Is Robustly Induced in Human Macrophages and Monocytes in Inflammatory Conditions', *Front Immunol*, 9: 1593.
- Asthana, S., C. Toso, G. Meeberg, D. L. Bigam, A. Mason, J. Shapiro, and N. M. Kneteman. 2011. 'The impact of sirolimus on hepatitis C recurrence after liver transplantation', *Can J Gastroenterol*, 25: 28-34.
- Atlas, The Human Protein. 2023. 'ENSG00000173269-MMRN2', Accessed December 2023. <https://www.proteinatlas.org/ENSG00000173269-MMRN2/single+cell+type>.
- Auvynet, Constance, Samadhi Moreno, Erika Melchy, Iris Coronado-Martínez, Jose Luis Montiel, Irma Aguilar-Delfin, and Yvonne Rosenstein. 2012. 'Galectin-1 promotes human neutrophil migration', *Glycobiology*, 23: 32-42.
- Axford, J. S., N. Sumar, A. Alavi, D. A. Isenberg, A. Young, K. B. Bodman, and I. M. Roitt. 1992. 'Changes in normal glycosylation mechanisms in autoimmune rheumatic disease', *J Clin Invest*, 89: 1021-31.
- Ayona, D., P. E. Fournier, B. Henrissat, and B. Desnues. 2020. 'Utilization of Galectins by Pathogens for Infection', *Front Immunol*, 11: 1877.
- Baeriswyl, D. C., I. Prionisti, T. Peach, G. Tsolkas, K. Y. Chooi, J. Vardakis, S. Morel, M. R. Diagbougua, P. Bijlenga, S. Cuhlmann, P. Evans, B. R. Kwak, Y. Ventikos, and R. Krams. 2019. 'Disturbed flow induces a sustained, stochastic NF-

- kappaB activation which may support intracranial aneurysm growth in vivo', *Sci Rep*, 9: 4738.
- Bänfer, S., and R. Jacob. 2020. 'Galectins in Intra- and Extracellular Vesicles', *Biomolecules*, 10.
- Baum, L. G., J. J. Seilhamer, M. Pang, W. B. Levine, D. Beynon, and J. A. Berliner. 1995. 'Synthesis of an endogeneous lectin, galectin-1, by human endothelial cells is up-regulated by endothelial cell activation', *Glycoconj J*, 12: 63-8.
- Bevilacqua, M. P., J. S. Pober, D. L. Mendrick, R. S. Cotran, and M. A. Gimbrone, Jr. 1987. 'Identification of an inducible endothelial-leukocyte adhesion molecule', *Proc Natl Acad Sci U S A*, 84: 9238-42.
- Bi, Shuguang, Patrick W. Hong, Benhur Lee, and Linda G. Baum. 2011. 'Galectin-9 binding to cell surface protein disulfide isomerase regulates the redox environment to enhance T-cell migration and HIV entry', *Proceedings of the National Academy of Sciences*, 108: 10650-55.
- Blanda, V., U. M. Bracale, M. D. Di Taranto, and G. Fortunato. 2020. 'Galectin-3 in Cardiovascular Diseases', *Int J Mol Sci*, 21.
- Bocci, V. 1991. 'Interleukins. Clinical pharmacokinetics and practical implications', *Clin Pharmacokinet*, 21: 274-84.
- Bourguignon, L. Y., P. A. Singleton, F. Diedrich, R. Stern, and E. Gilad. 2004. 'CD44 interaction with Na⁺-H⁺ exchanger (NHE1) creates acidic microenvironments leading to hyaluronidase-2 and cathepsin B activation and breast tumor cell invasion', *J Biol Chem*, 279: 26991-7007.
- Buckley, C. D., E. A. Ross, H. M. McGettrick, C. E. Osborne, O. Haworth, C. Schmutz, P. C. Stone, M. Salmon, N. M. Matharu, R. K. Vohra, G. B. Nash, and G. E. Rainger. 2006. 'Identification of a phenotypically and functionally distinct population of long-lived neutrophils in a model of reverse endothelial migration', *J Leukoc Biol*, 79: 303-11.
- Camby, Isabelle, Marie Le Mercier, Florence Lefranc, and Robert Kiss. 2006. 'Galectin-1: a small protein with major functions', *Glycobiology*, 16: 137R-57R.
- Cattaneo, Valentina, María Virginia Tribulatti, Julieta Carabelli, Agostina Carestia, Mirta Schattner, and Oscar Campetella. 2014. 'Galectin-8 elicits pro-inflammatory activities in the endothelium', *Glycobiology*, 24: 966-73.
- Ceroni, A., K. Maass, H. Geyer, R. Geyer, A. Dell, and S. M. Haslam. 2008. 'GlycoWorkbench: a tool for the computer-assisted annotation of mass spectra of glycans', *J Proteome Res*, 7: 1650-9.
- Cervantes-Alvarez, E., N. L. la Rosa, M. S. la Mora, P. Valdez-Sandoval, M. Palacios-Jimenez, F. Rodriguez-Alvarez, B. I. Vera-Maldonado, E. Aguirre-Aguilar, J. M. Escobar-Valderrama, J. Alanis-Mendizabal, O. Mendez-Guerrero, F. Tejeda-Dominguez, J. Torres-Ruiz, D. Gomez-Martin, K. L. Colborn, D. Kershenovich, C. A. Huang, and N. Navarro-Alvarez. 2022. 'Galectin-3 as a potential

- prognostic biomarker of severe COVID-19 in SARS-CoV-2 infected patients', *Sci Rep*, 12: 1856.
- Chakraborty, A., C. Staudinger, S. L. King, F. C. Erickson, L. S. Lau, A. Bernasconi, F. W. Lusinskas, C. Perlyn, and C. J. Dimitroff. 2021. 'Galectin-9 bridges human B cells to vascular endothelium while programming regulatory pathways', *J Autoimmun*, 117: 102575.
- Chandrasekharan, U. M., M. Siemionow, M. Unsal, L. Yang, E. Poptic, J. Bohn, K. Ozer, Z. Zhou, P. H. Howe, M. Penn, and P. E. DiCorleto. 2007. 'Tumor necrosis factor alpha (TNF-alpha) receptor-II is required for TNF-alpha-induced leukocyte-endothelial interaction in vivo', *Blood*, 109: 1938-44.
- Charles River Laboratories International, Inc. 2012. "C57BL/6 Mouse Hematology." In, edited by C57BL/6 Mouse Hematology North American Colonies*. Charles River Laboratories International, Inc.
- Chen, C., C. A. Duckworth, Q. Zhao, D. M. Pritchard, J. M. Rhodes, and L. G. Yu. 2013. 'Increased circulation of galectin-3 in cancer induces secretion of metastasis-promoting cytokines from blood vascular endothelium', *Clin Cancer Res*, 19: 1693-704.
- Chi, J. T., H. Y. Chang, G. Haraldsen, F. L. Jahnsen, O. G. Troyanskaya, D. S. Chang, Z. Wang, S. G. Rockson, M. van de Rijn, D. Botstein, and P. O. Brown. 2003. 'Endothelial cell diversity revealed by global expression profiling', *Proc Natl Acad Sci U S A*, 100: 10623-8.
- Chien, S. 2007. 'Mechanotransduction and endothelial cell homeostasis: the wisdom of the cell', *Am J Physiol Heart Circ Physiol*, 292: H1209-24.
- Chiu, J. J., L. J. Chen, C. I. Lee, P. L. Lee, D. Y. Lee, M. C. Tsai, C. W. Lin, S. Usami, and S. Chien. 2007. 'Mechanisms of induction of endothelial cell E-selectin expression by smooth muscle cells and its inhibition by shear stress', *Blood*, 110: 519-28.
- Cinamon, Guy, Vera Shinder, and Ronen Alon. 2001. 'Shear forces promote lymphocyte migration across vascular endothelium bearing apical chemokines', *Nature Immunology*, 2: 515-22.
- Colladel, R., R. Pellicani, E. Andreuzzi, A. Paulitti, G. Tarticchio, F. Todaro, A. Colombatti, and M. Mongiat. 2016. 'MULTIMERIN2 binds VEGF-A primarily via the carbohydrate chains exerting an angiostatic function and impairing tumor growth', *Oncotarget*, 7: 2022-37.
- Colomb, F., W. Wang, D. Simpson, M. Zafar, R. Beynon, J. M. Rhodes, and L. G. Yu. 2017. 'Galectin-3 interacts with the cell-surface glycoprotein CD146 (MCAM, MUC18) and induces secretion of metastasis-promoting cytokines from vascular endothelial cells', *J Biol Chem*, 292: 8381-89.

- Conant, K., Y. Wang, A. Szklarczyk, A. Dudak, M. P. Mattson, and S. T. Lim. 2010. 'Matrix metalloproteinase-dependent shedding of intercellular adhesion molecule-5 occurs with long-term potentiation', *Neuroscience*, 166: 508-21.
- Consortium, The UniProt. 2020. 'UniProt: the universal protein knowledgebase in 2021', *Nucleic Acids Research*, 49: D480-D89.
- Cooke, B. M., S. Usami, I. Perry, and G. B. Nash. 1993. 'A simplified method for culture of endothelial cells and analysis of adhesion of blood cells under conditions of flow', *Microvasc Res*, 45: 33-45.
- Cooper, D., A. J. Iqbal, B. R. Gittens, C. Cervone, and M. Perretti. 2012. 'The effect of galectins on leukocyte trafficking in inflammation: sweet or sour?', *Ann N Y Acad Sci*, 1253: 181-92.
- Cooper, Dianne, Lucy V. Norling, and Mauro Perretti. 2008. 'Novel insights into the inhibitory effects of Galectin-1 on neutrophil recruitment under flow', *Journal of Leukocyte Biology*, 83: 1459-66.
- Cooper, GM. 2000. 'The Cell: A Molecular Approach. 2nd edition.' in (Sinauer Associates: Sunderland (MA)).
- Cosgun, Z. C., B. Fels, and K. Kusche-Vihrog. 2020. 'Nanomechanics of the Endothelial Glycocalyx: From Structure to Function', *Am J Pathol*, 190: 732-41.
- Crainiciuc, G., M. Palomino-Segura, M. Molina-Moreno, J. Sicilia, D. G. Aragonés, J. L. Y. Li, R. Madurga, J. M. Adrover, A. Aroca-Crevillen, S. Martín-Salamanca, A. S. Del Valle, S. D. Castillo, H. C. E. Welch, O. Soehnlein, M. Graupera, F. Sanchez-Cabo, A. Zarbock, T. E. Smithgall, M. Di Pilato, T. R. Mempel, P. L. Tharaux, S. F. Gonzalez, A. Ayuso-Sacido, L. G. Ng, G. F. Calvo, I. Gonzalez-Diaz, F. Diaz-de-Maria, and A. Hidalgo. 2022. 'Behavioural immune landscapes of inflammation', *Nature*, 601: 415-21.
- Cunningham, Kristopher S., and Avrum I. Gotlieb. 2005. 'The role of shear stress in the pathogenesis of atherosclerosis', *Laboratory Investigation*, 85: 9-23.
- Dange, M. C., N. Srinivasan, S. K. More, S. M. Bane, A. Upadhyaya, A. D. Ingle, R. P. Gude, R. Mukhopadhyaya, and R. D. Kalraiya. 2014. 'Galectin-3 expressed on different lung compartments promotes organ specific metastasis by facilitating arrest, extravasation and organ colonization via high affinity ligands on melanoma cells', *Clin Exp Metastasis*, 31: 661-73.
- Deaglio, S., R. Mallone, G. Baj, A. Arnulfo, N. Surico, U. Dianzani, K. Mehta, and F. Malavasi. 2000. 'CD38/CD31, a receptor/ligand system ruling adhesion and signaling in human leukocytes', *Chem Immunol*, 75: 99-120.
- Demetriou, M., M. Granovsky, S. Quaggin, and J. W. Dennis. 2001. 'Negative regulation of T-cell activation and autoimmunity by Mgat5 N-glycosylation', *Nature*, 409: 733-9.
- Eckardt, Veit, Michelle C Miller, Xavier Blanchet, Rundan Duan, Julian Leberzammer, Johan Duchene, Oliver Soehnlein, Remco TA Megens, Anna-Kristin Ludwig,

- Aurelio Dregni, Alexander Faussner, Kanin Wichapong, Hans Ippel, Ingrid Dijkgraaf, Herbert Kaltner, Yvonne Döring, Kiril Bidzhekov, Tilman M Hackeng, Christian Weber, Hans-Joachim Gabius, Philipp von Hundelshausen, and Kevin H Mayo. 2020. 'Chemokines and galectins form heterodimers to modulate inflammation', *EMBO reports*, 21: e47852.
- Ensembl. 2023. 'Human (GRCh38.p14)', Accessed December 2023. https://www.ensembl.org/Homo_sapiens/Info/Index.
- Favero, G., C. Paganelli, B. Buffoli, L. F. Rodella, and R. Rezzani. 2014. 'Endothelium and its alterations in cardiovascular diseases: life style intervention', *Biomed Res Int*, 2014: 801896.
- Fernandez-Martin, J. C., A. M. Espinosa-Oliva, I. Garcia-Dominguez, I. Rosado-Sanchez, Y. M. Pacheco, R. Moyano, J. G. Monterde, J. L. Venero, and R. M. de Pablos. 2022. 'Gal3 Plays a Deleterious Role in a Mouse Model of Endotoxemia', *Int J Mol Sci*, 23.
- Filippi, Marie-Dominique. 2019. 'Neutrophil transendothelial migration: updates and new perspectives', *Blood*, 133: 2149-58.
- Fine, N., N. Tasevski, C. A. McCulloch, H. C. Tenenbaum, and M. Glogauer. 2020. 'The Neutrophil: Constant Defender and First Responder', *Front Immunol*, 11: 571085.
- Finger, E. B., K. D. Puri, R. Alon, M. B. Lawrence, U. H. von Andrian, and T. A. Springer. 1996. 'Adhesion through L-selectin requires a threshold hydrodynamic shear', *Nature*, 379: 266-9.
- Ge, S. X., E. W. Son, and R. Yao. 2018. 'iDEP: an integrated web application for differential expression and pathway analysis of RNA-Seq data', *BMC Bioinformatics*, 19: 534.
- Ge, X. N., N. S. Bahaie, B. N. Kang, M. R. Hosseinkhani, S. G. Ha, E. M. Frenzel, F. T. Liu, S. P. Rao, and P. Sriramaraio. 2010. 'Allergen-induced airway remodeling is impaired in galectin-3-deficient mice', *J Immunol*, 185: 1205-14.
- Gimbrone, M. A., Jr., and G. Garcia-Cardena. 2016. 'Endothelial Cell Dysfunction and the Pathobiology of Atherosclerosis', *Circ Res*, 118: 620-36.
- Gittens, B. R. 2014. 'Investigating novel roles for exogenous and endogenous Galectin-3 in leukocyte recruitment to the inflamed microcirculation', Queen Mary University of London.
- Gittens, B. R., J. V. Bodkin, S. Nourshargh, M. Perretti, and D. Cooper. 2017. 'Galectin-3: A Positive Regulator of Leukocyte Recruitment in the Inflamed Microcirculation', *J Immunol*, 198: 4458-69.
- Go, Y. M., D. J. Son, H. Park, M. Orr, L. Hao, W. Takabe, S. Kumar, D. W. Kang, C. W. Kim, H. Jo, and D. P. Jones. 2014. 'Disturbed flow enhances inflammatory signaling and atherogenesis by increasing thioredoxin-1 level in endothelial cell nuclei', *PLoS One*, 9: e108346.

- Granger, D. N. 1999. 'Ischemia-reperfusion: mechanisms of microvascular dysfunction and the influence of risk factors for cardiovascular disease', *Microcirculation*, 6: 167-78.
- Hadi, H. A., and J. A. Suwaidi. 2007. 'Endothelial dysfunction in diabetes mellitus', *Vasc Health Risk Manag*, 3: 853-76.
- Hara, Akira, Masayuki Niwa, Kei Noguchi, Tomohiro Kanayama, Ayumi Niwa, Mikiko Matsuo, Yuichiro Hatano, and Hiroyuki Tomita. 2020. 'Galectin-3 as a Next-Generation Biomarker for Detecting Early Stage of Various Diseases', *Biomolecules*, 10: 389.
- Harrison, D. G., J. Widder, I. Grumbach, W. Chen, M. Weber, and C. Searles. 2006. 'Endothelial mechanotransduction, nitric oxide and vascular inflammation', *J Intern Med*, 259: 351-63.
- Haydon, G. H., and J. Neuberger. 2000. 'PBC: an infectious disease?', *Gut*, 47: 586-8.
- He, J., and L. G. Baum. 2006. 'Endothelial cell expression of galectin-1 induced by prostate cancer cells inhibits T-cell transendothelial migration', *Lab Invest*, 86: 578-90.
- Hellberg, C., L. Molony, L. Zheng, and T. Andersson. 1996. 'Ca²⁺ signalling mechanisms of the beta 2 integrin on neutrophils: involvement of phospholipase C gamma 2 and Ins(1,4,5)P₃', *Biochem J*, 317 (Pt 2): 403-9.
- Herter, J., and A. Zarbock. 2013. 'Integrin Regulation during Leukocyte Recruitment', *J Immunol*, 190: 4451-7.
- Hirabayashi, J., T. Hashidate, Y. Arata, N. Nishi, T. Nakamura, M. Hirashima, T. Urashima, T. Oka, M. Futai, W. E. Muller, F. Yagi, and K. Kasai. 2002. 'Oligosaccharide specificity of galectins: a search by frontal affinity chromatography', *Biochim Biophys Acta*, 1572: 232-54.
- Huang, Haozhong, Peile Ren, Yiwei Zhao, Huimin Weng, Chunsen Jia, Fengxu Yu, and Yongmei Nie. 2023. 'Low shear stress induces inflammatory response via CX3CR1/NF- κ B signal pathway in human umbilical vein endothelial cells', *Tissue and Cell*, 82: 102043.
- ibidi-AN03, GmbH. 2022. "Application Note 03 - Cell Culture in ibidi Channel Slides: Using the μ -Slide VI 0.4 as an Example.". https://ibidi.com/img/cms/support/AN/AN03_Cell_Culture_in_ibidi_Channel_Slides.pdf
- ibidi-AN13, GmbH. 2022. "Application Note 13 - Endothelial Cell Culture Under Perfusion with the ibidi Pump System and μ -Slide I 0.6 Luer.". https://ibidi.com/img/cms/support/AN/AN13_Endothelial_Cells_Under_Perfusion.pdf

- Illumina-AN:Sequencing. 2015. "NextSeq 500 System WGS Solution." .
<https://www.illumina.com/documents/products/appnotes/appnote-nextseq-500-wgs.pdf>
- imagej.net. 2012. 'ImageJ User Guide. Section 30.13 Analyze Gels'.
<https://imagej.net/ij/docs/guide/146-30.html#sec:Analyze-Menu>.
- Imaizumi, Tadaatsu, Mika Kumagai, Naoko Sasaki, Hidekachi Kurotaki, Fumiaki Mori, Masako Seki, Nozomu Nishi, Koji Fujimoto, Kunikazu Tanji, Takeo Shibata, Wakako Tamo, Tomoh Matsumiya, Hidemi Yoshida, Xue-Fan Cui, Shingo Takanashi, Katsumi Hanada, Ken Okumura, Soroku Yagihashi, Koichi Wakabayashi, Takanori Nakamura, Mitsuomi Hirashima, and Kei Satoh. 2002. 'Interferon- γ stimulates the expression of galectin-9 in cultured human endothelial cells', *Journal of Leukocyte Biology*, 72: 486-91.
- Iqbal, A. J., F. Krautter, I. A. Blacksell, R. D. Wright, S. N. Austin-Williams, M. B. Voisin, M. T. Hussain, H. L. Law, T. Niki, M. Hirashima, M. Bombardieri, C. Pitzalis, A. Tiwari, G. B. Nash, L. V. Norling, and D. Cooper. 2022. 'Galectin-9 mediates neutrophil capture and adhesion in a CD44 and beta2 integrin-dependent manner', *FASEB J*, 36: e22065.
- Iqbal, A. J., A. L. Sampaio, F. Maione, K. V. Greco, T. Niki, M. Hirashima, M. Perretti, and D. Cooper. 2011. 'Endogenous galectin-1 and acute inflammation: emerging notion of a galectin-9 pro-resolving effect', *Am J Pathol*, 178: 1201-9.
- Ishikawa, A., T. Imaizumi, H. Yoshida, N. Nishi, T. Nakamura, M. Hirashima, and K. Satoh. 2004. 'Double-stranded RNA enhances the expression of galectin-9 in vascular endothelial cells', *Immunol Cell Biol*, 82: 410-4.
- Jiang, H. R., Z. Al Rasebi, E. Mensah-Brown, A. Shahin, D. Xu, C. S. Goodyear, S. Y. Fukada, F. T. Liu, F. Y. Liew, and M. L. Lukic. 2009. 'Galectin-3 deficiency reduces the severity of experimental autoimmune encephalomyelitis', *J Immunol*, 182: 1167-73.
- Joeh, E., T. O'Leary, W. Li, R. Hawkins, J. R. Hung, C. G. Parker, and M. L. Huang. 2020. 'Mapping glycan-mediated galectin-3 interactions by live cell proximity labeling', *Proc Natl Acad Sci U S A*, 117: 27329-38.
- Joeh, E., A. E. Reeves, C. G. Parker, and M. L. Huang. 2021. 'Mapping Interactions between Glycans and Glycan-Binding Proteins by Live Cell Proximity Tagging', *Curr Protoc*, 1: e104.
- Jumper, J., R. Evans, A. Pritzel, T. Green, M. Figurnov, O. Ronneberger, K. Tunyasuvunakool, R. Bates, A. Zidek, A. Potapenko, A. Bridgland, C. Meyer, S. A. A. Kohl, A. J. Ballard, A. Cowie, B. Romera-Paredes, S. Nikolov, R. Jain, J. Adler, T. Back, S. Petersen, D. Reiman, E. Clancy, M. Zielinski, M. Steinegger, M. Pacholska, T. Berghammer, S. Bodenstein, D. Silver, O. Vinyals, A. W. Senior, K. Kavukcuoglu, P. Kohli, and D. Hassabis. 2021. 'Highly accurate protein structure prediction with AlphaFold', *Nature*, 596: 583-89.

- Khan, K. A., A. J. Naylor, A. Khan, P. J. Noy, M. Mambretti, P. Lodhia, J. Athwal, A. Korzystka, C. D. Buckley, B. E. Willcox, F. Mohammed, and R. Bicknell. 2017. 'Multimerin-2 is a ligand for group 14 family C-type lectins CLEC14A, CD93 and CD248 spanning the endothelial pericyte interface', *Oncogene*, 36: 6097-108.
- Kinashi, Tatsuo. 2005. 'Intracellular signalling controlling integrin activation in lymphocytes', *Nature Reviews Immunology*, 5: 546-59.
- Kitayama, J., A. Hidemura, H. Saito, and H. Nagawa. 2000. 'Shear stress affects migration behavior of polymorphonuclear cells arrested on endothelium', *Cell Immunol*, 203: 39-46.
- Krautter, F., M. T. Hussain, Z. Zhi, D. R. Lezama, J. E. Manning, E. Brown, N. Marigliano, F. Raucci, C. Recio, M. Chimen, F. Maione, A. Tiwari, H. M. McGettrick, D. Cooper, E. A. Fisher, and A. J. Iqbal. 2022. 'Galectin-9: A novel promoter of atherosclerosis progression', *Atherosclerosis*, 363: 57-68.
- Krautter, F., C. Recio, M. T. Hussain, D. R. Lezama, F. Maione, M. Chimen, and A. J. Iqbal. 2020. 'Characterisation of endogenous Galectin-1 and -9 expression in monocyte and macrophage subsets under resting and inflammatory conditions', *Biomed Pharmacother*, 130: 110595.
- Krautter, Franziska, and Asif J. Iqbal. 2021. 'Glycans and Glycan-Binding Proteins as Regulators and Potential Targets in Leukocyte Recruitment', *Frontiers in Cell and Developmental Biology*, 9.
- Kunkel, E. J., and K. Ley. 1996. 'Distinct phenotype of E-selectin-deficient mice. E-selectin is required for slow leukocyte rolling in vivo', *Circ Res*, 79: 1196-204.
- La, Mylinh, Thong V. Cao, Graziela Cerchiaro, Kathya Chilton, Jun Hirabayashi, Ken-ichi Kasai, Sonia M. Oliani, Yuti Chernajovsky, and Mauro Perretti. 2003. 'A novel biological activity for galectin-1: inhibition of leukocyte-endothelial cell interactions in experimental inflammation', *The American journal of pathology*, 163: 1505-15.
- Lagana, A., J. G. Goetz, P. Cheung, A. Raz, J. W. Dennis, and I. R. Nabi. 2006. 'Galectin binding to Mgat5-modified N-glycans regulates fibronectin matrix remodeling in tumor cells', *Mol Cell Biol*, 26: 3181-93.
- Lakshminarayan, R., C. Wunder, U. Becken, M. T. Howes, C. Benzing, S. Arumugam, S. Sales, N. Ariotti, V. Chambon, C. Lamaze, D. Loew, A. Shevchenko, K. Gaus, R. G. Parton, and L. Johannes. 2014. 'Galectin-3 drives glycosphingolipid-dependent biogenesis of clathrin-independent carriers', *Nat Cell Biol*, 16: 595-606.
- Lawrence, M. B., G. S. Kansas, E. J. Kunkel, and K. Ley. 1997. 'Threshold levels of fluid shear promote leukocyte adhesion through selectins (CD62L,P,E)', *J Cell Biol*, 136: 717-27.
- LexogenGmbH. 2023. 'QuantSeq 3' mRNA-Seq (Illumina) V1', Accessed December 2023. <https://www.lexogen.com/docs/quantseq/>.

- Ley, K., M. Allietta, D. C. Bullard, and S. Morgan. 1998. 'Importance of E-selectin for firm leukocyte adhesion in vivo', *Circ Res*, 83: 287-94.
- Ley, K., C. Laudanna, M. I. Cybulsky, and S. Nourshargh. 2007. 'Getting to the site of inflammation: the leukocyte adhesion cascade updated', *Nat Rev Immunol*, 7: 678-89.
- Lightfoot, Abbey, Helen M. McGettrick, and Asif J. Iqbal. 2021. 'Vascular Endothelial Galectins in Leukocyte Trafficking', *Frontiers in Immunology*, 12.
- Liu, Fu-Tong, and Gabriel A. Rabinovich. 2010. 'Galectins: regulators of acute and chronic inflammation', *Annals of the New York Academy of Sciences*, 1183: 158-82.
- Liu, S., Q. Wu, S. Zhang, Z. Wang, H. Liu, L. Teng, P. Xiao, Y. Lu, X. Wang, C. Dong, J. Xiao, and J. Zhang. 2022. 'Serum Galectin-3 levels and all-cause and cardiovascular mortality in maintenance hemodialysis patients: a prospective cohort study', *BMC Nephrol*, 23: 5.
- Livak, K. J., and T. D. Schmittgen. 2001. 'Analysis of relative gene expression data using real-time quantitative PCR and the 2(-Delta Delta C(T)) Method', *Methods*, 25: 402-8.
- Lu, G., N. Nishio, N. S. van den Berg, B. A. Martin, S. Fakurnejad, S. van Keulen, A. D. Colevas, G. M. Thurber, and E. L. Rosenthal. 2020. 'Co-administered antibody improves penetration of antibody-dye conjugate into human cancers with implications for antibody-drug conjugates', *Nat Commun*, 11: 5667.
- Lupu, Florea, Gary Kinasewitz, and Kenneth Dormer. 2020. 'The role of endothelial shear stress on haemodynamics, inflammation, coagulation and glycocalyx during sepsis', *Journal of Cellular and Molecular Medicine*, 24: 12258-71.
- Mansour, A. A., F. Raucci, M. Sevim, A. Saviano, J. Begum, Z. Zhi, L. Pezhman, S. Tull, F. Maione, and A. J. Iqbal. 2022. 'Galectin-9 supports primary T cell transendothelial migration in a glycan and integrin dependent manner', *Biomed Pharmacother*, 151: 113171.
- Marino, K. V., A. J. Cagnoni, D. O. Croci, and G. A. Rabinovich. 2023. 'Targeting galectin-driven regulatory circuits in cancer and fibrosis', *Nat Rev Drug Discov*, 22: 295-316.
- Marki, Alex, Jeffrey D. Esko, Axel R. Pries, and Klaus Ley. 2015. 'Role of the endothelial surface layer in neutrophil recruitment', *Journal of Leukocyte Biology*, 98: 503-15.
- Marshall, B. T., M. Long, J. W. Piper, T. Yago, R. P. McEver, and C. Zhu. 2003. 'Direct observation of catch bonds involving cell-adhesion molecules', *Nature*, 423: 190-3.
- Mason, A. L. 2018. 'Is PBC a viral infectious disease?', *Best Pract Res Clin Gastroenterol*, 34-35: 27-39.

- Mason, A. L., L. Xu, L. Guo, S. Munoz, J. B. Jaspan, M. Bryer-Ash, Y. Cao, D. M. Sander, Y. Shoenfeld, A. Ahmed, J. Van de Water, M. E. Gershwin, and R. F. Garry. 1998. 'Detection of retroviral antibodies in primary biliary cirrhosis and other idiopathic biliary disorders', *Lancet*, 351: 1620-4.
- Matharu, N. M., G. E. Rainger, R. Vohra, and G. B. Nash. 2006. 'Effects of disturbed flow on endothelial cell function: Pathogenic implications of modified leukocyte recruitment', *Biorheology*, 43: 31-44.
- Matsumoto, Ryoji, Hiroyuki Matsumoto, Masako Seki, Mitsumi Hata, Yusuke Asano, Shiro Kanegasaki, Richard L. Stevens, and Mitsuomi Hirashima. 1998. 'Human Ecalectin, a Variant of Human Galectin-9, Is a Novel Eosinophil Chemoattractant Produced by T Lymphocytes *', *Journal of Biological Chemistry*, 273: 16976-84.
- Maurya, M. R., S. Gupta, J. Y. Li, N. E. Ajami, Z. B. Chen, J. Y. Shyy, S. Chien, and S. Subramaniam. 2021. 'Longitudinal shear stress response in human endothelial cells to atheroprone and atheroprotective conditions', *Proc Natl Acad Sci U S A*, 118.
- Meisner, J. K., S. Sumer, K. P. Murrell, T. J. Higgins, and R. J. Price. 2012. 'Laser speckle flowmetry method for measuring spatial and temporal hemodynamic alterations throughout large microvascular networks', *Microcirculation*, 19: 619-31.
- Meng, E. C., T. D. Goddard, E. F. Pettersen, G. S. Couch, Z. J. Pearson, J. H. Morris, and T. E. Ferrin. 2023. 'UCSF ChimeraX: Tools for structure building and analysis', *Protein Sci*, 32: e4792.
- Mirdita, Milot, Konstantin Schütze, Yoshitaka Moriwaki, Lim Heo, Sergey Ovchinnikov, and Martin Steinegger. 2022. 'ColabFold: making protein folding accessible to all', *Nature Methods*, 19: 679-82.
- Mishani, S., H. Belhoul-Fakir, C. Lagat, S. Jansen, B. Evans, and M. Lawrence-Brown. 2021. 'Stress distribution in the walls of major arteries: implications for atherogenesis', *Quant Imaging Med Surg*, 11: 3494-505.
- Mitchell, M. J., K. S. Lin, and M. R. King. 2014. 'Fluid shear stress increases neutrophil activation via platelet-activating factor', *Biophys J*, 106: 2243-53.
- Mitra, R., G. L. O'Neil, I. C. Harding, M. J. Cheng, S. A. Mensah, and E. E. Ebong. 2017. 'Glycocalyx in Atherosclerosis-Relevant Endothelium Function and as a Therapeutic Target', *Curr Atheroscler Rep*, 19: 63.
- Miyata, S. 2015. 'New aspects in fenestrated capillary and tissue dynamics in the sensory circumventricular organs of adult brains', *Front Neurosci*, 9: 390.
- Moazzam, F., F. A. DeLano, B. W. Zweifach, and G. W. Schmid-Schonbein. 1997. 'The leukocyte response to fluid stress', *Proc Natl Acad Sci U S A*, 94: 5338-43.

- Modenutti, Carlos P., Juan I. Blanco Capurro, Santiago Di Lella, and Marcelo A. Martí. 2019. 'The Structural Biology of Galectin-Ligand Recognition: Current Advances in Modeling Tools, Protein Engineering, and Inhibitor Design', *Frontiers in Chemistry*, 7.
- Morra, M., M. Zubiaur, C. Terhorst, J. Sancho, and F. Malavasi. 1998. 'CD38 is functionally dependent on the TCR/CD3 complex in human T cells', *FASEB J*, 12: 581-92.
- Munir, H., G. E. Rainger, G. B. Nash, and H. McGettrick. 2015. 'Analyzing the effects of stromal cells on the recruitment of leukocytes from flow', *J Vis Exp*: e52480.
- Mura, M., R. K. Swain, X. Zhuang, H. Vorschmitt, G. Reynolds, S. Durant, J. F. Beesley, J. M. Herbert, H. Sheldon, M. Andre, S. Sanderson, K. Glen, N. T. Luu, H. M. McGettrick, P. Antczak, F. Falciani, G. B. Nash, Z. S. Nagy, and R. Bicknell. 2012a. 'Identification and angiogenic role of the novel tumor endothelial marker CLEC14A', *Oncogene*, 31: 293-305.
- Mura, M., R. K. Swain, X. Zhuang, H. Vorschmitt, G. Reynolds, S. Durant, J. F. J. Beesley, J. M. J. Herbert, H. Sheldon, M. Andre, S. Sanderson, K. Glen, N. T. Luu, H. M. McGettrick, P. Antczak, F. Falciani, G. B. Nash, Z. S. Nagy, and R. Bicknell. 2012b. 'Identification and angiogenic role of the novel tumor endothelial marker CLEC14A', *Oncogene*, 31: 293-305.
- Nabi, Ivan R., Jay Shankar, and James W. Dennis. 2015. 'The galectin lattice at a glance', *Journal of Cell Science*, 128: 2213-19.
- Nangia-Makker, P., V. Hogan, Y. Honjo, S. Baccarini, L. Tait, R. Bresalier, and A. Raz. 2002. 'Inhibition of human cancer cell growth and metastasis in nude mice by oral intake of modified citrus pectin', *J Natl Cancer Inst*, 94: 1854-62.
- Nangia-Makker, P., Y. Honjo, R. Sarvis, S. Akahani, V. Hogan, K. J. Pienta, and A. Raz. 2000. 'Galectin-3 induces endothelial cell morphogenesis and angiogenesis', *Am J Pathol*, 156: 899-909.
- Nangia-Makker, P., S. Nakahara, V. Hogan, and A. Raz. 2007. 'Galectin-3 in apoptosis, a novel therapeutic target', *J Bioenerg Biomembr*, 39: 79-84.
- Nash, G. B., C. D. Buckley, and G. Ed Rainger. 2004. 'The local physicochemical environment conditions the proinflammatory response of endothelial cells and thus modulates leukocyte recruitment', *FEBS Lett*, 569: 13-7.
- Naylor, A. J., H. M. McGettrick, W. D. Maynard, P. May, F. Barone, A. P. Croft, S. Egginton, and C. D. Buckley. 2014. 'A differential role for CD248 (Endosialin) in PDGF-mediated skeletal muscle angiogenesis', *PLoS One*, 9: e107146.
- Neag, Georgiana. 2022. 'Targeting the novel CD248-MMRN2-CLEC14A pathway in age-related bone loss', University of Birmingham.
- Nielsen, M. I., J. Stegmayr, O. C. Grant, Z. Yang, U. J. Nilsson, I. Boos, M. C. Carlsson, R. J. Woods, C. Unverzagt, H. Leffler, and H. H. Wandall. 2018. 'Galectin binding to cells and glycoproteins with genetically modified glycosylation

- reveals galectin-glycan specificities in a natural context', *J Biol Chem*, 293: 20249-62.
- Nieminen, Julie, Atsushi Kuno, Jun Hirabayashi, and Sachiko Sato. 2007. 'Visualization of Galectin-3 Oligomerization on the Surface of Neutrophils and Endothelial Cells Using Fluorescence Resonance Energy Transfer*', *Journal of Biological Chemistry*, 282: 1374-83.
- Norling, Lucy V., André L. F. Sampaio, Dianne Cooper, and Mauro Perretti. 2008. 'Inhibitory control of endothelial galectin-1 on in vitro and in vivo lymphocyte trafficking', *The FASEB Journal*, 22: 682-90.
- Nourshargh, S., and R. Alon. 2014. 'Leukocyte migration into inflamed tissues', *Immunity*, 41: 694-707.
- Noy, P. J., J. Yang, J. S. Reyat, A. L. Matthews, A. E. Charlton, J. Furmston, D. A. Rogers, G. E. Rainger, and M. G. Tomlinson. 2016. 'TspanC8 Tetraspanins and A Disintegrin and Metalloprotease 10 (ADAM10) Interact via Their Extracellular Regions: EVIDENCE FOR DISTINCT BINDING MECHANISMS FOR DIFFERENT TspanC8 PROTEINS', *J Biol Chem*, 291: 3145-57.
- O'Brien, Martin J., Qiang Shu, W. Alexander Stinson, Pei-Suen Tsou, Jeffrey H. Ruth, Takeo Isozaki, Phillip L. Campbell, Ray A. Ohara, Alisa E. Koch, David A. Fox, and M. Asif Amin. 2018. 'A unique role for galectin-9 in angiogenesis and inflammatory arthritis', *Arthritis research & therapy*, 20: 31-31.
- Ohtsubo, K., and J. D. Marth. 2006. 'Glycosylation in cellular mechanisms of health and disease', *Cell*, 126: 855-67.
- Oliveira, R. M., T. L. Teixeira, C. C. Rodrigues, A. A. da Silva, B. C. Borges, R. T. S. Brigido, S. C. Teixeira, M. A. Dos Santos, J. P. S. Servato, O. Santos D. de, M. J. B. Silva, L. R. Goulart, and C. V. da Silva. 2021. 'Galectin-3 plays a protective role in Leishmania (Leishmania) amazonensis infection', *Glycobiology*, 31: 1378-89.
- Ostermann, G., K. S. Weber, A. Zerneck, A. Schröder, and C. Weber. 2002. 'JAM-1 is a ligand of the beta(2) integrin LFA-1 involved in transendothelial migration of leukocytes', *Nat Immunol*, 3: 151-8.
- Pai, C. H., S. R. Lin, C. H. Liu, S. Y. Pan, H. Hsu, Y. T. Chen, C. T. Yen, I. S. Yu, H. L. Wu, S. L. Lin, and S. W. Lin. 2020. 'Targeting fibroblast CD248 attenuates CCL17-expressing macrophages and tissue fibrosis', *Sci Rep*, 10: 16772.
- Panda, S. K. and Ravindran, B. 2013. 'Isolation of Human PBMCs', *bio-protocol*, 3.
- Parmar, K. M., H. B. Larman, G. Dai, Y. Zhang, E. T. Wang, S. N. Moorthy, J. R. Kratz, Z. Lin, M. K. Jain, M. A. Gimbrone, Jr., and G. Garcia-Cardena. 2006. 'Integration of flow-dependent endothelial phenotypes by Kruppel-like factor 2', *J Clin Invest*, 116: 49-58.

- Patnaik, S. K., B. Potvin, S. Carlsson, D. Sturm, H. Leffler, and P. Stanley. 2006. 'Complex N-glycans are the major ligands for galectin-1, -3, and -8 on Chinese hamster ovary cells', *Glycobiology*, 16: 305-17.
- Pellicani, R., E. Poletto, E. Andreuzzi, A. Paulitti, R. Doliana, D. Bizzotto, P. Braghetta, R. Colladel, G. Tarticchio, P. Sabatelli, F. Bucciotti, G. Bressan, R. V. Iozzo, A. Colombatti, P. Bonaldo, and M. Mongiat. 2020. 'Multimerin-2 maintains vascular stability and permeability', *Matrix Biol*, 87: 11-25.
- Perez-Del-Pulgar, S., P. Pizcueta, P. Engel, J. Bosch, and J. Rodes. 2001. 'Neutrophil adhesion is impaired in the mesentery but not in the liver sinusoids of portal hypertensive rats', *Am J Physiol Gastrointest Liver Physiol*, 280: G1351-9.
- Pettersen, E. F., T. D. Goddard, C. C. Huang, E. C. Meng, G. S. Couch, T. I. Croll, J. H. Morris, and T. E. Ferrin. 2021. 'UCSF ChimeraX: Structure visualization for researchers, educators, and developers', *Protein Sci*, 30: 70-82.
- Piedra-Quintero, Z. L., Z. Wilson, P. Nava, and M. Guerau-de-Arellano. 2020. 'CD38: An Immunomodulatory Molecule in Inflammation and Autoimmunity', *Front Immunol*, 11: 597959.
- Platanias, L. C. 2005. 'Mechanisms of type-I- and type-II-interferon-mediated signalling', *Nat Rev Immunol*, 5: 375-86.
- Qiu, Y., S. Xu, X. Chen, X. Wu, Z. Zhou, J. Zhang, Q. Tu, B. Dong, Z. Liu, J. He, X. Zhang, S. Liu, C. Su, H. Huang, W. Xia, and J. Tao. 2023. 'NAD(+) exhaustion by CD38 upregulation contributes to blood pressure elevation and vascular damage in hypertension', *Signal Transduct Target Ther*, 8: 353.
- Rabinovich, G. A., F.-T. Liu, M. Hirashima, and A. Anderson. 2007. 'An Emerging Role for Galectins in Tuning the Immune Response: Lessons from Experimental Models of Inflammatory Disease, Autoimmunity and Cancer', *Scandinavian Journal of Immunology*, 66: 143-58.
- Rabinovich, G. A., and M. A. Toscano. 2009. 'Turning 'sweet' on immunity: galectin-glycan interactions in immune tolerance and inflammation', *Nat Rev Immunol*, 9: 338-52.
- Rampart, M., W. Fiers, W. de Smet, and A. G. Herman. 1989. 'Different pro-inflammatory profiles of interleukin 1 (IL 1) and tumor necrosis factor (TNF) in an in vivo model of inflammation', *Agents Actions*, 26: 186-8.
- Rao, S. P., Z. Wang, R. I. Zuberi, L. Sikora, N. S. Bahaie, B. L. Zuraw, F. T. Liu, and P. Sriramara. 2007a. 'Galectin-3 functions as an adhesion molecule to support eosinophil rolling and adhesion under conditions of flow', *J Immunol*, 179: 7800-7.
- Rao, Savita P., Zhuangzhi Wang, Riaz I. Zuberi, Lyudmila Sikora, Nooshin S. Bahaie, Bruce L. Zuraw, Fu-Tong Liu, and P. Sriramara. 2007b. 'Galectin-3 Functions as an Adhesion Molecule to Support Eosinophil Rolling and Adhesion under Conditions of Flow', *The Journal of Immunology*, 179: 7800-07.

- Reily, C., T. J. Stewart, M. B. Renfrow, and J. Novak. 2019. 'Glycosylation in health and disease', *Nat Rev Nephrol*, 15: 346-66.
- Reitsma, Sietze, Dick W. Slaaf, Hans Vink, Marc A. M. J. van Zandvoort, and Mirjam G. A. oude Egbrink. 2007. 'The endothelial glycocalyx: composition, functions, and visualization', *Pflugers Archiv : European journal of physiology*, 454: 345-59.
- Roh, J. S., and D. H. Sohn. 2018. 'Damage-Associated Molecular Patterns in Inflammatory Diseases', *Immune Netw*, 18: e27.
- Ronny, Racine, and E. Mummert Mark. 2012. 'Hyaluronan Endocytosis: Mechanisms of Uptake and Biological Functions.' in Ceresa Brian (ed.), *Molecular Regulation of Endocytosis* (IntechOpen: Rijeka).
- Rose, S., A. Misharin, and H. Perlman. 2012. 'A novel Ly6C/Ly6G-based strategy to analyze the mouse splenic myeloid compartment', *Cytometry A*, 81: 343-50.
- Saeed, M. E. M., J. C. Boulous, S. B. Mucklich, E. Leich, M. Chatterjee, S. M. Klauck, and T. Efferth. 2022. 'Disruption of Lipid Raft Microdomains, Regulation of CD38, TP53, and MYC Signaling, and Induction of Apoptosis by Lomitapide in Multiple Myeloma Cells', *Cancer Genomics Proteomics*, 19: 540-55.
- Salmi, M., G. G. Yegutkin, R. Lehvonen, K. Koskinen, T. Salminen, and S. Jalkanen. 2001. 'A cell surface amine oxidase directly controls lymphocyte migration', *Immunity*, 14: 265-76.
- Sano, Hideki, Daniel K. Hsu, Lan Yu, John R. Apgar, Ichiro Kuwabara, Tohru Yamanaka, Mitsuomi Hirashima, and Fu-Tong Liu. 2000. 'Human Galectin-3 Is a Novel Chemoattractant for Monocytes and Macrophages', *The Journal of Immunology*, 165: 2156-64.
- Sanz-Moncasi, M. P., P. Garin-Chesa, E. Stockert, E. A. Jaffe, L. J. Old, and W. J. Rettig. 1994. 'Identification of a high molecular weight endothelial cell surface glycoprotein, endoGlyx-1, in normal and tumor blood vessels', *Lab Invest*, 71: 366-73.
- Schindelin, J., I. Arganda-Carreras, E. Frise, V. Kaynig, M. Longair, T. Pietzsch, S. Preibisch, C. Rueden, S. Saalfeld, B. Schmid, J. Y. Tinevez, D. J. White, V. Hartenstein, K. Eliceiri, P. Tomancak, and A. Cardona. 2012. 'Fiji: an open-source platform for biological-image analysis', *Nat Methods*, 9: 676-82.
- Sedlar, A., M. Travnickova, P. Bojarova, M. Vlachova, K. Slamova, V. Kren, and L. Bacakova. 2021. 'Interaction between Galectin-3 and Integrins Mediates Cell-Matrix Adhesion in Endothelial Cells and Mesenchymal Stem Cells', *Int J Mol Sci*, 22.
- Sheikh, S., M. Rahman, Z. Gale, N. T. Luu, P. C. Stone, N. M. Matharu, G. E. Rainger, and G. B. Nash. 2005. 'Differing mechanisms of leukocyte recruitment and sensitivity to conditioning by shear stress for endothelial cells treated with

- tumour necrosis factor-alpha or interleukin-1beta', *Br J Pharmacol*, 145: 1052-61.
- Sheikh, Sajila, G. Ed Rainger, Zoe Gale, Mahbub Rahman, and Gerard B. Nash. 2003. 'Exposure to fluid shear stress modulates the ability of endothelial cells to recruit neutrophils in response to tumor necrosis factor- α : a basis for local variations in vascular sensitivity to inflammation', *Blood*, 102: 2828-34.
- Shetty, S., P. F. Lalor, and D. H. Adams. 2018. 'Liver sinusoidal endothelial cells - gatekeepers of hepatic immunity', *Nat Rev Gastroenterol Hepatol*, 15: 555-67.
- Shuang, Chen, M. H. Wong, D. J. Schulte, M. Arditi, and K. S. Michelsen. 2007. 'Differential expression of Toll-like receptor 2 (TLR2) and responses to TLR2 ligands between human and murine vascular endothelial cells', *J Endotoxin Res*, 13: 281-96.
- Sieve, Irina, Anja K. Münster-Kühnel, and Denise Hilfiker-Kleiner. 2018. 'Regulation and function of endothelial glycocalyx layer in vascular diseases', *Vascular Pharmacology*, 100: 26-33.
- Sigma-Aldrich. 2020. 'Product Information: Histopaque-1119'. <https://www.sigmaaldrich.com/deepweb/assets/sigmaaldrich/product/documents/173/546/11191pis.pdf>.
- Simoncini, T., G. Varone, L. Fornari, P. Mannella, M. Luisi, F. Labrie, and A. R. Genazzani. 2002. 'Genomic and nongenomic mechanisms of nitric oxide synthesis induction in human endothelial cells by a fourth-generation selective estrogen receptor modulator', *Endocrinology*, 143: 2052-61.
- South Dakota State University. 2023. 'iDEP.96', Accessed December 2023. <http://bioinformatics.sdstate.edu/idep96/>.
- Sperandio, M., A. Thatte, D. Foy, L. G. Ellies, J. D. Marth, and K. Ley. 2001. 'Severe impairment of leukocyte rolling in venules of core 2 glucosaminyltransferase-deficient mice', *Blood*, 97: 3812-9.
- Stillman, Brianna N., Daniel K. Hsu, Mabel Pang, C. Fred Brewer, Pauline Johnson, Fu-Tong Liu, and Linda G. Baum. 2006. 'Galectin-3 and Galectin-1 Bind Distinct Cell Surface Glycoprotein Receptors to Induce T Cell Death', *The Journal of Immunology*, 176: 778-89.
- Szklarczyk, D., A. L. Gable, D. Lyon, A. Junge, S. Wyder, J. Huerta-Cepas, M. Simonovic, N. T. Doncheva, J. H. Morris, P. Bork, L. J. Jensen, and C. V. Mering. 2019. 'STRING v11: protein-protein association networks with increased coverage, supporting functional discovery in genome-wide experimental datasets', *Nucleic Acids Res*, 47: D607-D13.
- Tanaka, A., P. S. C. Leung, and M. E. Gershwin. 2019. 'Pathogen infections and primary biliary cholangitis', *Clin Exp Immunol*, 195: 25-34.

- Thijssen, V. L., B. Barkan, H. Shoji, I. M. Aries, V. Mathieu, L. Deltour, T. M. Hackeng, R. Kiss, Y. Kloog, F. Poirier, and A. W. Griffioen. 2010. 'Tumor cells secrete galectin-1 to enhance endothelial cell activity', *Cancer Res*, 70: 6216-24.
- Thijssen, V. L., S. Hulsmans, and A. W. Griffioen. 2008. 'The galectin profile of the endothelium: altered expression and localization in activated and tumor endothelial cells', *Am J Pathol*, 172: 545-53.
- Tsai, H. F., C. S. Wu, Y. L. Chen, H. J. Liao, I. T. Chyuan, and P. N. Hsu. 2016. 'Galectin-3 suppresses mucosal inflammation and reduces disease severity in experimental colitis', *J Mol Med (Berl)*, 94: 545-56.
- Vasudev, N. S., and A. R. Reynolds. 2014. 'Anti-angiogenic therapy for cancer: current progress, unresolved questions and future directions', *Angiogenesis*, 17: 471-94.
- Velasco, V., M. Gruenthal, E. Zusstone, J. M. Thomas, R. E. Berson, R. S. Keynton, and S. J. Williams. 2016. 'An orbital shear platform for real-time, in vitro endothelium characterization', *Biotechnol Bioeng*, 113: 1336-44.
- Vermes, I., C. Haanen, and C. Reutelingsperger. 2000. 'Flow cytometry of apoptotic cell death', *Journal of Immunological Methods*, 243: 167-90.
- Vicuna, L., E. Pardo, C. Curkovic, R. Doger, C. Oyanadel, C. Metz, L. Massardo, A. Gonzalez, and A. Soza. 2013. 'Galectin-8 binds to LFA-1, blocks its interaction with ICAM-1 and is counteracted by anti-Gal-8 autoantibodies isolated from lupus patients', *Biol Res*, 46: 275-80.
- Wang, N., H. Miao, Y. S. Li, P. Zhang, J. H. Haga, Y. Hu, A. Young, S. Yuan, P. Nguyen, C. C. Wu, and S. Chien. 2006. 'Shear stress regulation of Krüppel-like factor 2 expression is flow pattern-specific', *Biochem Biophys Res Commun*, 341: 1244-51.
- Wang, X., and R. A. Khalil. 2018. 'Matrix Metalloproteinases, Vascular Remodeling, and Vascular Disease', *Adv Pharmacol*, 81: 241-330.
- Wasilenko, S. T., G. E. Mason, and A. L. Mason. 2009. 'Primary biliary cirrhosis, bacteria and molecular mimicry: what's the molecule and where's the mimic?', *Liver Int*, 29: 779-82.
- Watson, C., S. Whittaker, N. Smith, A. J. Vora, D. C. Dumonde, and K. A. Brown. 1996. 'IL-6 acts on endothelial cells to preferentially increase their adherence for lymphocytes', *Clin Exp Immunol*, 105: 112-9.
- Wilhelm, A., V. Aldridge, D. Haldar, A. J. Naylor, C. J. Weston, D. Hedegaard, A. Garg, J. Fear, G. M. Reynolds, A. P. Croft, N. C. Henderson, C. D. Buckley, and P. N. Newsome. 2016. 'CD248/endosialin critically regulates hepatic stellate cell proliferation during chronic liver injury via a PDGF-regulated mechanism', *Gut*, 65: 1175-85.

- Wilkinson, Alex L., Maria Qurashi, and Shishir Shetty. 2020. 'The Role of Sinusoidal Endothelial Cells in the Axis of Inflammation and Cancer Within the Liver', *Frontiers in Physiology*, 11.
- Woodfin, A., M. B. Voisin, M. Beyrau, B. Colom, D. Caille, F. M. Diapouli, G. B. Nash, T. Chavakis, S. M. Albelda, G. E. Rainger, P. Meda, B. A. Imhof, and S. Nourshargh. 2011. 'The junctional adhesion molecule JAM-C regulates polarized transendothelial migration of neutrophils in vivo', *Nat Immunol*, 12: 761-9.
- Woodfin, A., M. B. Voisin, B. A. Imhof, E. Dejana, B. Engelhardt, and S. Nourshargh. 2009. 'Endothelial cell activation leads to neutrophil transmigration as supported by the sequential roles of ICAM-2, JAM-A, and PECAM-1', *Blood*, 113: 6246-57.
- Wragg, J. W., S. Durant, H. M. McGettrick, K. M. Sample, S. Egginton, and R. Bicknell. 2014. 'Shear stress regulated gene expression and angiogenesis in vascular endothelium', *Microcirculation*, 21: 290-300.
- Wu, Kan Xing, Natalie Jia Ying Yeo, Chun Yi Ng, Florence Wen Jing Chioh, Qiao Fan, Xianfeng Tian, Binxia Yang, Gunaseelan Narayanan, Hui Min Tay, Han Wei Hou, N. Ray Dunn, Xinyi Su, Chui Ming Gemmy Cheung, and Christine Cheung. 2022. 'Hyaluronidase-1-mediated glycocalyx impairment underlies endothelial abnormalities in polypoidal choroidal vasculopathy', *BMC Biology*, 20: 47.
- Xu, L., Z. Shen, L. Guo, B. Fodera, A. Keogh, R. Joplin, B. O'Donnell, J. Aitken, W. Carman, J. Neuberger, and A. Mason. 2003. 'Does a betaretrovirus infection trigger primary biliary cirrhosis?', *Proc Natl Acad Sci U S A*, 100: 8454-9.
- Xu, Qichao, Wenqi Zhao, Mingyang Yan, and Hongxia Mei. 2022. 'Neutrophil reverse migration', *Journal of Inflammation*, 19: 22.
- Yamamoto, Hitomi, Nozomu Nishi, Hiroki Shoji, Aiko Itoh, Liang-Hao Lu, Mitsuomi Hirashima, and Takanori Nakamura. 2007. 'Induction of Cell Adhesion by Galectin-8 and its Target Molecules in Jurkat T-Cells', *The Journal of Biochemistry*, 143: 311-24.
- Yang, X., Y. Chang, and W. Wei. 2016. 'Endothelial Dysfunction and Inflammation: Immunity in Rheumatoid Arthritis', *Mediators Inflamm*, 2016: 6813016.
- Yin, Y., MØ Jensen, E. Tajkhorshid, and K. Schulten. 2006. 'Sugar binding and protein conformational changes in lactose permease', *Biophys J*, 91: 3972-85.
- Young, R. E., R. D. Thompson, and S. Nourshargh. 2002. 'Divergent mechanisms of action of the inflammatory cytokines interleukin 1-beta and tumour necrosis factor-alpha in mouse cremasteric venules', *Br J Pharmacol*, 137: 1237-46.
- Zhang, Y., Y. He, S. Bharadwaj, N. Hammam, K. Carnagey, R. Myers, A. Atala, and M. Van Dyke. 2009. 'Tissue-specific extracellular matrix coatings for the

promotion of cell proliferation and maintenance of cell phenotype', *Biomaterials*, 30: 4021-8.

Zhou, X., F. Motta, C. Selmi, W. M. Ridgway, M. E. Gershwin, and W. Zhang. 2021. 'Antibody glycosylation in autoimmune diseases', *Autoimmun Rev*, 20: 102804.